NASA TECHNICAL NOTE

NASA TN D-4139

C.1

STATIC LONGITUDINAL AERODYNAMIC CHARACTERISTICS OF A HAMMERHEAD-SHAPED LITTLE JOE II - LUNAR MODULE MODEL AT MACH 0.30 TO 1.20

by Arvo A. Luoma and Charles D. Harris

Langley Research Center
Langley Station, Hampton, Va.

NATIONAL AERONAUTICS AND SPACE ADMINISTRATION • WASHINGTON, D. C. • OCTOBER 1967

NASA TN D-4139

STATIC LONGITUDINAL AERODYNAMIC CHARACTERISTICS OF A HAMMERHEAD-SHAPED LITTLE JOE II — LUNAR MODULE MODEL AT MACH 0.30 TO 1.20

By Arvo A. Luoma and Charles D. Harris

Langley Research Center
Langley Station, Hampton, Va.

NATIONAL AERONAUTICS AND SPACE ADMINISTRATION

For sale by the Clearinghouse for Federal Scientific and Technical Information
Springfield, Virginia 22151 – CFSTI price $3.00

STATIC LONGITUDINAL AERODYNAMIC CHARACTERISTICS OF A HAMMERHEAD-SHAPED LITTLE JOE II — LUNAR MODULE MODEL AT MACH 0.30 TO 1.20

By Arvo A. Luoma and Charles D. Harris
Langley Research Center

SUMMARY

An investigation of the static longitudinal aerodynamic characteristics of a 0.03-scale model of a proposed Little Joe II — lunar module suborbital space vehicle was made in the Langley 8-foot transonic pressure tunnel at Mach numbers from 0.30 to 1.20 and at angles of attack from approximately -12° to 12°. This configuration was of the hammerhead type, in that the diameter of the lunar module shroud was larger than the diameter of the Little Joe II launch vehicle. Three sizes of stabilizing fins, three nose shapes on the lunar module aerodynamic shroud, and two shroud skirts, which extended over the converging juncture between the shroud and the launch vehicle, were investigated. Flap-type trailing-edge controls on the stabilizing fins were uniformly deflected for pitch control. Control hinge moments were measured on the small fins. Limited transition-strip studies were made on one of the configurations.

All configurations investigated had static longitudinal instability at all test conditions about a moment reference center 1.3 base diameters forward of the base. Severe model buffeting occurred at a Mach number of 0.90 in two narrow ranges of angles of attack near -7° and 7° for the configuration with a shroud nose consisting of a blunt-nosed cone of 30° half-angle and a frustum of a cone of 15° half-angle. Associated with the severe model buffeting were abrupt changes in the magnitudes of the aerodynamic forces and moments as the angle of attack was increased through the critical range. The addition of transition strips extended the Mach number range in which model buffeting and abrupt changes in aerodynamic forces and moments occurred to a Mach number of 1.00. The addition of a boattailed shroud skirt to the smooth configuration substantially reduced the model buffeting and the extent of the abrupt changes in forces and moments at a Mach number of 0.90. The trailing-edge controls on all three sizes of stabilizing fins were effective for pitch control at all test conditions, although reductions in control effectiveness occurred at high control deflections and also at the highest angles of attack at Mach numbers of 0.95 and 1.00.

INTRODUCTION

The National Aeronautics and Space Administration at the Langley Research Center has investigated several configurations of the Little Joe II launch vehicle in combination with an aerodynamic shroud which will house the lunar module (LM) during the boost phase of suborbital flights for LM systems testing. The main objective of the investigations was to determine the longitudinal stability and aerodynamic control characteristics of the Little Joe II — LM space vehicle and the effect of fin size and shape of the LM aerodynamic shroud on these characteristics. The attitude control system of the Little Joe II launch vehicle consists of a combination of aerodynamic control from trailing-edge flap-type controls on the four stabilizing fins and reaction control with fixed nozzles at the roots of the fins.

The results of an investigation in the Langley 8-foot transonic pressure tunnel of the static longitudinal stability, longitudinal aerodynamic control, and trailing-edge control hinge moments of a 0.03-scale model of a proposed Little Joe II — LM suborbital space vehicle are presented herein. Three sizes of stabilizing fins (with full-scale planform areas per fin of 4.65, 7.33, and 9.30 square meters), three nose shapes on the LM aerodynamic shroud, and two LM shroud skirts, which extended over the converging juncture between the shroud and the launch vehicle, were tested. The investigation was made at Mach numbers from 0.30 to 1.20, at angles of attack from approximately -12° to 12°, and with the trailing-edge controls uniformly deflected from 0° to -30° for pitch control. Control-surface hinge moments were investigated for deflections of 0° and -10° on one of the small fins. Test Reynolds numbers based on the diameter of the base of the model varied over the Mach number range from approximately 0.70×10^{6} to 1.60×10^{6}.

The most promising of the three nose shapes on the LM aerodynamic shroud has been investigated with the intermediate and the large stabilizing fins at supersonic speeds also; these results are reported in reference 1. References 2 to 4 report the results of similar tests of the Little Joe II launch vehicle in combination with the Apollo spacecraft at Mach numbers from low subsonic to supersonic.

SYMBOLS

The aerodynamic force and moment data are referred to both the body and wind axes, the origin being on the model reference line and 1.3 reference diameters forward of the model base as shown in figure 1. The hinge-moment data (obtained only with 4.65-square-meter fins) are referred to the hinge line of the trailing-edge control.

C_A axial-force coefficient corrected for base pressure, $\left(\frac{\text{Axial force uncorrected for base pressure}}{qS} - C_{A,b}\right)$

$C_{A,b}$ base axial-force coefficient, $-\left[\left(C_{p,b,1}\right)\left(\frac{A_{b,1}}{S}\right) + \left(C_{p,b,2}\right)\left(\frac{A_{b,2}}{S}\right)\right]$

C_D drag coefficient corrected for base pressure, $\left(C_A \cos \alpha + C_N \sin \alpha\right)$

$C_{h,2}$ hinge-moment coefficient of trailing-edge control on fin 2 (see fig. 1(a)), $\frac{\text{Hinge moment}}{qS_c\bar{c}_c}$

C_L lift coefficient corrected for base pressure, $\left(C_N \cos \alpha - C_A \sin \alpha\right)$

C_m pitching-moment coefficient, $\frac{\text{Pitching moment}}{qSd_{ref}}$

C_N normal-force coefficient, $\frac{\text{Normal force}}{qS}$

$C_{p,b,1}$ pressure coefficient in balance chamber, $\frac{p_{b,1} - p}{q}$

$C_{p,b,2}$ pressure coefficient at rim of model base, $\frac{p_{b,2} - p}{q}$

$A_{b,1}$ area of sting hole in booster airframe

$A_{b,2}$ area of rim at base of booster airframe

$\bar{c}_c$ mean aerodynamic chord (rearward of hinge line) of single trailing-edge control

d diameter

d_{ref} reference length (base diameter)

L/D lift-drag ratio, C_L/C_D

M Mach number of undisturbed stream

p static pressure of undisturbed stream

$p_{b,1}$ static pressure in balance chamber

$p_{b,2}$ static pressure at rim of model base

q dynamic pressure of undisturbed stream

R Reynolds number, based on reference length d_{ref}

r radius

S reference area, $\frac{\pi}{4}(d_{ref})^2$

S_c area rearward of hinge line of single trailing-edge control

x_{cp} longitudinal distance of center of pressure (point on model reference line through which line of action of resultant of normal and axial forces passes) from model base; positive direction forward

x_{cp}/d_{ref} center-of-pressure parameter

α angle of attack, based on model reference line

δ deflection of trailing-edge control measured in plane perpendicular to hinge line; positive direction when trailing edge is down; all four controls had same deflection

$C_{h_\alpha} = \frac{dC_{h,2}}{d\alpha}$, per deg

$C_{h_\delta} = \frac{dC_{h,2}}{d\delta}$, per deg

$C_{m_{C_N}} = \frac{dC_m}{dC_N}$

$C_{m_\alpha} = \frac{dC_m}{d\alpha}$, per deg

$$C_{m_\delta} = \frac{dC_m}{d\delta}, \text{ per deg}$$

$$\frac{C_{m_\delta}}{C_{h_\delta}} = \frac{dC_m}{dC_h}$$

$$C_{N_\alpha} = \frac{dC_N}{d\alpha}, \text{ per deg}$$

$$C_{N_\delta} = \frac{dC_N}{d\delta}, \text{ per deg}$$

APPARATUS

Tunnel

The investigation was made in the Langley 8-foot transonic pressure tunnel. The test section in this tunnel is square in cross section with the upper and lower walls axially slotted to permit changing the test section Mach number continuously from 0 to over 1.20 with negligible effects of choking and blockage. The total pressure of the tunnel air can be varied from a minimum value of about 0.25 atmosphere (0.25×10^5 N/m^2) at all test Mach numbers to a maximum value of about 1.5 atmospheres (1.52×10^5 N/m^2) at transonic Mach number and about 2.0 atmospheres (2.03×10^5 N/m^2) at Mach numbers of 0.40 or less. The stagnation temperature of the tunnel air is automatically controlled and is usually held constant at 120° F (49° C). The tunnel air is dried until the dewpoint temperature in the test section is reduced sufficiently to avoid condensation effects.

Model

The model used in the present investigation was a 0.03-scale model of a proposed Little Joe II — LM suborbital space vehicle which consisted of the Little Joe II launch vehicle and an aerodynamic shroud to house the LM. Four stabilizing fins with trailing-edge controls were spaced 90° apart at the base of the launch vehicle. The model was supported in the tunnel by a sting which had a ratio of sting diameter to model base diameter of 0.30. A drawing of the model is given in figure 1, and photographs of several of the configurations are shown as figure 2. Peripheral corrugations, evident in the photographs of the Little Joe II launch vehicle, have been left off the drawing in figure 1(a) for simplicity; the dimensions of the corrugations are given in reference 3. Geometric characteristics of the model are given in table I.

Three sizes of stabilizing fin with planform areas (full scale) per fin of 4.65, 7.33, and 9.30 square meters (identified herein as small, intermediate, and large, respectively) were investigated. The fins had wedge-shaped sections with blunt trailing edges and 45° sweepback of the leading edge. Aerodynamic control on the Little Joe II launch vehicle is achieved by the use of a flap-type control surface at the trailing edge of each fin. Various deflections of the trailing-edge controls were obtained by the use of deflection-setting plates bent to the proper angles. Details of the fins are given in figure 3. For part of the investigation, a trailing-edge control with a hinge-moment beam for hinge-moment measurements was used on fin 2 of the small fins. (See fig. 3(b).) Hydraulic actuator fairings near the midspan of the fins and reaction control fairings at the roots of the fins as shown in figures 1(a), 2, and 3 were included on the configurations.

Three nose shapes on the LM aerodynamic shroud, identified herein as shroud noses 1, 2, and 3, were investigated. Photographs and drawings of the shroud noses are given in figures 2 and 4, respectively. Shroud nose 1 was a blunt-nosed cone of 15° half-angle. Shroud nose 2 was a combination of a blunt-nosed cone of 30° half-angle and a frustum of a cone of 15° half-angle. Shroud nose 3 was a combination of a blunt-nosed cone of 60° half-angle and a frustum of a cone of 15° half-angle. All shroud noses were attached to the cylindrical portion of the LM shroud as shown by the drawings.

The cylindrical portion of the LM shroud was extended rearward 1.905 meters (full scale) over the launch vehicle in several tests by two types of shroud skirt in an attempt to improve the static longitudinal stability characteristics: a 4° boattailed shroud skirt and a cylindrical (0° boattail) shroud skirt as shown in figure 5.

Instrumentation

Aerodynamic forces and moments were measured with a six-component internal strain-gage balance housed in the model launch vehicle airframe. The model and balance were supported by a 3.49-centimeter-diameter sting which, in turn, was attached to the remotely operated tunnel central support system. A one-component strain gage mounted in the trailing-edge control of fin 2 of the small fins (see figs. 1(a) and 3(b)) was used for determining the hinge moment of the trailing-edge control.

A static-pressure orifice, located within the chamber surrounding the six-component strain-gage balance, and eight static-pressure orifices, located around the rim of the model base and manifolded to a single tube, were connected to pressure-sensitive electrical pickups. These static pressures were used in the base-pressure corrections.

The overall forces and moments on the model, the hinge moment of the trailing-edge control of fin 2 of the small fins, the angle of attack, and the static pressure in the

chamber surrounding the strain-gage balance and that on the rim of the model base were recorded electronically on punch cards.

TESTS, CORRECTIONS, AND ACCURACY

Tests

The model investigated consisted of the Little Joe II launch vehicle in combination with the LM aerodynamic shroud. Three nose shapes on the LM aerodynamic shroud, two shroud skirts, and three sizes of stabilizing fins were investigated. The model was also tested with the fins off. The configurations with the fins on always included the reaction control fairings and, except for one test, always included the hydraulic actuator fairings. Usually, the tests were made with the shroud skirts off.

The various configurations of the Little Joe II — LM space vehicle were investigated at Mach numbers from 0.30 to 1.20 and at angles of attack from approximately -12° to 12°. The stagnation temperature was 120° F (49° C) except at the two lowest Mach numbers where it was usually a few degrees less. The total pressure of the investigation was 1 atmosphere at Mach numbers up to 0.95 for most of the configurations; however, at high subsonic Mach numbers for configurations with large control-surface deflections, and at Mach numbers of 1.00 and 1.20 for all configurations, the total pressure was maintained at less than 1 atmosphere in order to stay within balance load limits. Table II gives the variation of Reynolds number with Mach number for the various configurations.

All configurations were investigated in pitch at a sideslip angle of 0°. Uniform deflections only of the four trailing-edge controls were investigated. The small fins were investigated at control deflections of 0° and -10°, the intermediate fins at control deflections of 0°, -10°, and -20°, and the large fins at control deflections of 0°, -5°, -10°, -20°, and -30°. The hinge moment of the trailing-edge control on fin 2 of the small fins was measured at deflections of 0° and -10° on the configurations with shroud noses 1 and 2 and shroud skirt off.

All configurations were tested with natural transition on the model. The configuration with shroud nose 2, shroud skirt off, and fins off was also tested with three 0.16-centimeter-wide strips of No. 60 carborundum grains located immediately aft of the surface junctures on the LM shroud as indicated in figure 1(b).

Corrections

The axial-force coefficient C_A includes the correction for the base axial-force coefficient $C_{A,b}$; the coefficients C_D and C_L, which are based on C_A and C_N,

are therefore also corrected for base pressure. The aerodynamic force and moment data presented herein are considered to be free of tunnel-boundary interference. No sting-interference corrections have been made to the data except to the extent of the partial correction for sting interference inherent in the base-pressure correction. The angle of attack has been corrected for the deflection of the balance and sting support under aerodynamic load.

Accuracy

The accuracy of the data, based primarily on the static calibrations and the repeatability of the data, is estimated to be as follows:

α, deg	±0.1
M	±0.005

At Mach numbers of 0.70 and above:

C_N	±0.02
C_A	±0.008
C_m	±0.01
C_L	±0.02
C_D	±0.008
$C_{h,2}$	±0.007

At Mach numbers less than 0.70, where the dynamic pressures were substantially less, the accuracy of the data expressed in aerodynamic-coefficient form was correspondingly poorer than that listed.

During the tests, the aerodynamic loading on the trailing-edge controls modified the no-load (M = 0) values of the control deflection. The actual values of the control deflection of the control instrumented for hinge-moment measurements (on fin 2 of small fins) are given by the following empirical equations for the two control deflections investigated:

$$\delta = 0^o - \left(K_{0^o}\right)\alpha M^2$$

$$\delta = -10^o + \left(K_{-10^o}\right)(12^o - \alpha)M^2$$

where α is in degrees, 0^o and -10^o are the no-load (M = 0) values of the control deflection, and the empirical constants K_{0^o} and K_{-10^o} are as follows:

M	K_{0^o}	K_{-10^o}
0 to 1.00	0.010	0.014
1.20	.008	.010

The trailing-edge controls which were not instrumented for hinge-moment measurements had a deflection flexibility which was estimated to be about one-half that of the instrumented trailing-edge control. In several of the figures presented herein, the no-load values of control deflection are used in identifying the data.

PRESENTATION OF RESULTS

The basic longitudinal aerodynamic data are presented in figures 6 to 14 as plots of aerodynamic coefficients against angle of attack. Hinge-moment characteristics are included in figures 11 and 14. The results have been arranged into groupings which make possible a more direct comparison of the effects of model components and control deflections; this arrangement necessitated the presentation of the results for some of the configurations more than once.

Center-of-pressure results are presented herein for the configurations with fins on and controls undeflected and with fins off. The value of the center-of-pressure parameter x_{cp}/d_{ref} shown herein at an angle of attack of 0^o was taken as the value of the average slope $\Delta C_m/\Delta C_N$ between angles of attack from approximately -1^o to 1^o; at angles of attack other than 0^o the value of x_{cp}/d_{ref} shown was obtained by using the following equation:

$$\frac{x_{cp}}{d_{ref}} = \frac{C_{m,\alpha=\alpha_1} - C_{m,C_N=0}}{C_{N,\alpha=\alpha_1}}$$

In this equation, $C_{m,\alpha=\alpha_1}$ and $C_{N,\alpha=\alpha_1}$ are the values of C_m and C_N, respectively, corresponding to a given value α_1 of angle of attack, and $C_{m,C_N=0}$ is the value of C_m when $C_N = 0$. The center-of-pressure location is referenced to the base of the model.

Summary longitudinal aerodynamic characteristics are shown plotted against Mach number in figures 15 to 24. Schlieren photographs are presented in figure 25. The slopes C_{N_α}, C_{m_α}, $C_{m_{C_N}}$, and C_{h_α} shown herein are average values between angles

of attack from approximately $-1\frac{1}{2}^{\circ}$ to $1\frac{1}{2}^{\circ}$. The slopes C_{h_δ}, C_{N_δ}, and C_{m_δ} shown herein are average values between control deflections from approximately 0° to approximately -10°. The results of this investigation are presented in the following figures:

DISCUSSION

Longitudinal Stability

All configurations tested had static longitudinal instability at all test conditions about a moment reference center 1.3 base diameters forward of the base. (For example, see fig. 13(d).) The longitudinal-stability parameter C_{m_α} increased (configuration became more unstable) as the Mach number was increased to about 0.95, then decreased

(configuration became less unstable) with further increase in Mach number to 1.00, and then either remained essentially constant (configuration instability remained same) or decreased (configuration became less unstable), depending on configuration, with further increase in Mach number above 1.00. (See figs. 20 and 24.)

Fin size.- Adding stabilizing fins to the configuration or increasing the size of the fins reduced the amount of static longitudinal instability as might be expected, but not enough to make the configuration stable. (See figs. 11(d), 12(d), 13(d), and 20.) The center-of-pressure location varied somewhat with change in angle of attack and Mach number, the location being farthest forward of the base usually at angles of attack near 0° and at Mach numbers near 0.95. For configurations with shroud nose 1, the center of pressure was forward of the model base by 3.5 to 5.3 base diameters for the fins-off configuration (fig. 11(h)), by 2.0 to 2.6 base diameters for the configuration with the small fins (fig. 11(h)), by 1.6 to 2.2 base diameters for the configuration with the intermediate fins (fig. 12(h)), and by 1.4 to 1.9 base diameters for the configuration with the large fins (fig. 13(h)).

Shroud-nose modifications.- The effect on the static longitudinal stability of changing the shape of the shroud nose was usually quite small. Shroud nose 2 reduced the static longitudinal instability at Mach numbers less than approximately 0.86 and at a Mach number of 1.20. Shroud nose 3 reduced somewhat more the static longitudinal instability at Mach numbers less than approximately 0.92. At the other Mach numbers, however, shroud noses 2 and 3 generally increased the static longitudinal instability. (See fig. 15 and compare figs. 17 and 19.) Shroud nose 2 caused a large shift in the pitching-moment curves and, in general, a reduction in the amount of static longitudinal instability at the higher angles of attack at a Mach number of 0.90 for the configuration with the transition strips both on and off, and at Mach numbers of 0.95 and 1.00 for the configuration with the transition strips on (fig. 14(d)). The effect of shroud nose 2 on the aerodynamic characteristics at these test conditions is discussed more fully in the section "Unsteady Flow."

Shroud skirts.- The effect of the shroud skirts on the static longitudinal stability was generally small, usually reducing the amount of static longitudinal instability at Mach numbers near 0.90, but increasing the amount of static longitudinal instability at the other Mach numbers. (See figs. 16 to 19.) However, the shroud skirts had a favorable effect on the undesirable aerodynamic characteristics observed for the configuration with shroud nose 2 at the higher angles of attack at a Mach number of 0.90 (fig. 10(d)); this effect is discussed further in the section "Unsteady Flow."

Unsteady Flow

Hammerhead-shaped configurations.- As figure 1 shows, the Little Joe II — LM space vehicle was of the hammerhead type, in that the diameter of the LM aerodynamic shroud was larger than the diameter of the Little Joe II launch vehicle. The ratio of these diameters was 1.38. As noted in references 5 to 7, pressure fluctuations exist in two types of flow regions on hammerhead-shaped configurations. First, at high subsonic free-stream Mach numbers there are the regions of flow expansions followed by shock waves (for example, at cone-cylinder junctures) in which there are extremely local but relatively high pressure fluctuations. Second, there are the regions of separated flow in which large areas may be subjected to unsteady flow and, hence, to pressure fluctuations. Flow separation due to the hammerhead configuration, particularly at subsonic Mach numbers, can result in the significant pressure fluctuations associated with buffeting. References 6 and 7 also point out that an abrupt body convergence angle between the shroud and the launch vehicle can extend the separation effects and pressure fluctuations to supersonic Mach numbers. In the present investigation, the body convergence was a frustum of a cone of 58.9° half-angle. This body convergence angle was abrupt, and schlieren photographs indicate that separation off the shroud occurred at all Mach numbers including 1.20.

Model buffeting and abrupt changes in forces and moments.- Severe model buffeting (visually observed) occurred at a Mach number of 0.90 for the configuration with shroud nose 2 and shroud skirt off in two narrow ranges of angles of attack near 7° and -7°. This buffeting occurred with the fins both on and off. The configurations with shroud noses 1 and 3, however, did not exhibit this severe buffeting.

Associated with the severe model buffeting were abrupt changes in the magnitudes of the aerodynamic forces and moments as the angle of attack was increased through the critical range (fig. 14). These abrupt changes included a large decrease in the magnitude of the pitching moment, a rearward movement of the center of pressure of about $1.2d_{ref}$ when the fins were on and about $2.5d_{ref}$ when the fins were off, an increase in normal force of about 25 percent when the fins were on and an insignificant amount when the fins were off, and an increase in axial force of about 25 percent.

Effect of transition strips.- Three transition strips of No. 60 carborundum grains were added to the configuration with shroud nose 2, fins off, and shroud skirt off, as indicated in figure 1(b). Brief tests of this configuration were made at Mach numbers from 0.80 to 1.00 to determine primarily the effect of the transition strips on the model buffeting and on the abrupt changes in the forces and moments observed at a Mach number of 0.90 for the configuration without the transition strips. Direct comparisons of the effect of the transition strips are available at test Mach numbers of 0.80, 0.90, and 1.00, where tests were made both with and without the transition strips. Tests were also

made at Mach numbers of 0.85 and 0.95 of the configuration with the transition strips on. (See fig. 14.)

The transition strips had no effect on the force and moment characteristics at a Mach number of 0.80. At a Mach number of 0.90, the transition strips had only a small effect on the magnitudes of the abrupt changes in pitching moment, center of pressure, and axial force, but did lower (by somewhat less than 1^{o}) the angle-of-attack range in which the abrupt changes occurred. At a Mach number of 1.00, the transition strips caused flow changes at angles of attack near 9^{o} which resulted in model buffeting and abrupt changes in pitching moment, center of pressure, normal force, and axial force. These characteristics were not observed at a Mach number of 1.00 for the configuration with the transition strips off. Addition of the transition strips also reduced the axial force and the base axial force at all angles of attack at a Mach number of 1.00.

At a Mach number of 0.95, the configuration with the transition strips experienced severe buffeting and the characteristic abrupt changes in pitching moment and center of pressure associated with the buffeting. These characteristics occurred at angles of attack near 6^{o} at a Mach number of 0.95. At a Mach number of 0.85, the configuration with the transition strips was not affected by buffeting or abrupt changes in forces and moments.

The results of reference 8 show that at Mach numbers less than 0.95 the flow rearward of the juncture on a 30^{o} half-angle cone-cylinder configuration was markedly affected by the presence of a transition strip located immediately aft of the juncture (the flow was attached when the transition strip was on, separated when the transition strip was off). A relative scarcity of roughness particles in a part of the transition strip due either to erosion or a lack of care in the application of the transition strip also was found to have an important effect on the separation characteristics. The flow on a 15^{o} half-angle cone-cylinder configuration, however, was essentially the same (that is, attached) whether the transition strip was on or off. In the present investigation, shroud nose 2 consisted of a blunt-nosed cone of 30^{o} half-angle and a frustum of a cone of 15^{o} half-angle followed by a cylinder. The sensitivity of the flow on the configuration with shroud nose 2 to transition-strip effects would be expected to be somewhat less than that of the flow on a 30^{o} half-angle cone-cylinder configuration but more than that of the flow on a 15^{o} half-angle cone-cylinder configuration.

Effect of shroud skirt.- Addition of the boattailed shroud skirt to the smooth configuration with shroud nose 2 and fins on (fig. 10) substantially reduced the model buffeting and the extent of the large abrupt changes in aerodynamic forces and moments at a Mach number of 0.90, and delayed the occurrence of these abrupt changes to somewhat higher angles of attack. At a Mach number of 0.95, the configuration with the boattailed shroud skirt did not buffet or show the abrupt changes in forces and moments

evident at a Mach number of 0.90. The cylindrical shroud skirt was not tested with shroud nose 2.

Schlieren photographs.- Schlieren photographs are shown in figure 25(a) for the configuration with shroud nose 1 and shroud skirt off at Mach numbers of 0.80 and 0.90 for angles of attack from 0° to 4° and in figure 25(b) for the configuration with shroud nose 2 and shroud skirt off at a Mach number of 0.90 for angles of attack from -7° to 8°. Typical regions of flow expansions followed by shock waves are evident at the sphere-cone juncture of shroud nose 1 (fig. 25(a)), the cone-cone juncture of shroud nose 2 (fig. 25(b)), and the cone-cylinder junctures of both shroud noses 1 and 2. At a Mach number of 0.90, a shock-wave system was located in the region of the converging juncture between the shroud and the launch vehicle for the configurations with both shroud noses 1 and 2. The schlieren photographs show that for the configuration with shroud nose 2 (fig. 25(b)) the shock-wave system on the windward surface of the shroud moved upstream and away from the converging juncture as the angle of attack was increased through the critical range. (Compare the schlieren photographs for angles of attack of -6° and -7° and for 6° and 8°.) Also evident in the schlieren photographs at an angle of attack of 8° is a small region of flow expansion at the beginning of the converging juncture. This region of flow expansion is evident to a lesser extent at an angle of attack of -7°, but not at lower angles of attack. Schlieren photographs were not obtained for the configuration with shroud nose 1 at these higher angles of attack or for the configurations with shroud skirt.

An explanation for the severe model buffeting at a Mach number of 0.90 is suggested by the observed facts that the buffeting was eliminated by the addition of the boattailed shroud skirt and that the buffeting did not occur for the configuration with shroud nose 1, and by a study of the schlieren photographs. The buffeting is possibly explained by the unsteady flow in the region of the converging juncture, the unsteadiness of this flow having been aggravated or intensified by the adverse effects of the interactions with the boundary layer of the shock waves in the regions of the converging juncture, the cone-cylinder juncture, and the cone-cone juncture. The strength and type of the shock waves in the regions of the cone-cylinder and the cone-cone junctures are dependent, of course, on the extent and degree of the flow expansions and the nature of the boundary layer preceding these shock waves.

Longitudinal Control

Longitudinal aerodynamic control on the Little Joe II — LM space vehicle is obtained from flap-type trailing-edge controls on the stabilizing fins. As figure 3 shows, the planforms of the controls used on the three sizes of fins tested in this investigation were dissimilar and, whereas full-span controls were used on the small and intermediate fins, only partial-span controls were used on the large fins.

The intermediate fins were approximately 50 percent larger than the small fins in both the total area of the fins and in the area of the control. The large fins were 100 percent larger than the small fins in the total area of the fins, but the area of the control on the large fins was actually less than the area of the control on the small fins.

The controls on all three sizes of stabilizing fins were found to be effective for pitch control at all test conditions. (See figs. 11(d), 12(d), 13(d), and 14(d).) However, there were reductions in control effectiveness at control deflections greater than -10^{o} for the controls on the intermediate fins (fig. 12(d)) and on the large fins (fig. 13(d)) at all angles of attack and Mach numbers. The controls on the small fins were not investigated at deflections greater than -10^{o} (figs. 11(d) and 14(d)). There were also losses in control effectiveness C_{m_δ} at all control deflections at the highest angles of attack at Mach numbers of 0.95 and 1.00 for the controls on the intermediate fins (fig. 12(d)) and on the large fins (fig. 13(d)), but not for the controls on the small fins (figs. 11(d) and 14(d)).

The variation with Mach number of the control-effectiveness parameter C_{m_δ} is shown in figure 20(b) for the controls on the three sizes of fins, and this variation is seen to be similar for all three sizes of fins. There was first a slight increase in control effectiveness as the Mach number was increased to about 0.85, then a more rapid increase in control effectiveness as the Mach number was further increased to about 0.90, and then a uniform reduction in control effectiveness as the Mach number was increased above 0.90, so that at a Mach number of 1.20 the control effectiveness was less than that at the lowest Mach numbers.

Figure 20(b) shows that the control effectiveness was greatest for the controls on the intermediate fins. This greater control effectiveness was due, of course, primarily to the fact that the area of the control on the intermediate fins was substantially larger than the area of the control on the large fins (56 percent larger) or the area of the control on the small fins (50 percent larger).

Control Hinge Moments

Hinge-moment data were obtained only for the control on fin 2 (fig. 1(a)) of the small fins. The variation of hinge-moment coefficient $C_{h,2}$ with angle of attack was approximately linear at subsonic Mach numbers for the two control deflections of 0^{o} and -10^{o} investigated. (See figs. 11(i) and 14(i).) The divergence from a linear variation of $C_{h,2}$ with angle of attack was greater at a Mach number of 1.00 than at the lower Mach numbers, and this divergence was still greater at a Mach number of 1.20.

The hinge-moment coefficient $C_{h,2}$ and the hinge-moment parameters C_{h_α} and C_{h_δ} are shown plotted against Mach number at an angle of attack of 0^{o} in

figures 21(b), 21(c), 24(b), and 24(c). The magnitude of the parameter C_{h_δ} is seen to be substantially greater at Mach numbers of 0.90 and above than at the lower Mach numbers.

The magnitudes of the hinge-moment results of the present investigation and the trends with angle of attack, control deflection, and Mach number check well with the corresponding results obtained in the investigation of reference 3 on the same fin-control configuration on the Little Joe II launch vehicle when tested in combination with the Apollo spacecraft. In the investigation of reference 3 the diameter of the Apollo spacecraft was the same as that of the Little Joe II launch vehicle, and the Apollo spacecraft, which was essentially conical of 33° half-angle, included the launch escape system.

The control-effectiveness hinge-moment parameter $C_{m_\delta}/C_{h_\delta}$ shown plotted against Mach number in figures 21(c) and 24(c) is a measure of the effectiveness of the control in producing a pitching moment in terms of the hinge moment developed on the control while producing this pitching moment. A large value of this parameter is desirable since such a value would tend to indicate good pitch effectiveness and low control hinge moments. It is seen in figures 21(c) and 24(c) that the control effectiveness parameter $C_{m_\delta}/C_{h_\delta}$ was, on the average, essentially invariant as the Mach number was increased to 0.80, but then decreased substantially with further increase in Mach number to 1.20.

CONCLUSIONS

An investigation of the static longitudinal aerodynamic characteristics of a 0.03-scale model of a proposed Little Joe II — lunar module suborbital space vehicle was made in the Langley 8-foot transonic pressure tunnel at Mach numbers from 0.30 to 1.20 and at angles of attack from approximately -12° to 12°. This configuration was of the hammerhead type, in that the diameter of the lunar module aerodynamic shroud was larger than the diameter of the Little Joe II launch vehicle. Three sizes of stabilizing fins, three nose shapes on the lunar module aerodynamic shroud, and two shroud skirts, which extended over the converging juncture between the shroud and the launch vehicle, were investigated. Flap-type trailing-edge controls on the stabilizing fins were uniformly deflected for pitch control from 0° to -10° on the small fins, from 0° to -20° on the intermediate fins, and from 0° to -30° on the large fins. Control hinge moments were measured on the small fins. Limited transition-strip studies were made on one of the configurations. The following conclusions are indicated:

1. All configurations investigated had static longitudinal instability at all test conditions about a moment reference center 1.3 base diameters forward of the base.

2. Depending on angle of attack and Mach number, the center of pressure was forward of the model base by 3.5 to 5.3 base diameters for the fins-off configuration, by 2.0 to 2.6 base diameters for the configuration with the small fins, by 1.6 to 2.2 base diameters for the configuration with the intermediate fins, and by 1.4 to 1.9 base diameters for the configuration with the large fins.

3. Shroud-nose changes or the addition of shroud skirts to the configuration usually had a small and variable effect on the static longitudinal stability. At a Mach number of 0.90, however, the flow on the configuration with one of the shroud noses was very critical to model attitude.

4. Severe model buffeting occurred at a Mach number of 0.90 in two narrow ranges of angles of attack near -7° and 7° for the configuration with a shroud nose consisting of a blunt-nosed cone of 30° half-angle and a frustum of a cone of 15° half-angle. Associated with the severe model buffeting were abrupt changes in the magnitudes of the aerodynamic forces and moments as the angle of attack was increased through the critical range.

5. The addition of transition strips to the surface junctures on the lunar module shroud had no beneficial effect on the severe model buffeting or the abrupt changes in forces and moments which occurred at a Mach number of 0.90, and actually precipitated model buffeting and abrupt changes in forces and moments at a Mach number of 1.00. Severe model buffeting and abrupt changes in forces and moments also occurred at a Mach number of 0.95 for the configuration with the transition strips on.

6. The addition of a boattailed shroud skirt to the smooth configuration substantially reduced the model buffeting and the extent of the abrupt changes in the aerodynamic forces and moments which occurred at a Mach number of 0.90 and delayed the occurrence of these abrupt changes to somewhat higher angles of attack. No model buffeting or abrupt changes in forces and moments occurred at a Mach number of 0.95 for the configuration with the shroud skirt.

7. The trailing-edge controls on all three sizes of stabilizing fins were effective for pitch control at all test conditions, although reductions in control effectiveness occurred at control deflections greater than -10° at all angles of attack and Mach numbers and also occurred at all control deflections for the controls on the intermediate and the large fins at the highest angles of attack at Mach numbers of 0.95 and 1.00.

8. The magnitude of the rate of change of hinge-moment coefficient with control deflection was greater at Mach numbers of 0.90 and above than at the lower Mach numbers.

9. The ratio of pitching moment produced by control deflection to hinge moment developed by control deflection was less at Mach numbers of 1.00 and 1.20 than at low subsonic Mach numbers.

Langley Research Center,
National Aeronautics and Space Administration,
Langley Station, Hampton, Va., May 2, 1967,
124-07-02-42-23.

REFERENCES

1. Fournier, Roger H.; and Wassum, Donald: Static Stability and Control Characteristics of a 0.030-Scale Model of a Little Joe II—LEM Space Vehicle at Mach 1.57 to 4.63. NASA TM X-1139, 1965.

2. Henderson, William P.: Subsonic Static Longitudinal Aerodynamic Characteristics at Angles of Attack From -2^{o} to 95^{o} of a Proposed Little Joe II — Apollo Space Vehicle. NASA TM X-751, 1963.

3. Luoma, Arvo A.: Longitudinal Stability and Control, Roll Control, and Hinge Moments of a Little Joe II — Apollo Model at Mach Numbers up to 1.20. NASA TM X-1002, 1964.

4. Fournier, Roger H.; and Silvers, H. Norman: Static Longitudinal Aerodynamic Characteristics of a 0.028-Scale Model of a Proposed Little Joe II — Apollo Space Vehicle at Mach Numbers From 1.50 to 2.16. NASA TM X-754, 1963.

5. Coe, Charles F.: Steady and Fluctuating Pressures at Transonic Speeds on Two Space-Vehicle Payload Shapes. NASA TM X-503, 1961.

6. Coe, Charles F.: The Effects of Some Variations in Launch-Vehicle Nose Shape on Steady and Fluctuating Pressures at Transonic Speeds. NASA TM X-646, 1962.

7. Coe, Charles F.; and Nute, James B.: Steady and Fluctuating Pressures at Transonic Speeds on Hammerhead Launch Vehicle. NASA TM X-778, 1962.

8. Kelly, Thomas C.: A Transonic Investigation of Base Pressures Associated With Shallow Three-Dimensional Rearward-Facing Steps. NASA TN D-2927, 1965.

TABLE I.- GEOMETRIC CHARACTERISTICS OF 0.03-SCALE MODEL OF PROPOSED LITTLE JOE II — LM SUBORBITAL SPACE VEHICLE

Little Joe II launch vehicle:	
Body:	
Cross-sectional area (reference area, S), m^2	0.0108
Diameter (reference length, d_{ref}), cm	11.73
Area of sting hole, $A_{b,1}$, m^2	0.0054
Area of rim, $A_{b,2}$, m^2	0.0055
Stabilizing fins (exposed, single-fin values given):	
Small fins (4.65 m^2 full scale):	
Airfoil section (parallel to root chord)	Wedge, 10^o total angle
Area (includes area of control), m^2	0.0042
Span, cm	7.087
Root chord, cm	6.688
Tip chord, cm	3.360
Aspect ratio	1.20
Sweepback of leading edge, deg	45
Trailing-edge control:	
Type	Flap
Area, aft of hinge line, S_c:	
m^2	0.0013
Percent of fin area	30
Mean aerodynamic chord, $\bar{c}_c$, cm	2.428
Intermediate fins (7.33 m^2 full scale):	
Airfoil section (parallel to root chord)	Wedge, 10^o total angle
Area (includes area of control), m^2	0.0066
Span, cm	8.659
Root chord, cm	9.078
Tip chord, cm	2.705
Aspect ratio	1.141
Sweepback of leading edge, deg	45
Trailing-edge control:	
Type	Flap
Area, aft of hinge line, S_c:	
m^2	0.0019
Percent of fin area	28.7
Mean aerodynamic chord, $\bar{c}_c$, cm	2.913

TABLE I.- GEOMETRIC CHARACTERISTICS OF 0.03-SCALE MODEL OF PROPOSED LITTLE JOE II — LM SUBORBITAL SPACE VEHICLE – Concluded

Large fins (9.30 m^2 full scale):	
Airfoil section (parallel to root chord)	Wedge, 10^o total angle
Area (includes area of control), m^2	0.0084
Span, cm	9.91
Root chord, cm	9.868
Tip chord, cm	4.57
Aspect ratio	1.17
Sweepback of leading edge, deg	45
Trailing-edge control:	
Type	Flap
Area, aft of hinge line, S_c:	
m^2	0.0012
Percent of fin area	14.3
Mean aerodynamic chord, $\bar{c}_c$, cm	2.743
LM aerodynamic shroud:	
Cylindrical section:	
Cross-sectional area, m^2	0.021
Diameter, cm	16.15
Shroud nose length:	
Shroud nose 1, cm	12.83
Shroud nose 2, cm	10.43
Shroud nose 3, cm	9.91
Overall length from nose of LM shroud to base of launch vehicle:	
Shroud nose 1, cm	52.98
Shroud nose 2, cm	50.60
Shroud nose 3, cm	50.06

TABLE II.- VARIATION OF REYNOLDS NUMBER WITH MACH NUMBER

Configuration				Reynolds number at –										
Shroud		Fins	δ, deg	M = 0.30	M = 0.50	M = 0.70	M = 0.80	M = 0.85	M = 0.90	M = 0.93	M = 0.95	M = 0.97	M = 1.00	M = 1.20
Nose	Skirt													
1	Off	Small	0	0.71×10^6	1.09×10^6	1.35×10^6	1.46×10^6	1.49×10^6	1.53×10^6	1.54×10^6	1.55×10^6	1.56×10^6	1.27×10^6	1.05×10^6
1	Off	Small	-10	.71	1.09	1.39	1.46	-------	1.53	-------	-------	-------	1.27	1.05
1	Off	Off		.71	1.07	1.35	1.46	1.50	1.54	-------	1.56	-------	1.27	1.06
1	Off	Intermediate	0	.70	1.08	1.36	1.47	1.49	1.54	-------	1.56	-------	1.12	.96
1	Off	Intermediate	-10	-------	1.08	1.35	1.46	-------	1.53	-------	1.56	-------	1.12	.96
1	Off	Intermediate	-20	-------	1.08	1.36	1.44	-------	1.53	-------	1.40	-------	.97	.82
1	Off	Large	0	.71	1.08	1.35	1.45	1.48	1.52	-------	1.56	-------	1.12	.97
1	Off	Large	-5	.70	1.08	-------	1.46	-------	1.54	-------	1.57	-------	1.12	.96
1	Off	Large	-10	.69	1.04	1.36	1.46	1.48	1.53	-------	1.56	-------	1.12	.96
1	Off	Large	-20	.70	1.07	1.36	1.46	1.49	1.54	-------	1.41	-------	.97	.81
1	Off	Large	-30	.70	1.07	-------	1.24	-------	1.30	-------	1.29	-------	.90	.77
2	Off	Small	0	.70	1.07	1.32	1.43	-------	1.51	-------	-------	-------	1.27	1.05
2	Off	Small	-10	.72	1.08	1.36	1.46	-------	1.53	-------	-------	-------	1.27	1.05
2	Off	Off		.71	1.07	1.35	1.46	-------	1.53	-------	-------	-------	1.27	1.05
[a]2	Off	Off		-------	-------	-------	1.46	1.51	1.53	-------	1.56	-------	1.12	-------
[a]2	Off	Off		-------	-------	-------	-------	-------	-------	-------	-------	-------	1.27	-------
3	Off	Off		.69	1.07	1.35	1.46	1.48	1.52	-------	1.56	-------	1.27	1.05
1	Cylindrical	Off		-------	-------	-------	-------	-------	1.54	-------	1.56	-------	1.27	1.06
1	Boattailed	Off		.71	1.08	1.36	1.46	1.51	1.53	-------	1.56	-------	1.27	1.05
1	Boattailed	Small	0	-------	-------	-------	-------	-------	-------	-------	1.55	-------	1.12	.96
1	Boattailed	Large	0	-------	-------	1.35	1.45	1.48	1.52	-------	1.56	-------	1.12	.96
2	Boattailed	Small	0	-------	-------	-------	1.22	1.47	1.52	-------	1.55	-------	1.12	.96

[a]With transition strips.

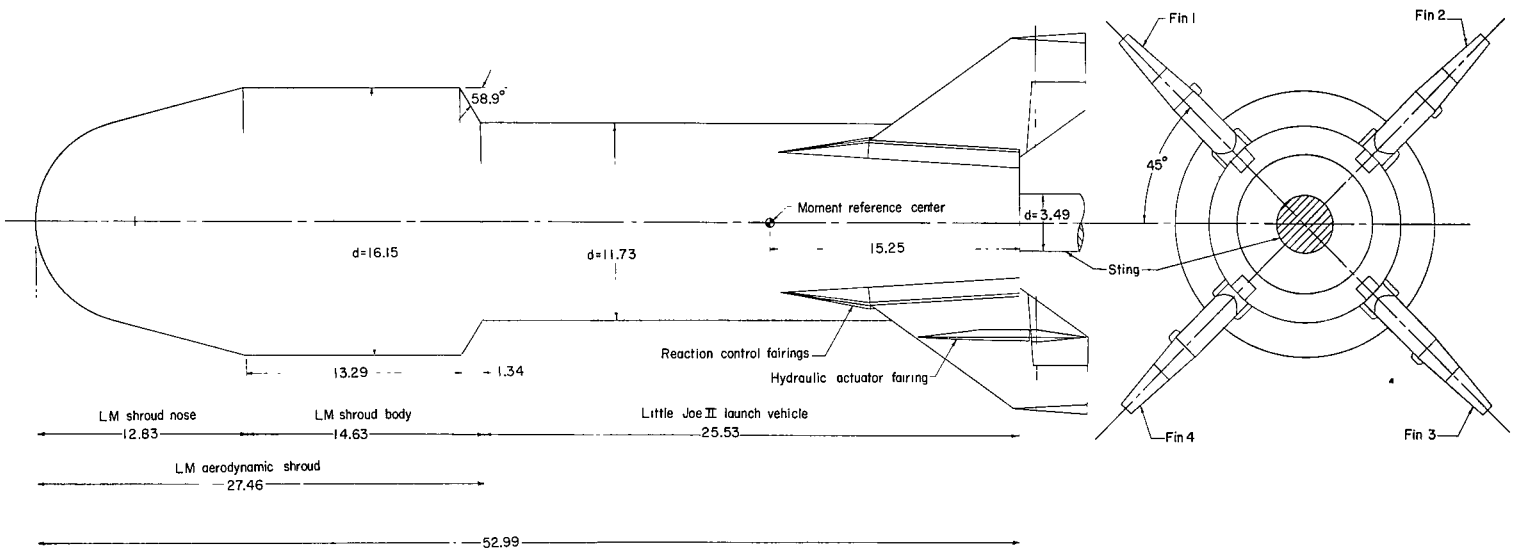

(a) Drawing. Shroud nose 1; large fins; $\delta = 0^0$.

Figure 1.- Drawing of 0.03-scale model of Little Joe II — LM space vehicle and location of transition strips on LM shroud. Shroud skirt off. All dimensions are in centimeters unless otherwise noted.

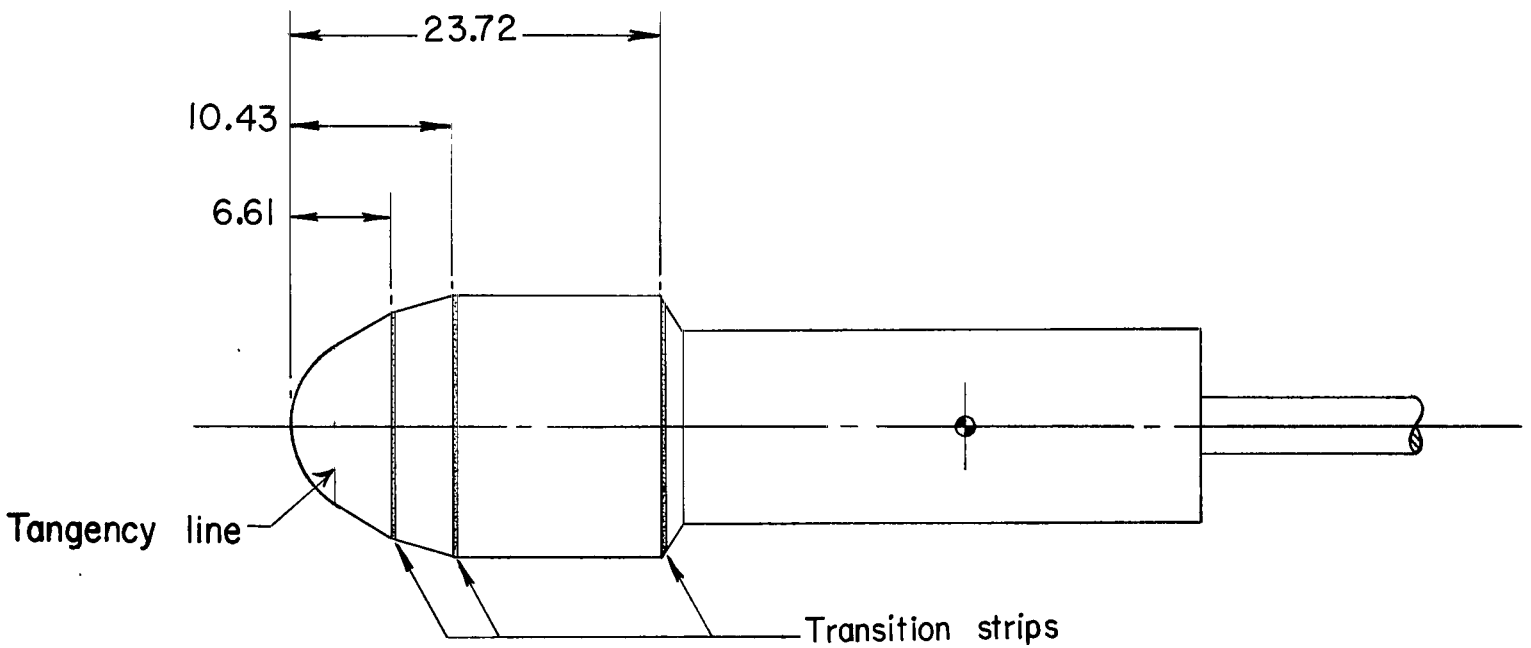

(b) Location of transition strips. Shroud nose 2; fins off.

Figure 1.- Concluded.

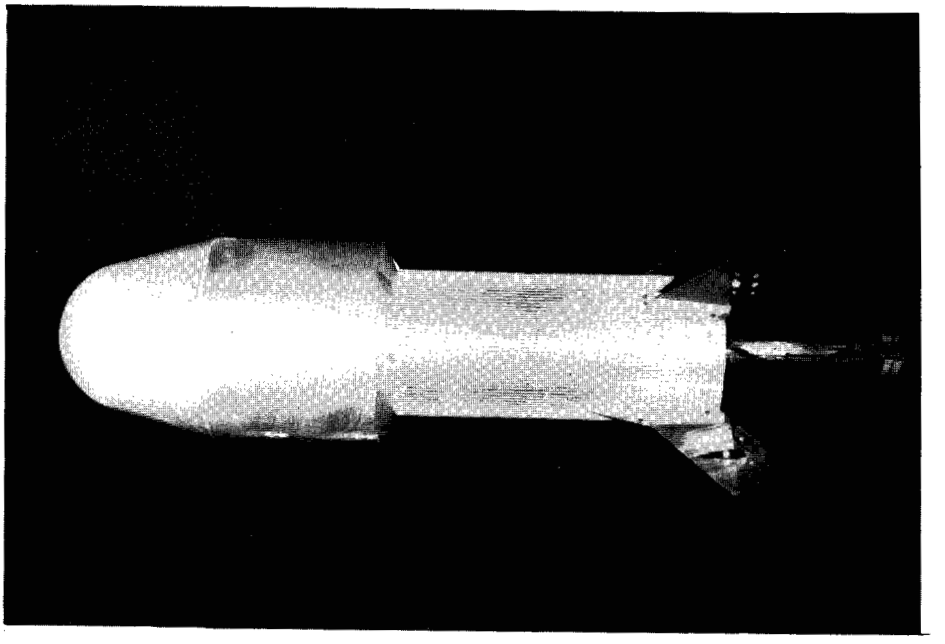

(a) Shroud nose 1; small fins; $\delta = -10^{0}$. L-63-9533

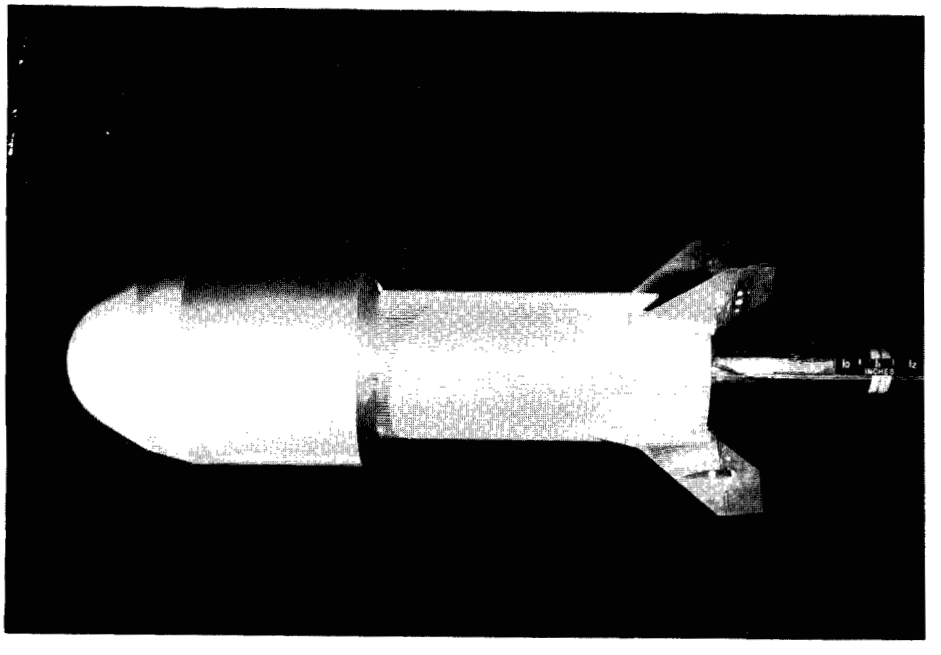

(b) Shroud nose 2; small fins; $\delta = -10^{0}$. L-63-9532

Figure 2.- Photographs of Little Joe II — LM model showing various configurations and model components.

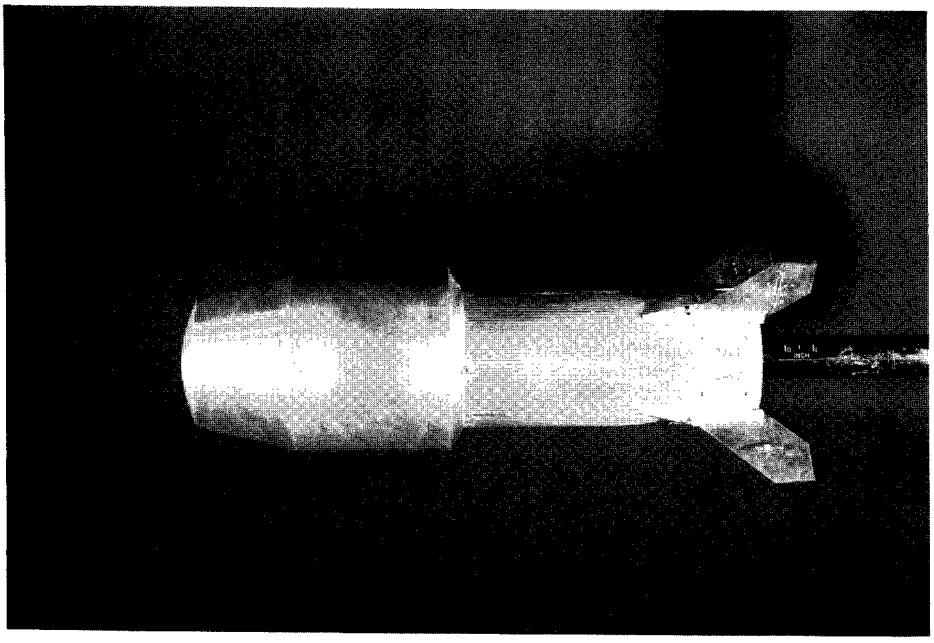

(c) Shroud nose 3; small fins; $\delta = 0^{o}$. L-64-2703

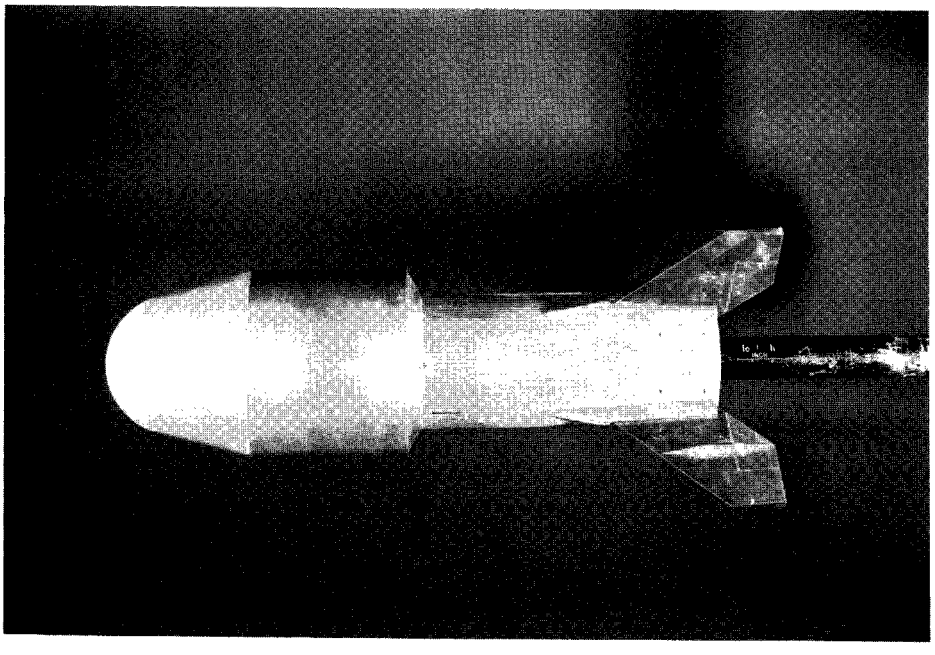

(d) Shroud nose 1; large fins; $\delta = 0^{o}$. L-64-2704

Figure 2.- Continued.

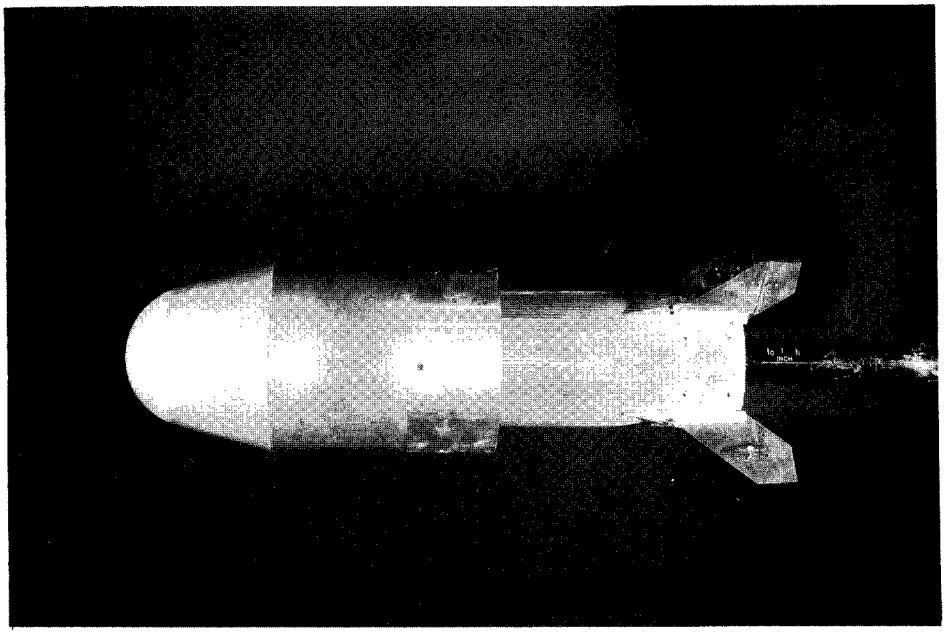

(e) Shroud nose 1; cylindrical shroud skirt; small fins; $\delta = 0^{o}$. L-64-2702

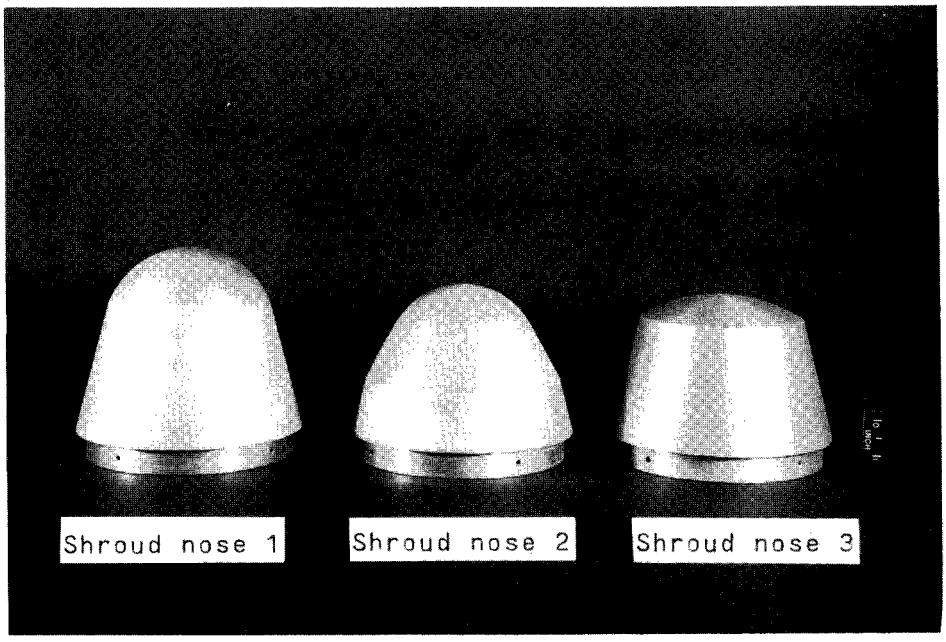

(f) LM shroud noses. L-64-2701

Figure 2.- Concluded.

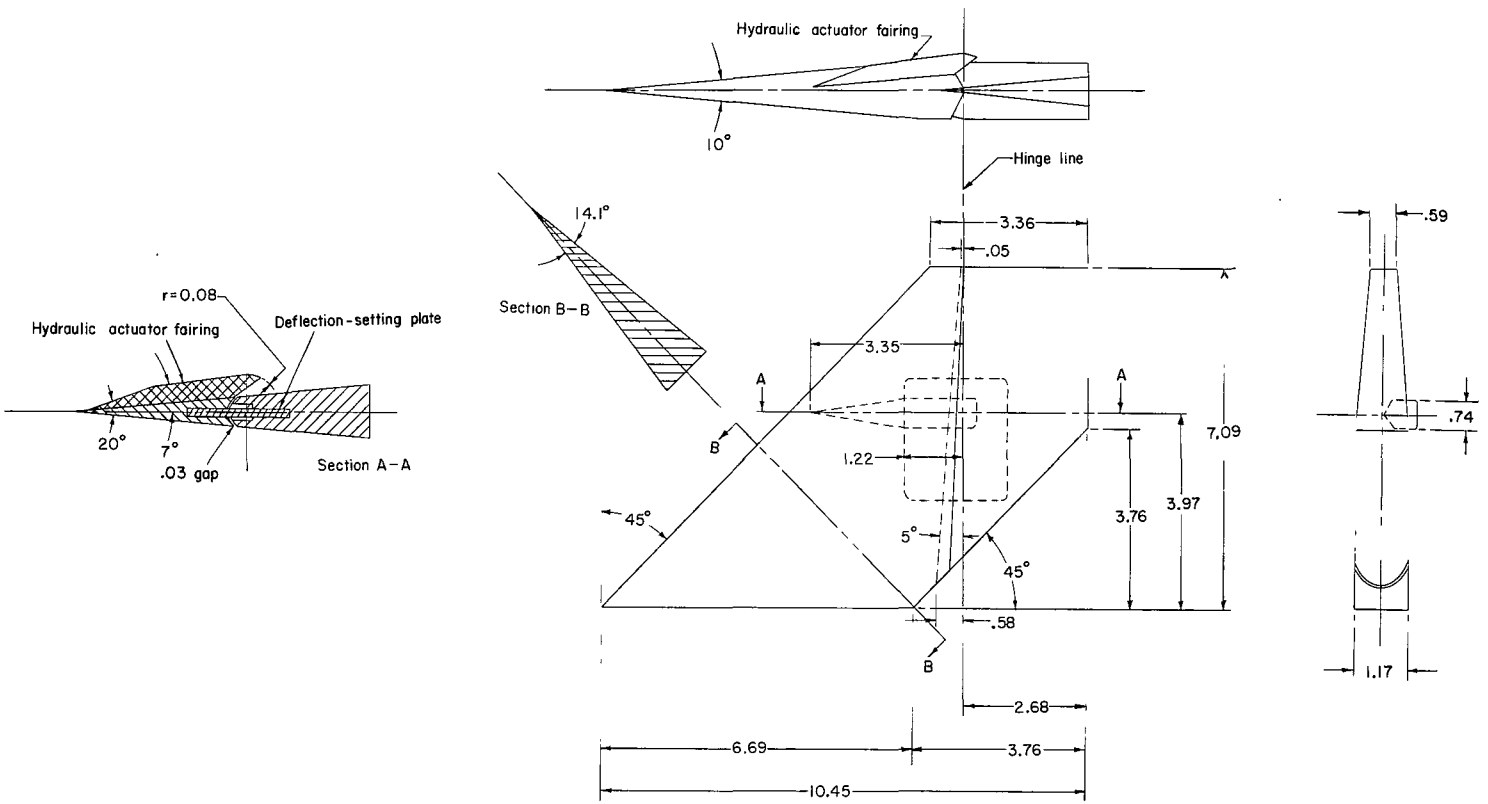

(a) Small (4.65 m^2) fin with uninstrumented trailing-edge control.

Figure 3.- Details of stabilizing fins. All dimensions are in cm unless otherwise noted.

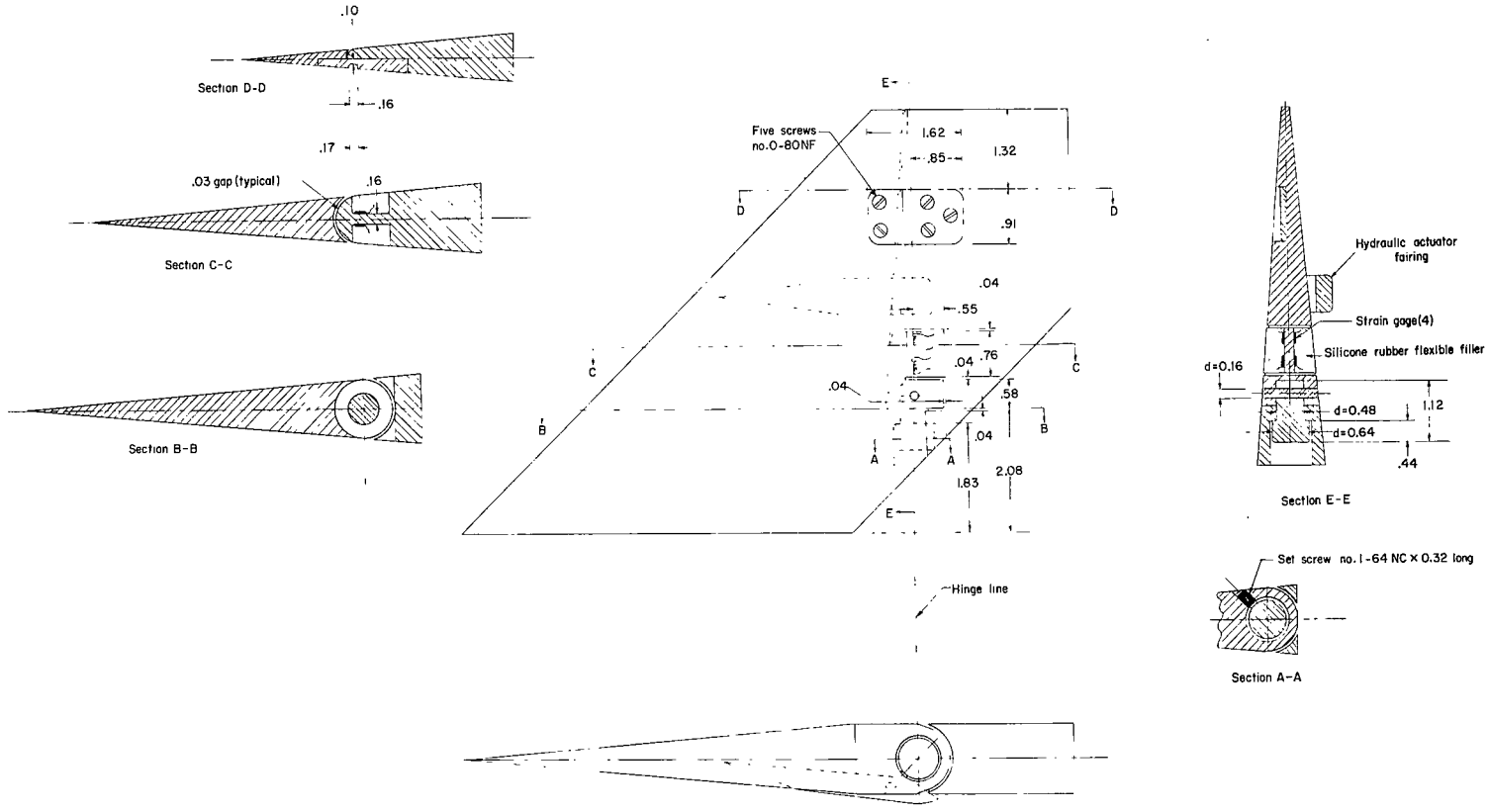

(b) Small (4.65 m^2) fin with instrumented trailing-edge control (fin 2).

Figure 3.- Continued.

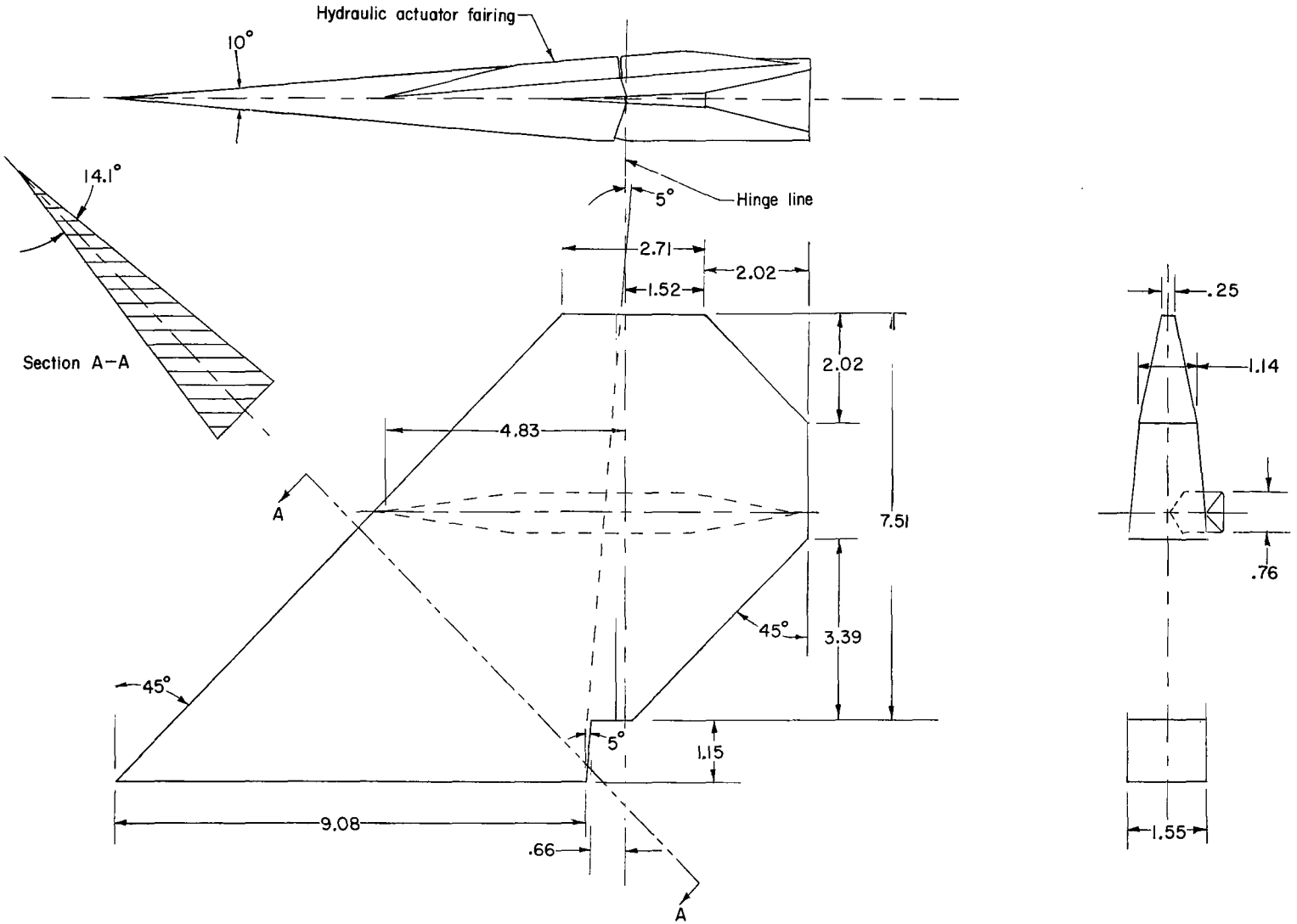

(c) Intermediate (7.33 m^2) fin.

Figure 3.- Continued.

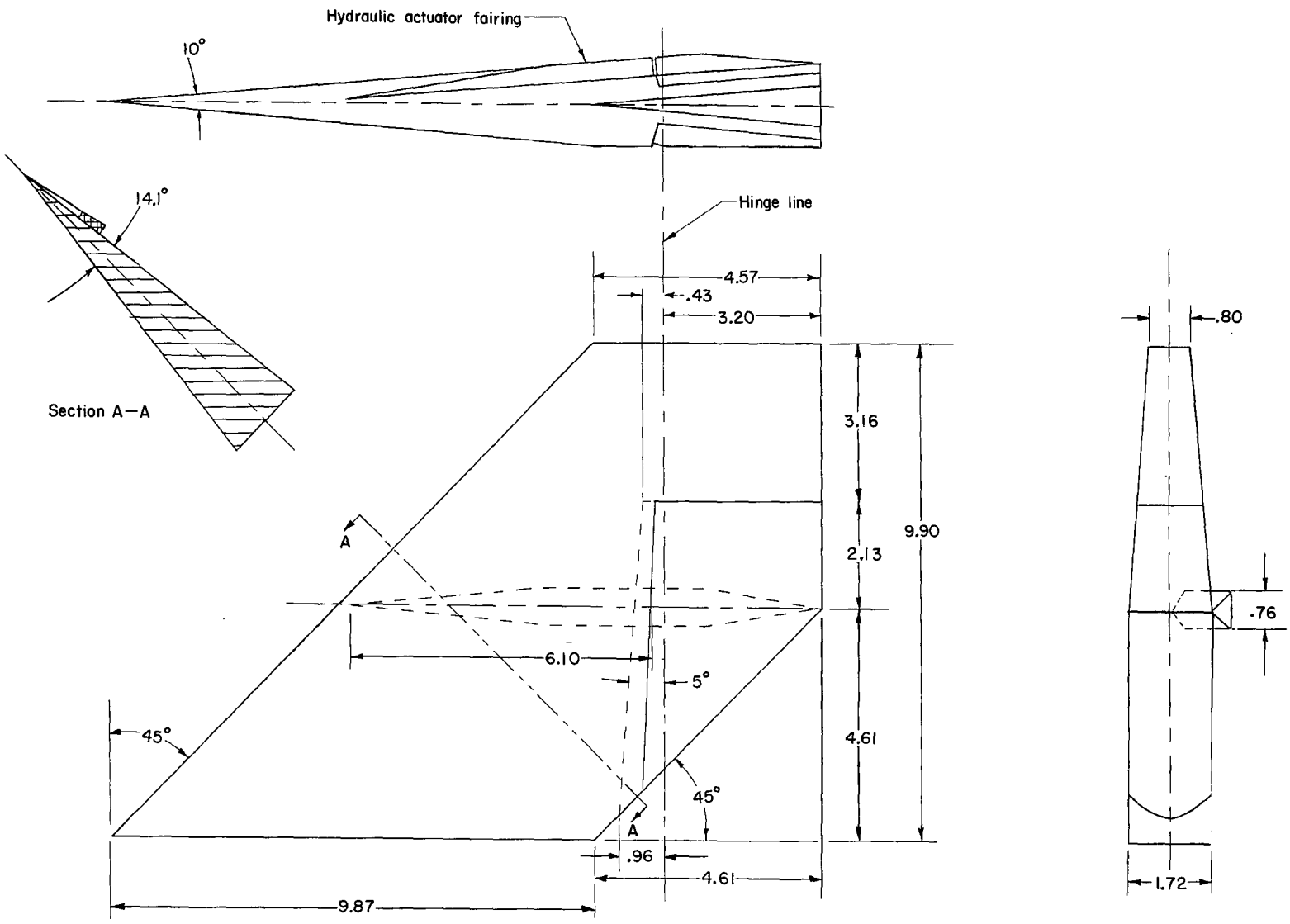

(d) Large (9.30 m^2) fin.

Figure 3.- Concluded.

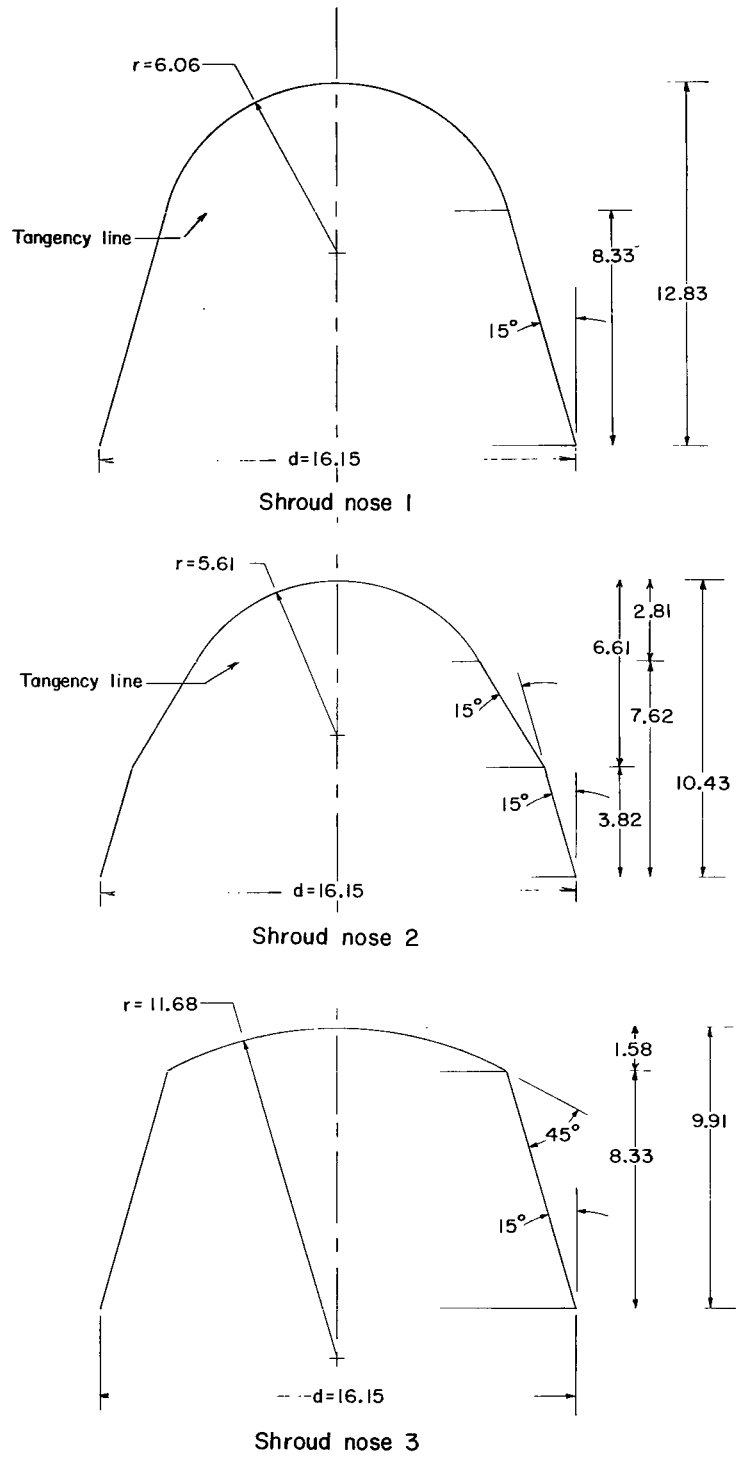

Figure 4.- Details of LM shroud noses. All dimensions are in cm unless otherwise noted.

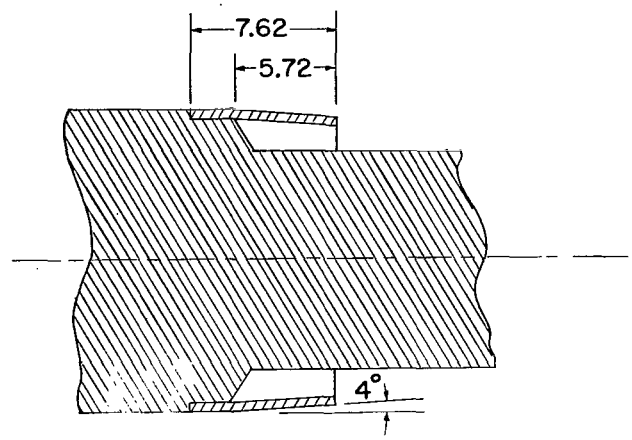

Boattailed shroud skirt

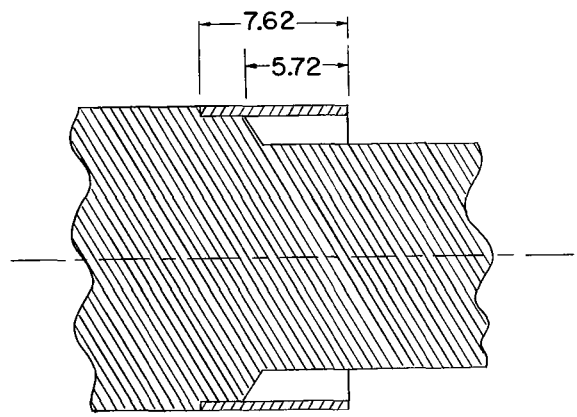

Cylindrical shroud skirt

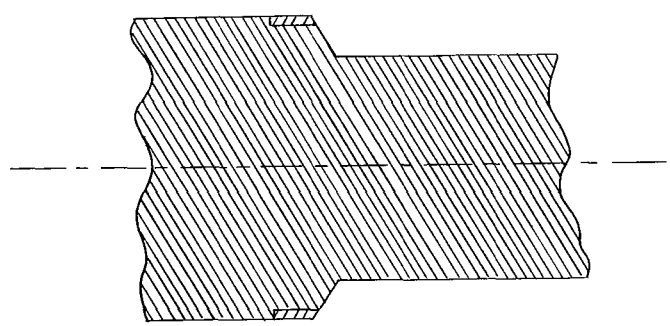

Shroud skirt off

Figure 5.- Details of LM shroud skirts. All dimensions are in cm unless otherwise noted.

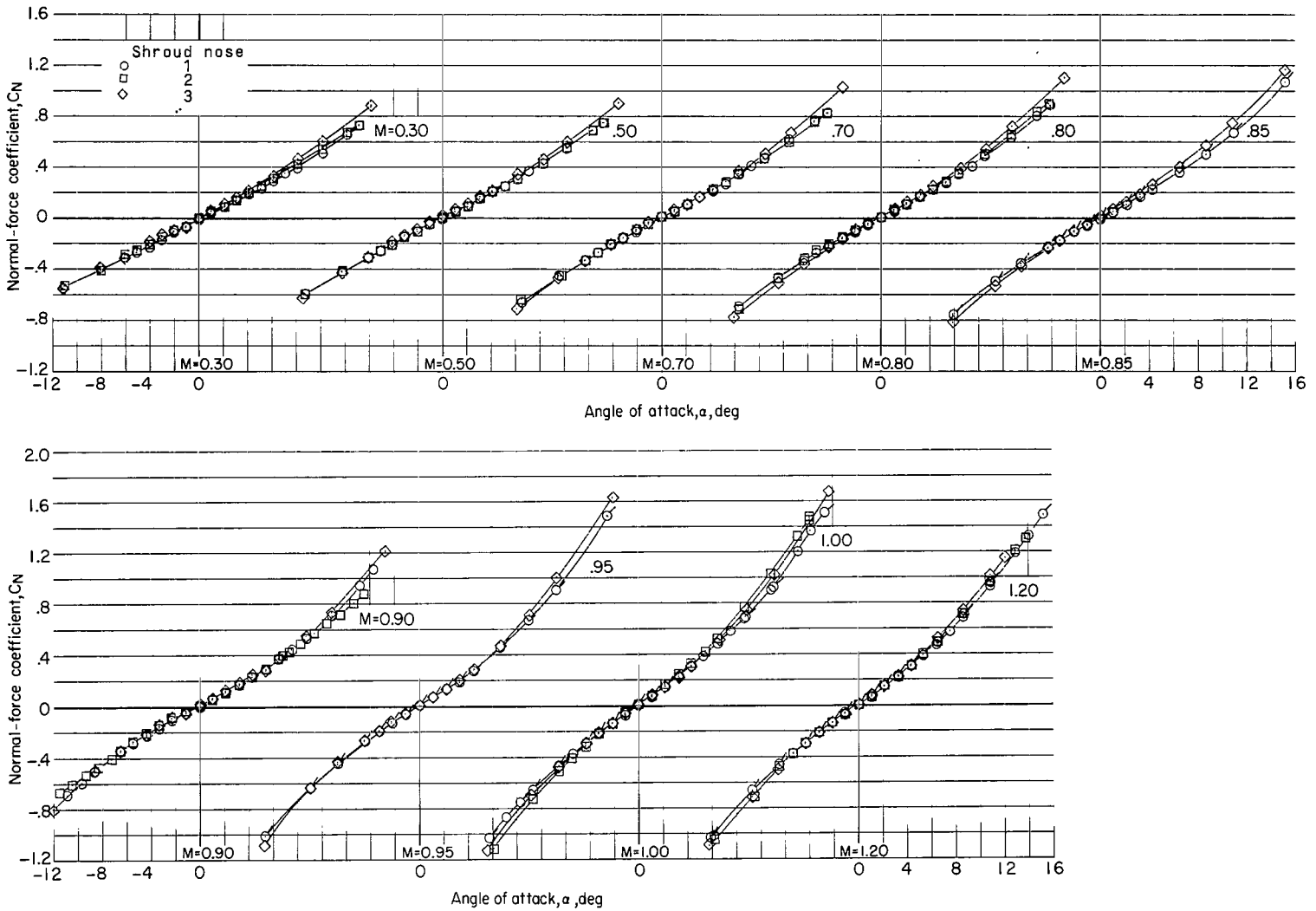

(a) C_N against α.

Figure 6.- Effect of shroud nose on longitudinal aerodynamic characteristics. Fins off; shroud skirt off. (Flagged symbols indicate points from repeat run.)

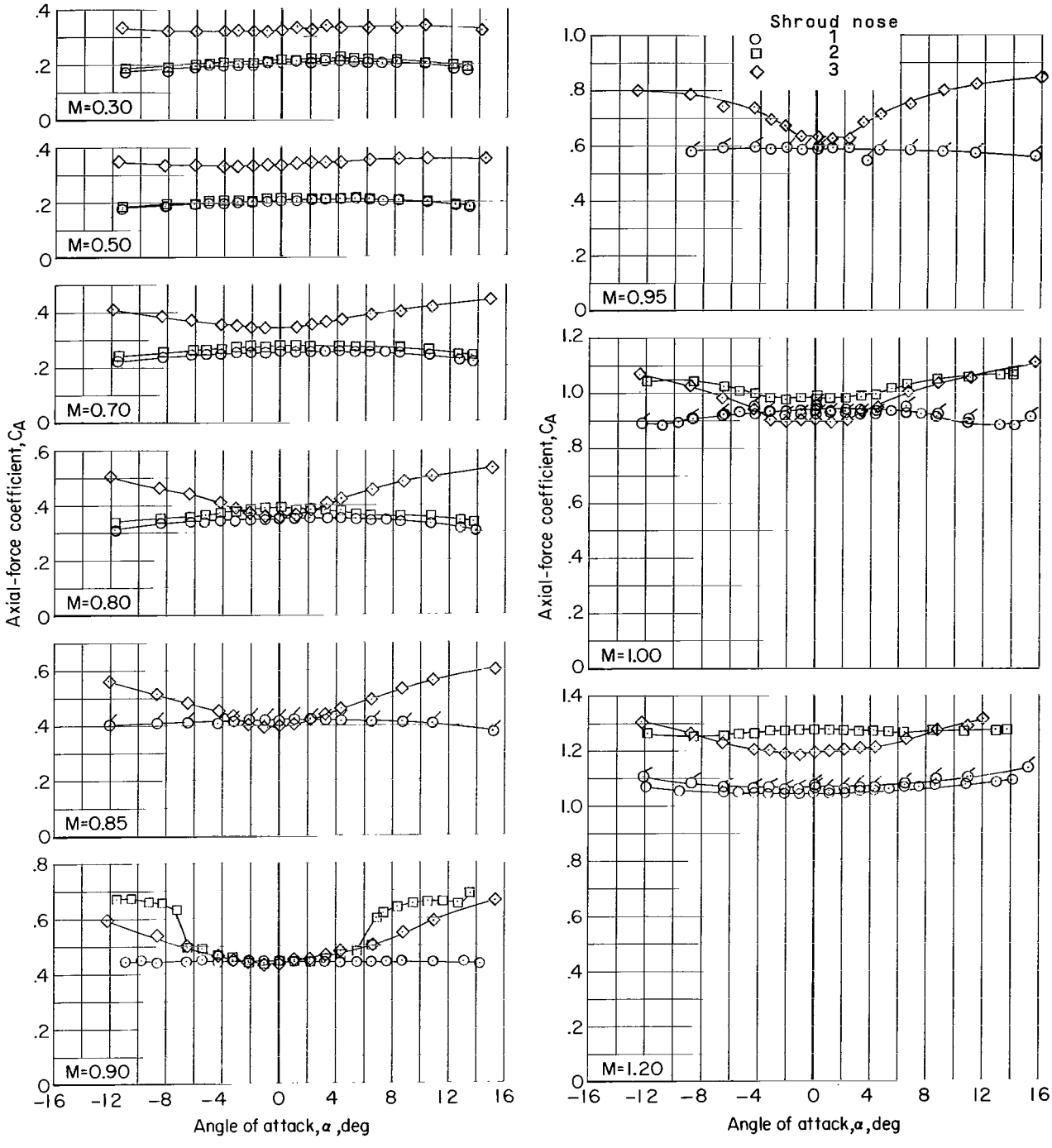

(b) C_A against α.

Figure 6.- Continued.

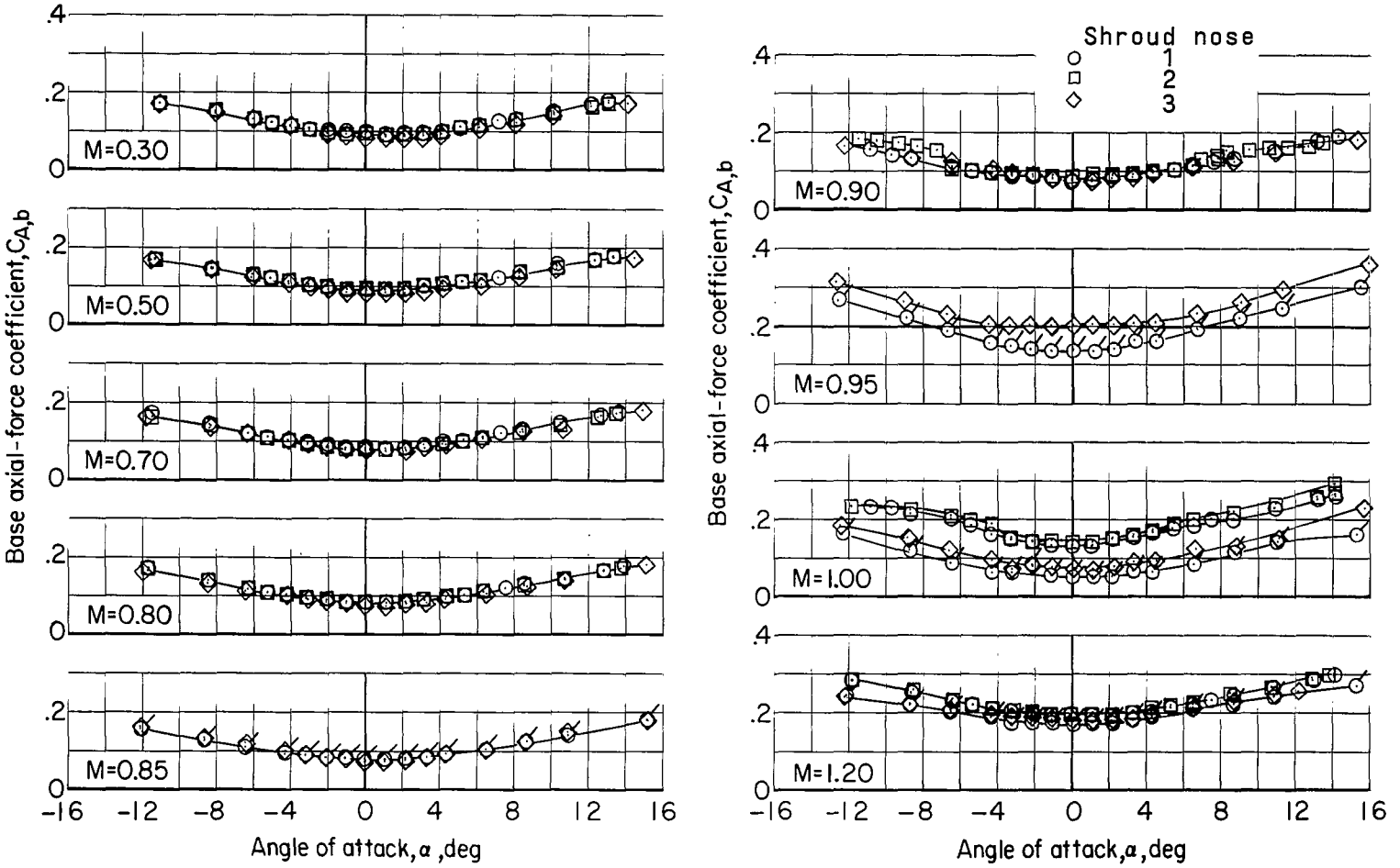

(c) $C_{A,b}$ against α.

Figure 6.- Continued.

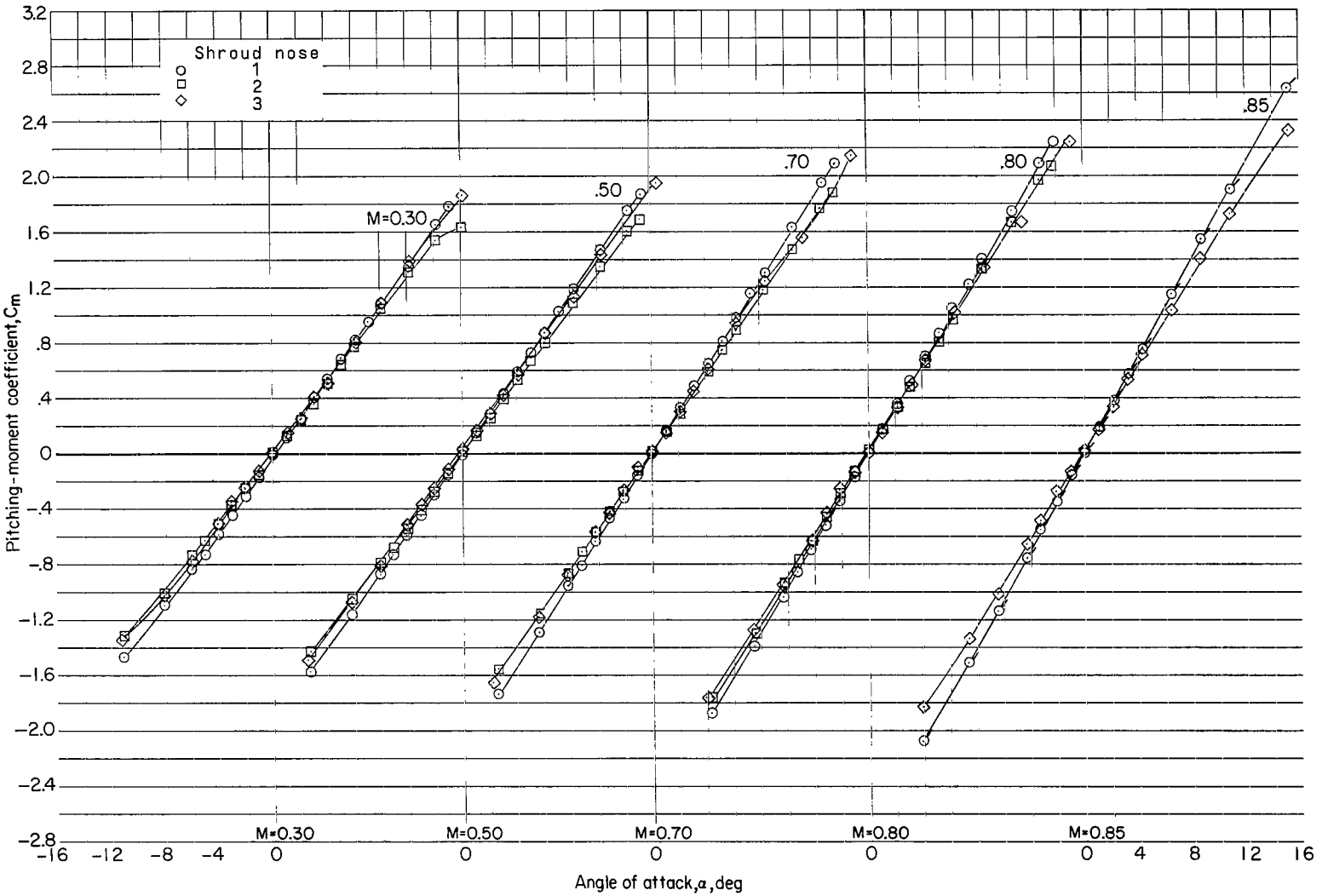

(d) C_m against α.

Figure 6.- Continued.

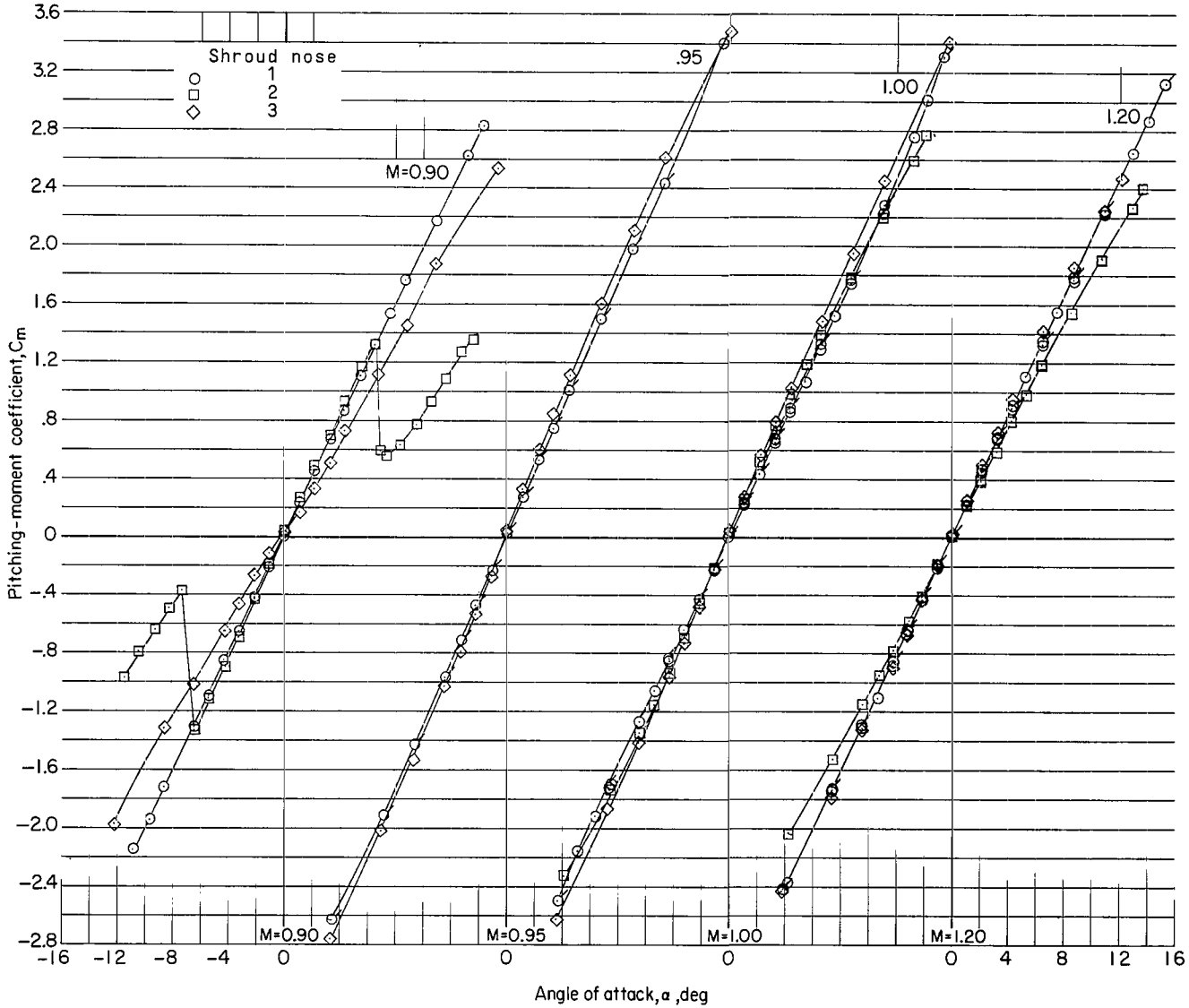

(d) C_m against α. Concluded.

Figure 6.- Continued.

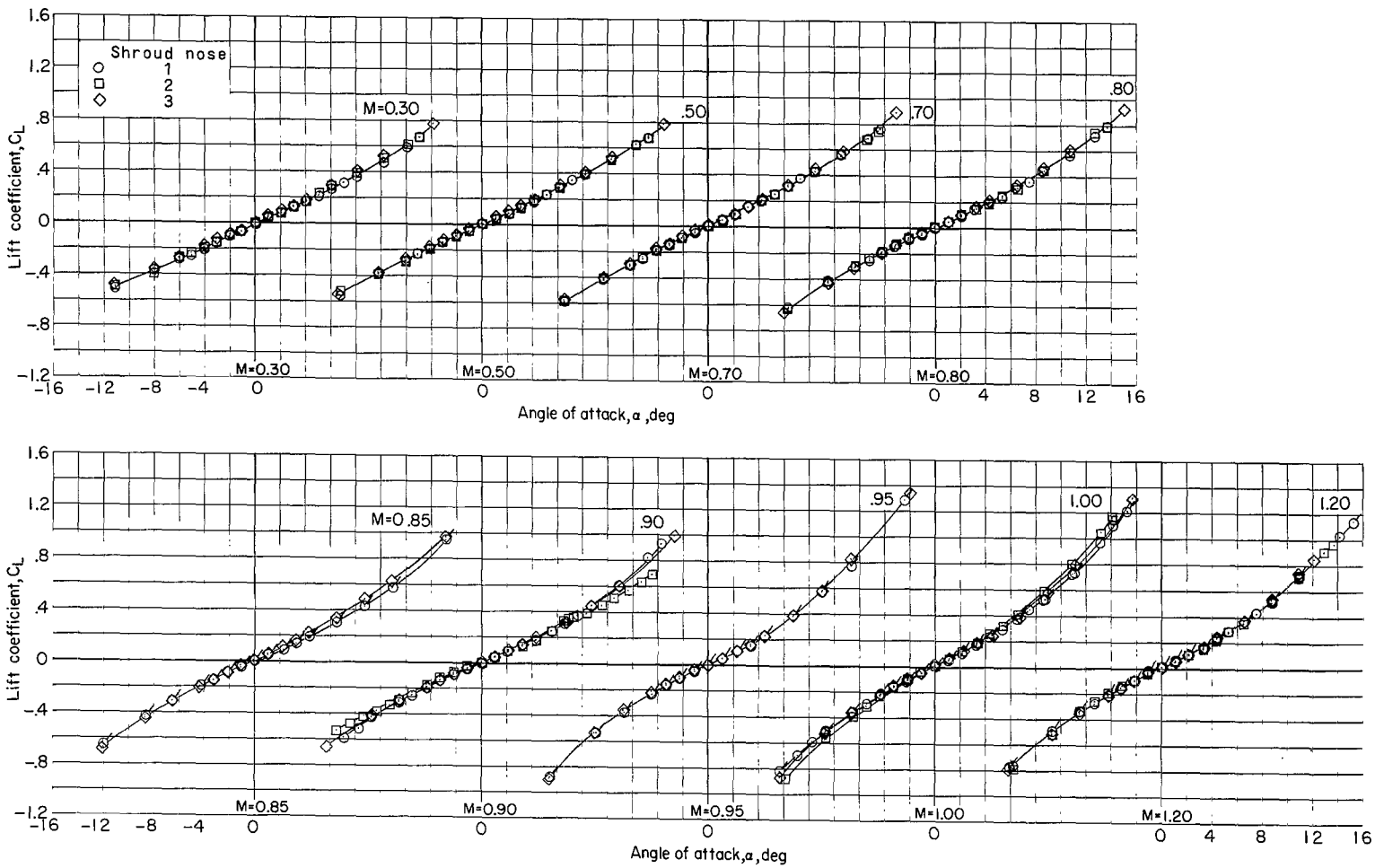

(e) C_L against α.

Figure 6.- Continued.

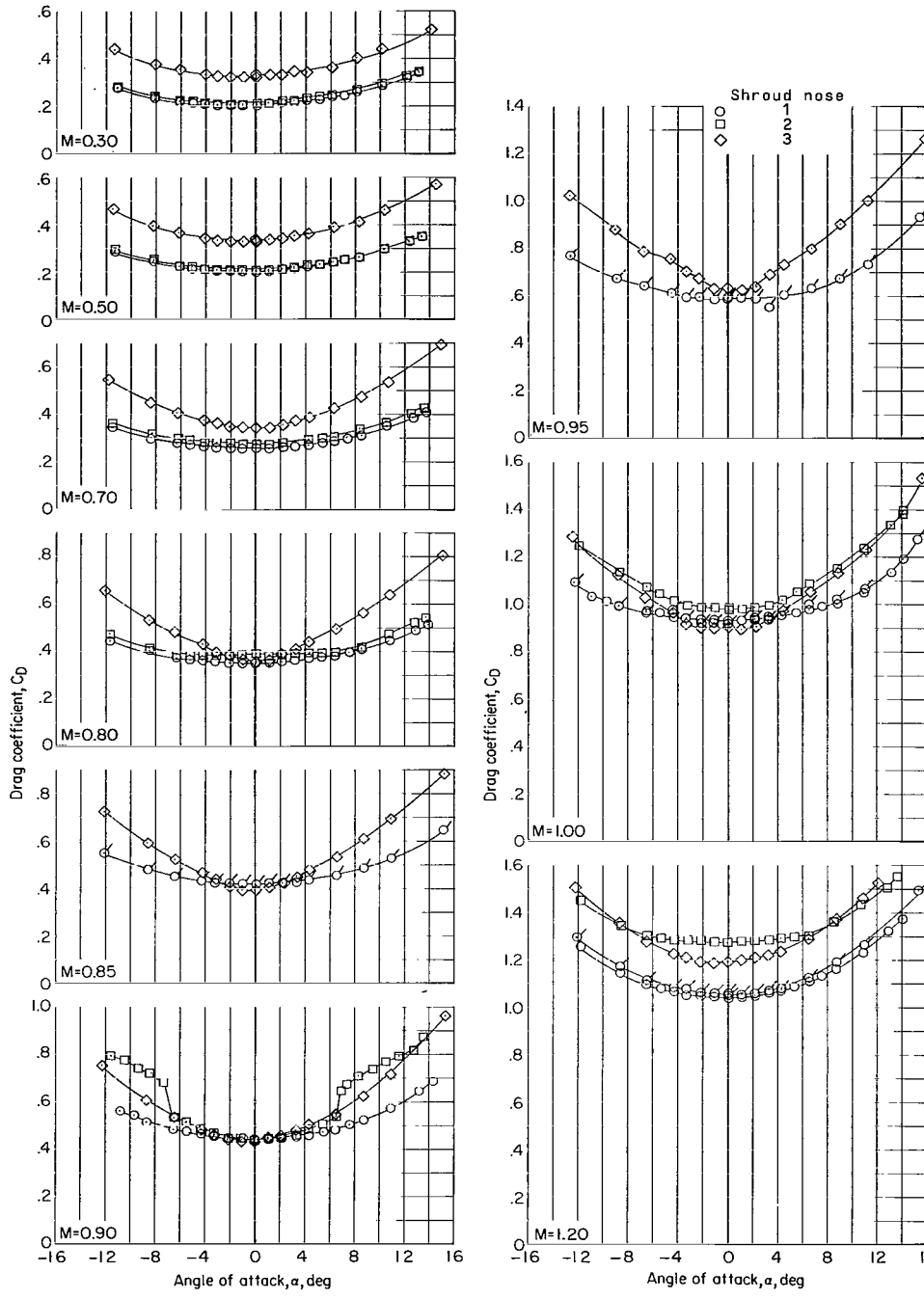

(f) C_D against α.

Figure 6.- Continued.

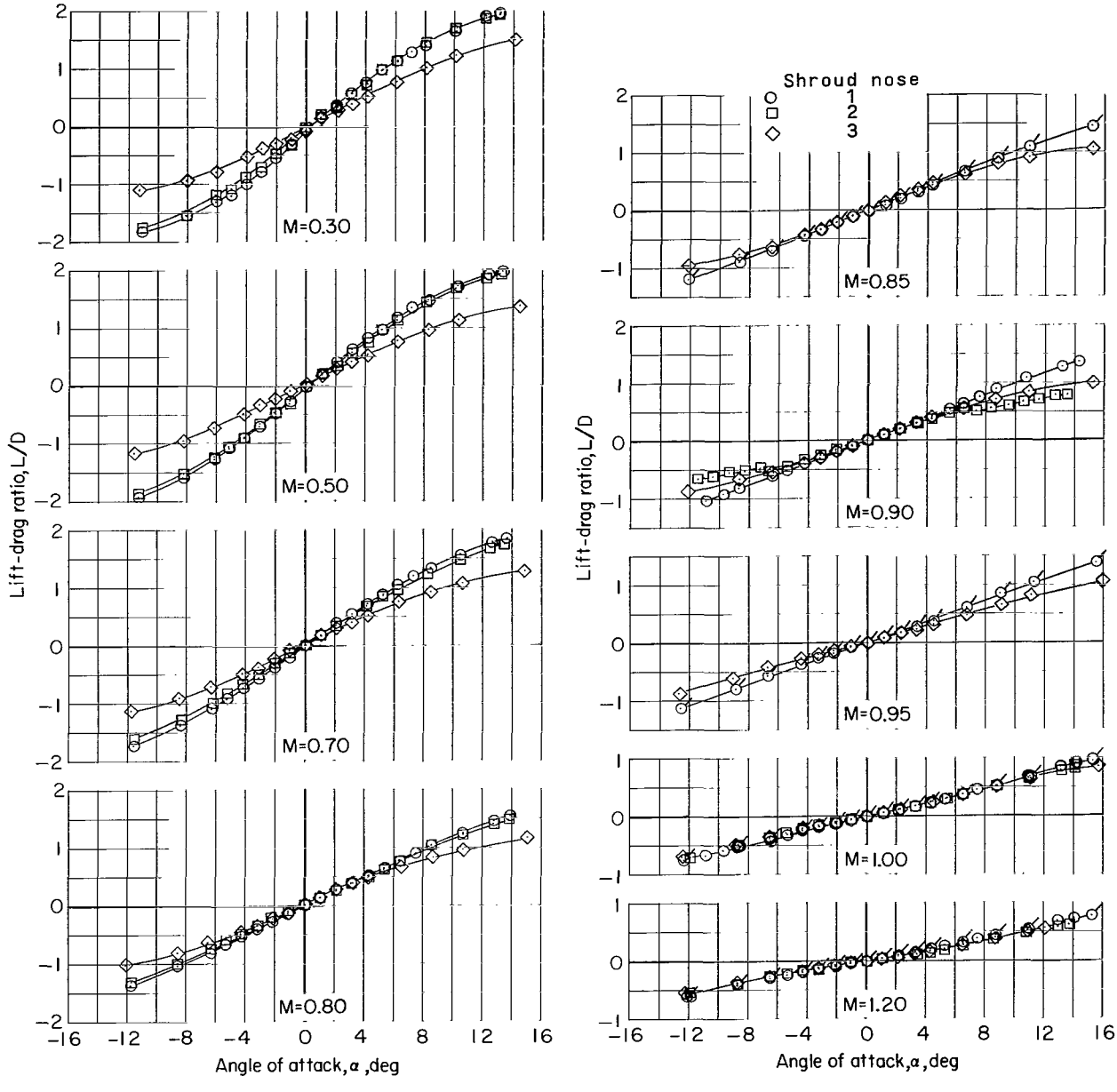

(g) L/D against α.

Figure 6.- Continued.

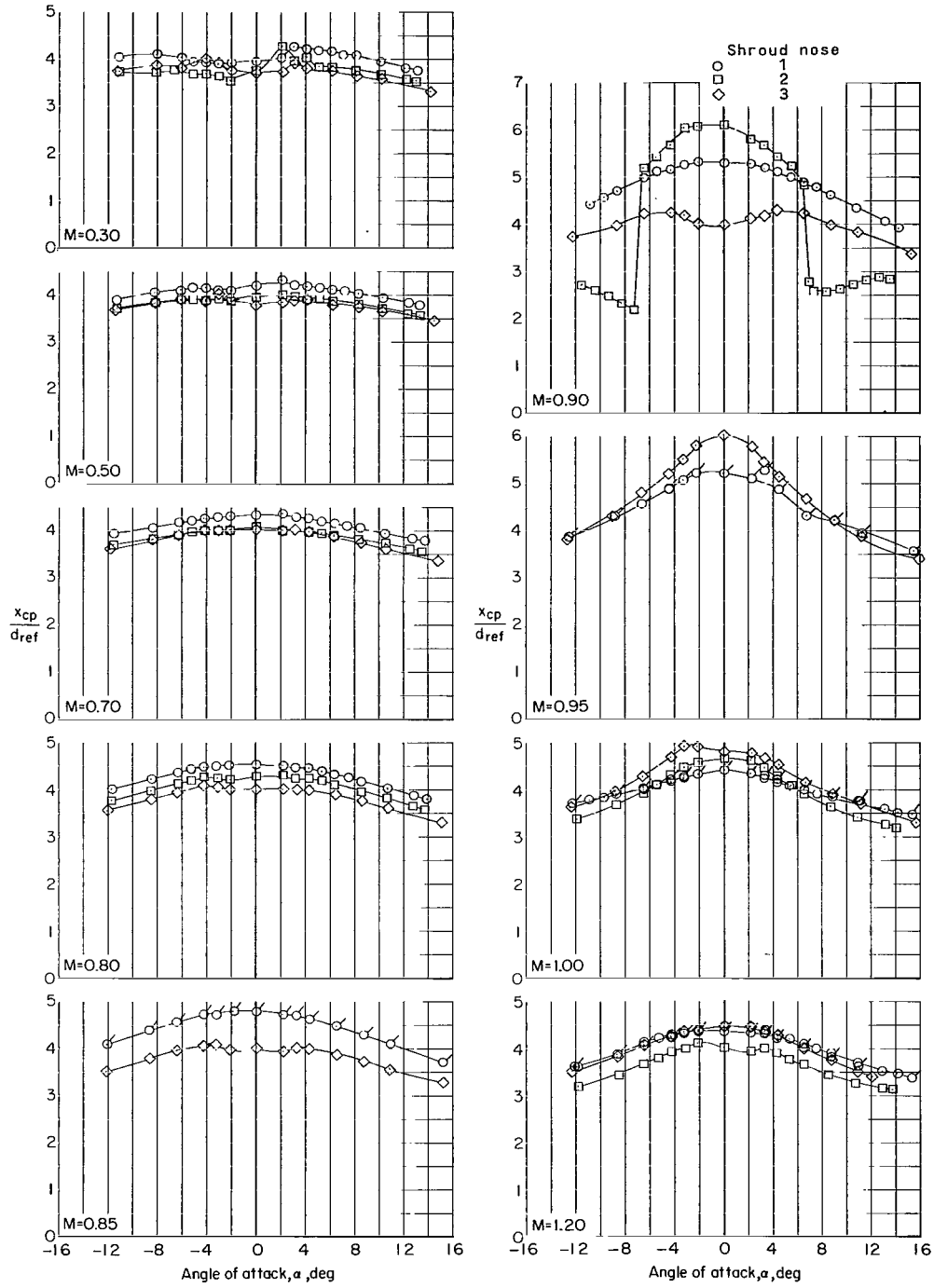

(h) x_{cp}/d_{ref} against α.

Figure 6.- Concluded.

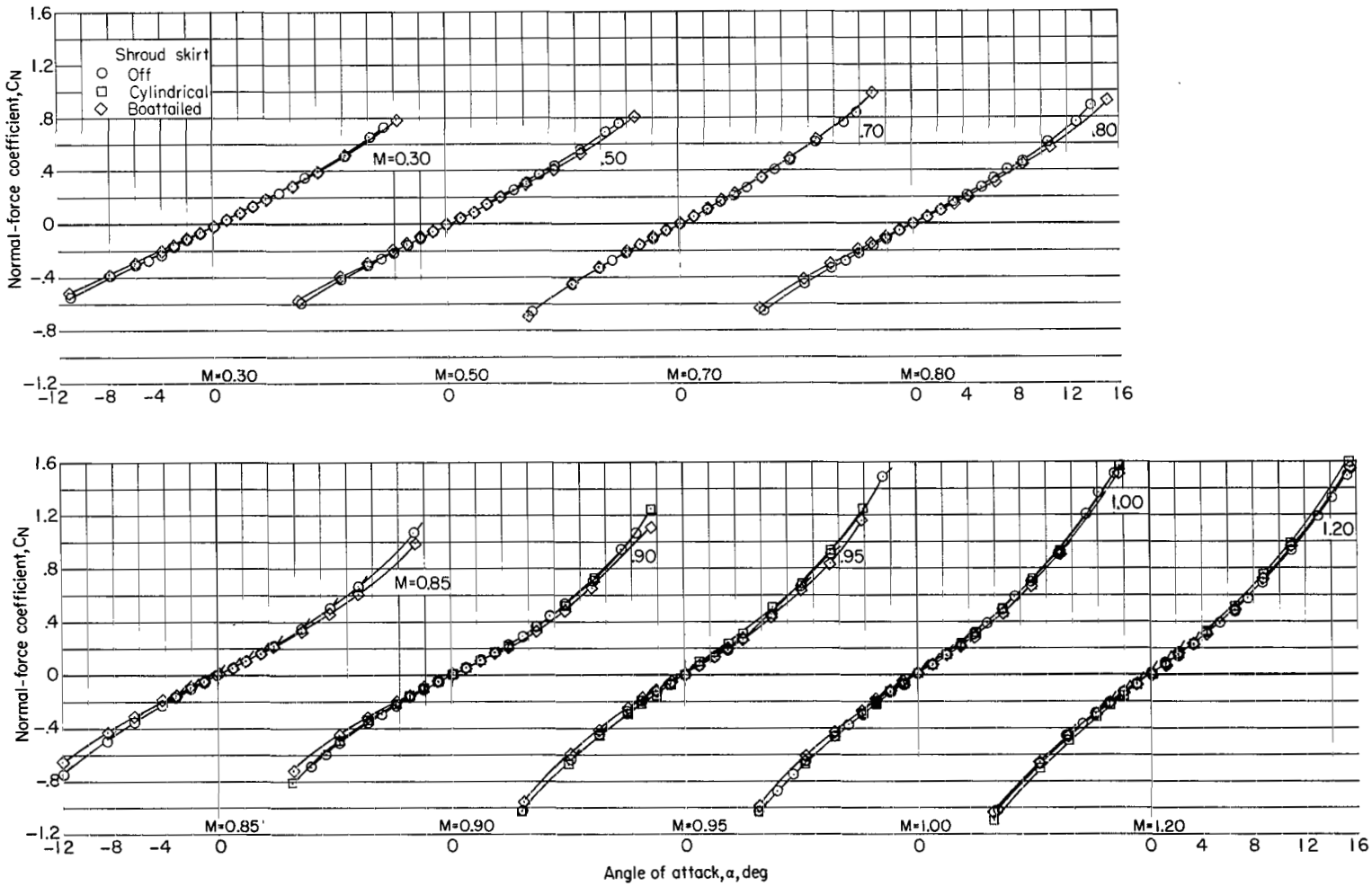

(a) C_N against α.

Figure 7.- Effect of cylindrical and boattailed shroud skirts on longitudinal aerodynamic characteristics. Shroud nose 1; fins off. (Flagged symbols indicate points from repeat run.)

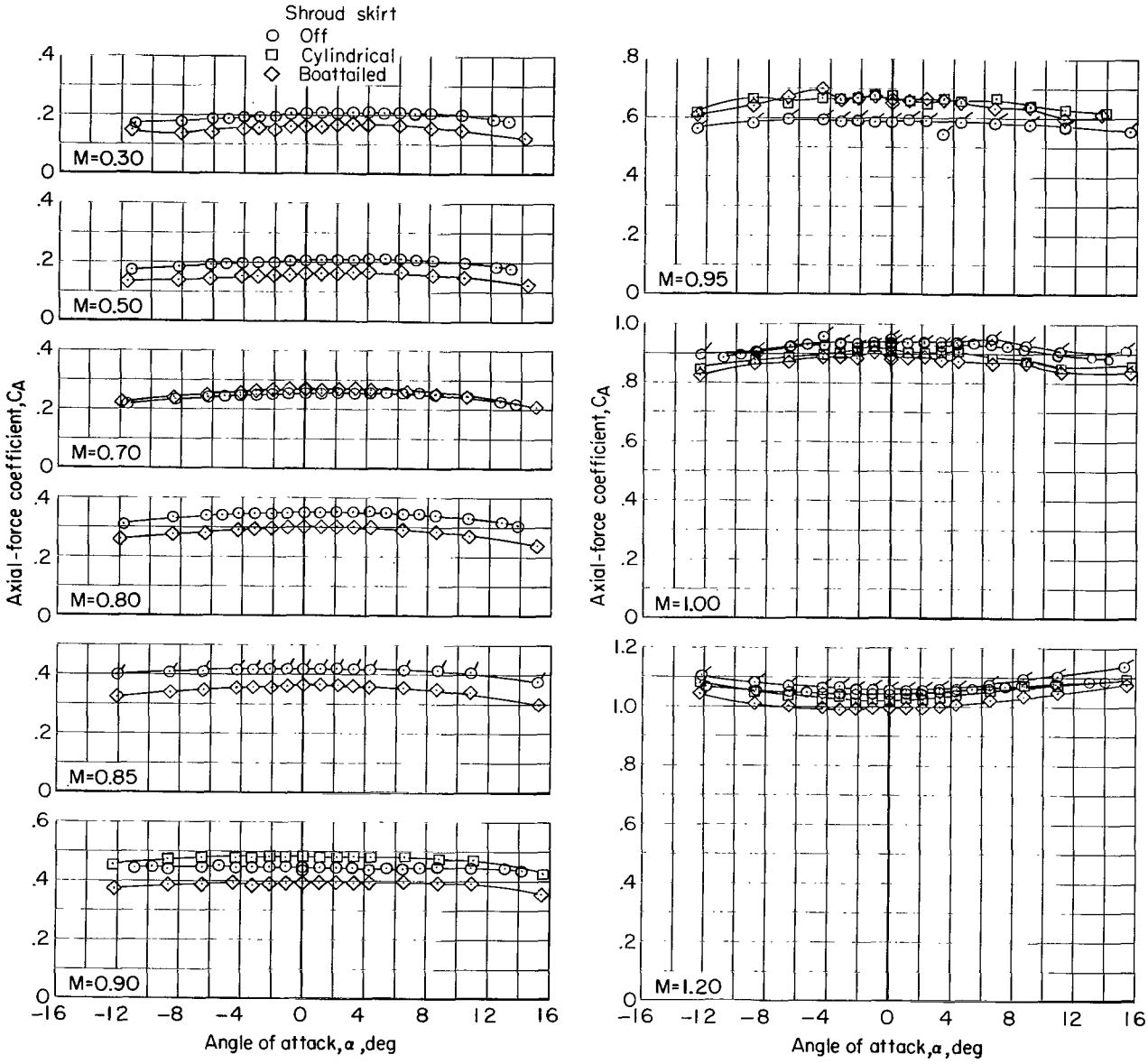

(b) C_A against α.

Figure 7.- Continued.

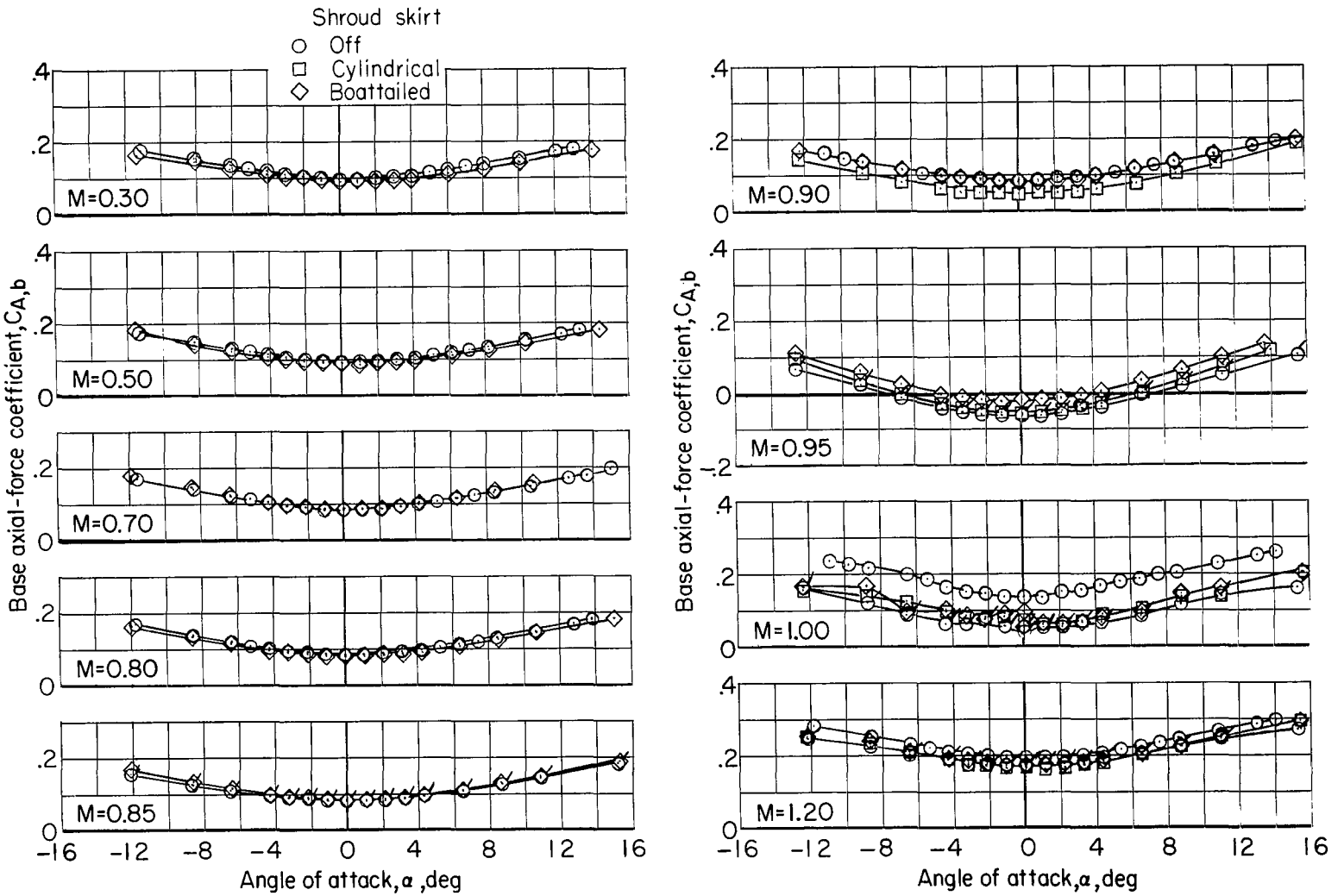

(c) $C_{A,b}$ against α.

Figure 7.- Continued.

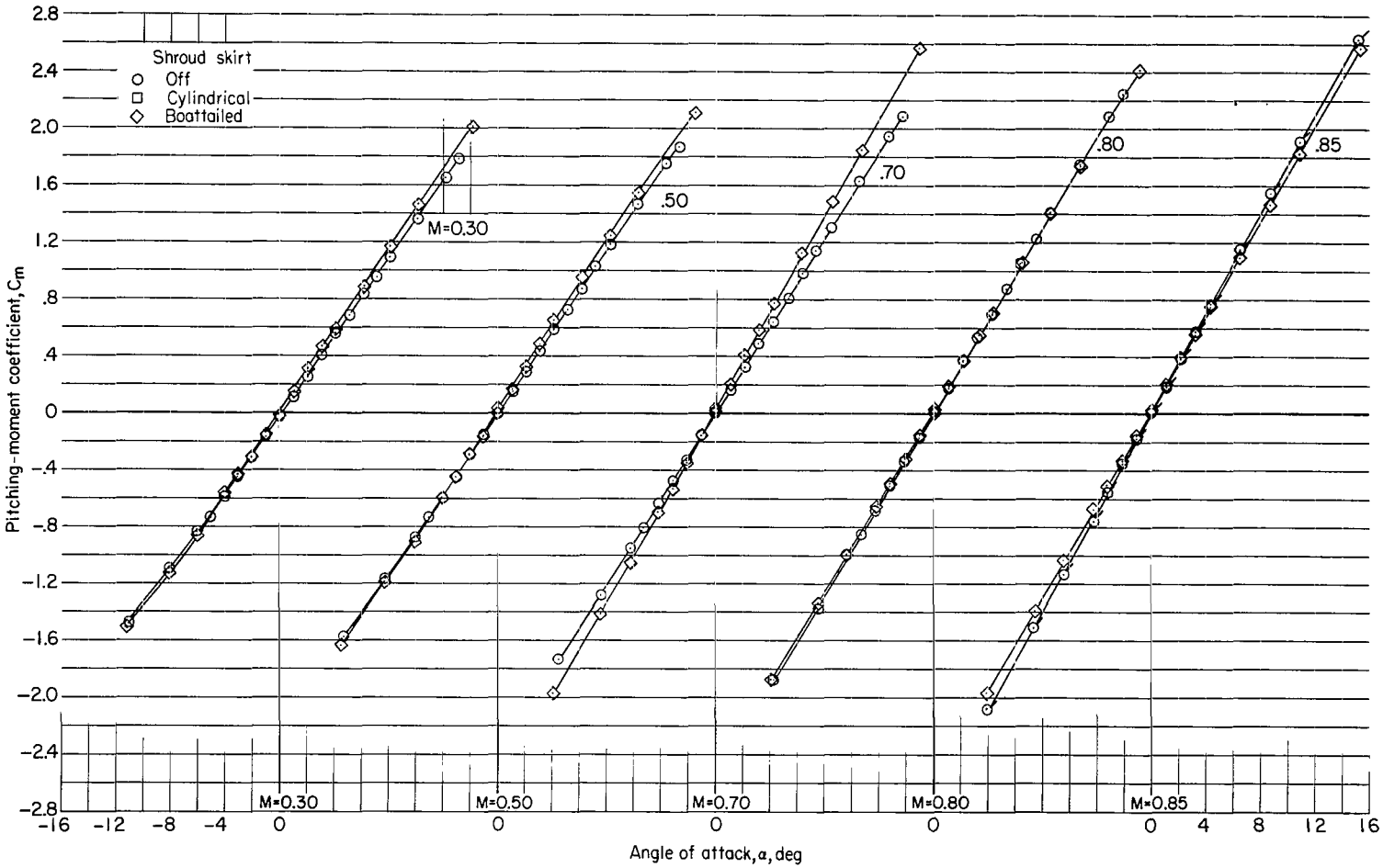

(d) C_m against α.

Figure 7.- Continued.

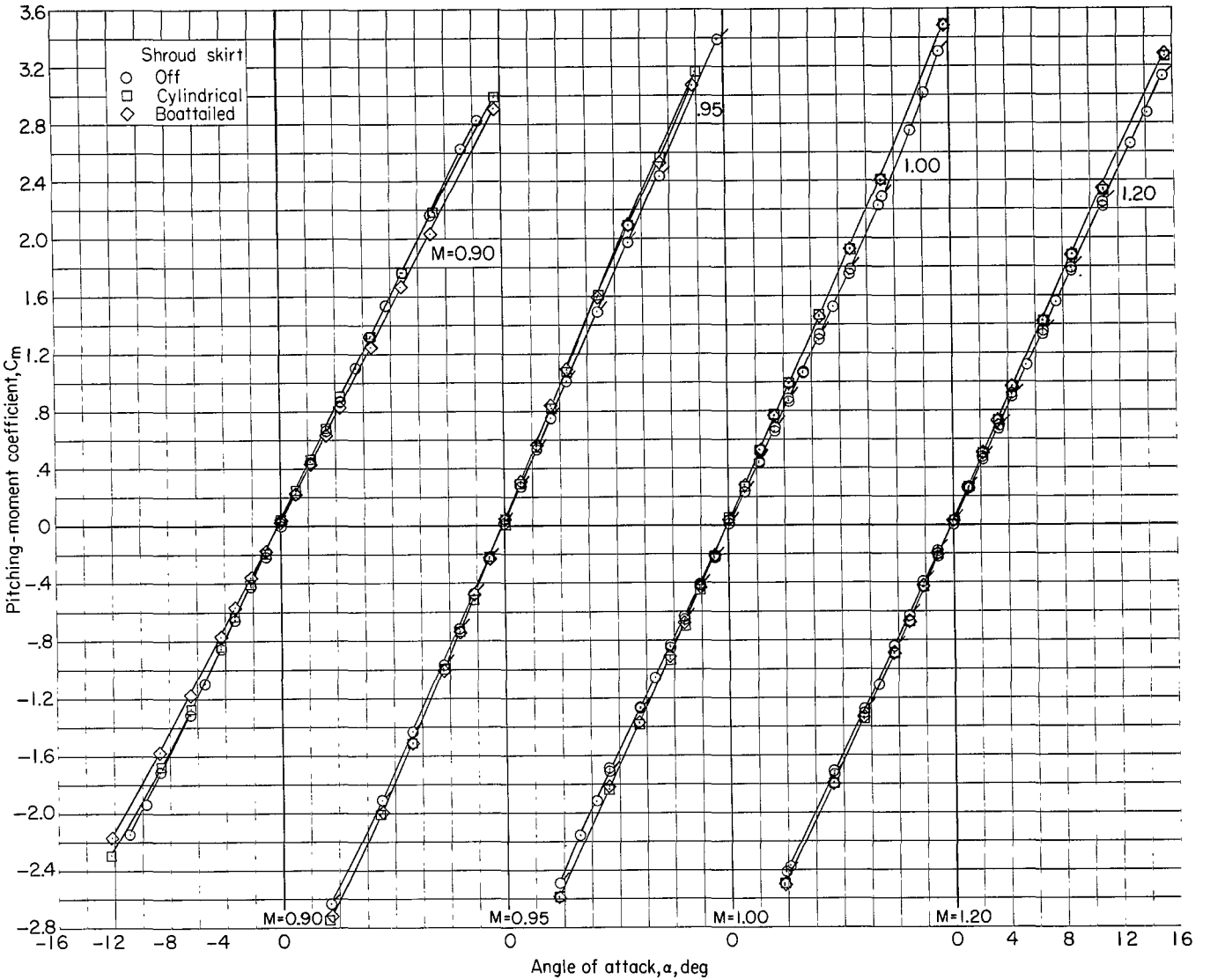

(d) C_m against α. Concluded.

Figure 7.- Continued.

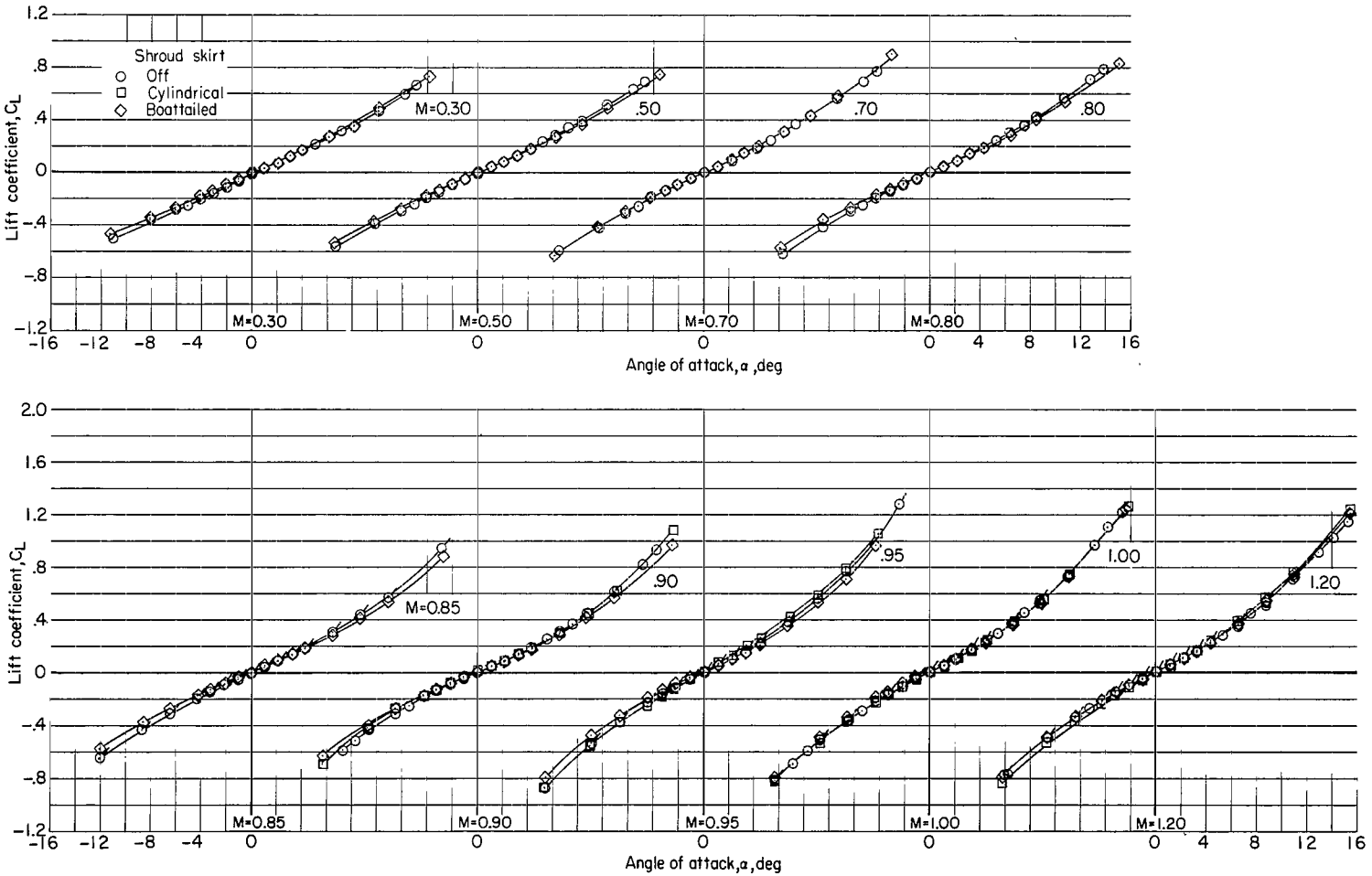

(e) C_L against α.

Figure 7.- Continued.

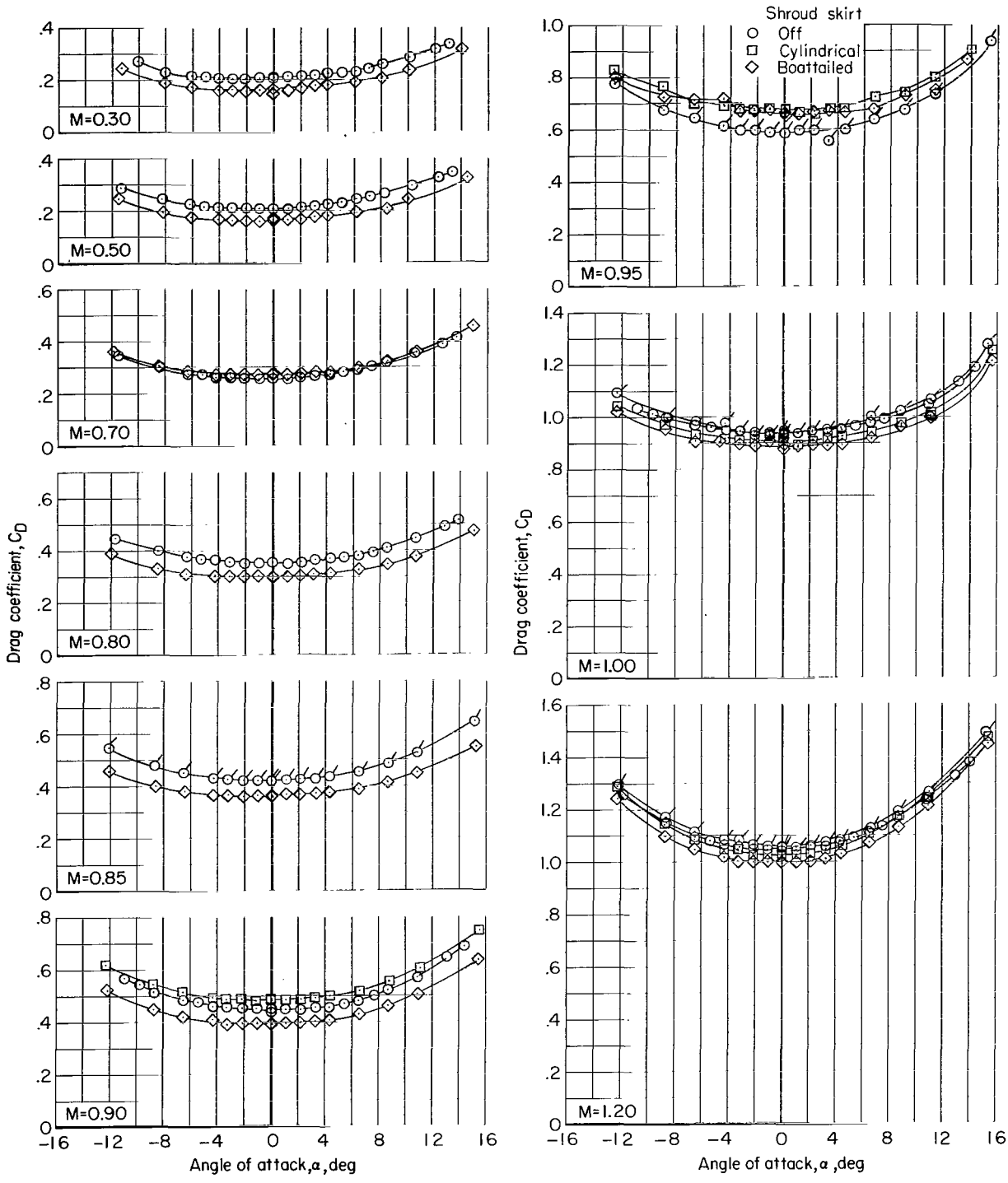

(f) C_D against α.

Figure 7.- Continued.

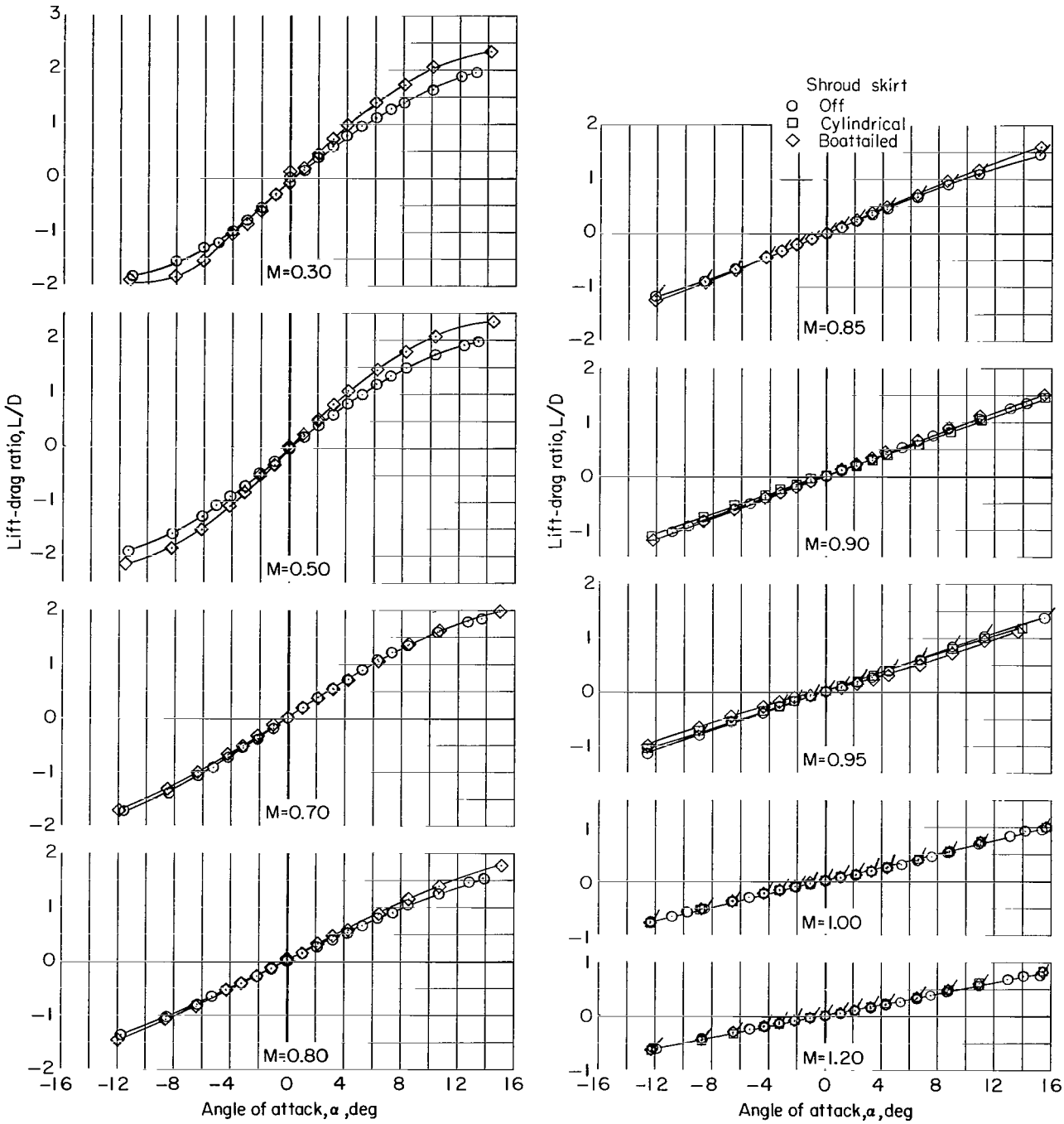

(g) L/D against α.

Figure 7.- Continued.

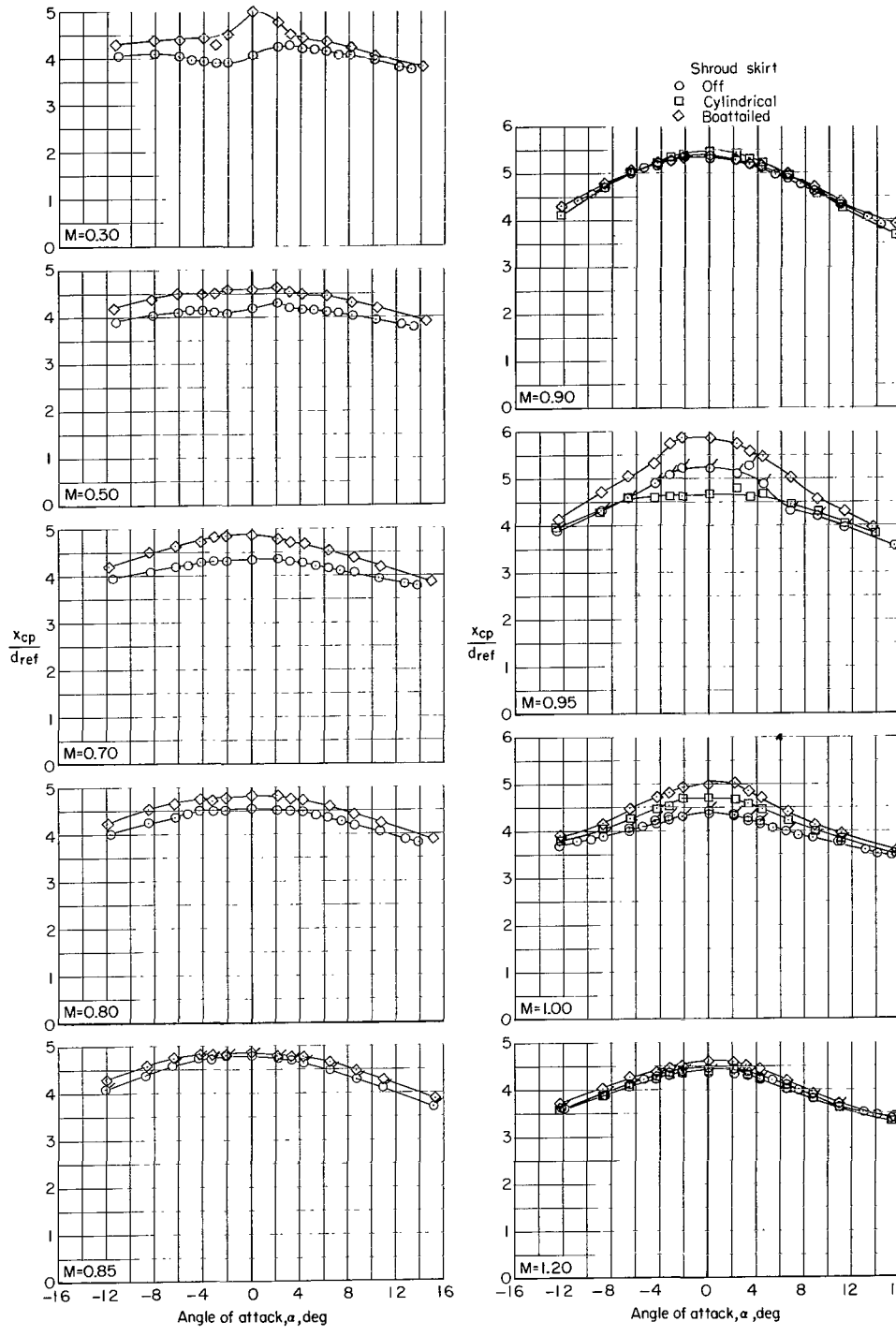

(h) x_{cp}/d_{ref} against α.

Figure 7.- Concluded.

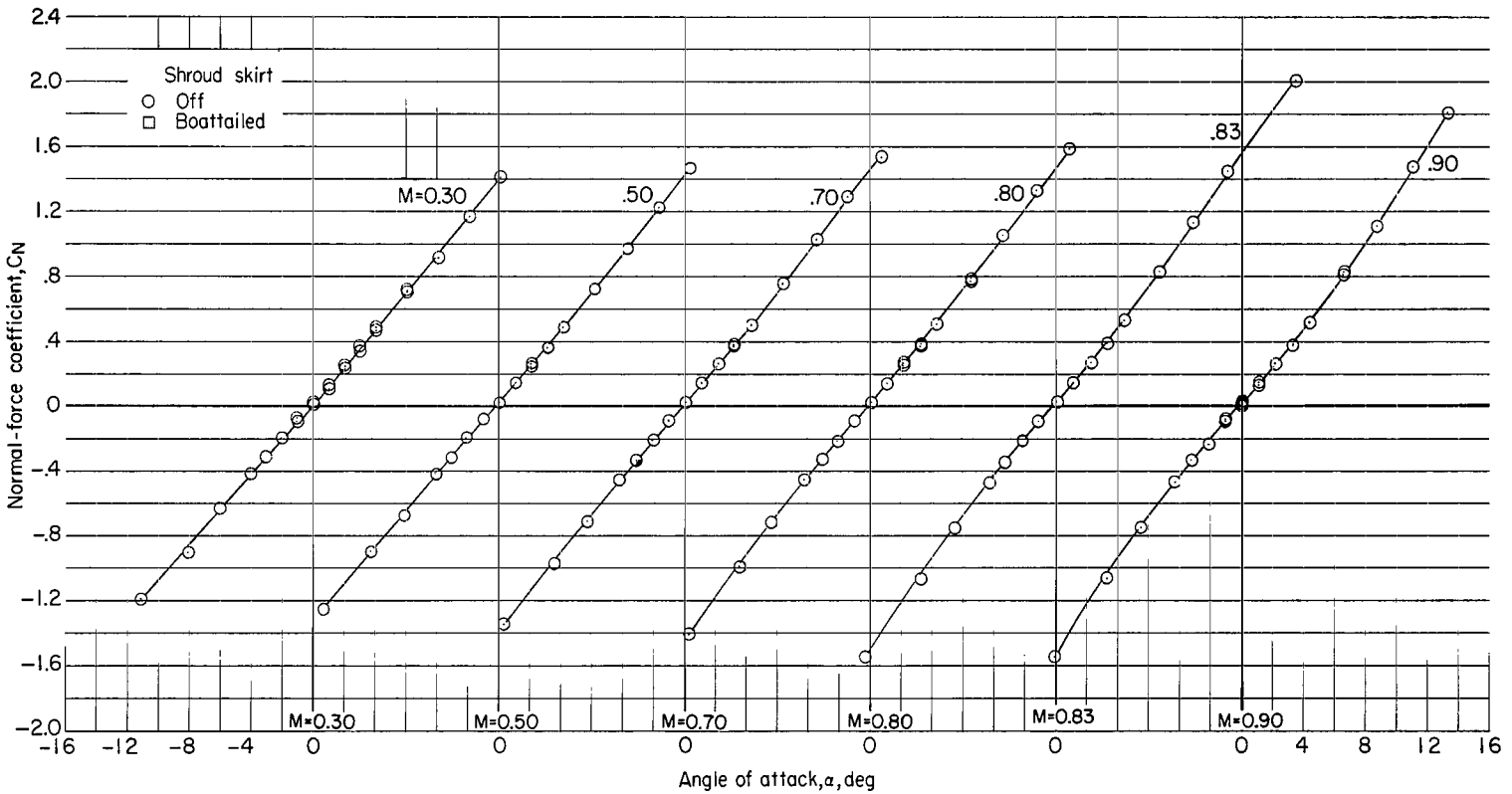

(a) C_N against α.

Figure 8.- Effect of boattailed shroud skirt on longitudinal aerodynamic characteristics. Shroud nose 1; small fins; $\delta = 0^0$.

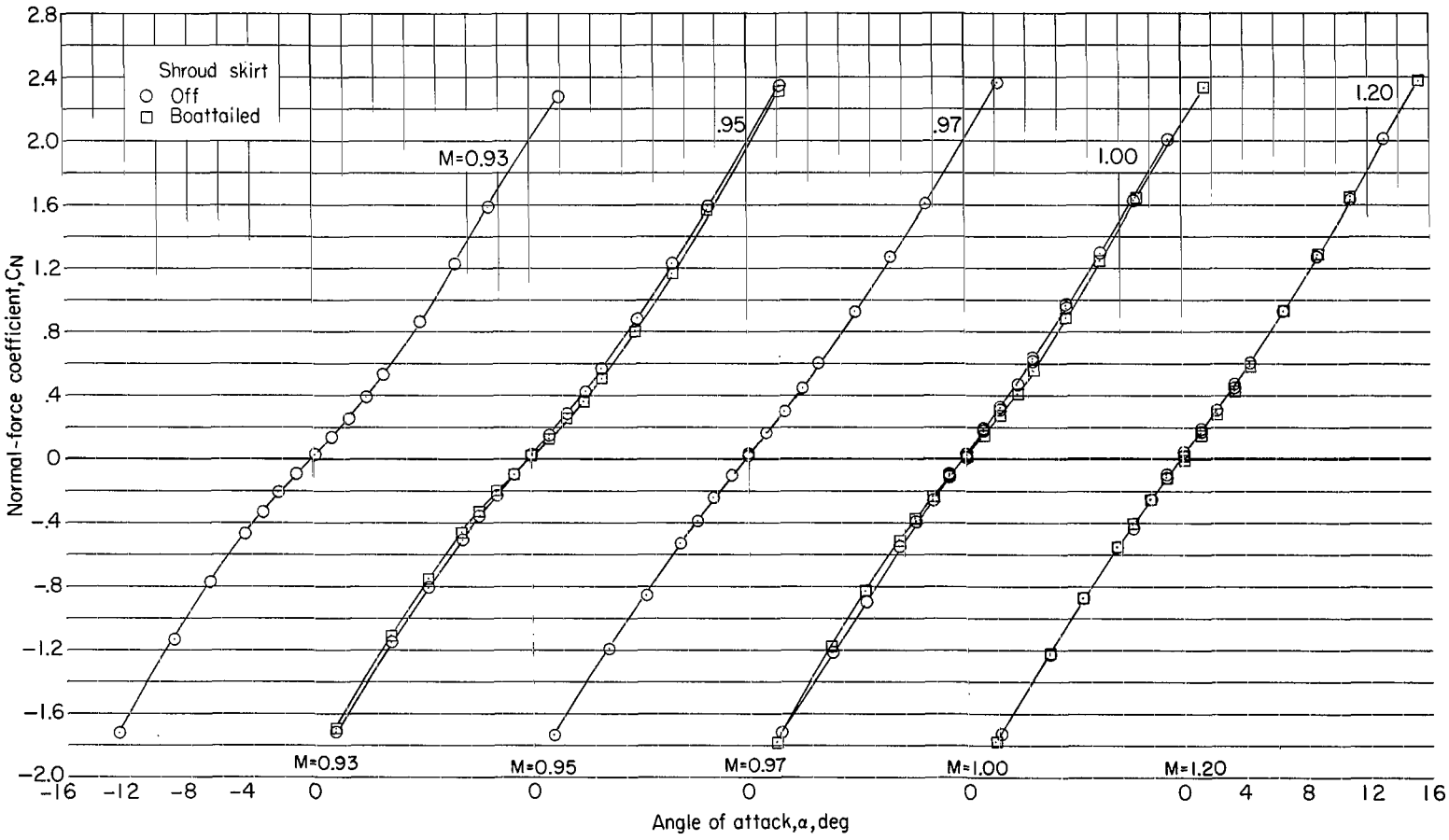

(a) C_N against α. Concluded.

Figure 8.- Continued.

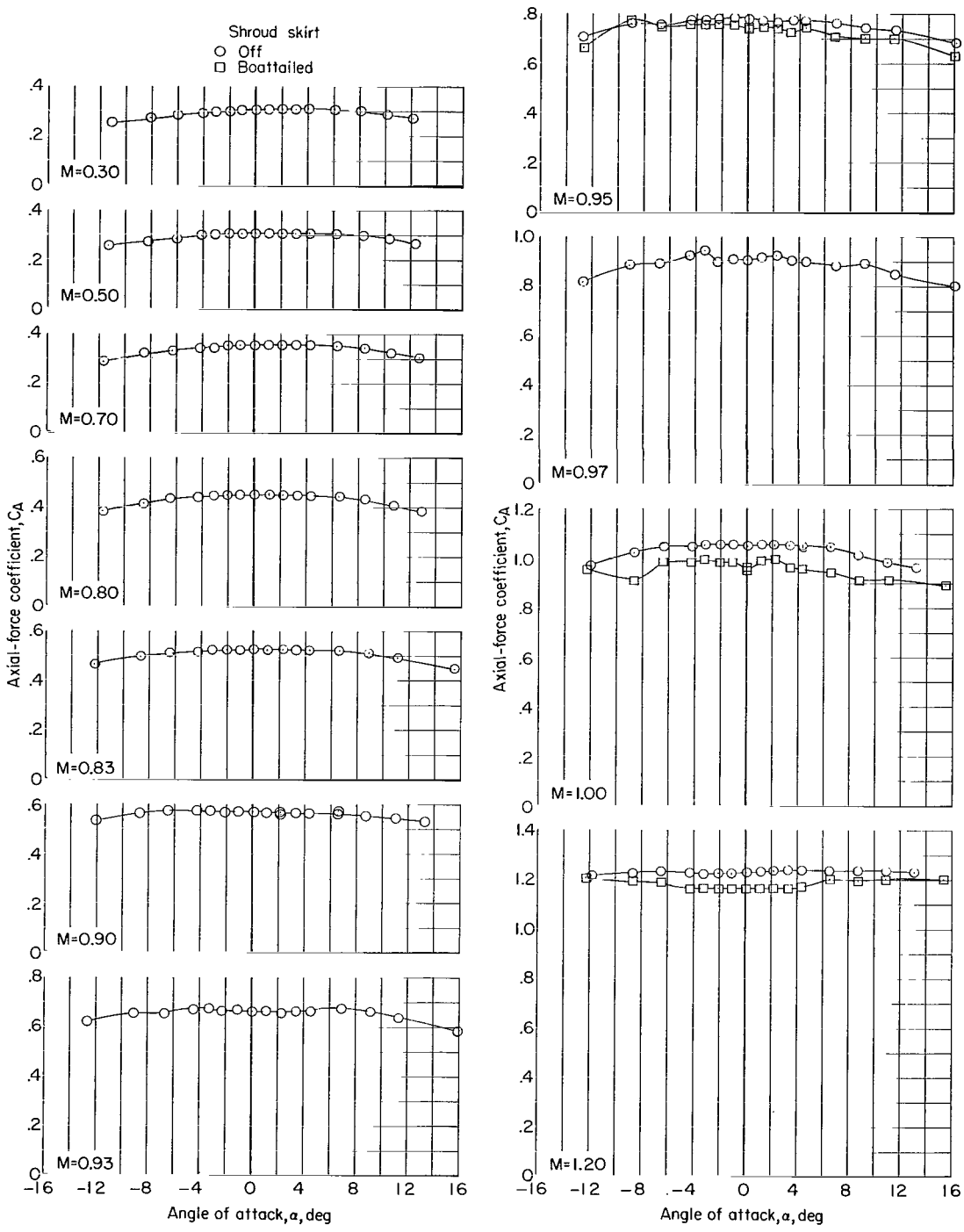

(b) C_A against α.

Figure 8.- Continued.

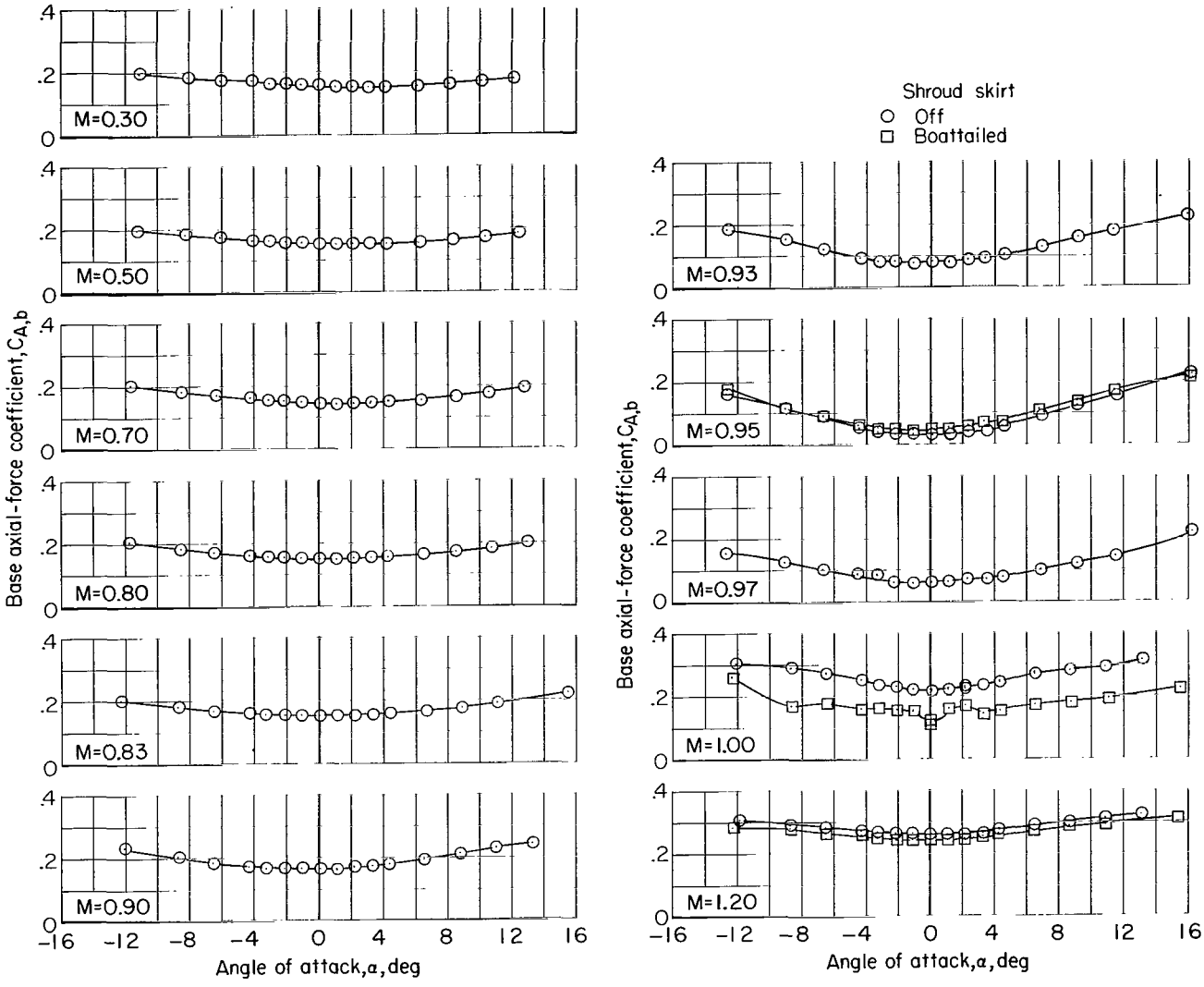

(c) $C_{A,b}$ against α.

Figure 8.- Continued.

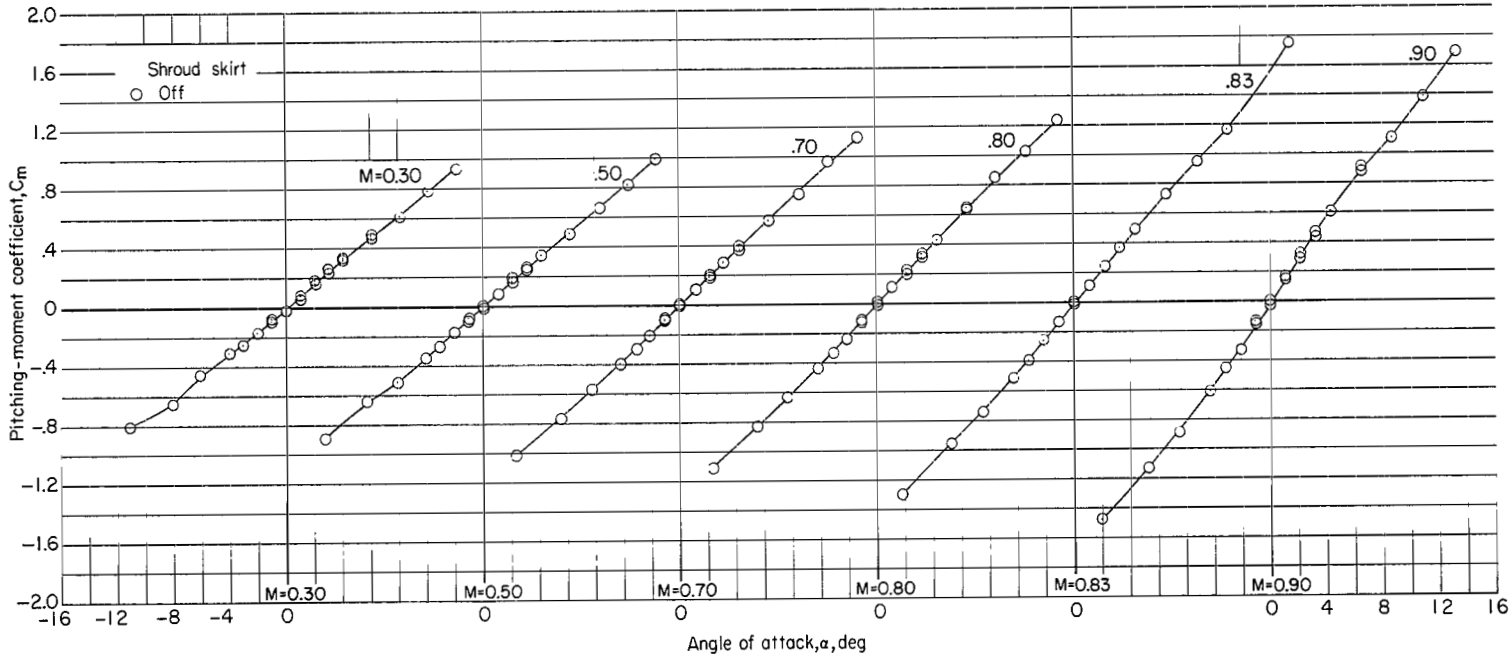

(d) C_m against α.

Figure 8.- Continued.

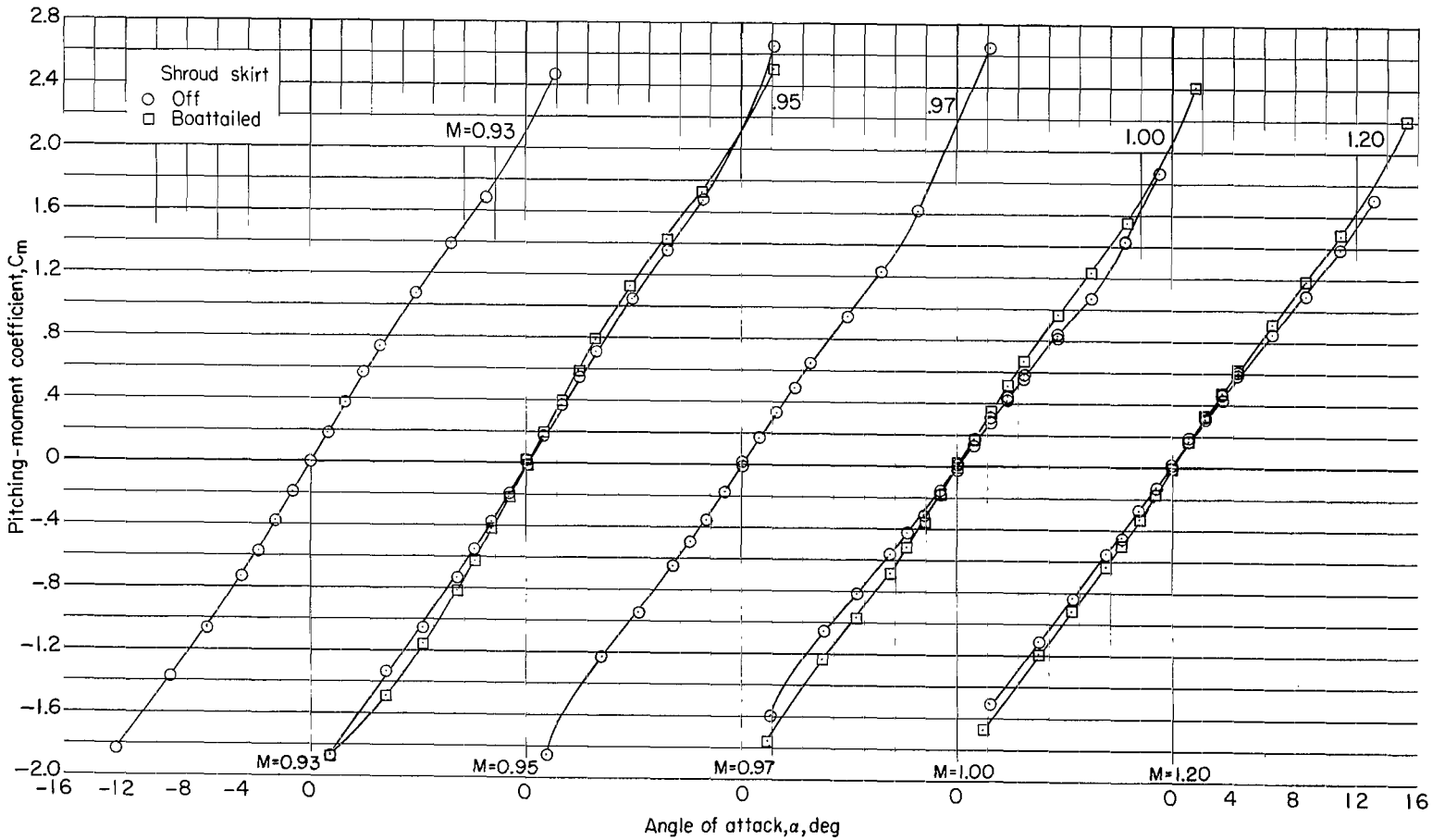

(d) C_m against α. Concluded.

Figure 8.- Continued.

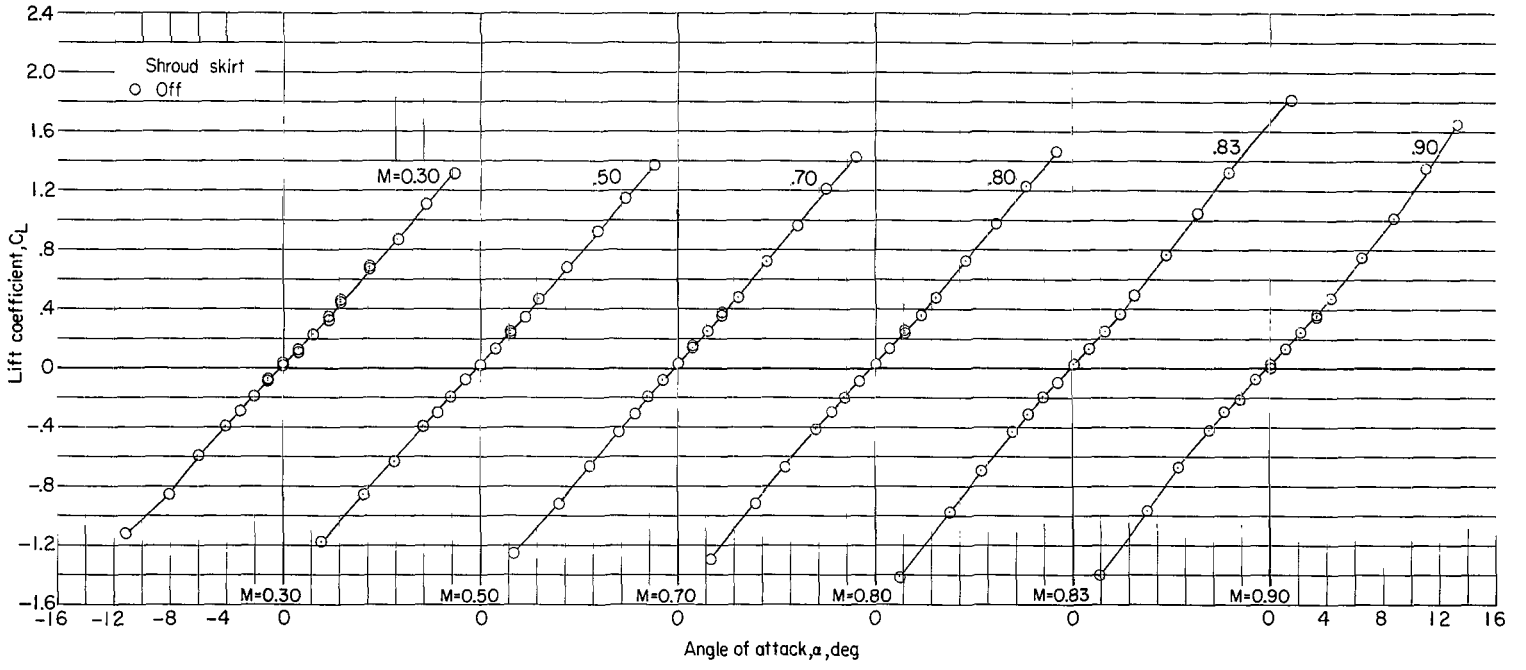

(e) C_L against α.

Figure 8.- Continued.

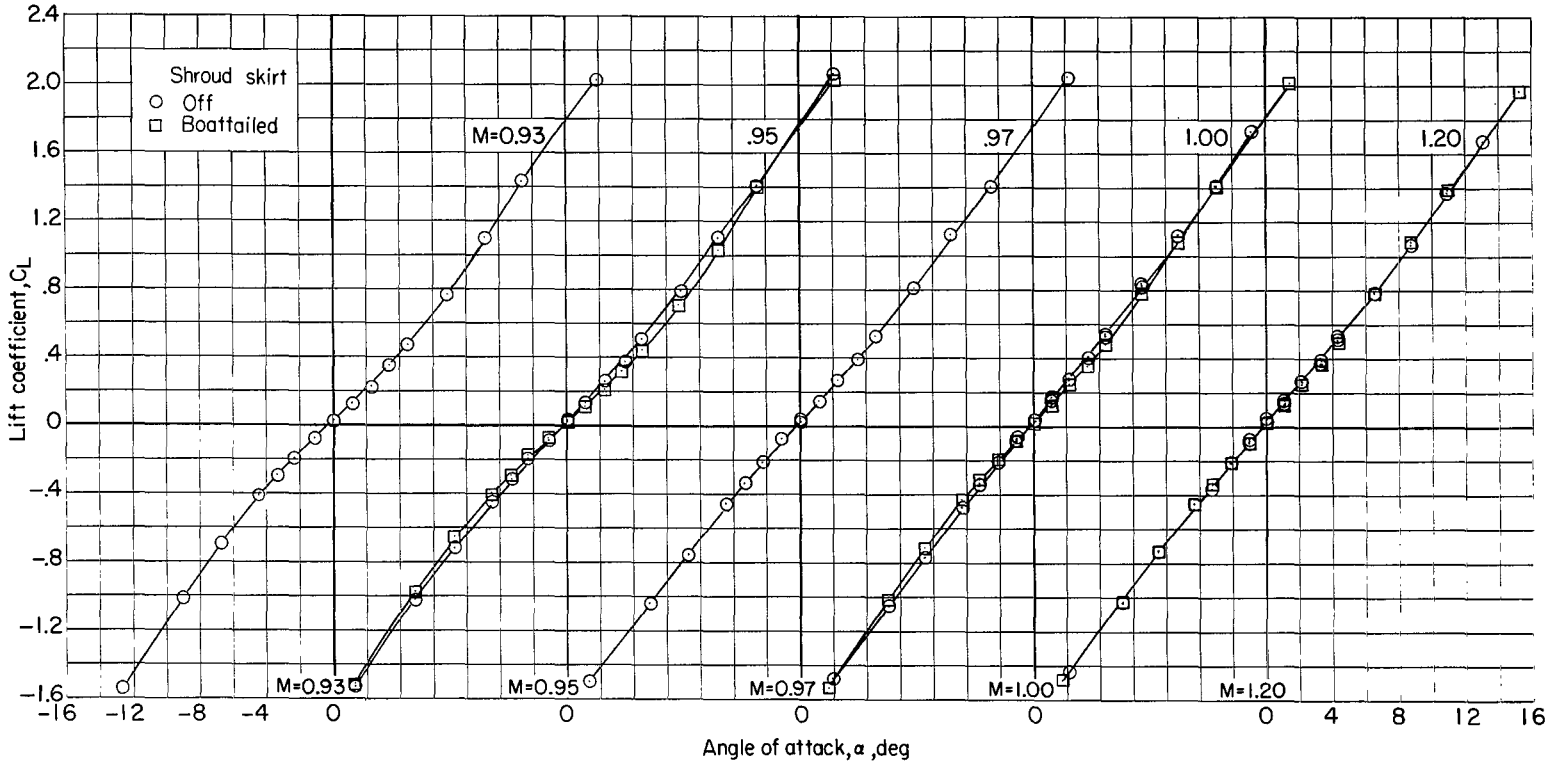

(e) C_L against α. Concluded.

Figure 8.- Continued.

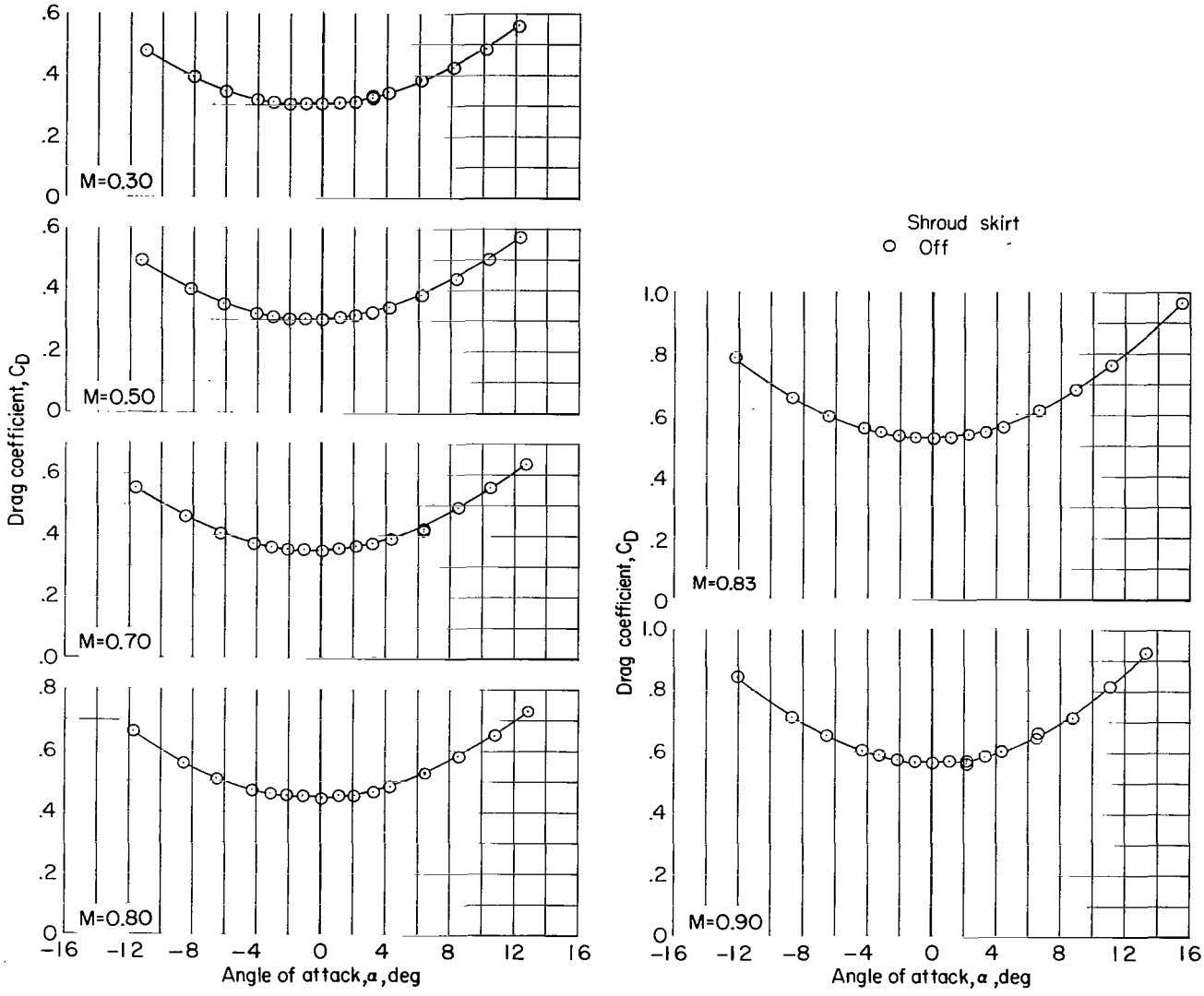

(f) C_D against α.

Figure 8.- Continued.

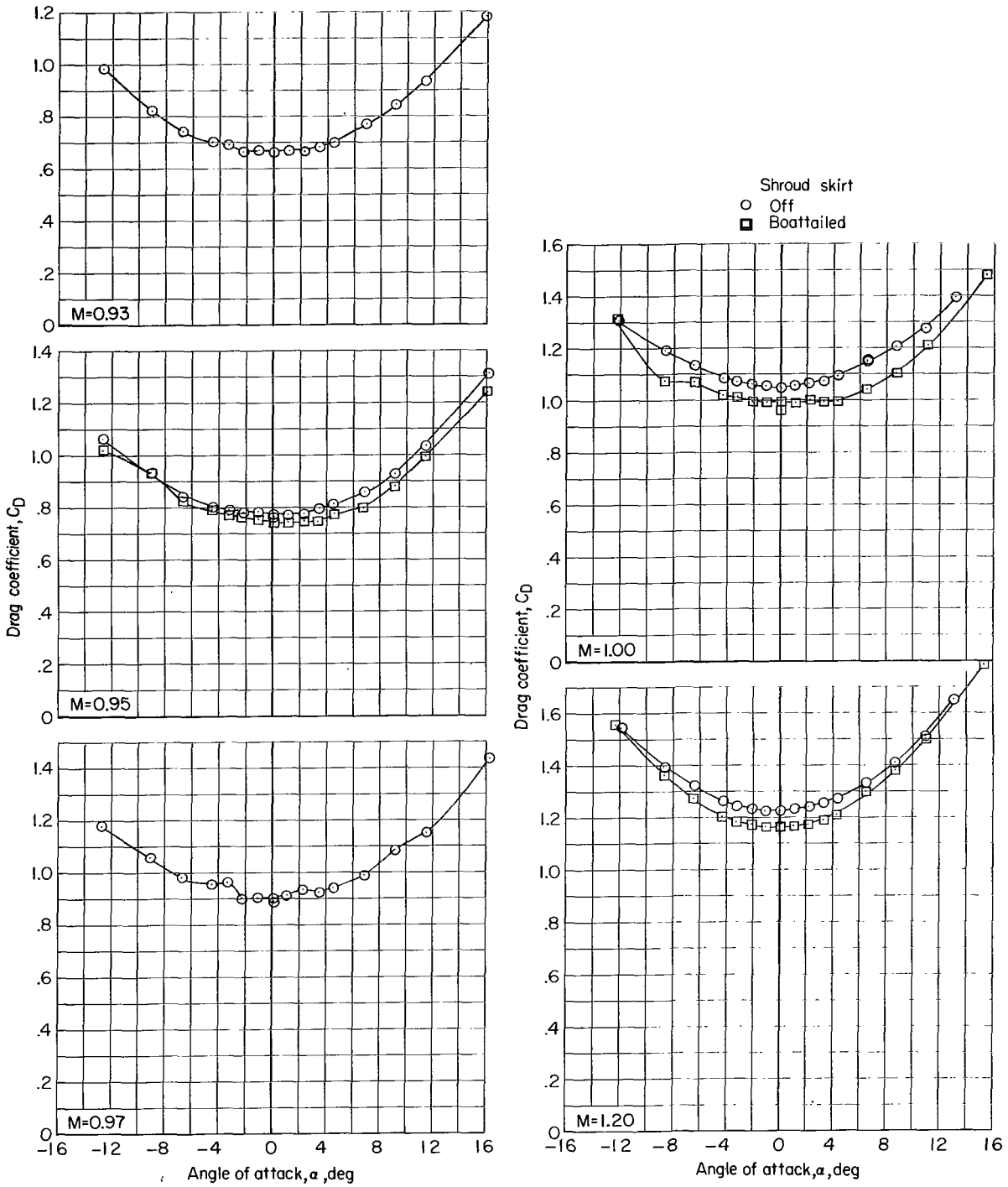

(f) C_D against α. Concluded.

Figure 8.- Continued.

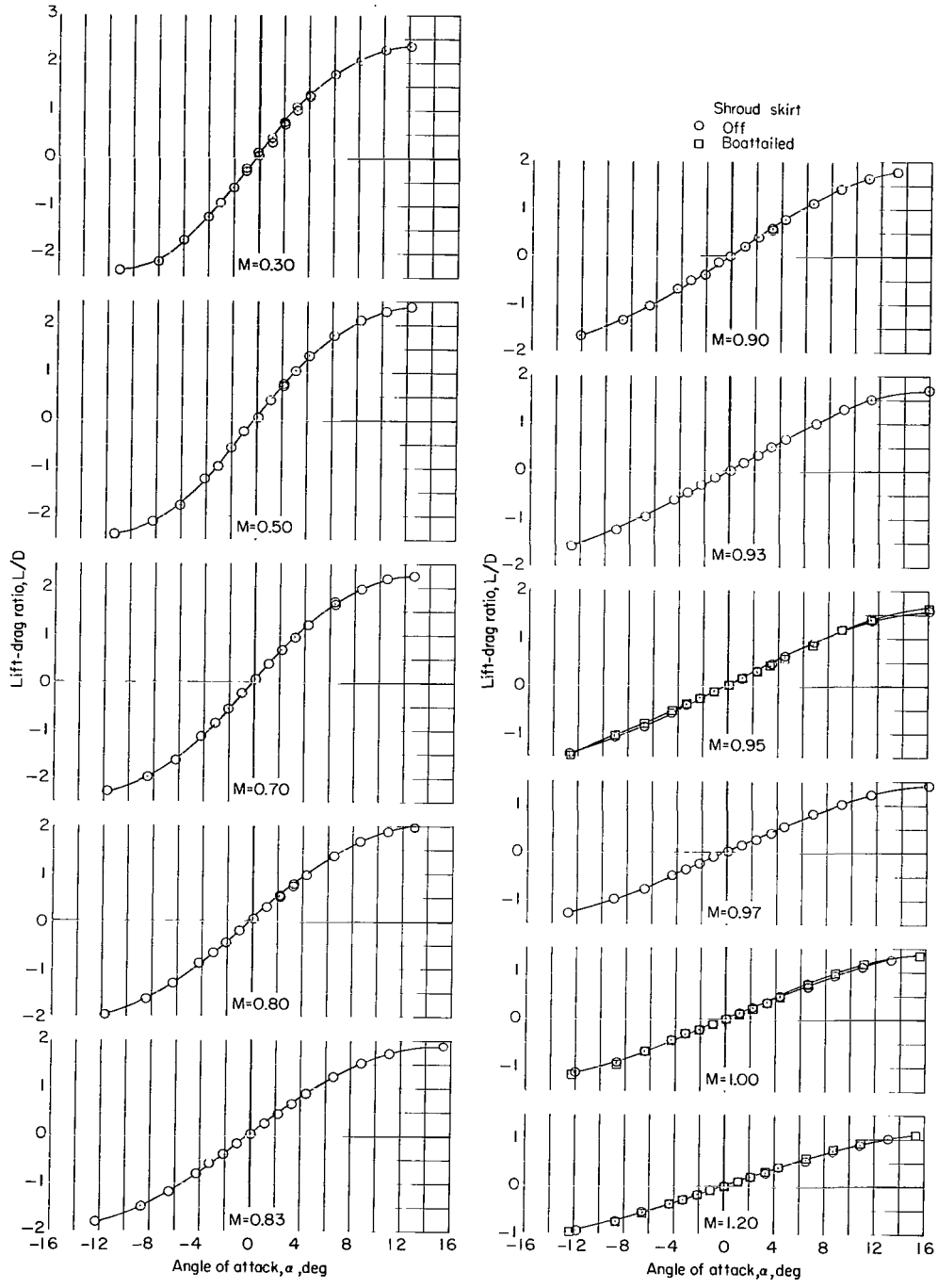

(g) L/D against α.

Figure 8.- Continued.

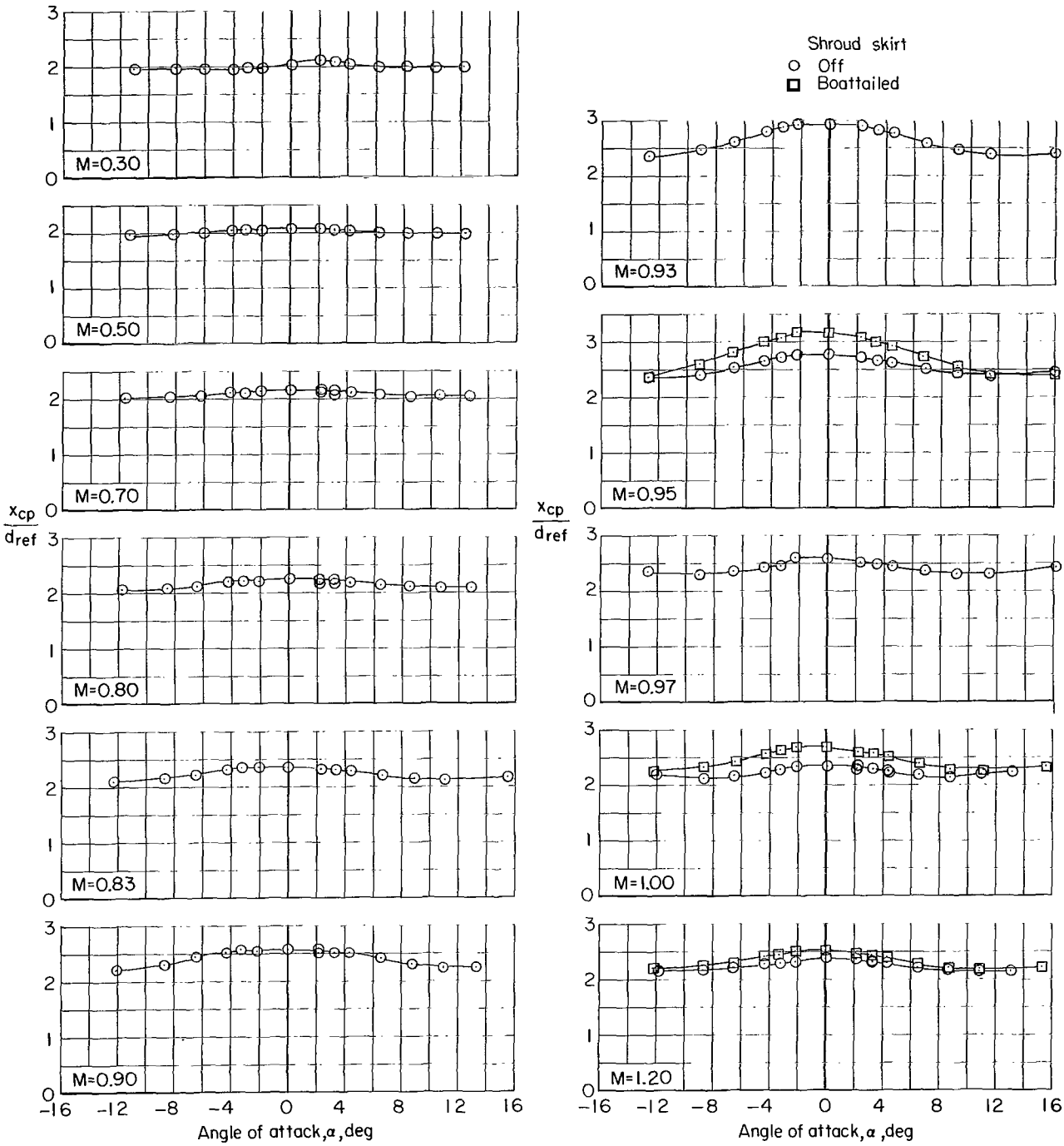

(h) x_{cp}/d_{ref} against α.

Figure 8.- Concluded.

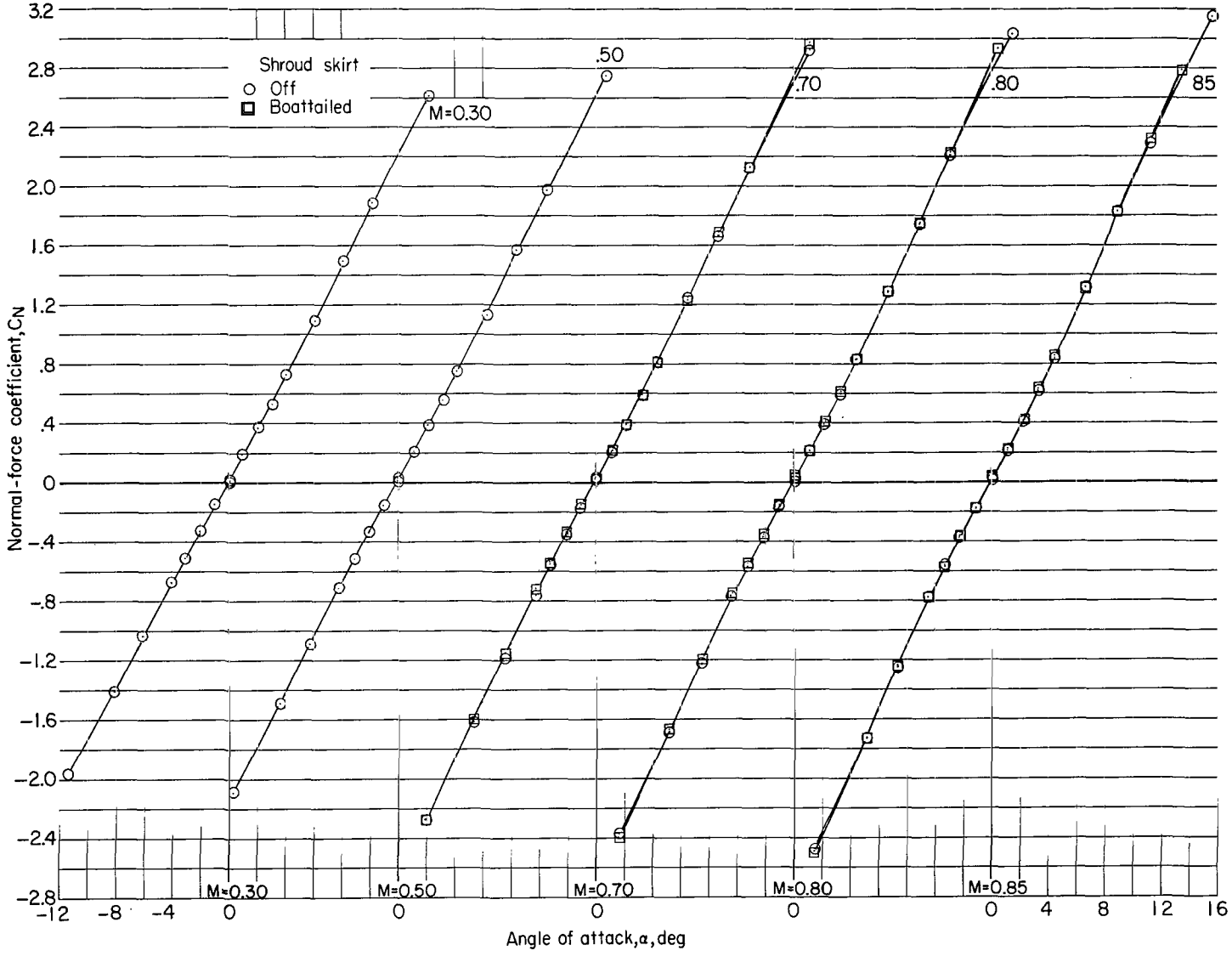

(a) C_N against α.

Figure 9.- Effect of boattailed shroud skirt on longitudinal aerodynamic characteristics. Shroud nose 1; large fins; $\delta = 0^0$.

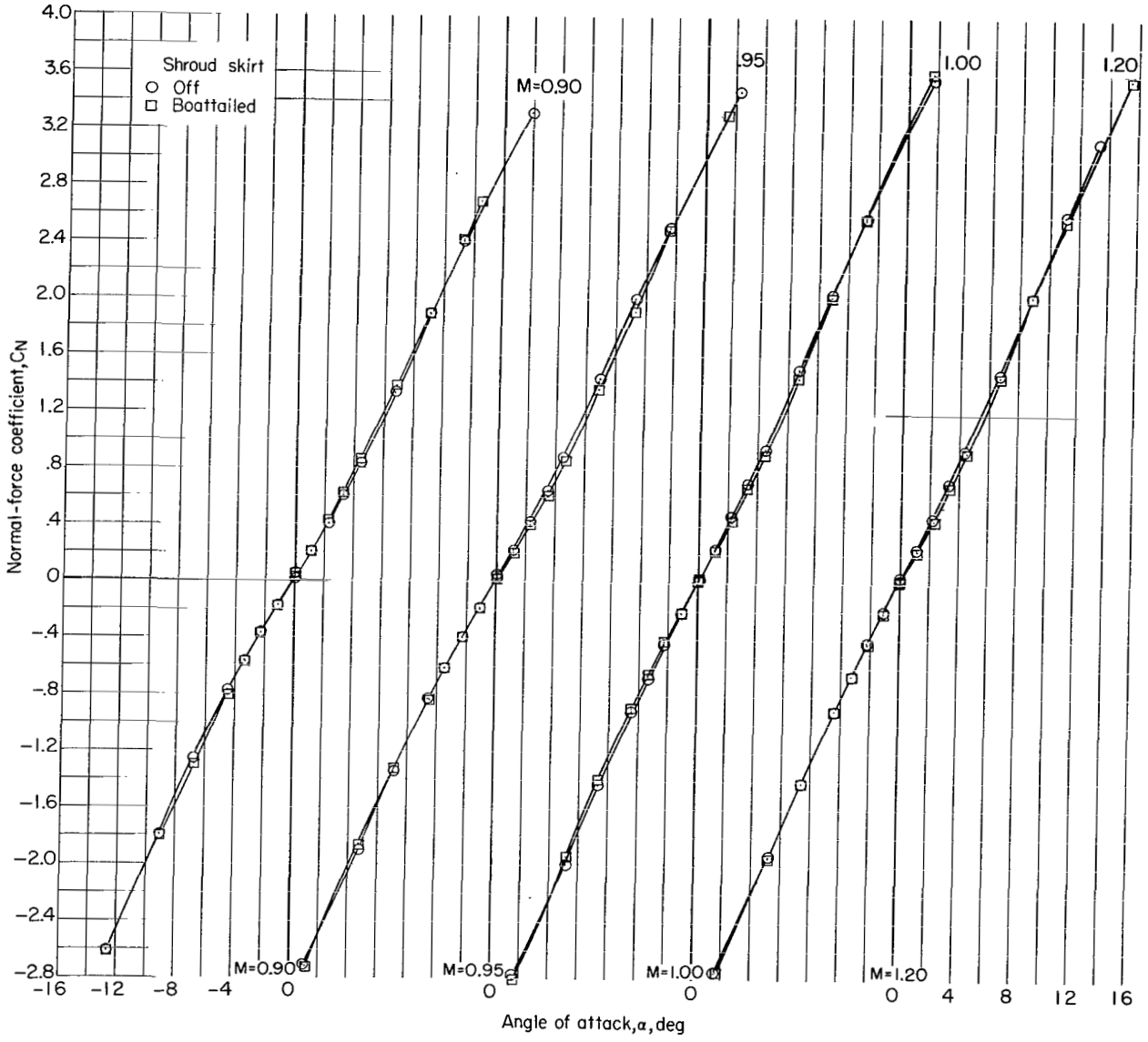

(a) C_N against α. Concluded.

Figure 9.- Continued.

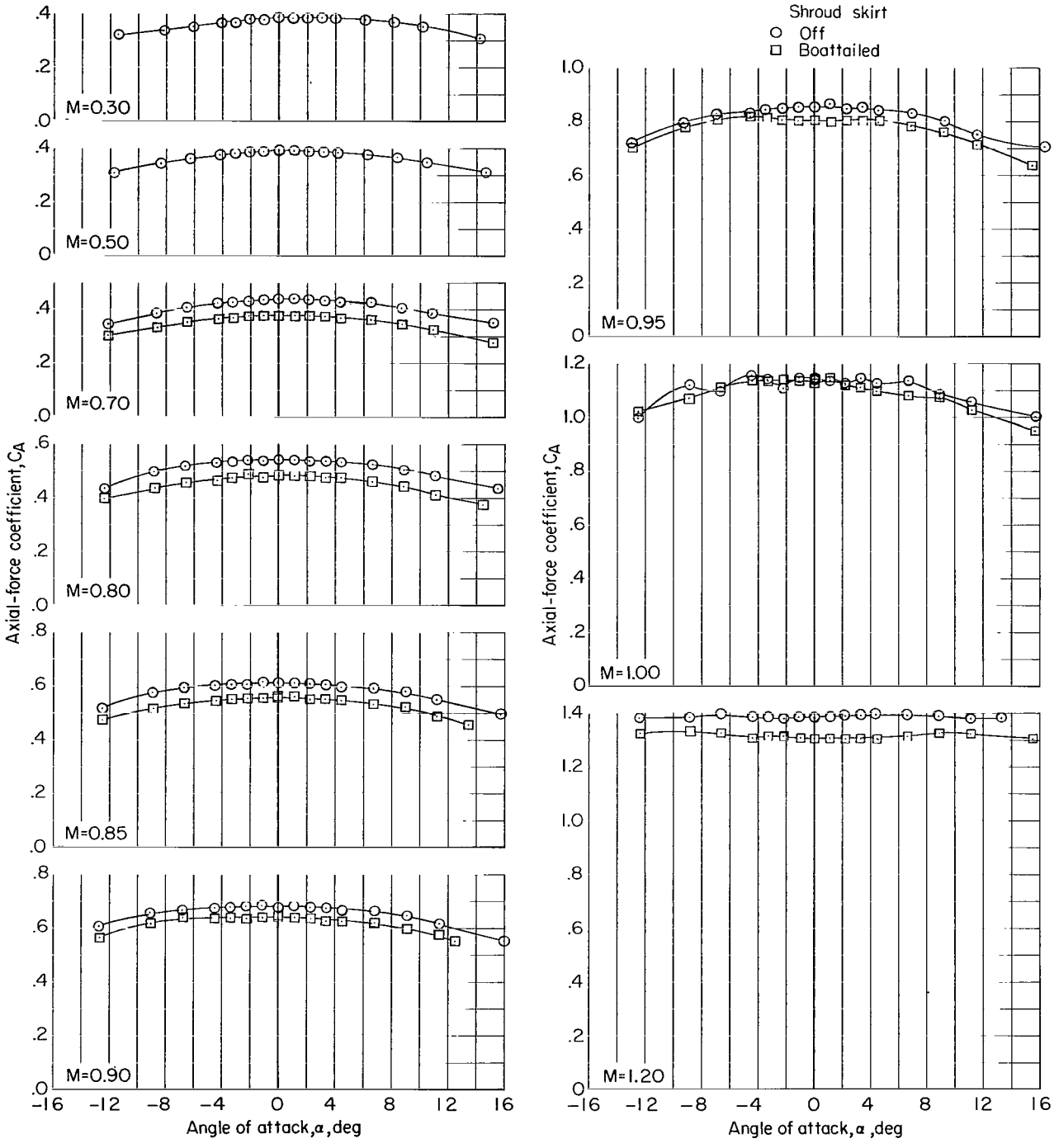

(b) C_A against α.

Figure 9.- Continued.

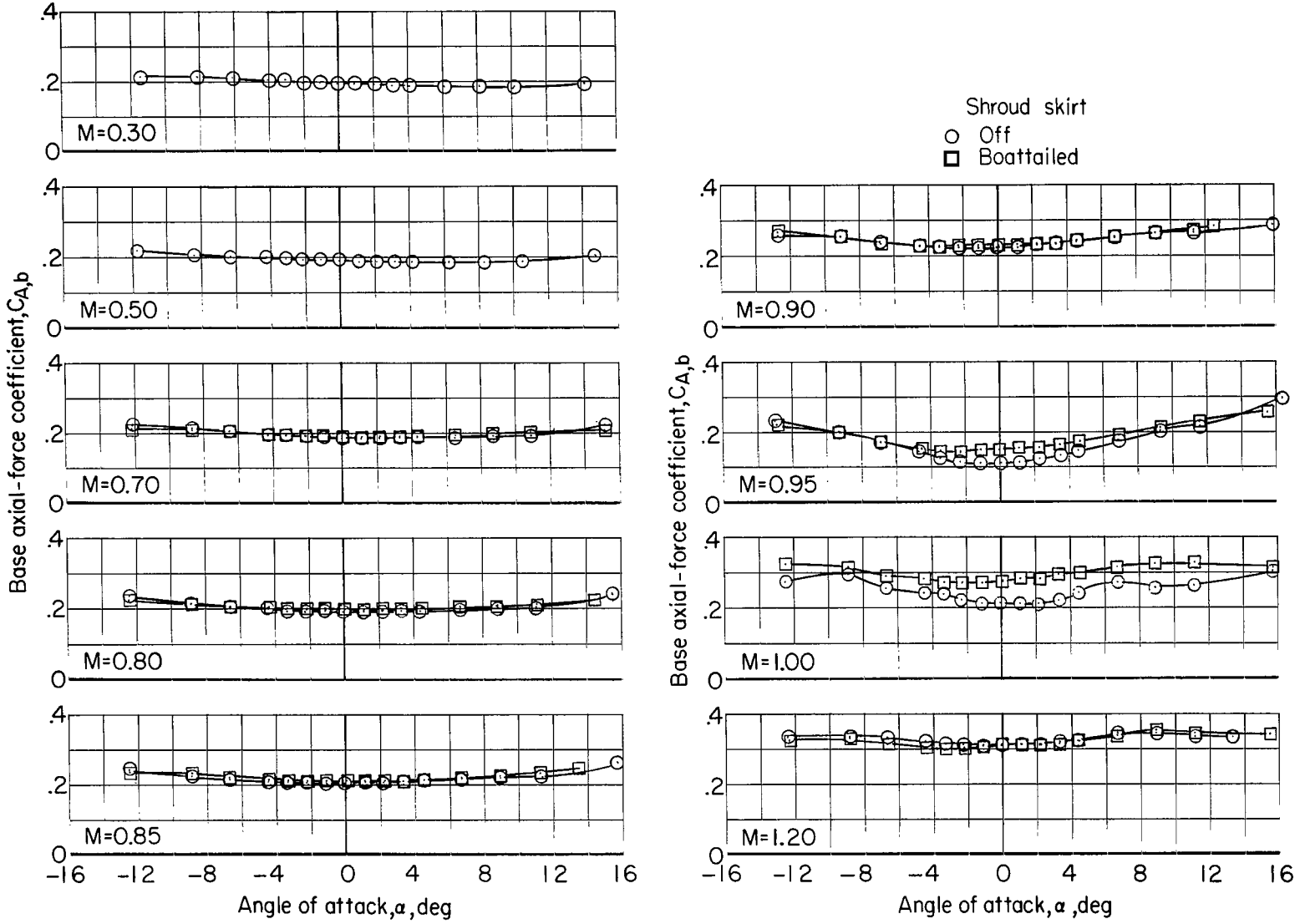

(c) $C_{A,b}$ against α.

Figure 9.- Continued.

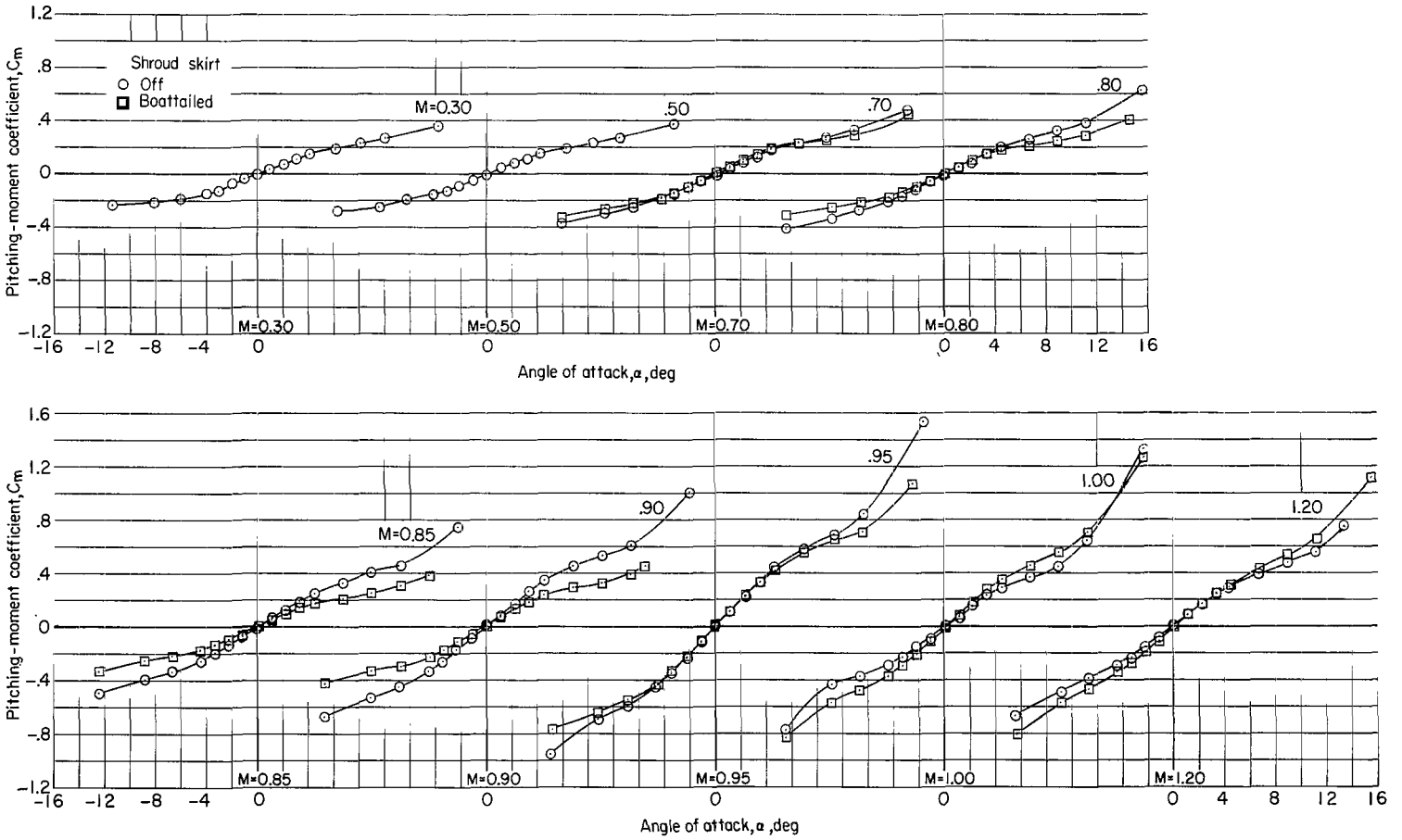

(d) C_m against α.

Figure 9.- Continued.

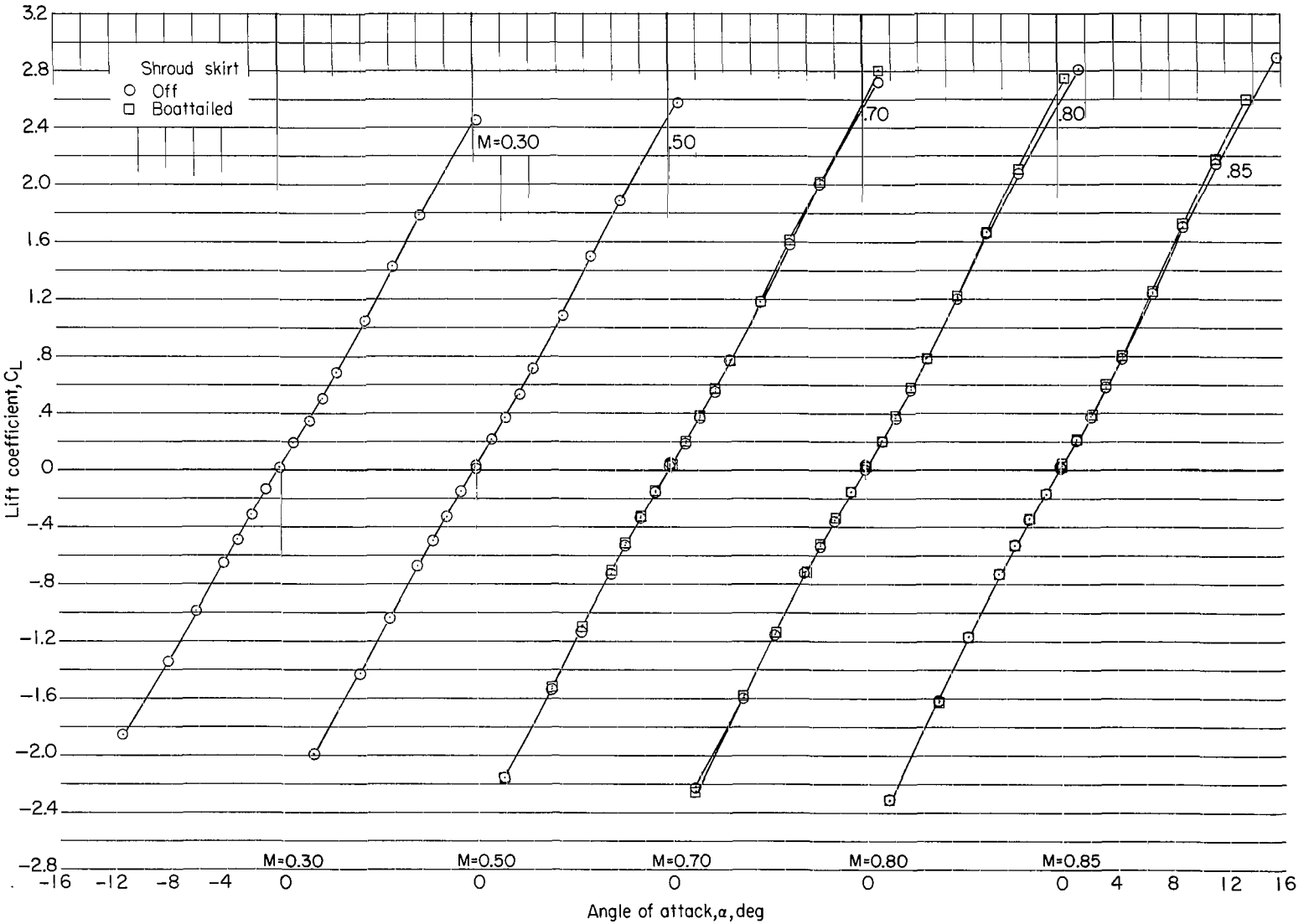

(e) C_L against α.

Figure 9.- Continued.

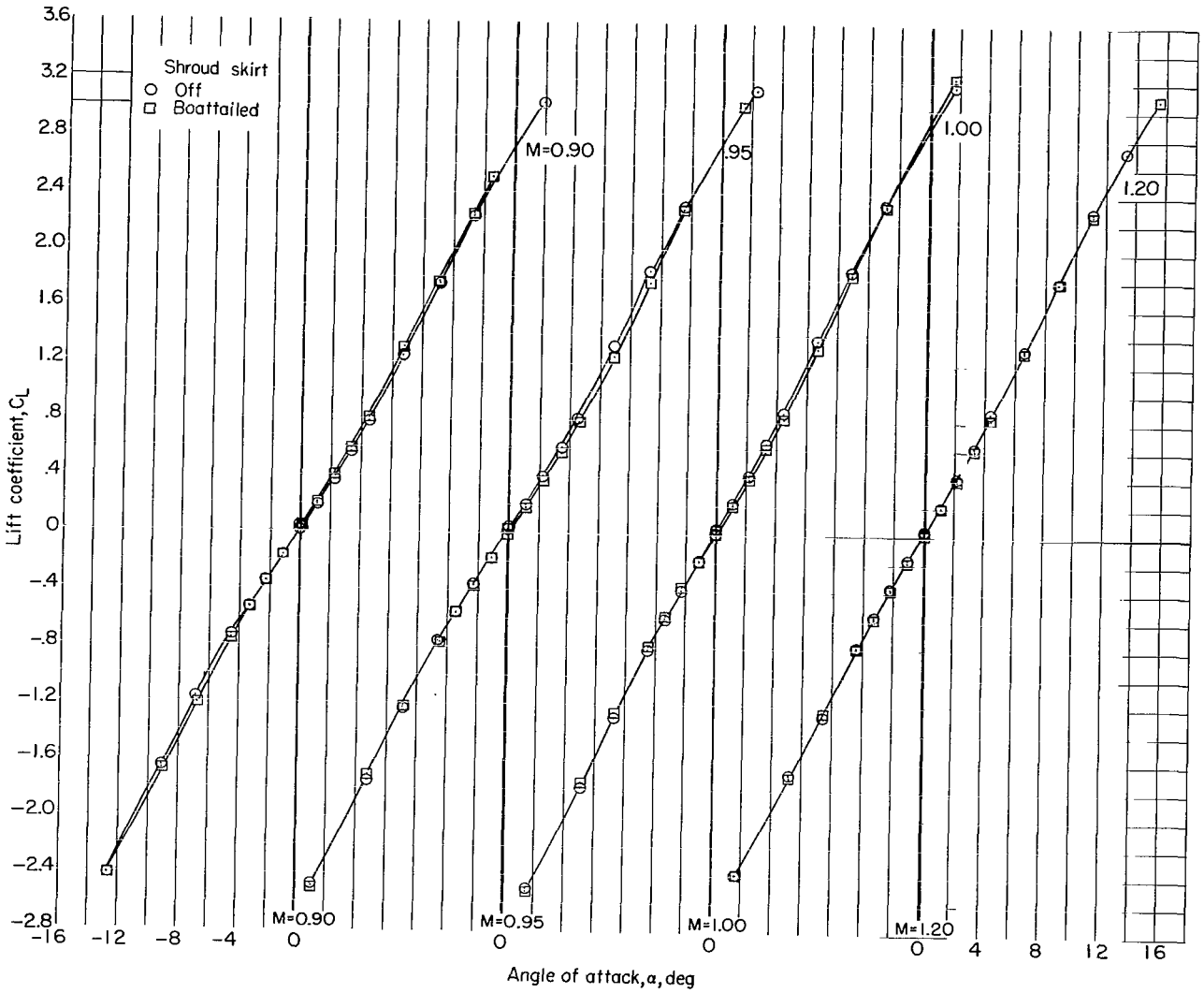

(e) C_L against α. Concluded.

Figure 9.- Continued.

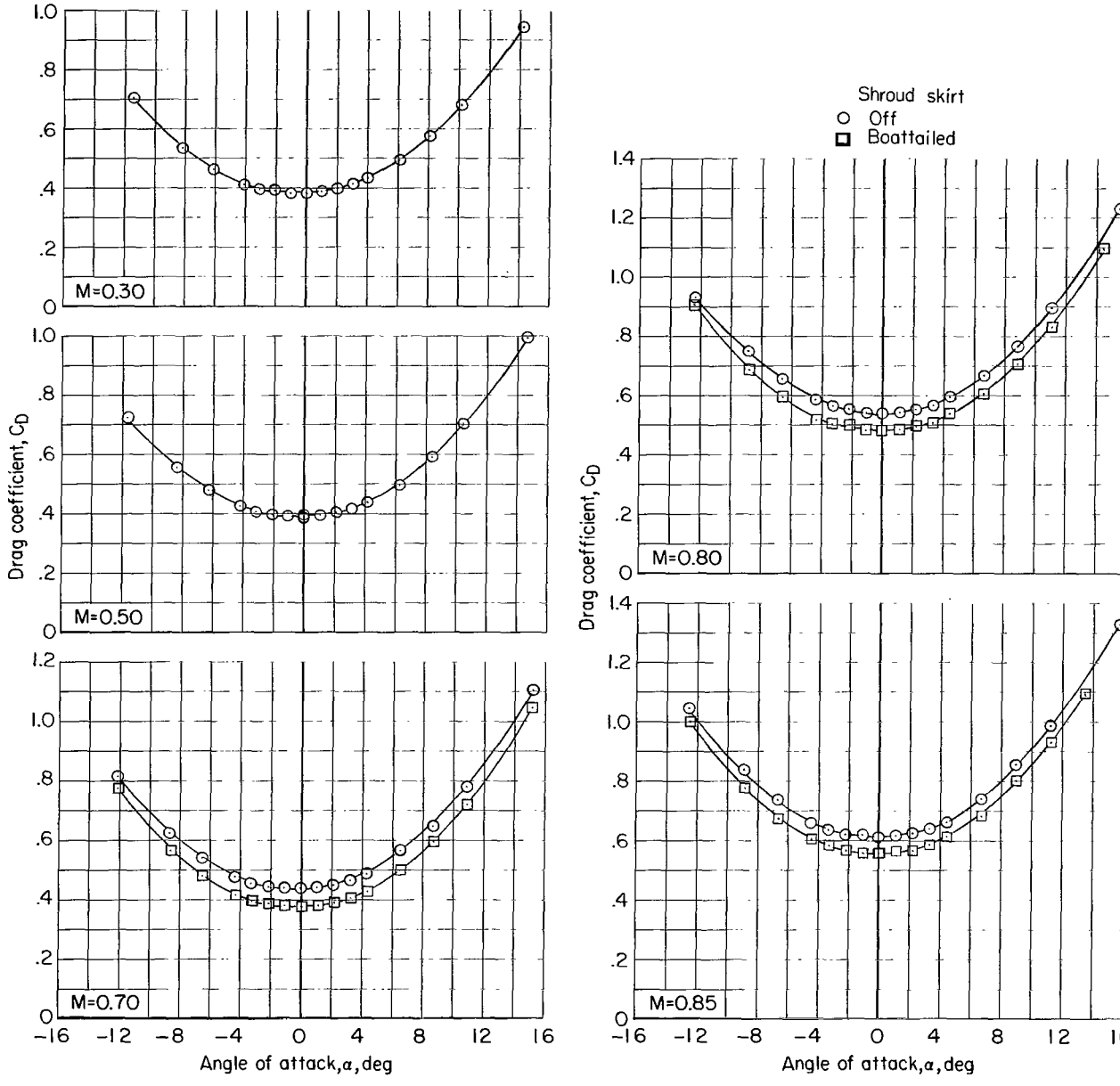

(f) C_D against α.

Figure 9.- Continued.

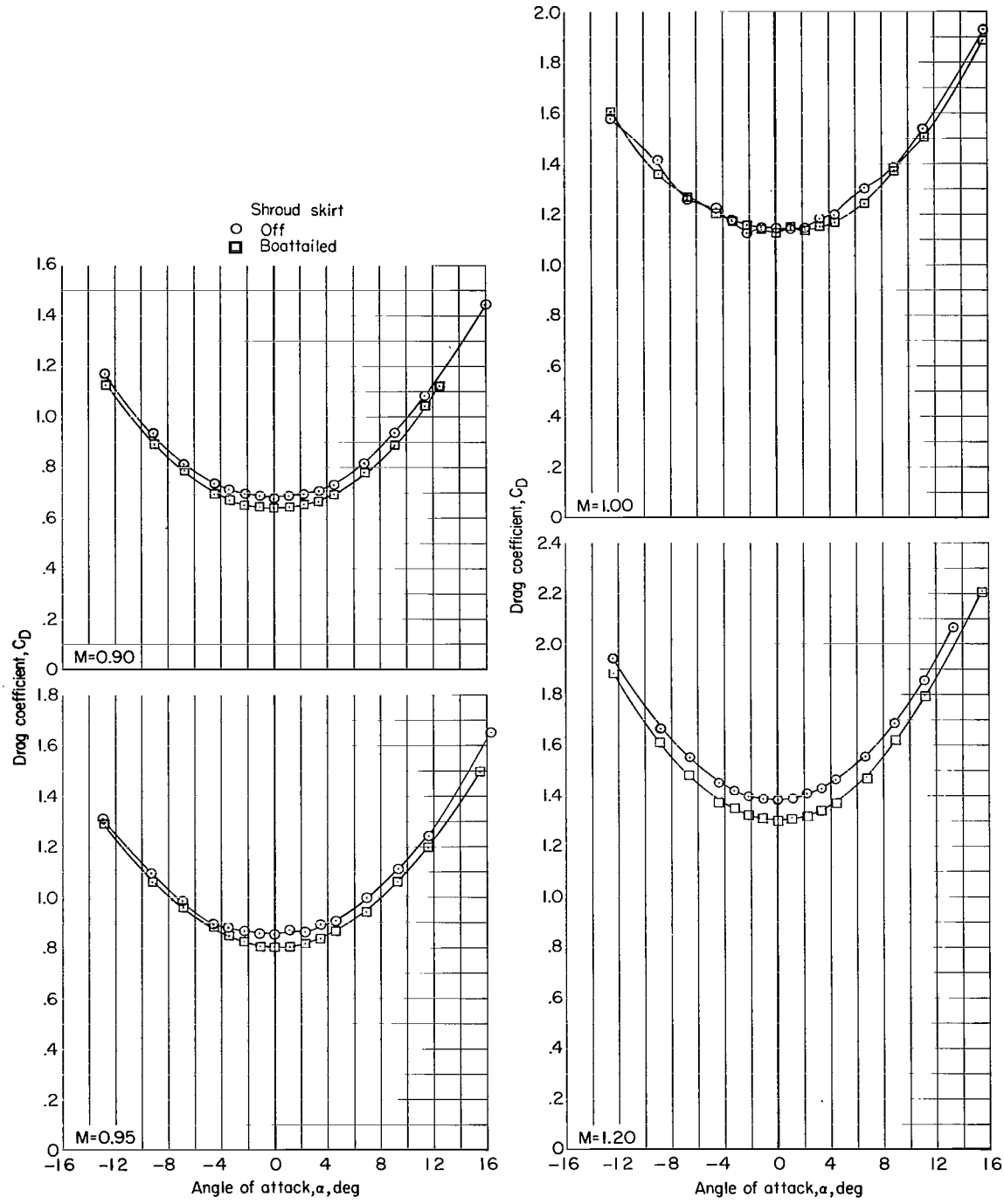

(f) C_D against α. Concluded.

Figure 9.- Continued.

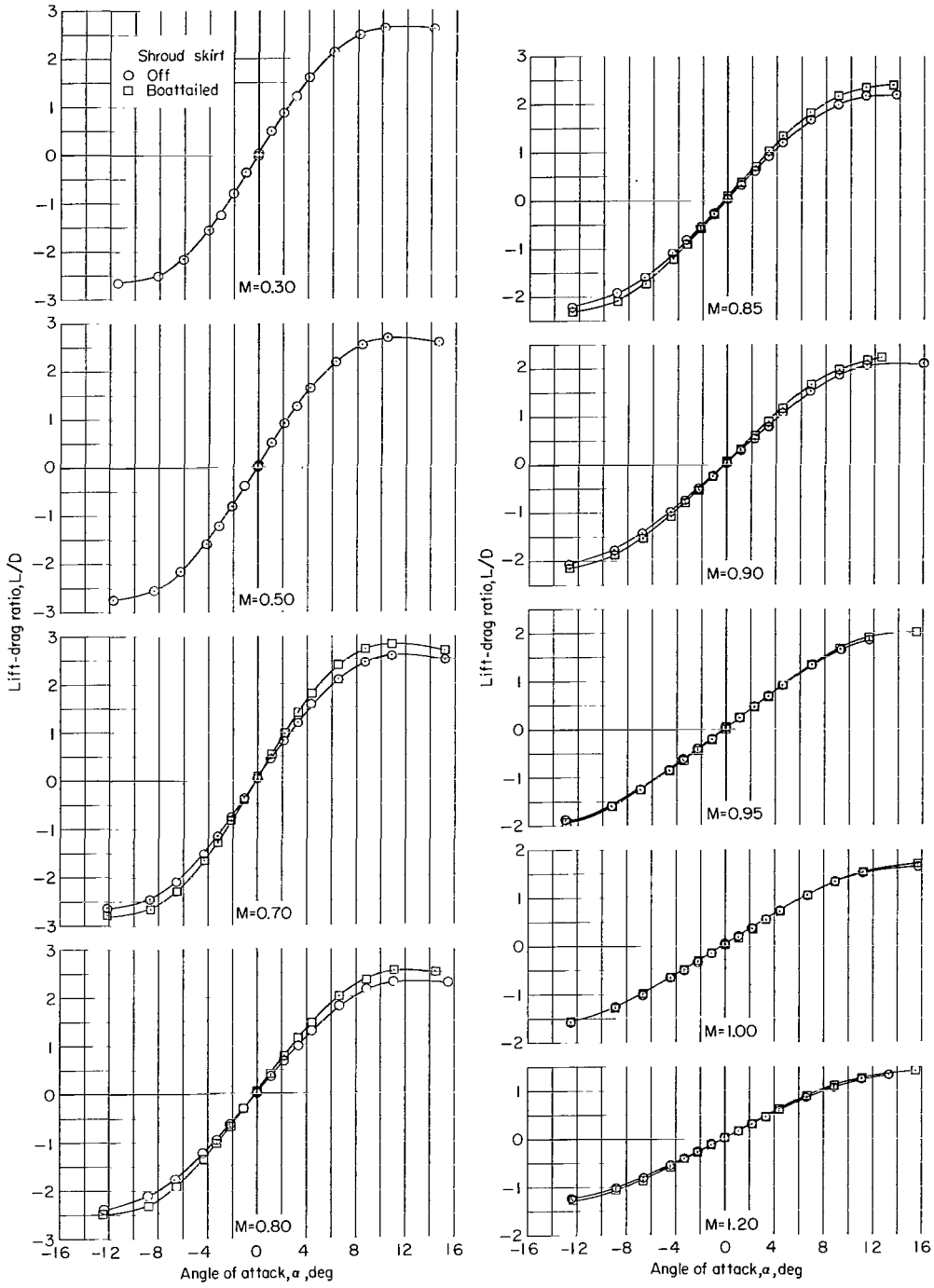

(g) L/D against α.

Figure 9.- Continued.

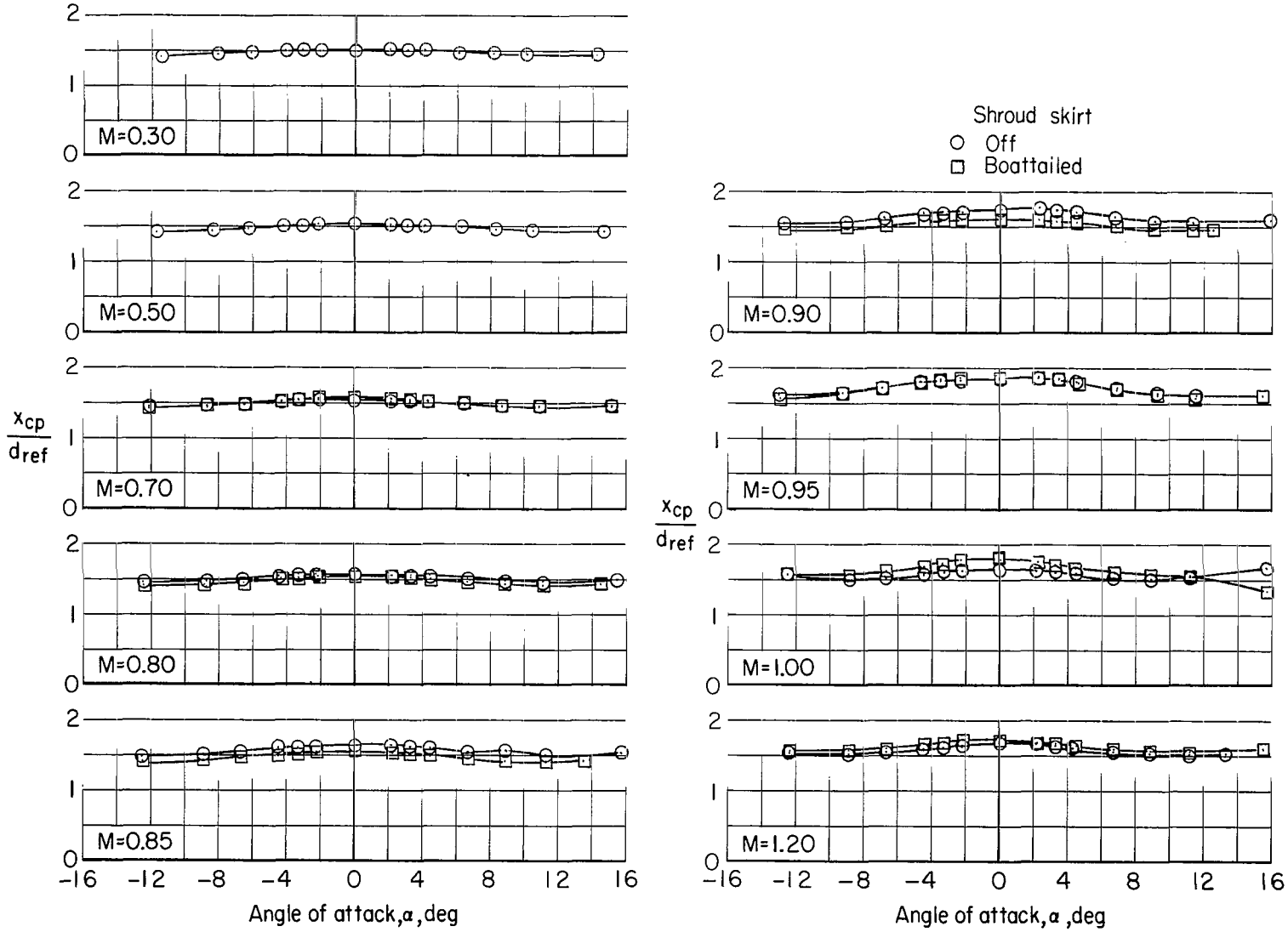

(h) x_{cp}/d_{ref} against α.

Figure 9.- Concluded.

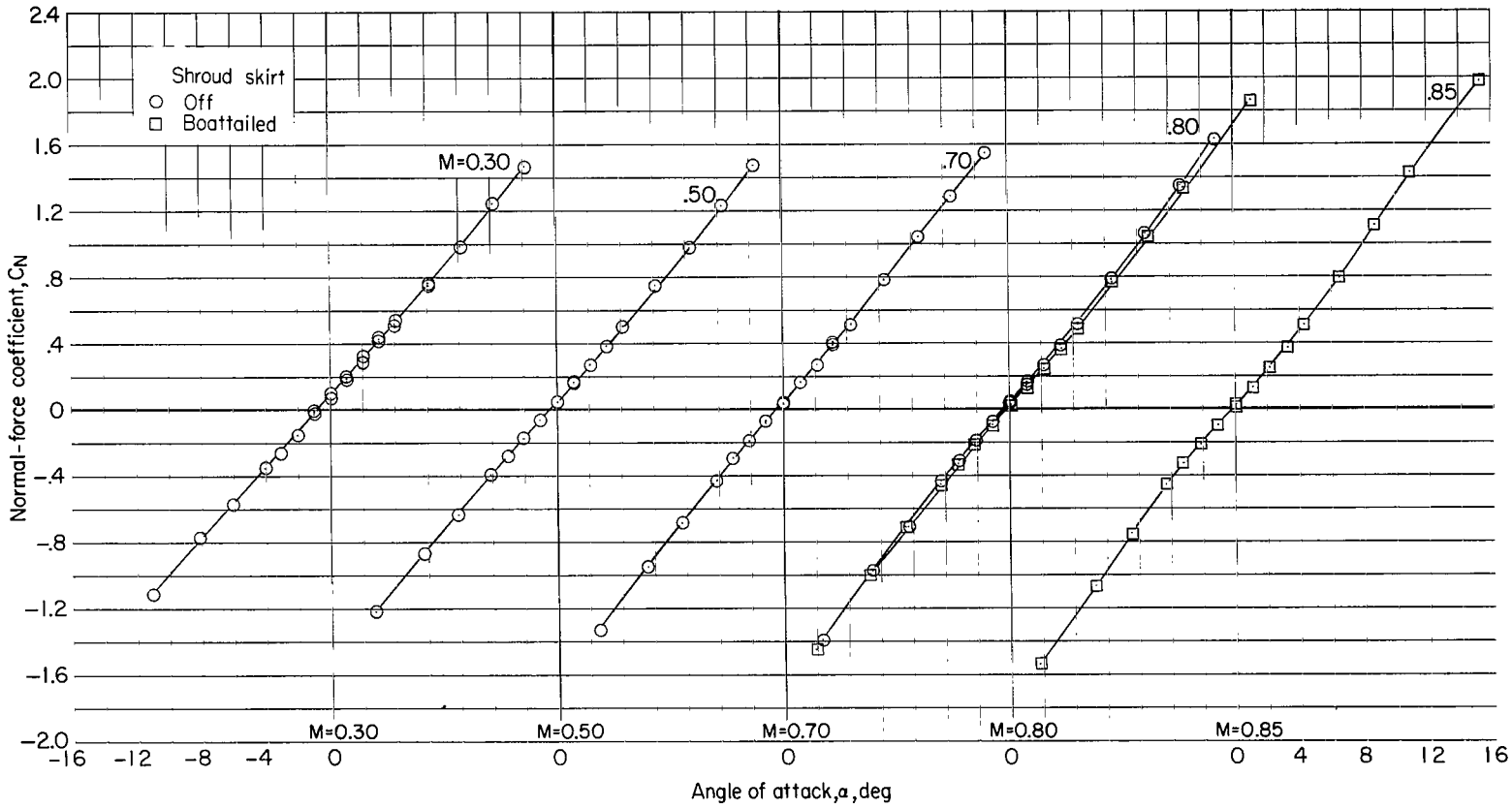

(a) C_N against α.

Figure 10.- Effect of boattailed shroud skirt on longitudinal aerodynamic characteristics. Shroud nose 2; small fins; $\delta = 0^0$.

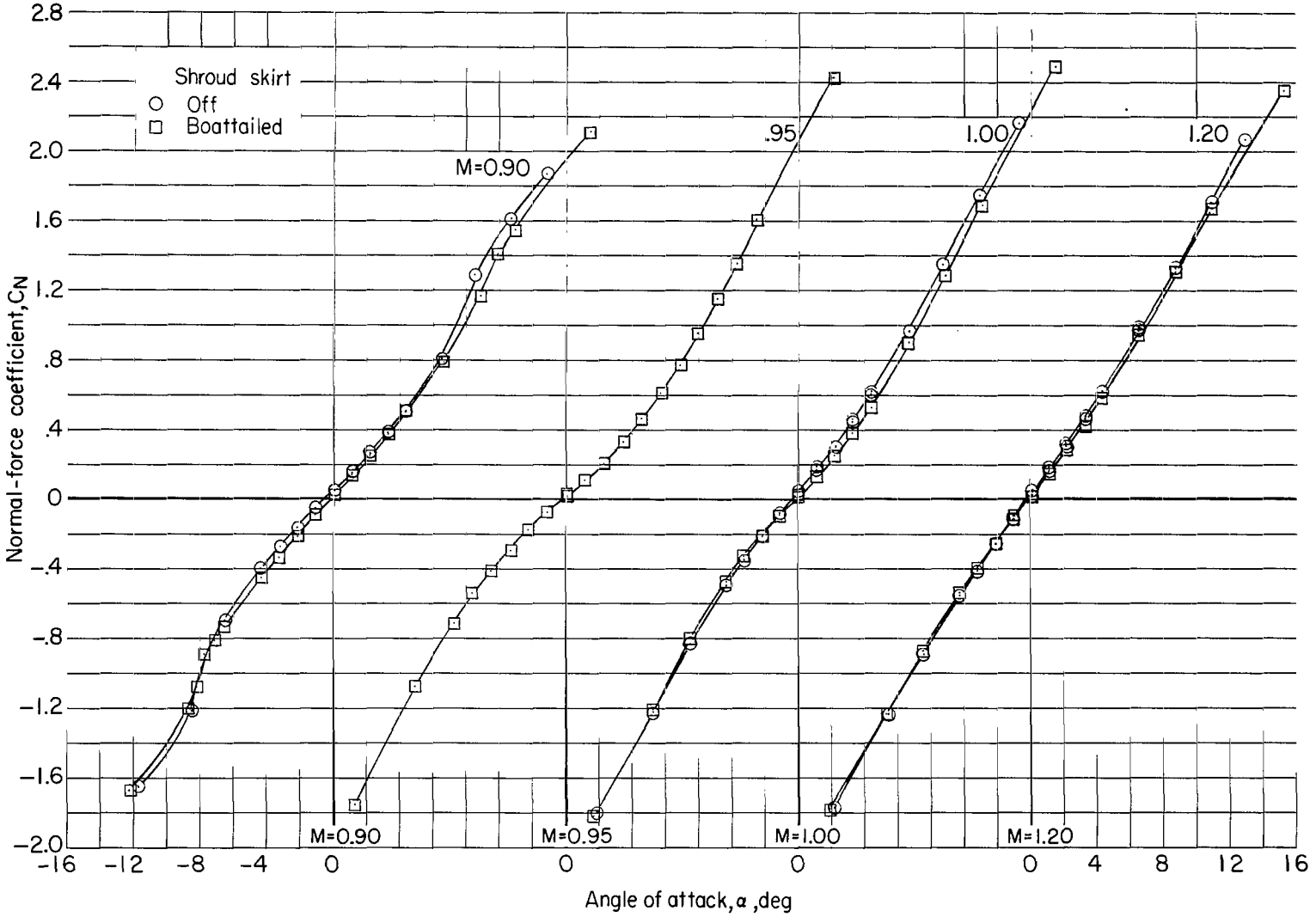

(a) C_N against α. Concluded.

Figure 10.- Continued.

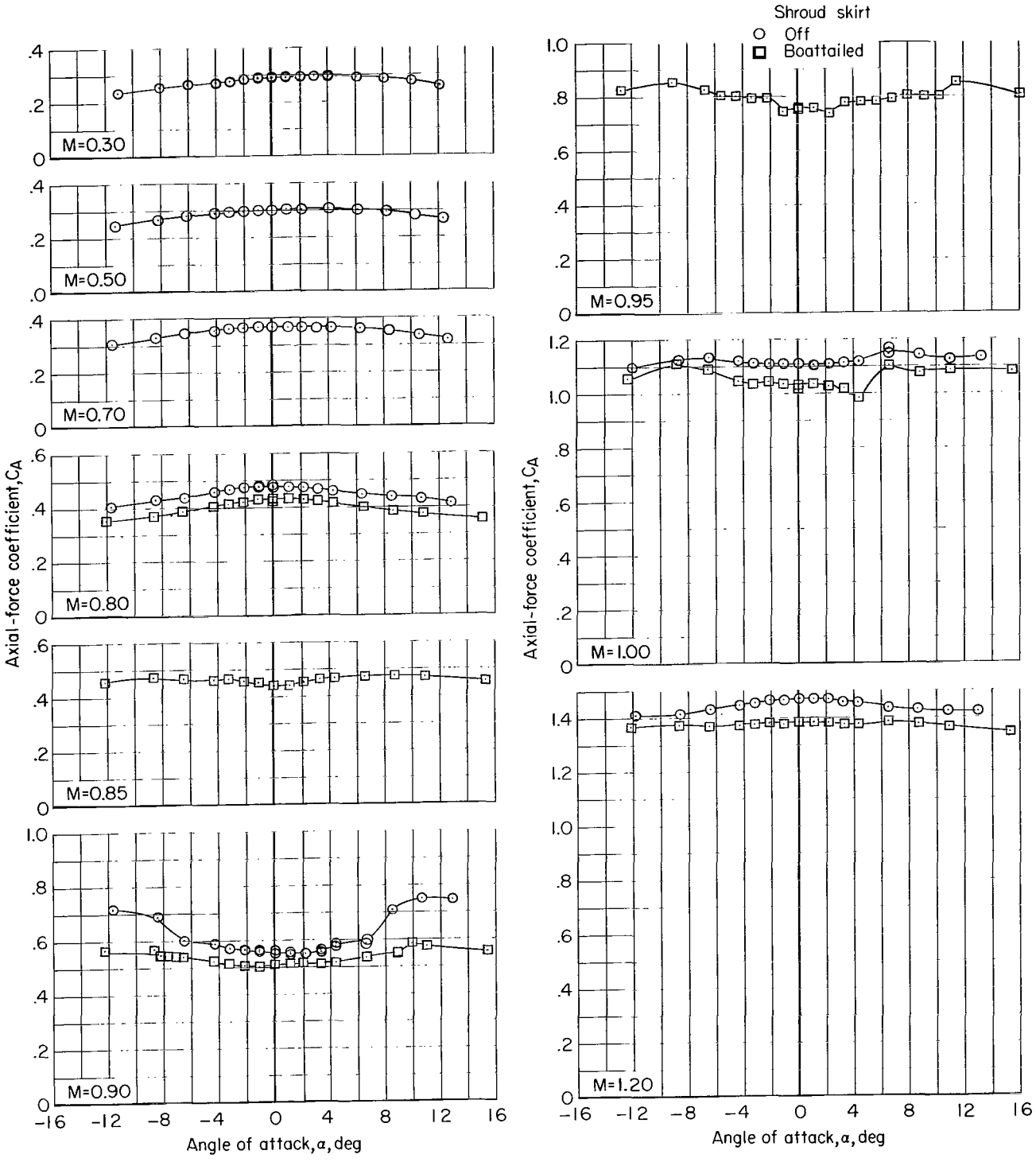

(b) C_A against α.

Figure 10.- Continued.

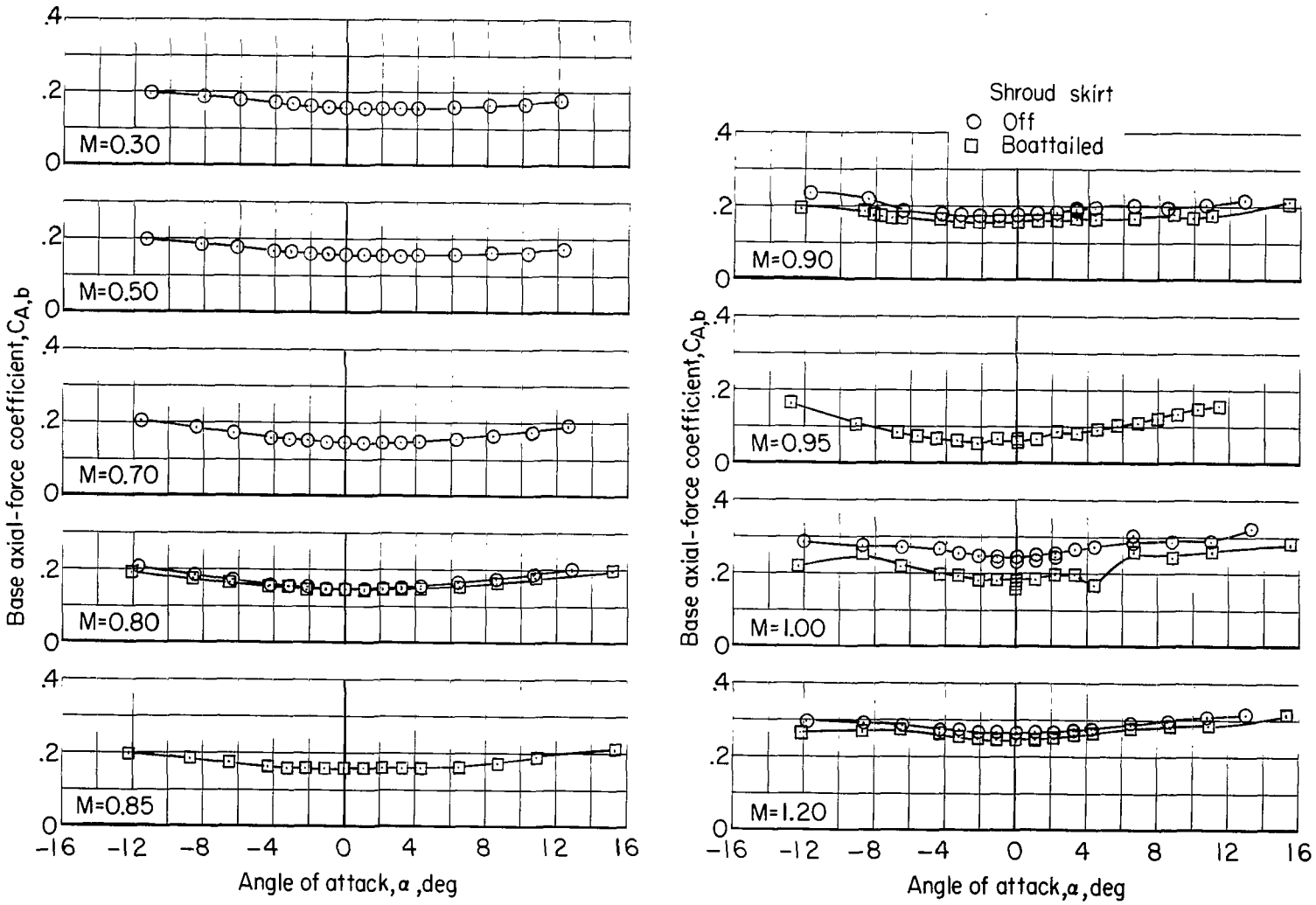

(c) $C_{A,b}$ against α.

Figure 10.- Continued.

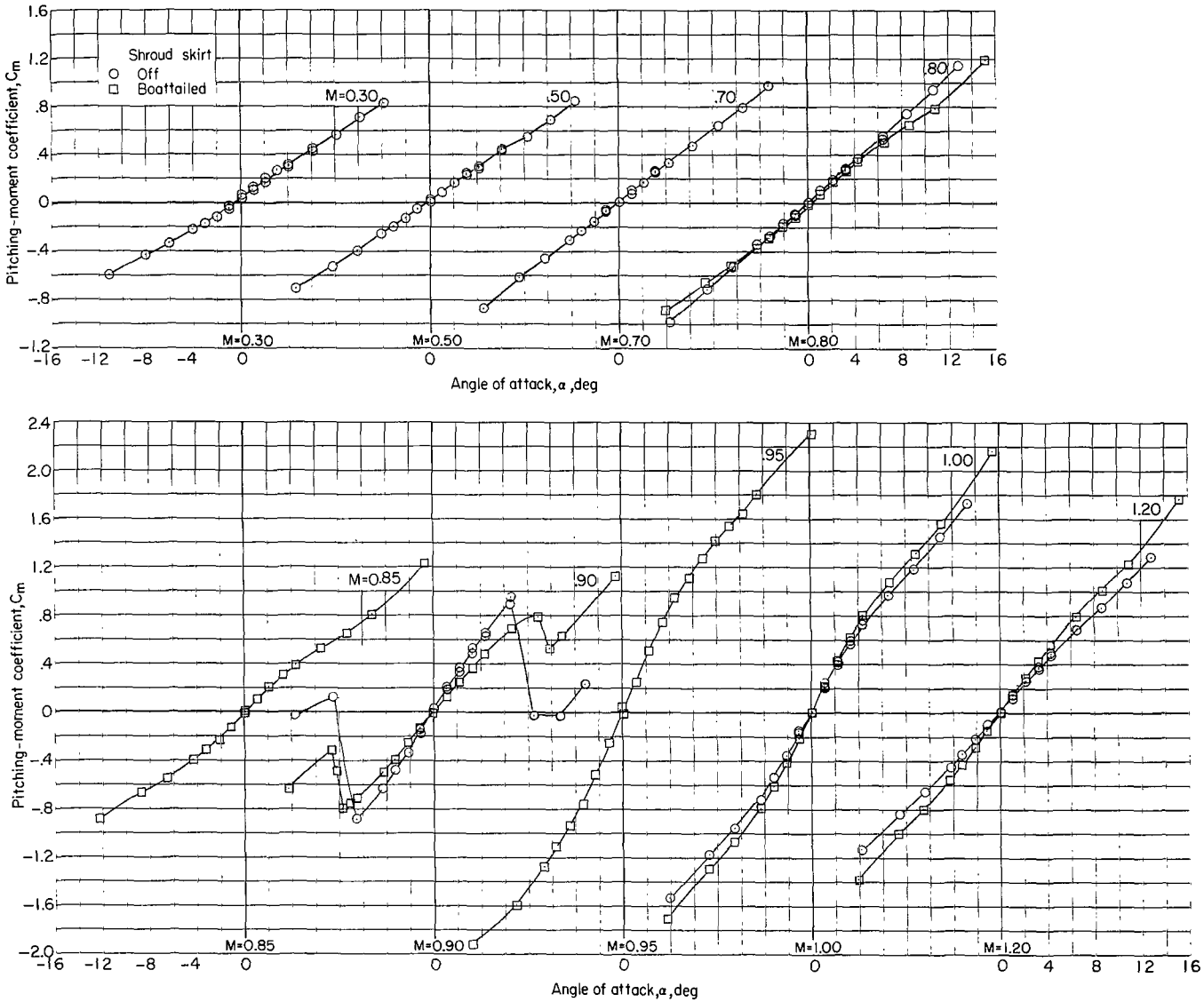

(d) C_m against α.

Figure 10.- Continued.

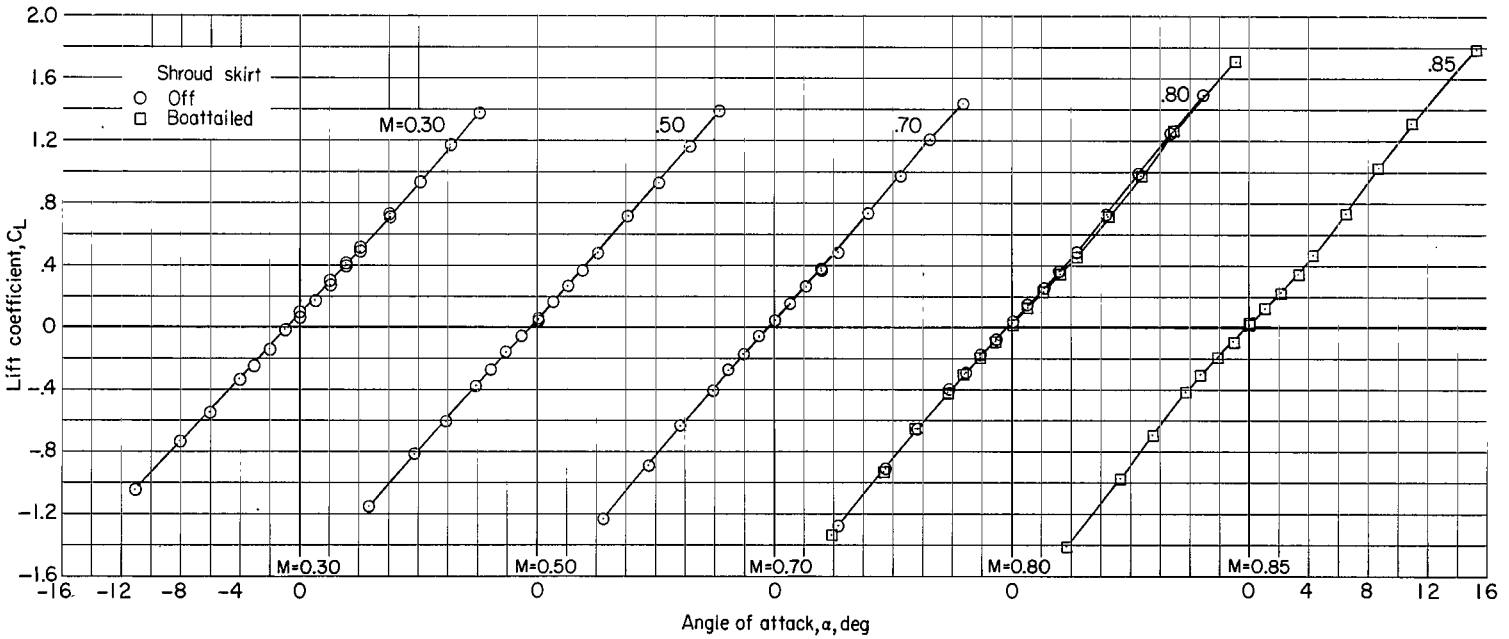

(e) C_L against α.

Figure 10.- Continued.

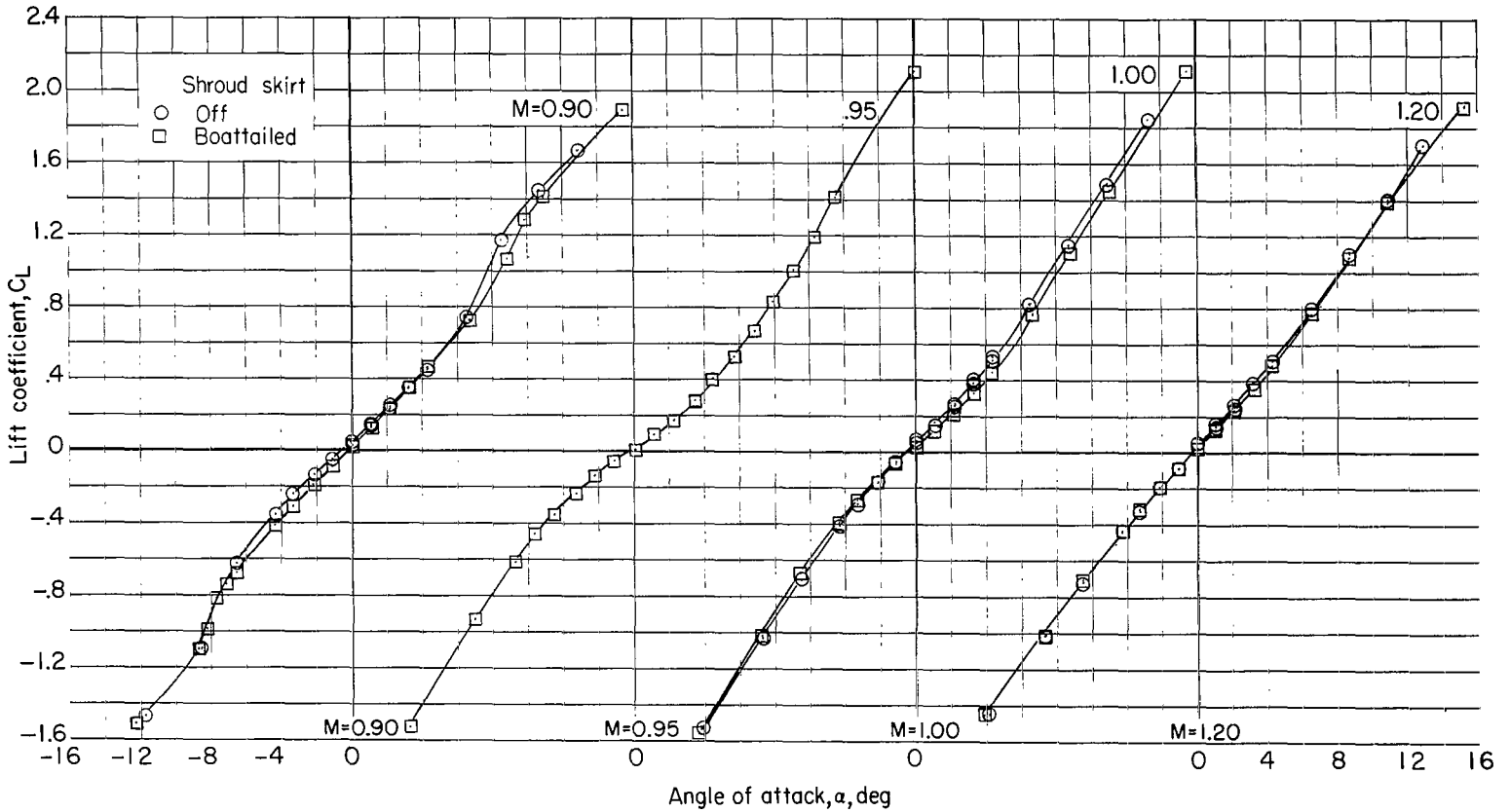

(e) C_L against α. Concluded.

Figure 10.- Continued.

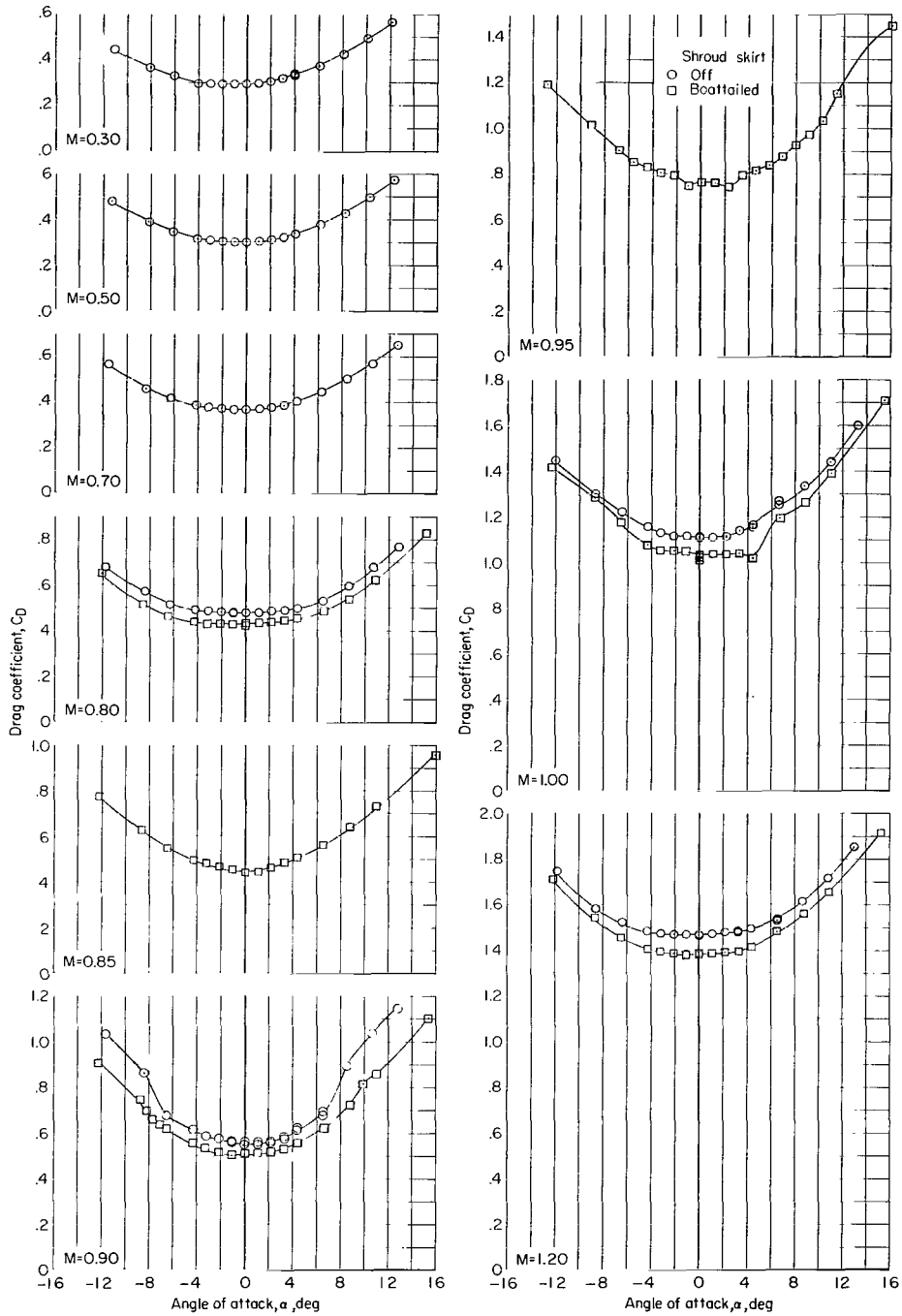

(f) C_D against α.

Figure 10.- Continued.

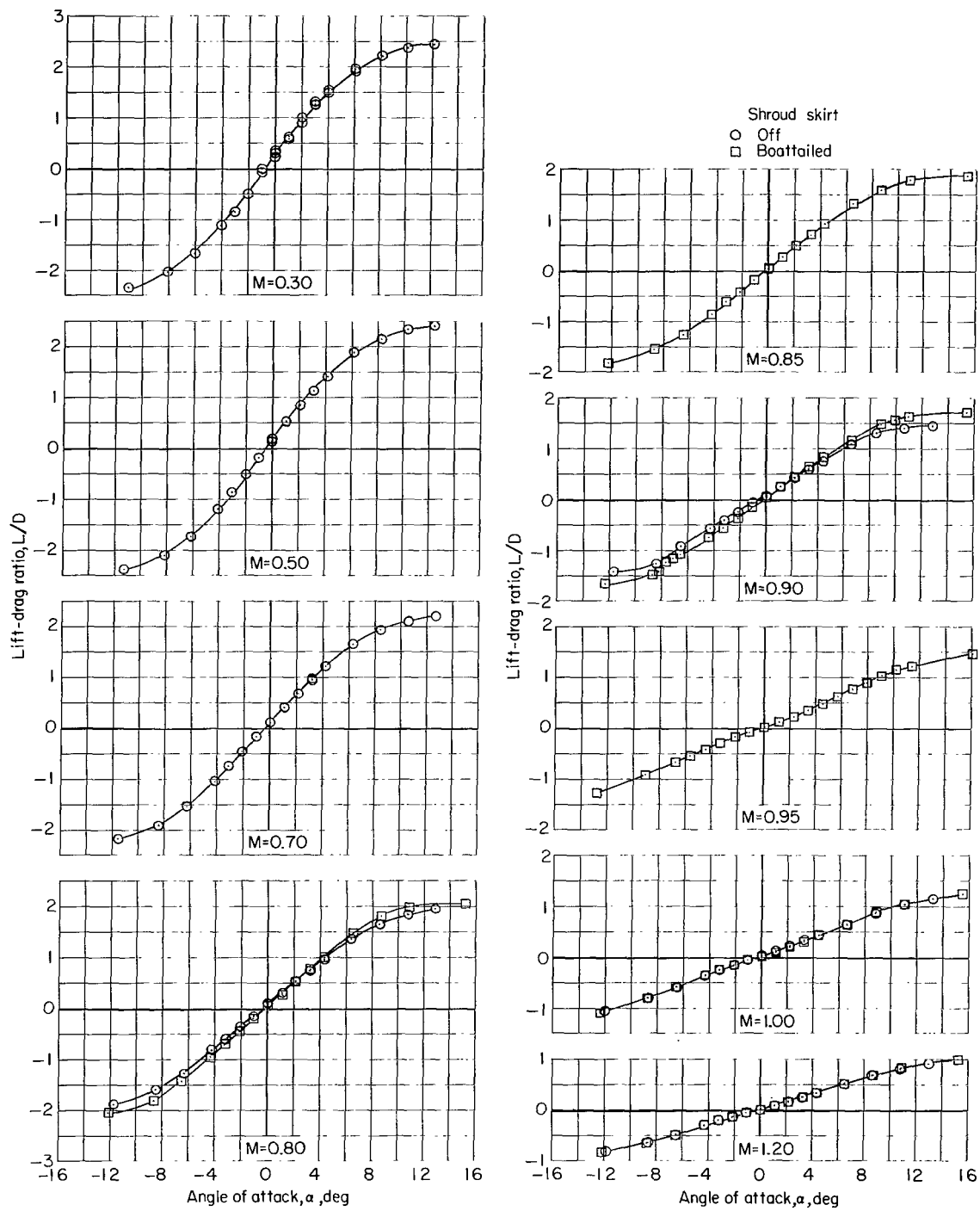

(g) L/D against α.

Figure 10.- Continued.

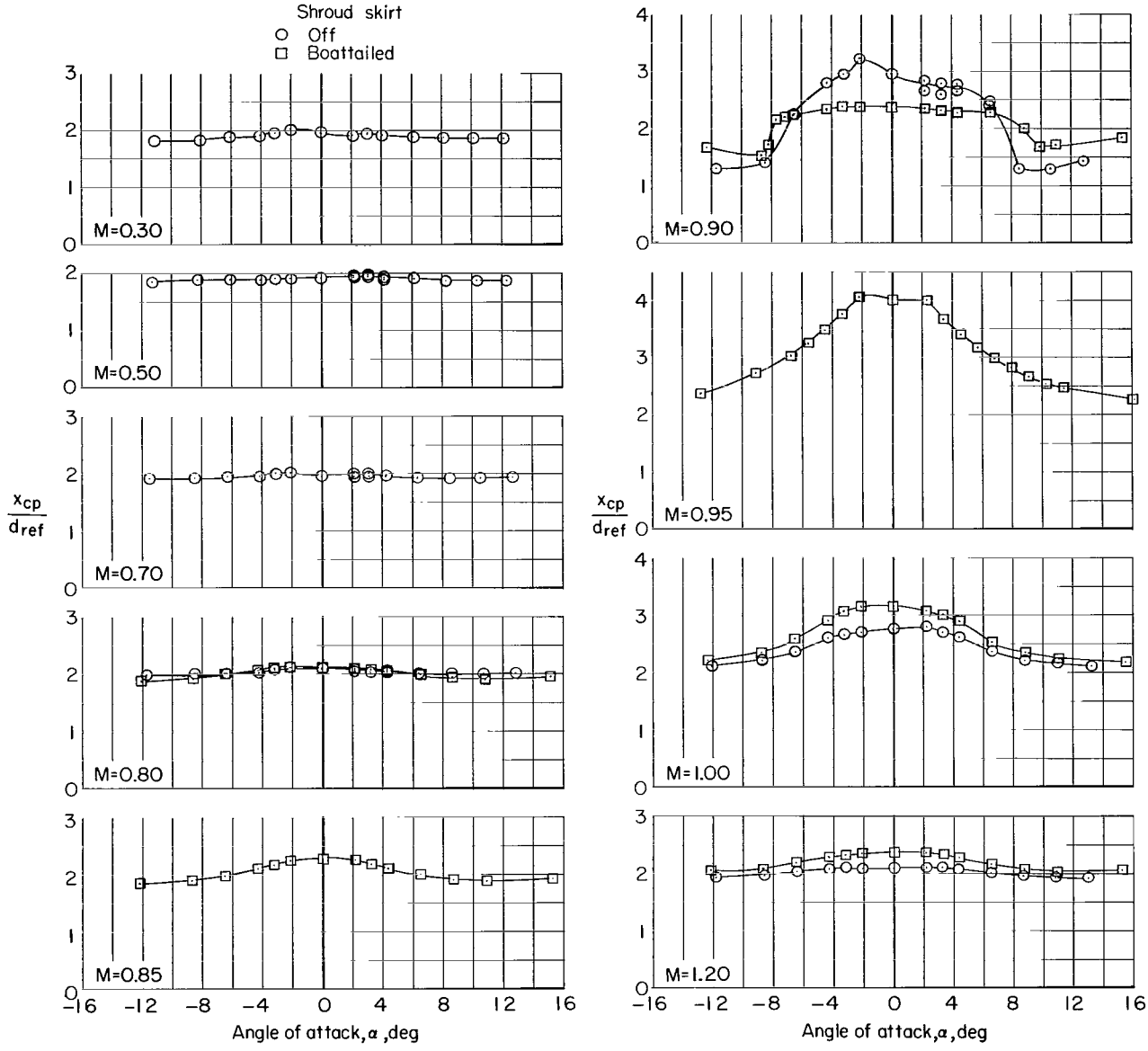

(h) x_{cp}/d_{ref} against α.

Figure 10.- Concluded.

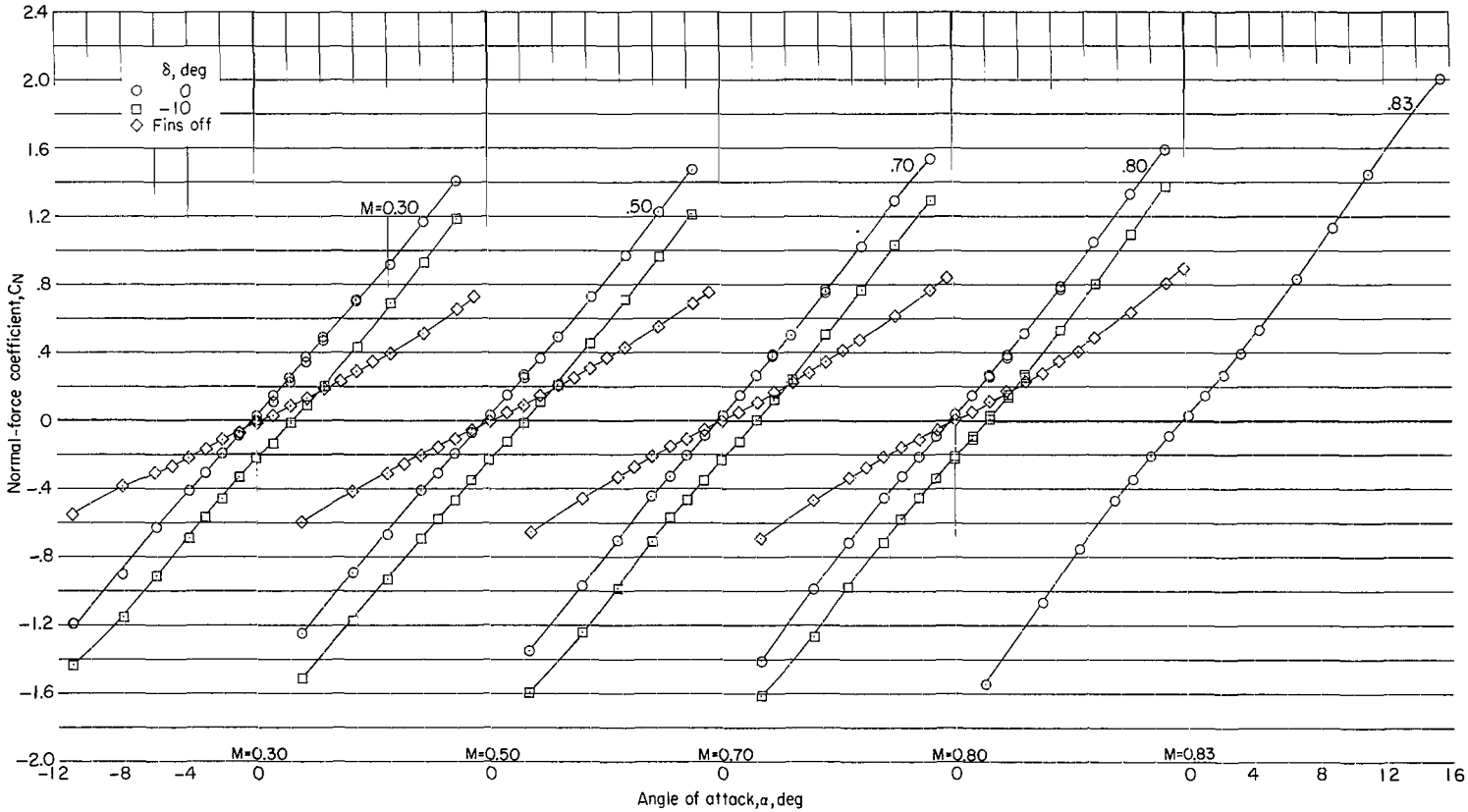

(a) C_N against α.

Figure 11.- Effect of deflection of trailing-edge controls on longitudinal aerodynamic characteristics and on hinge moments of control on fin 2. Shroud nose 1; small fins; shroud skirt off. (Flagged symbols indicate points from repeat run.)

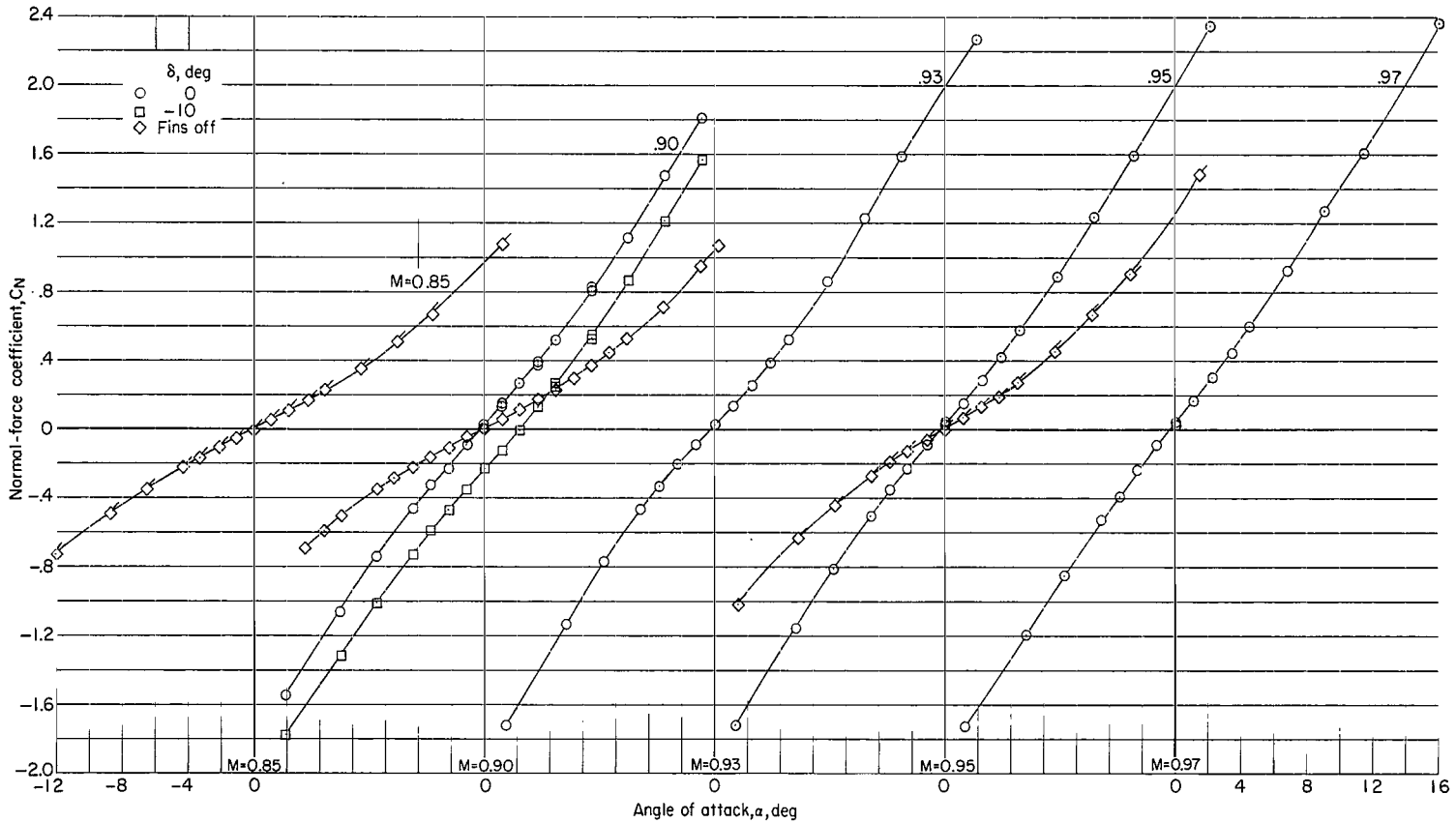

(a) C_N against α. Continued.

Figure 11.- Continued.

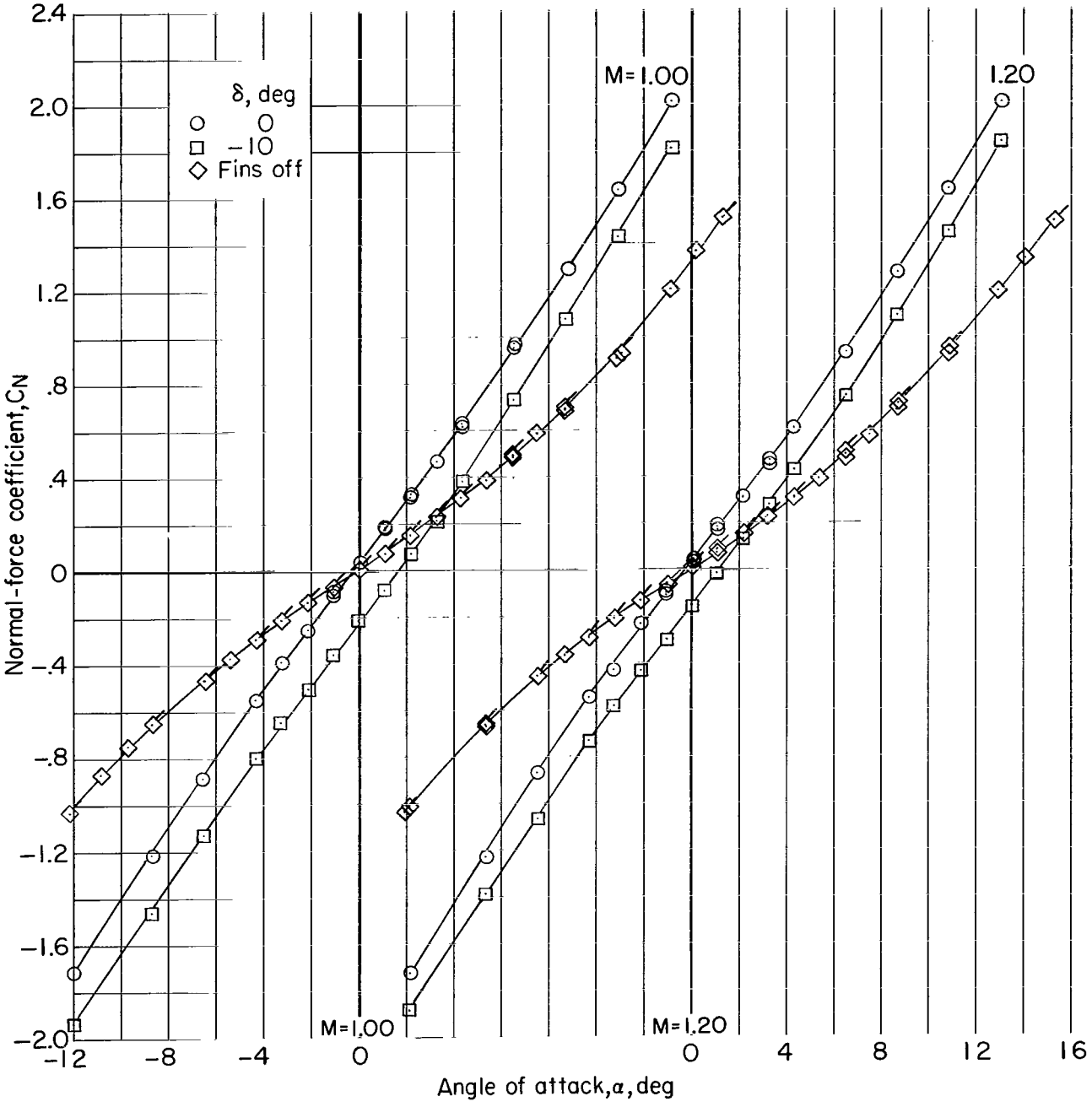

(a) C_N against α. Concluded.

Figure 11.- Continued.

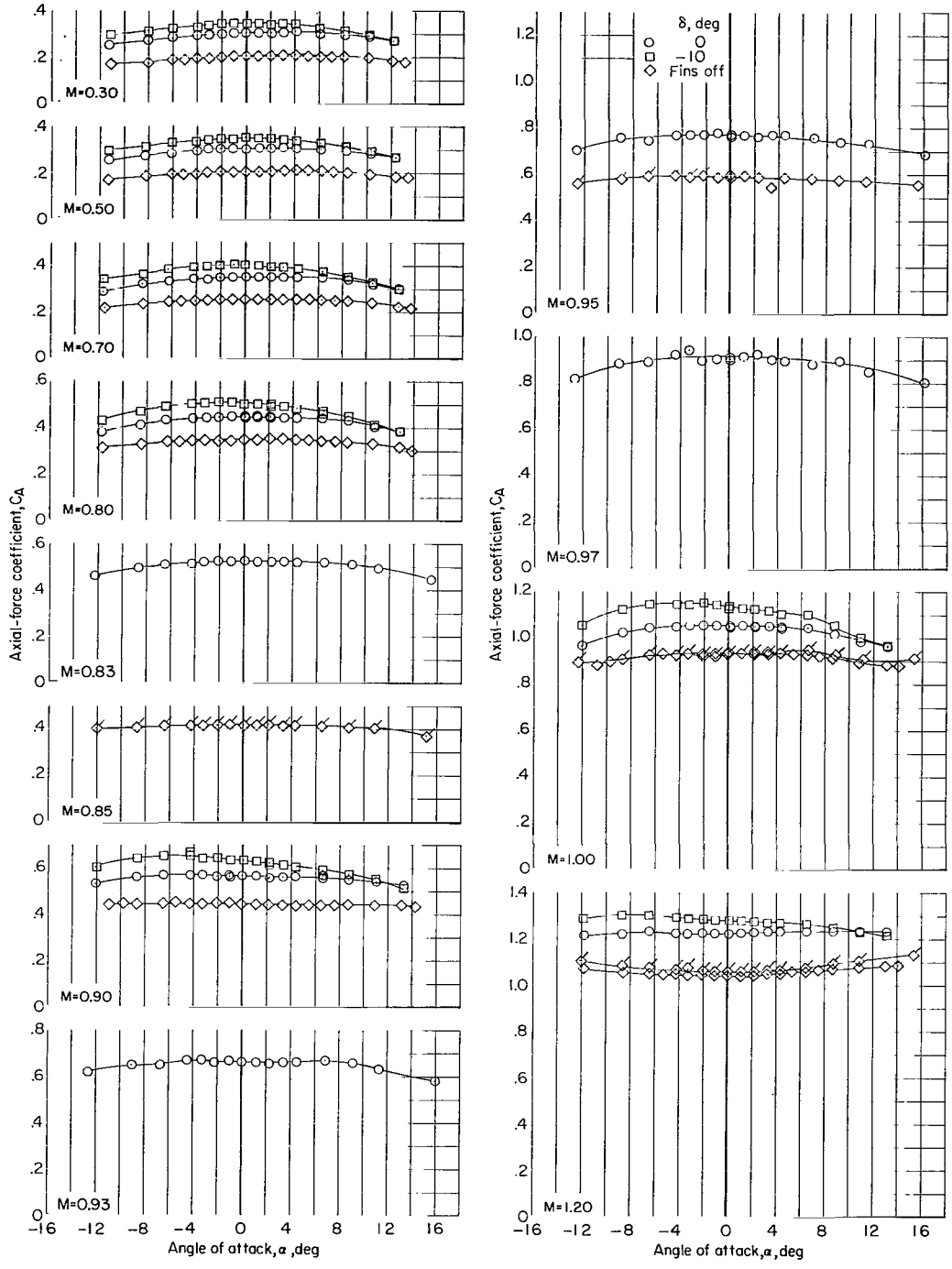

(b) C_A against α.

Figure 11.- Continued.

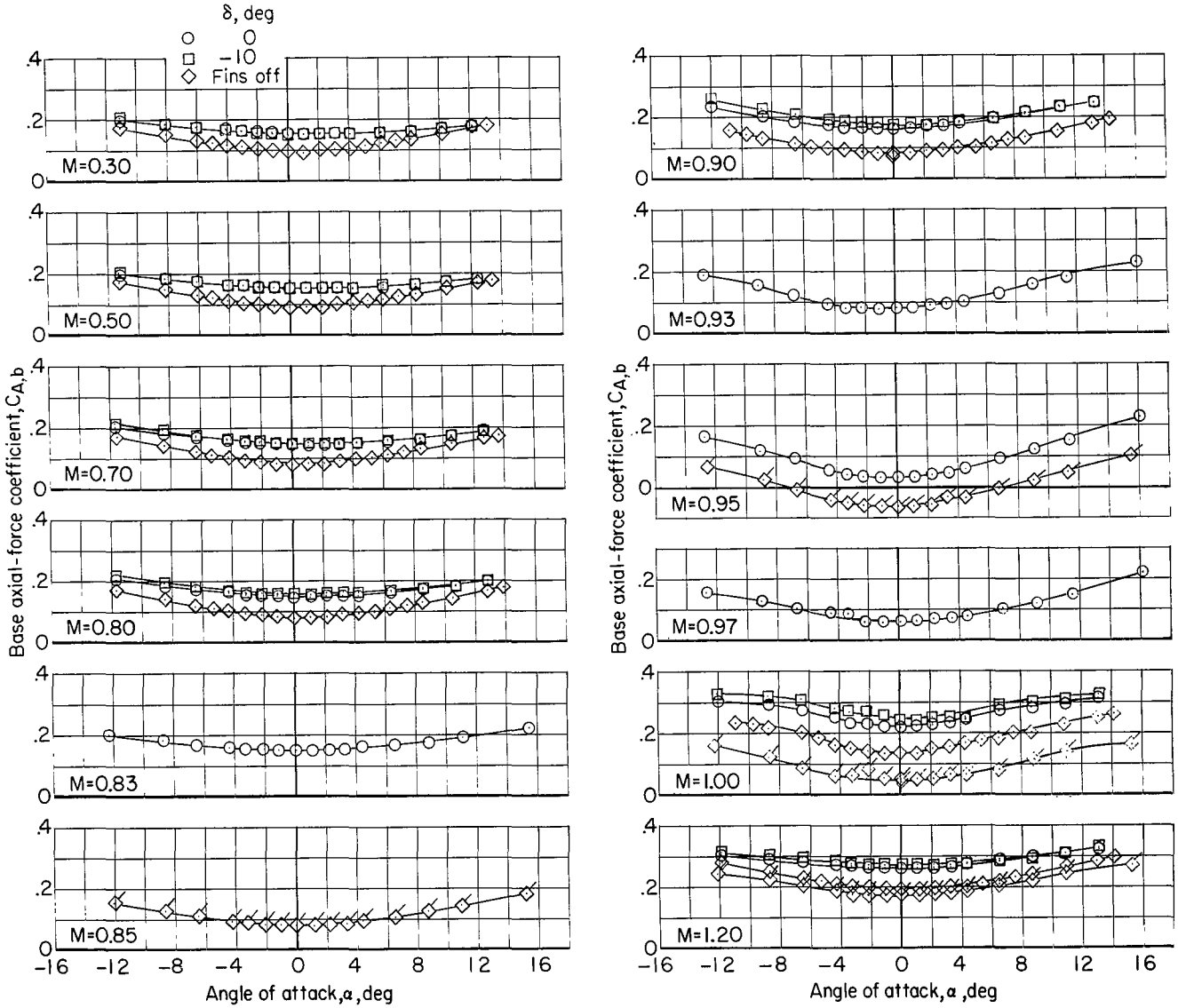

(c) $C_{A,b}$ against α.

Figure 11.- Continued.

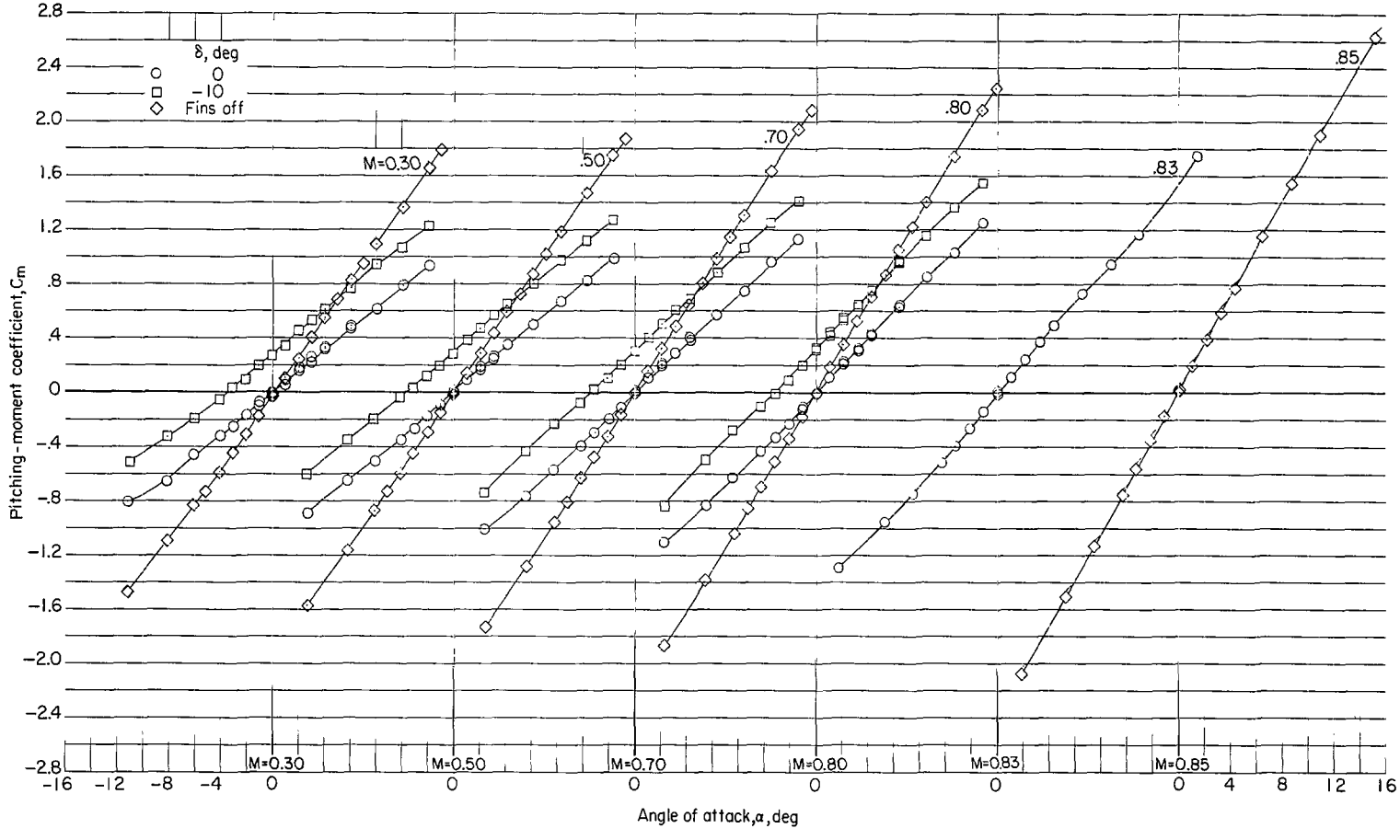

(d) C_m against α.

Figure 11.- Continued.

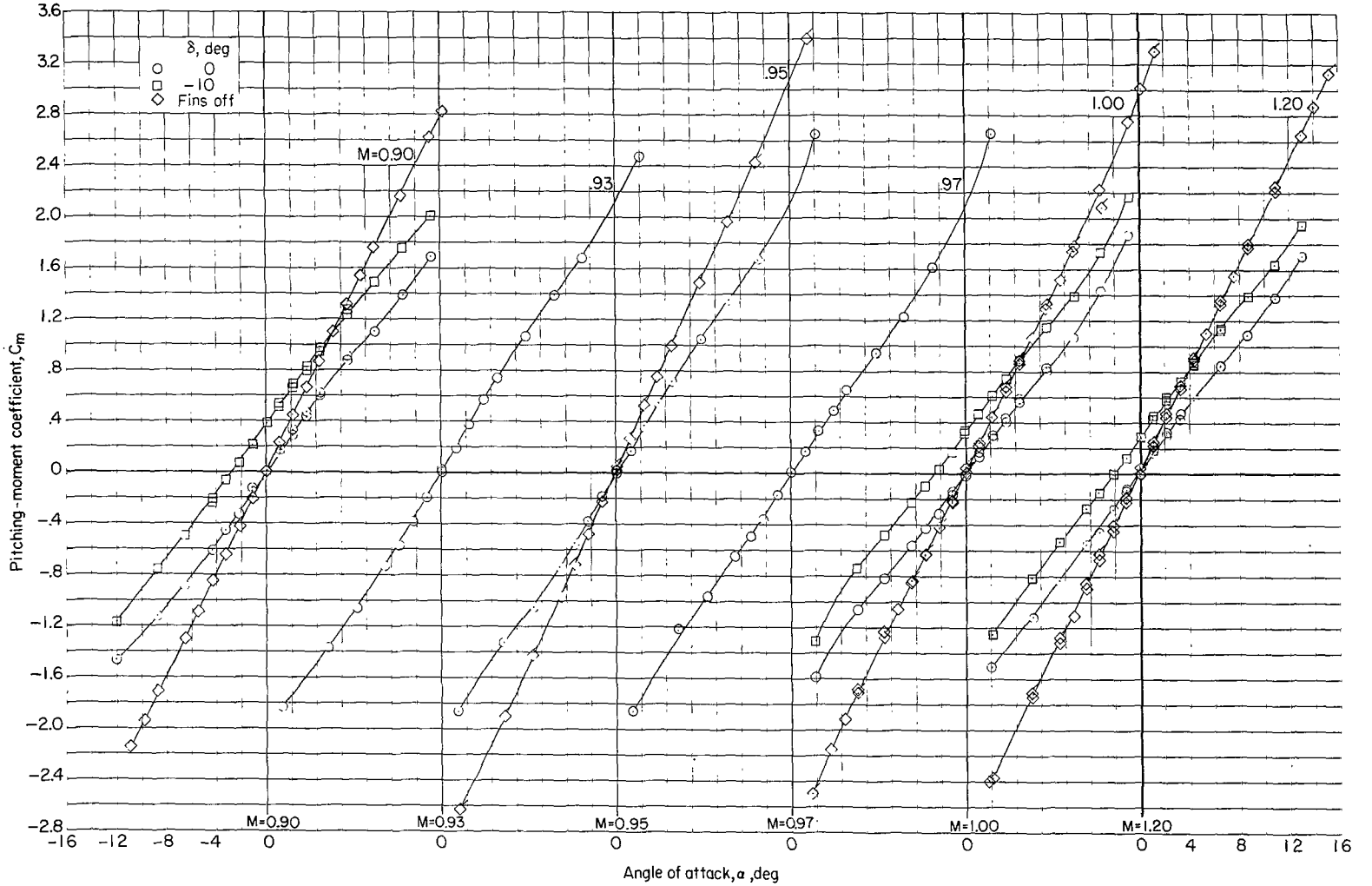

(d) C_m against α. Concluded.

Figure 11.- Continued.

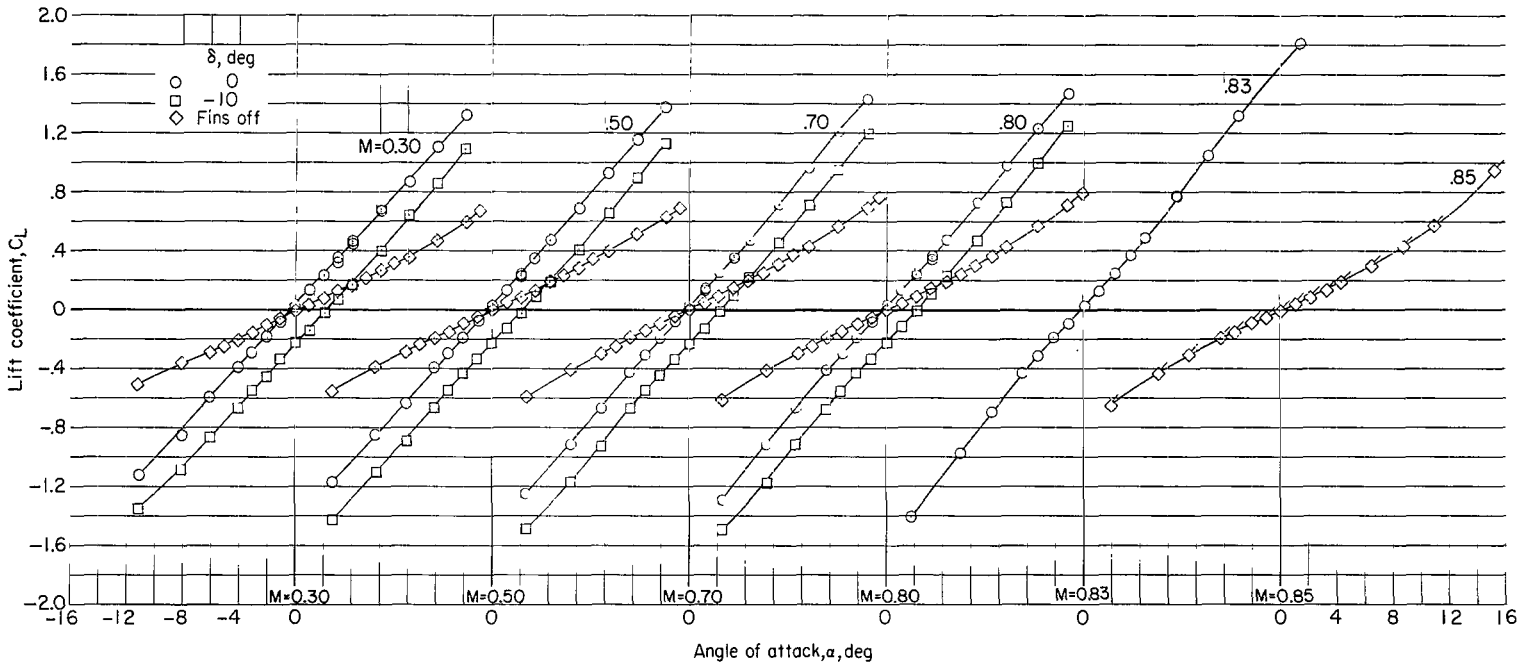

(e) C_L against α.

Figure 11.- Continued.

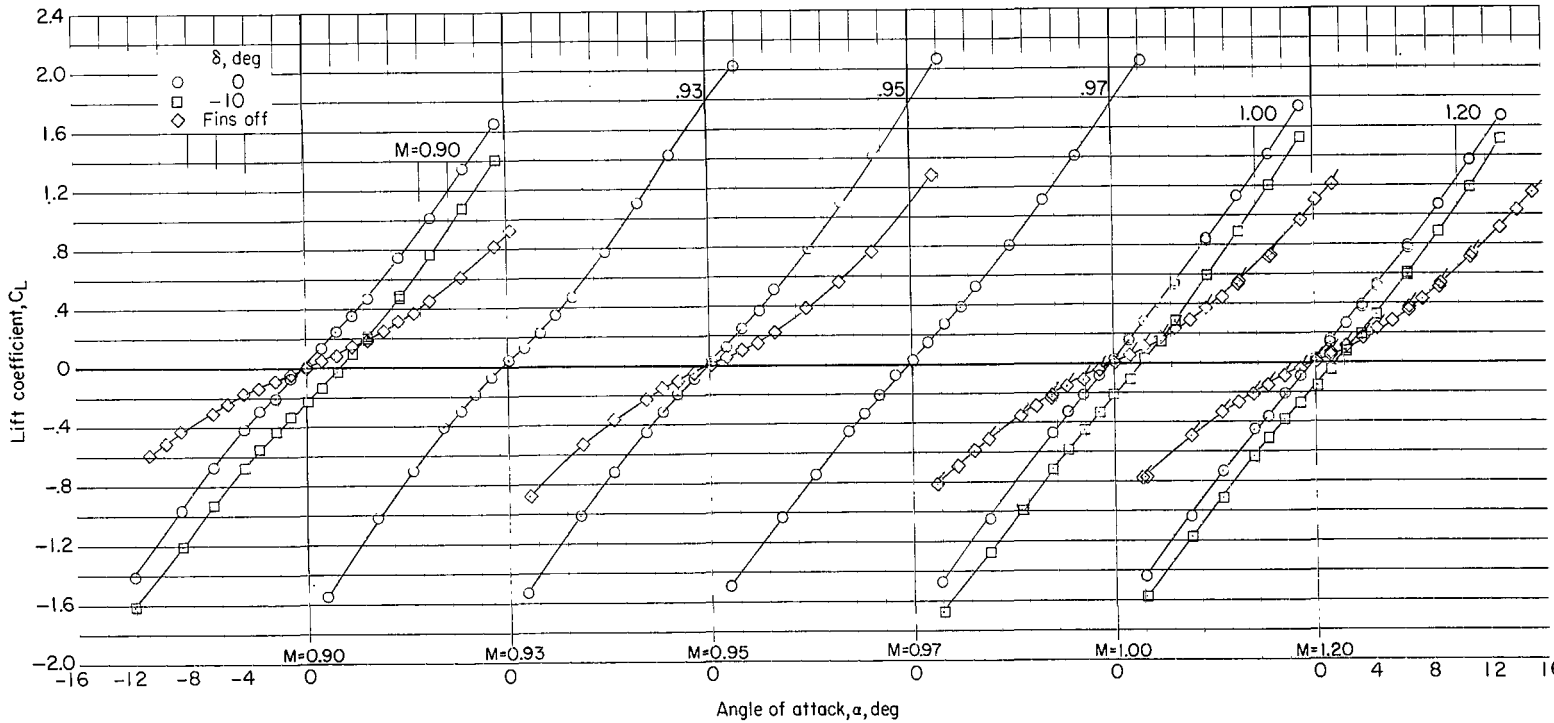

(e) C_L against α. Concluded.

Figure 11.- Continued.

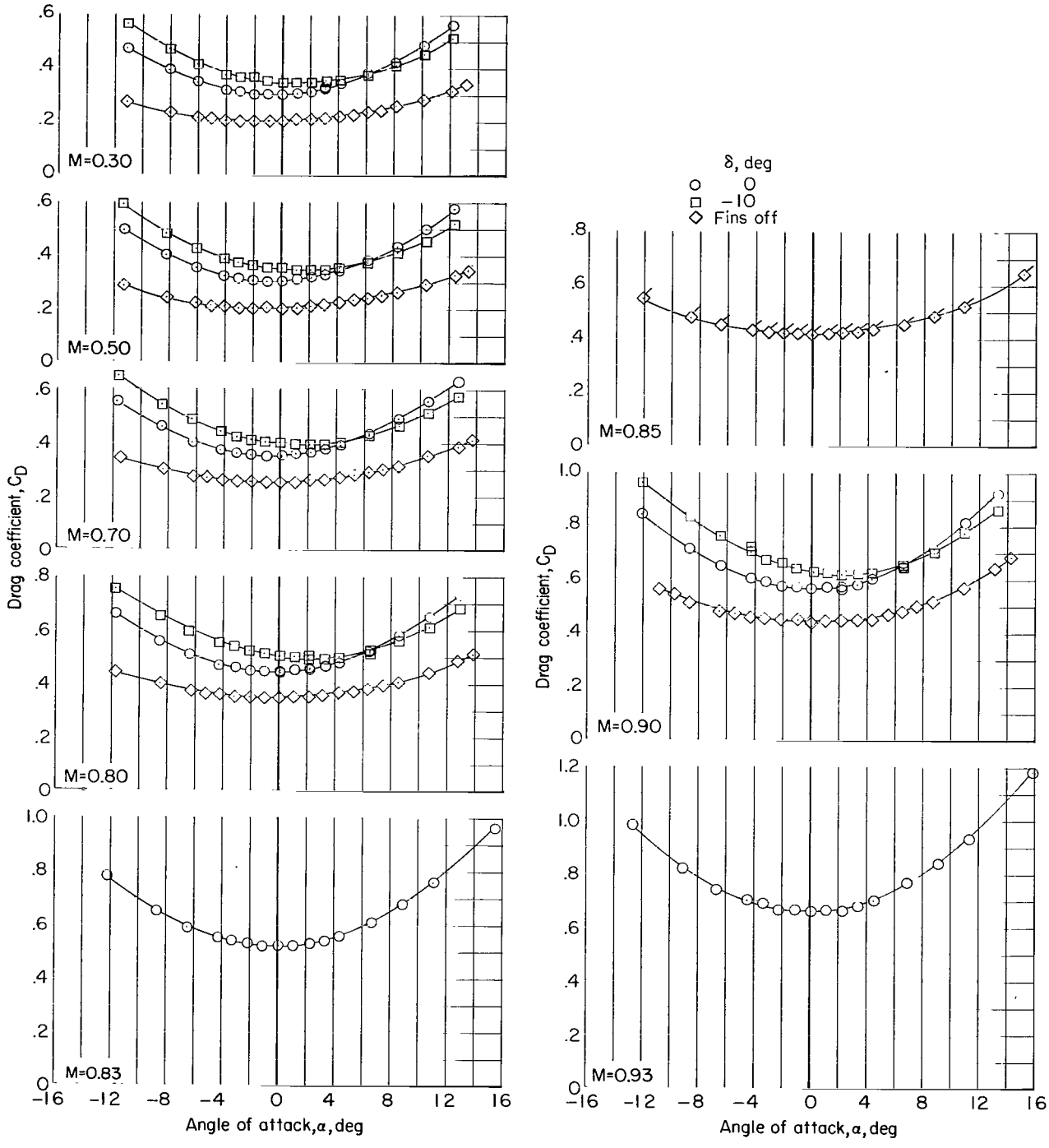

(f) C_D against α.

Figure 11.- Continued.

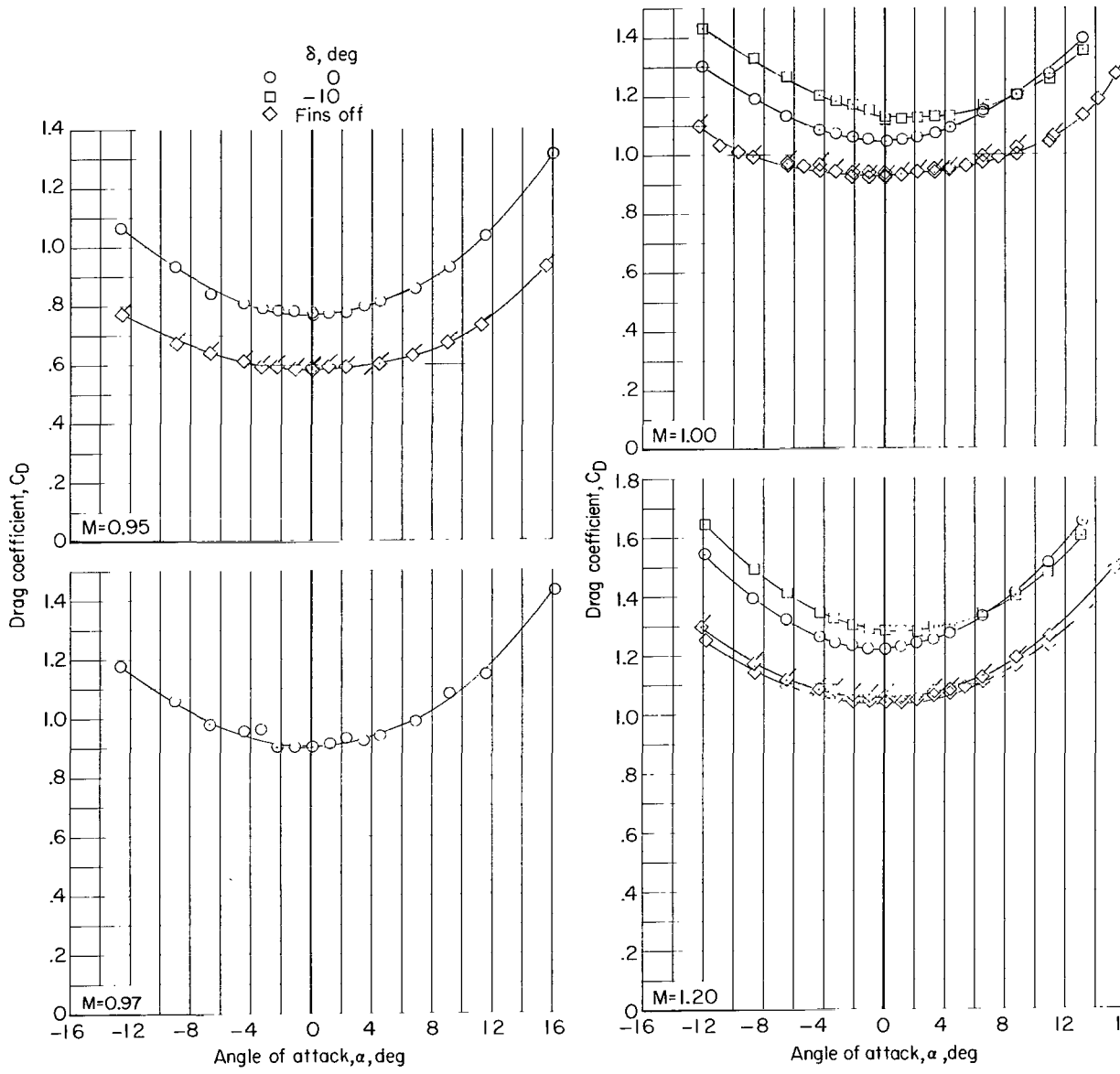

(f) C_D against α. Concluded.

Figure 11.- Continued.

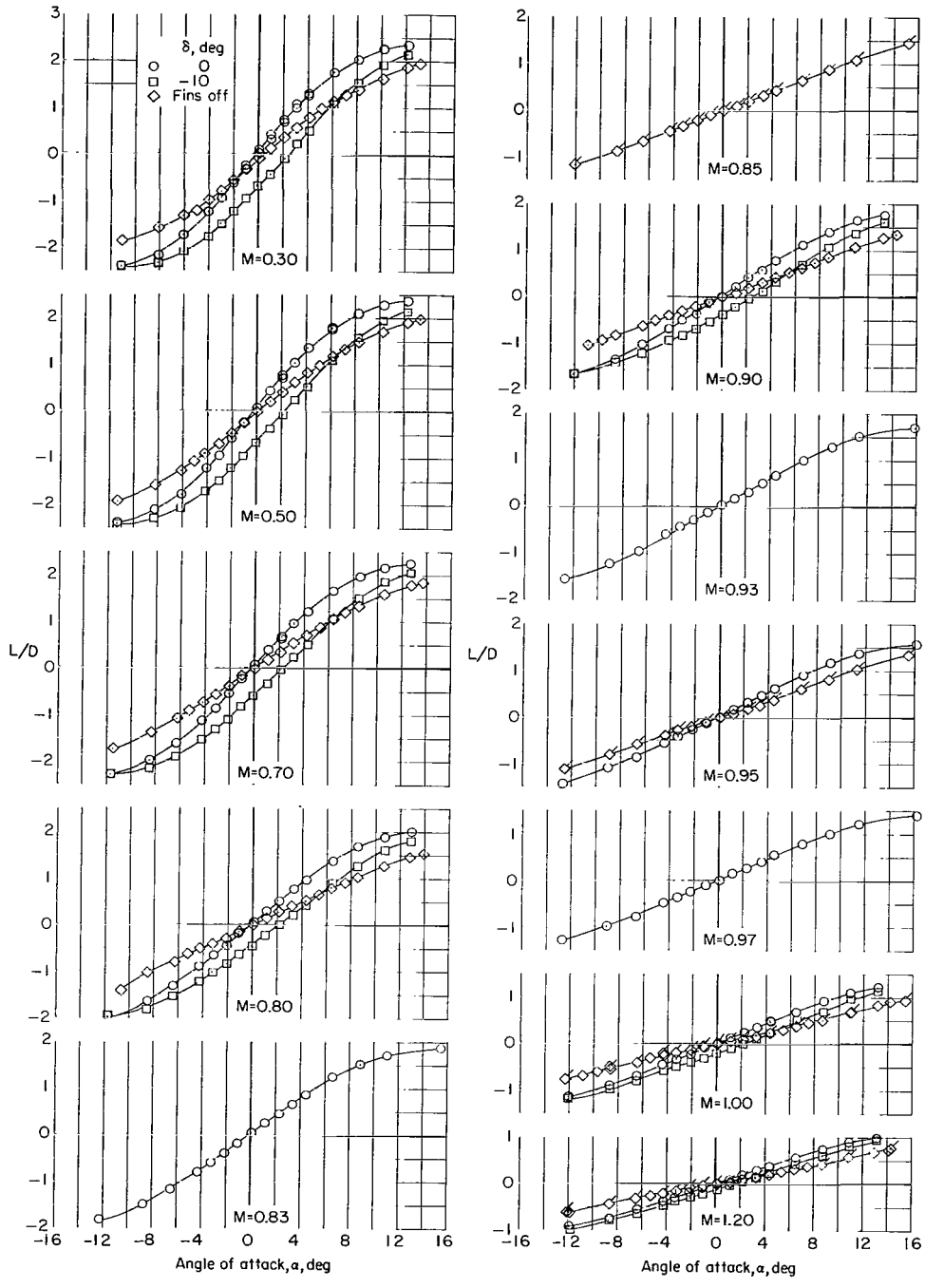

(g) L/D against α.

Figure 11.- Continued.

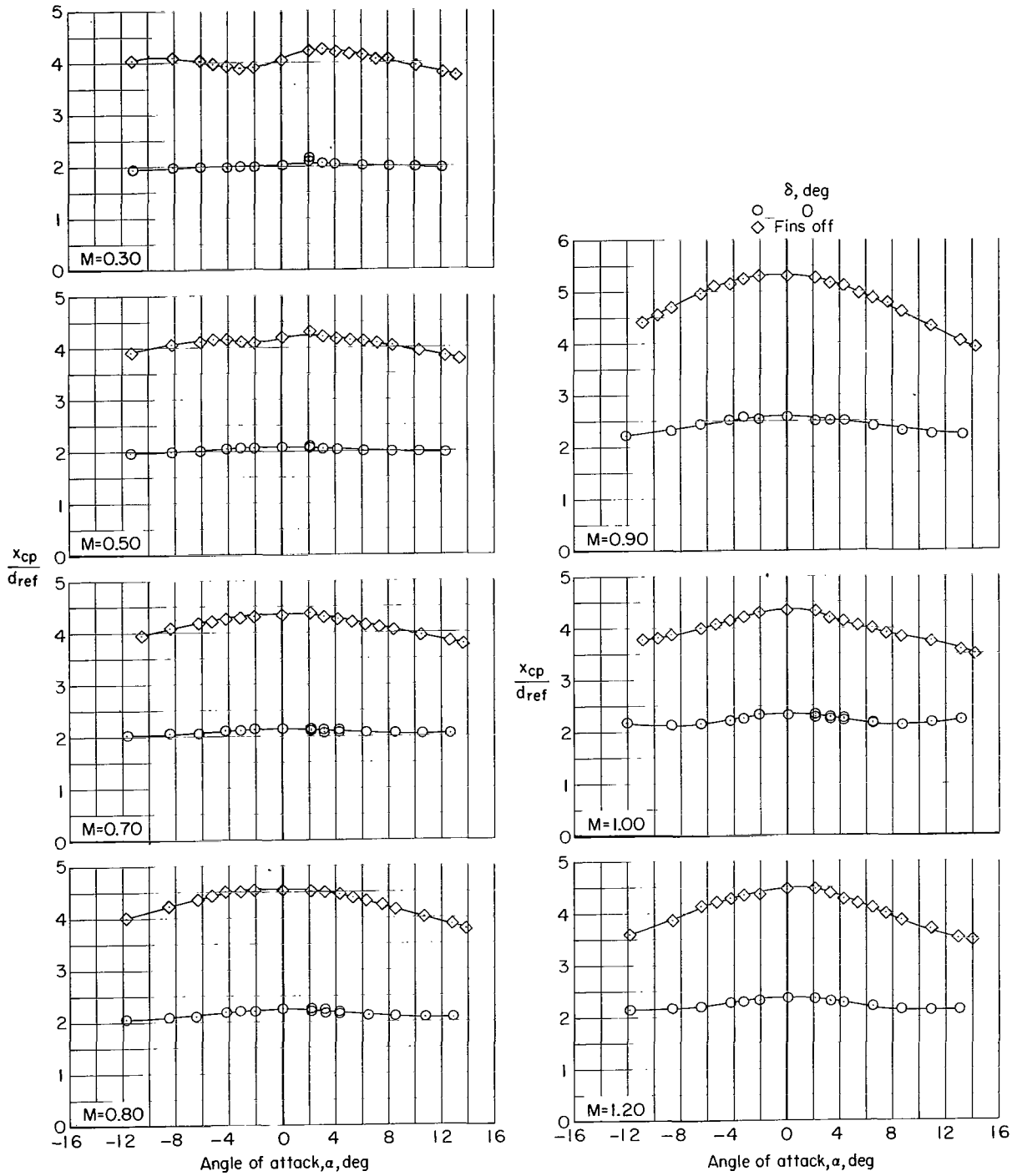

(h) x_{cp}/d_{ref} against α.

Figure 11.- Continued.

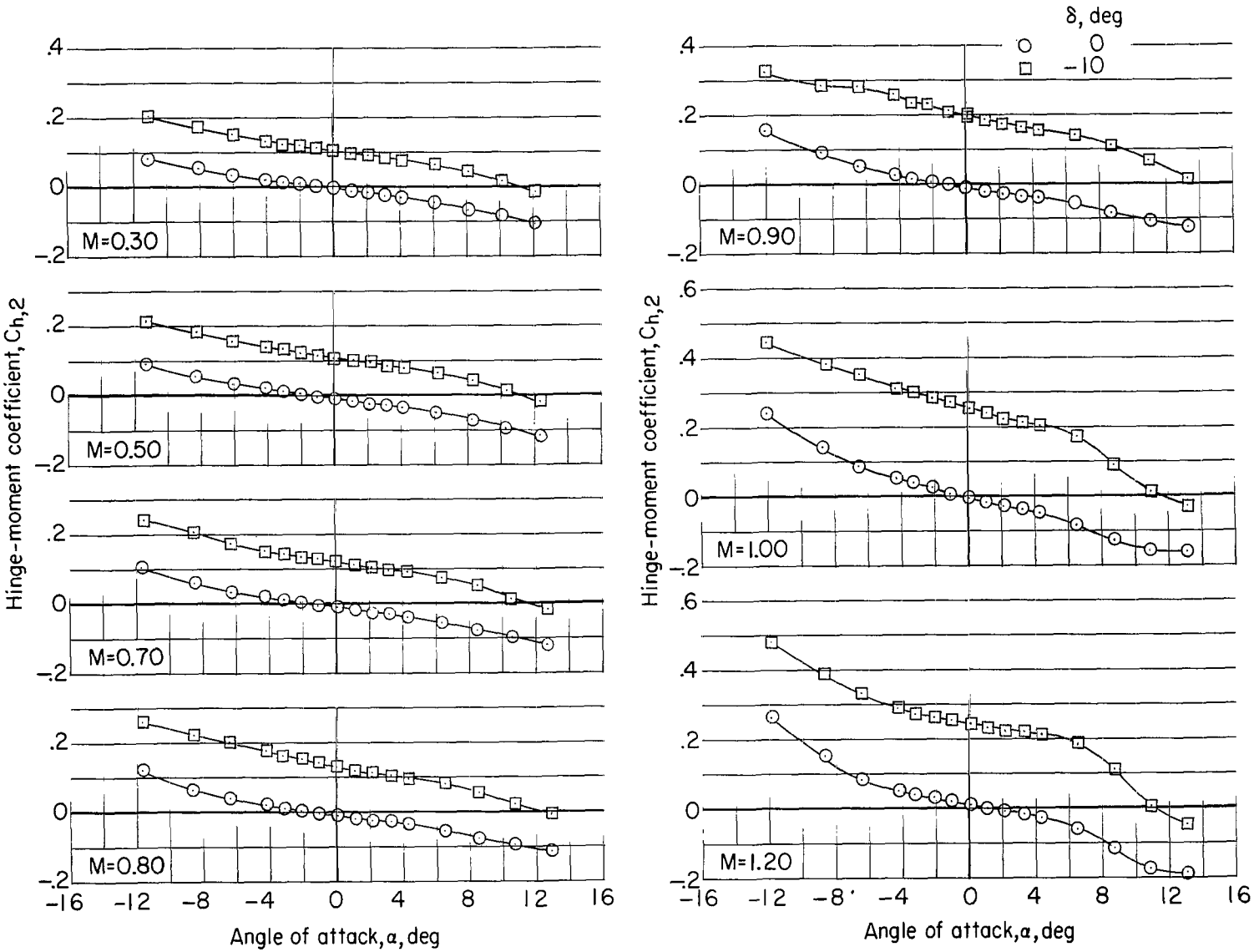

(i) $C_{h,2}$ against α.

Figure 11.- Concluded.

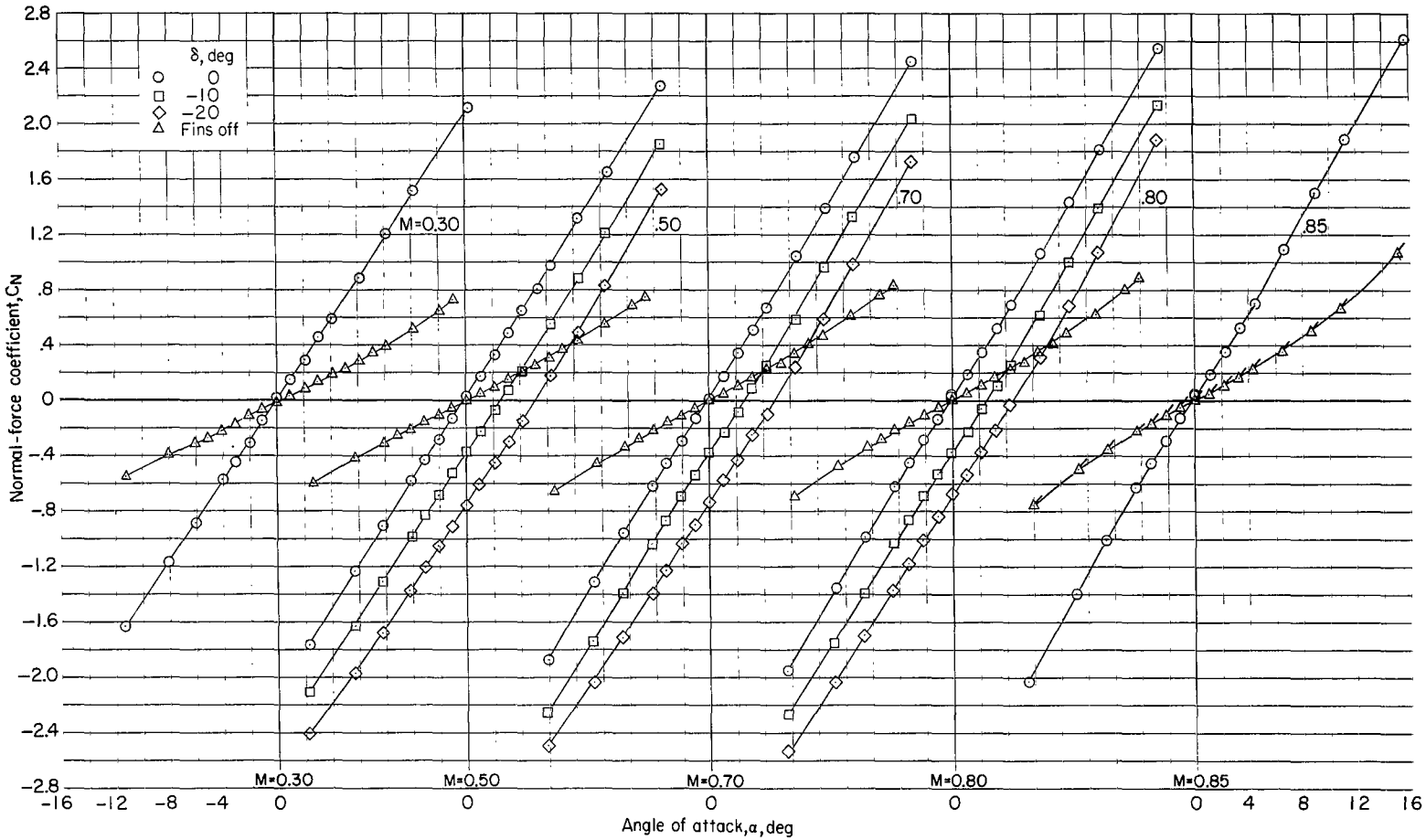

(a) C_N against α.

Figure 12.- Effect of deflection of trailing-edge controls on longitudinal aerodynamic characteristics. Shroud nose 1; intermediate fins; shroud skirt off. (Flagged symbols indicate points from repeat run.)

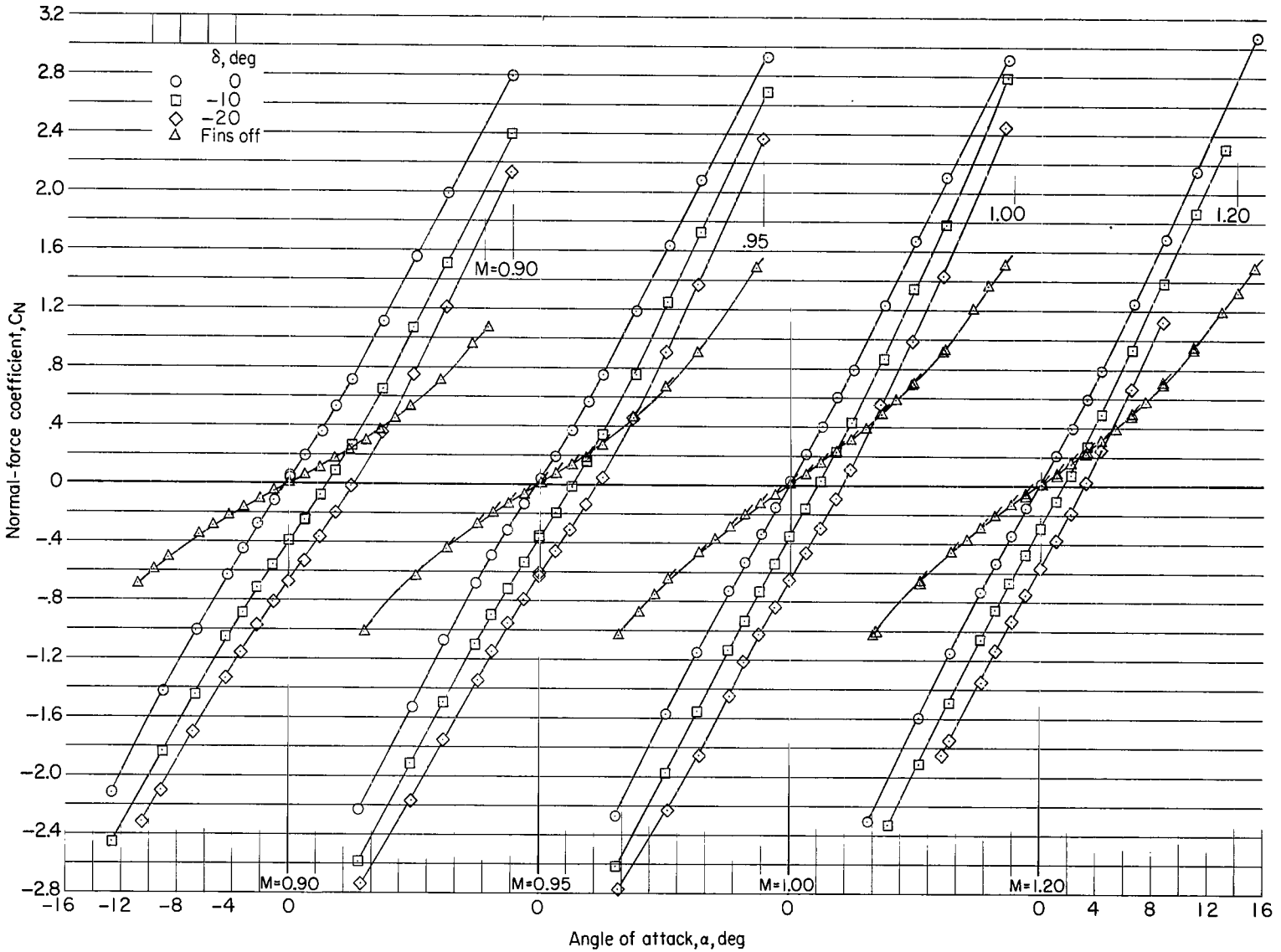

(a) C_N against α. Concluded.

Figure 12.- Continued.

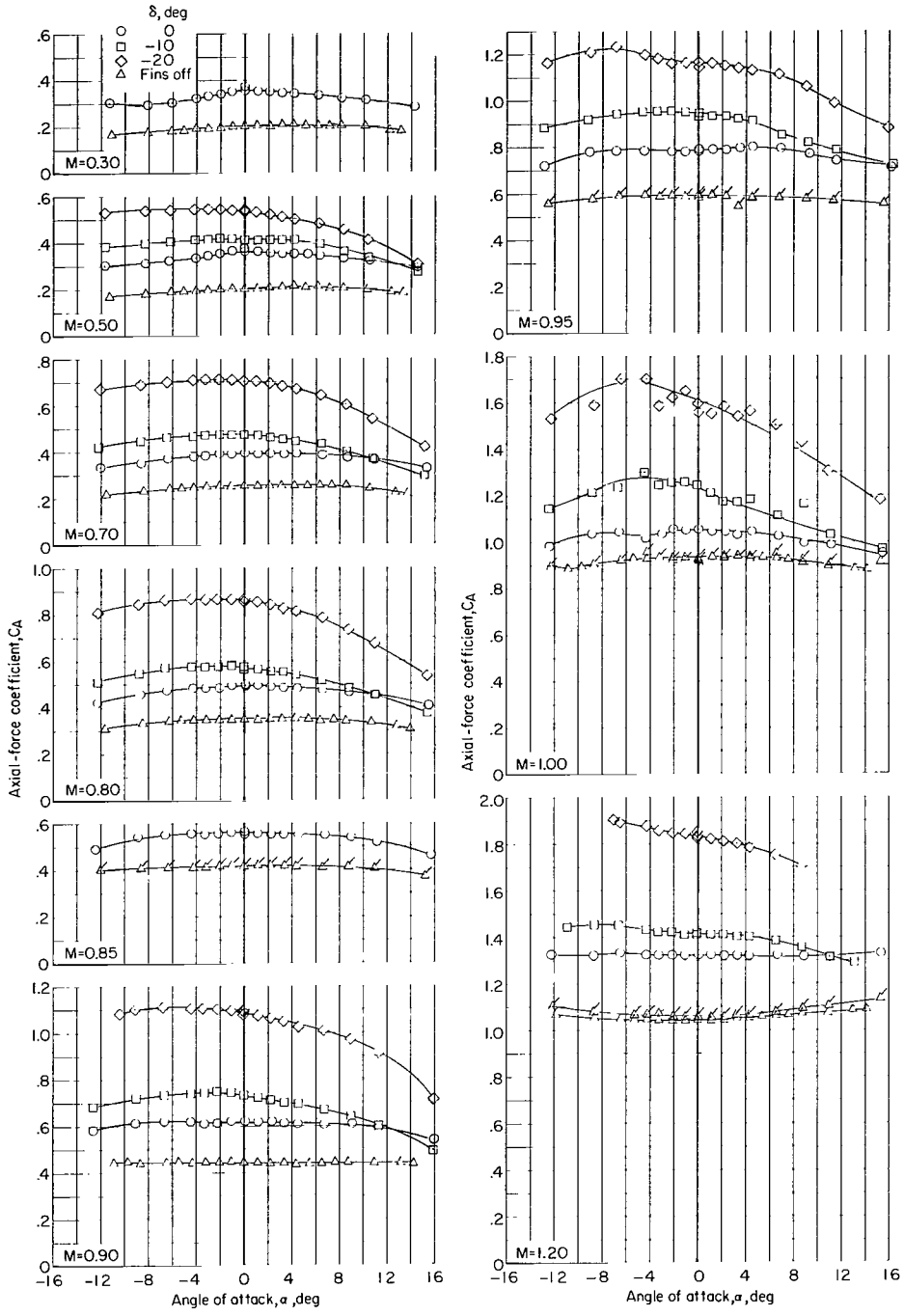

(b) C_A against α.

Figure 12.- Continued.

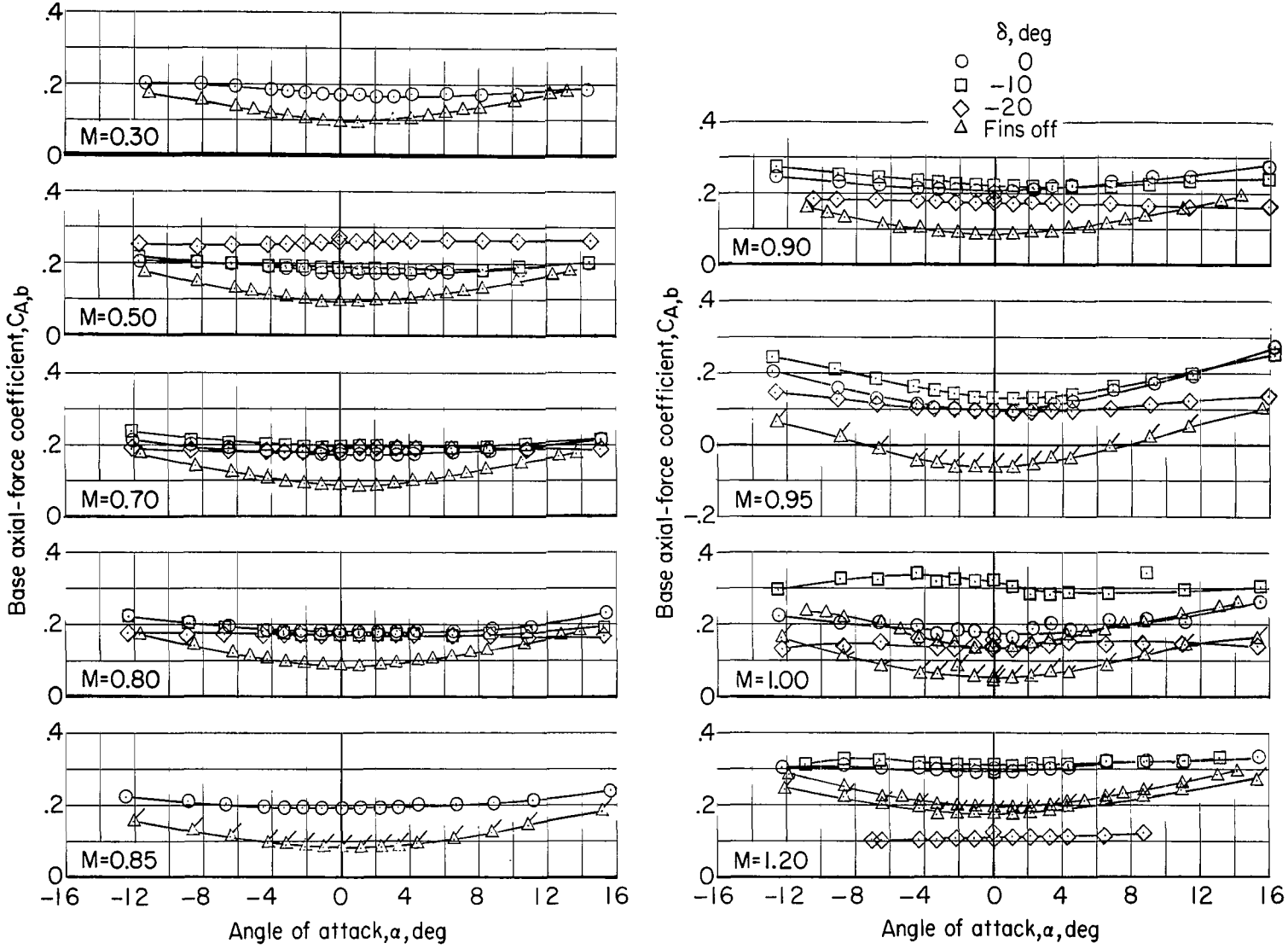

(c) $C_{A,b}$ against α.

Figure 12.- Continued.

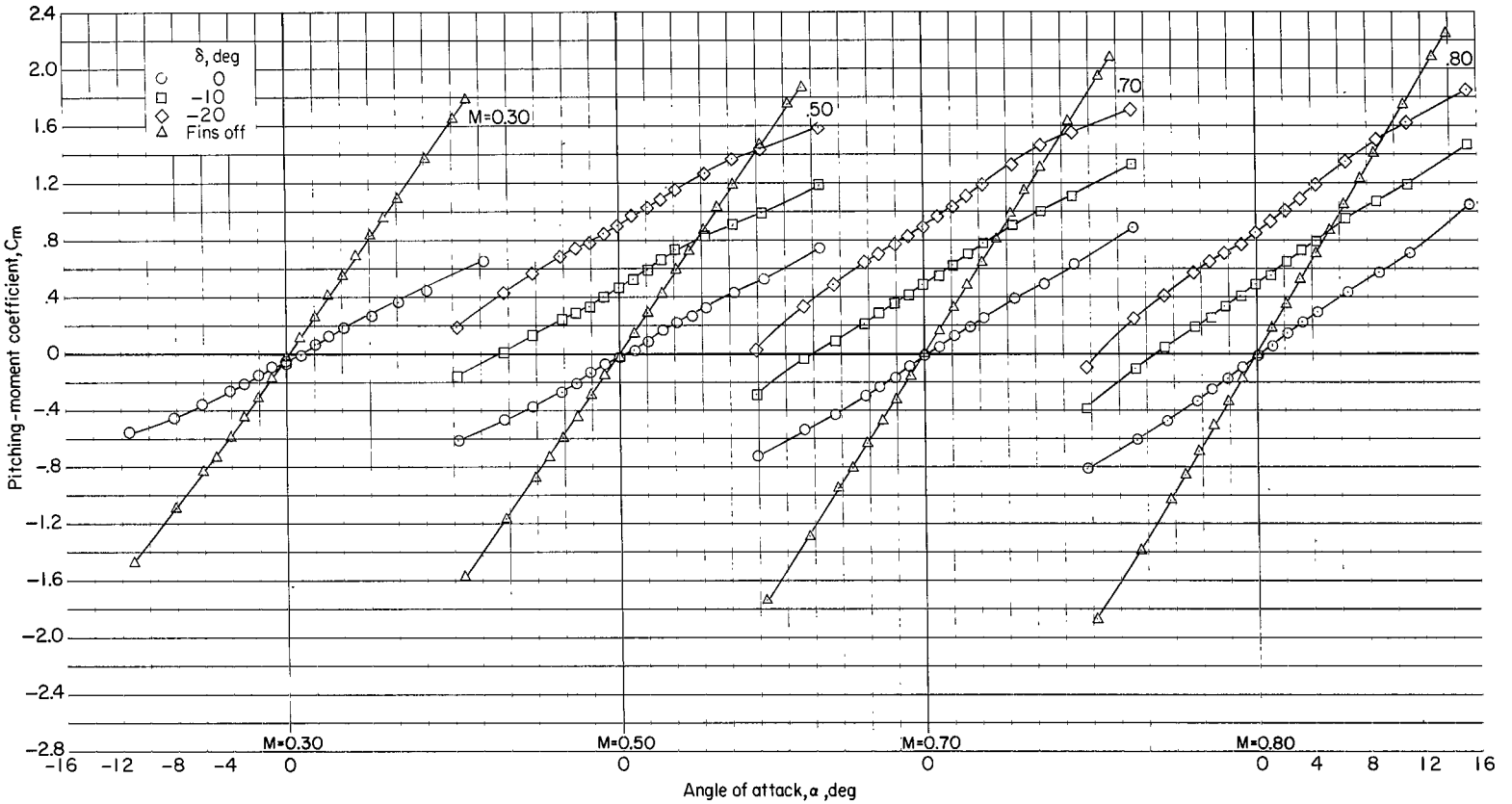

(d) C_m against α.

Figure 12.- Continued.

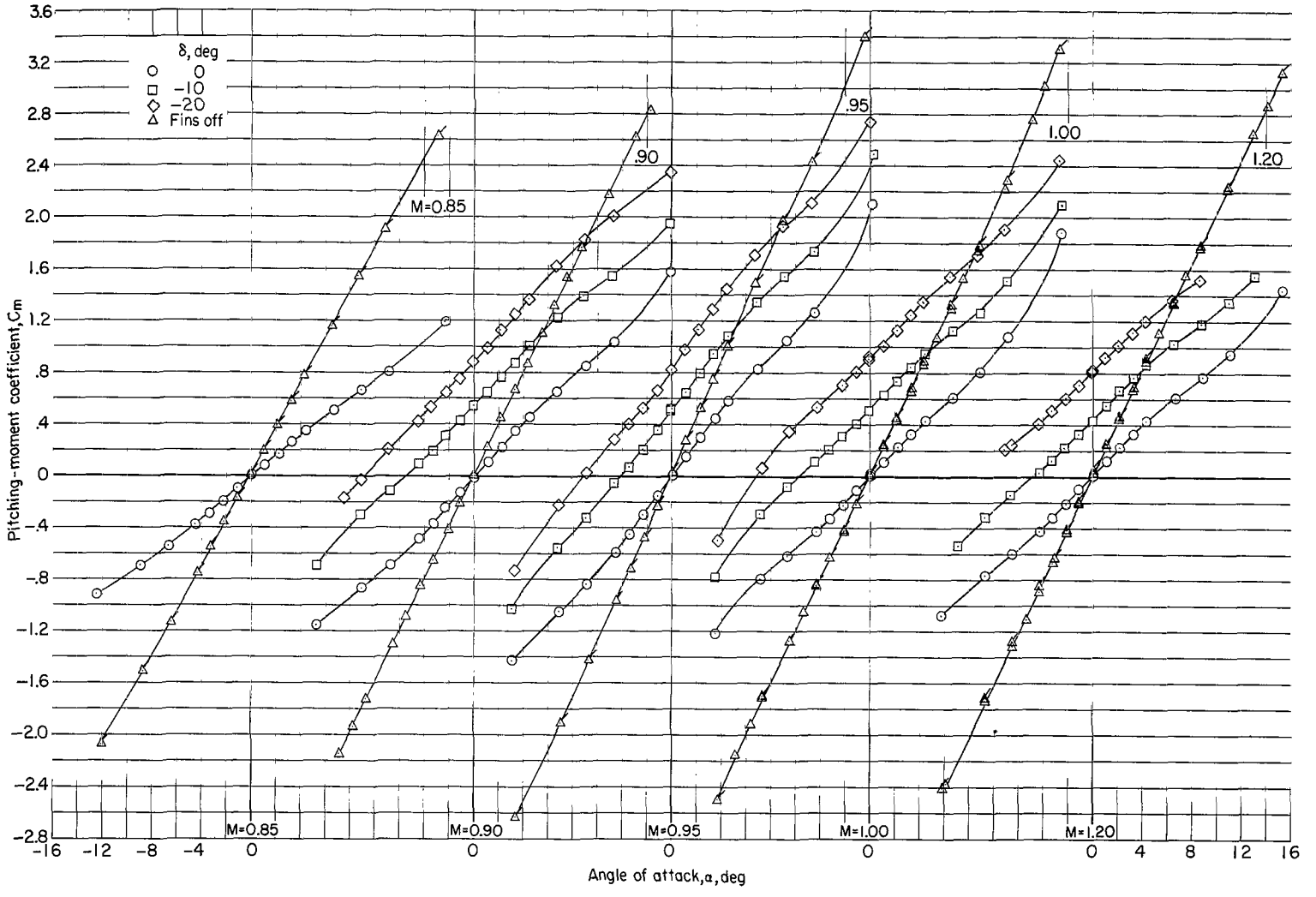

(d) C_m against α. Concluded.

Figure 12.- Continued.

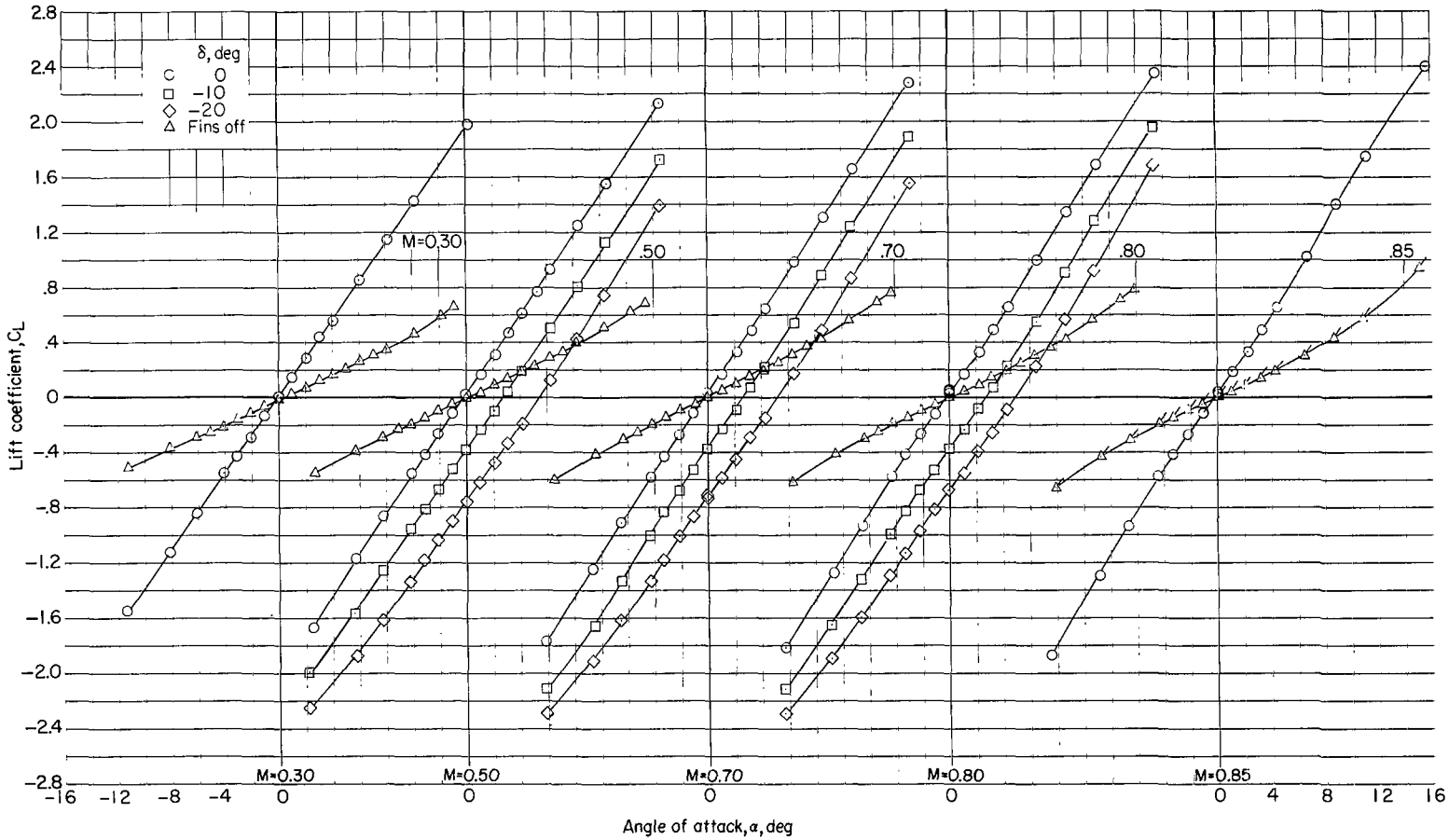

(e) C_L against α.

Figure 12.- Continued.

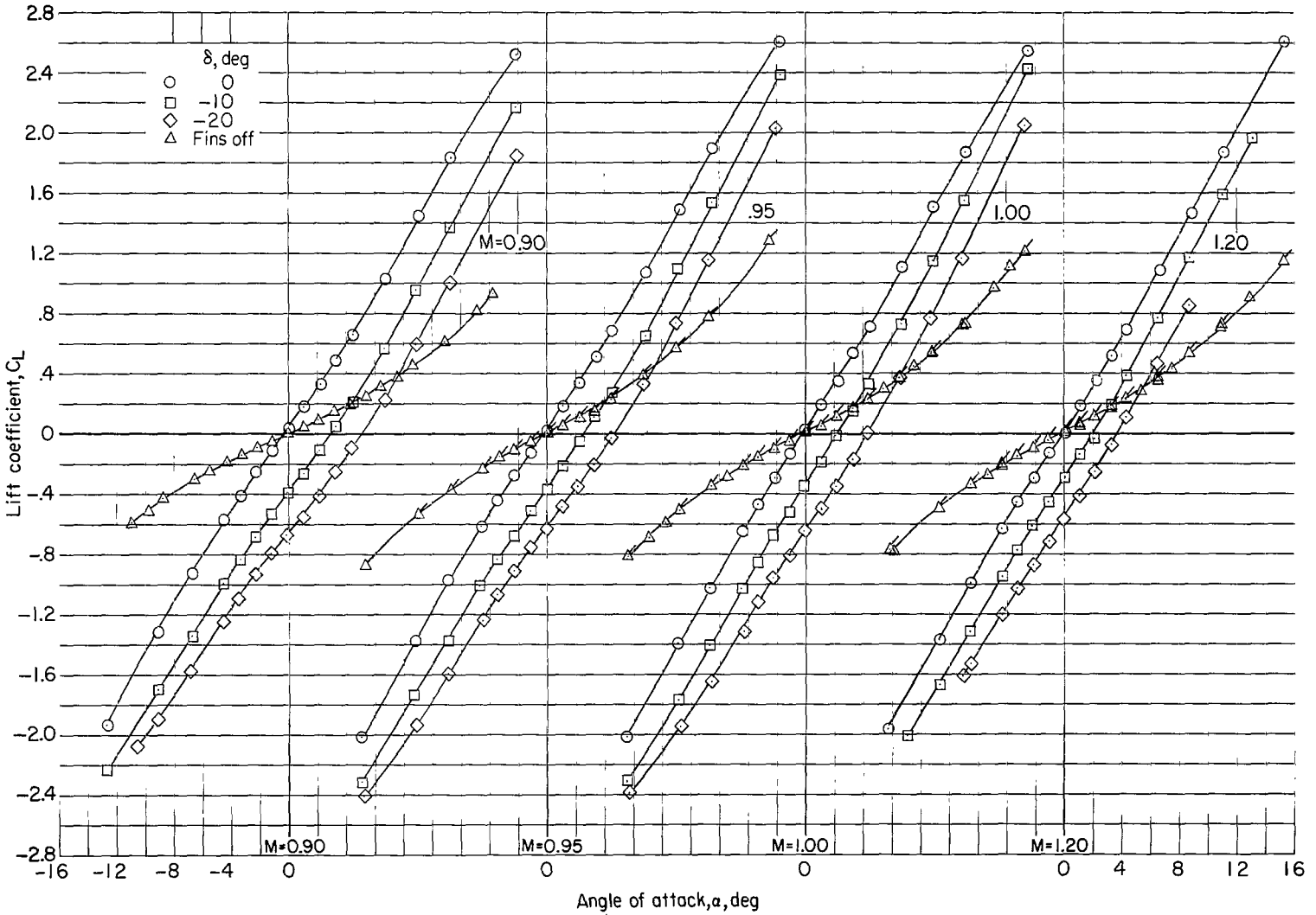

(e) C_L against α. Concluded.

Figure 12.- Continued.

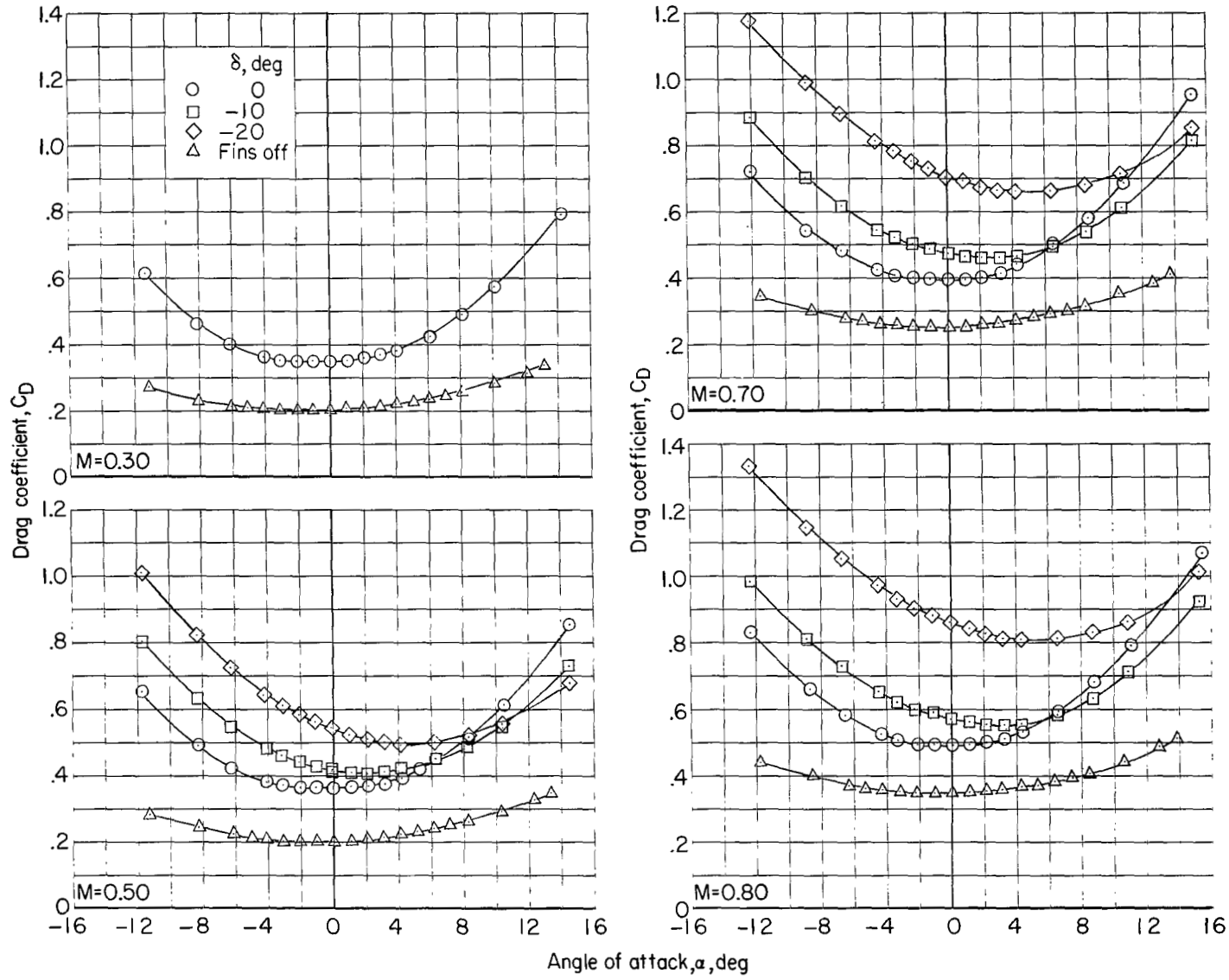

(f) C_D against α.

Figure 12.- Continued.

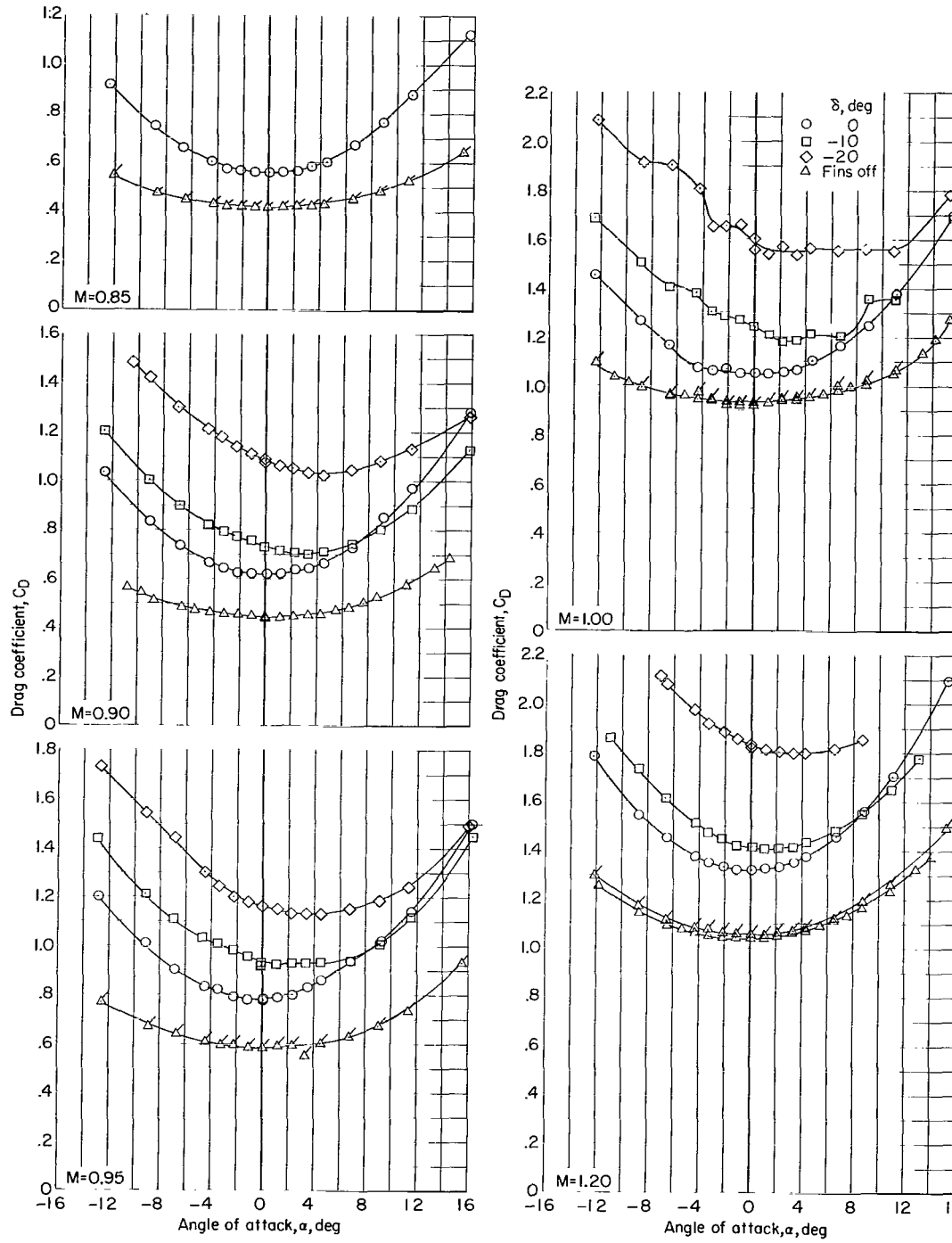

(f) C_D against α. Concluded.

Figure 12.- Continued.

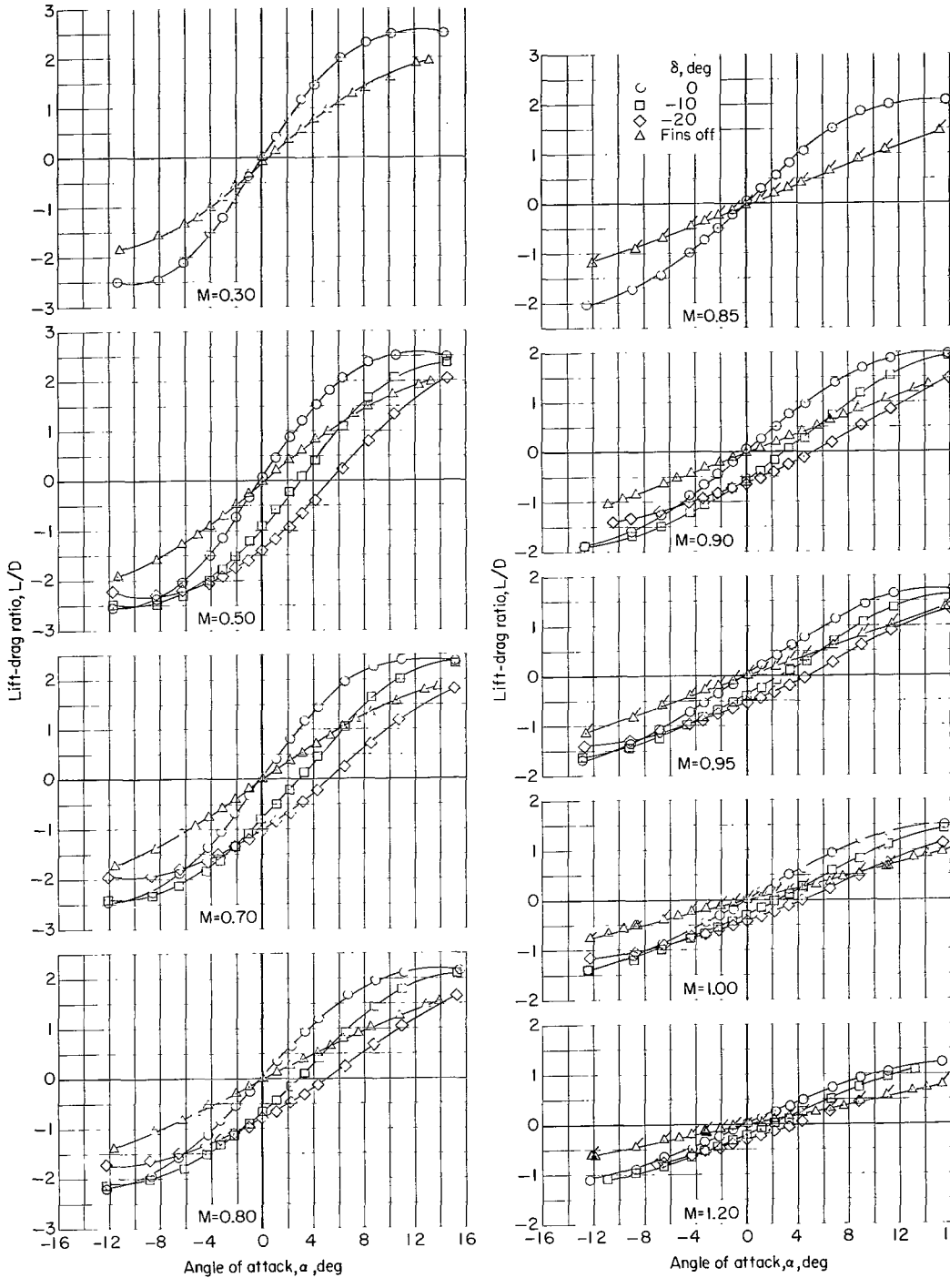

(g) L/D against α.

Figure 12.- Continued.

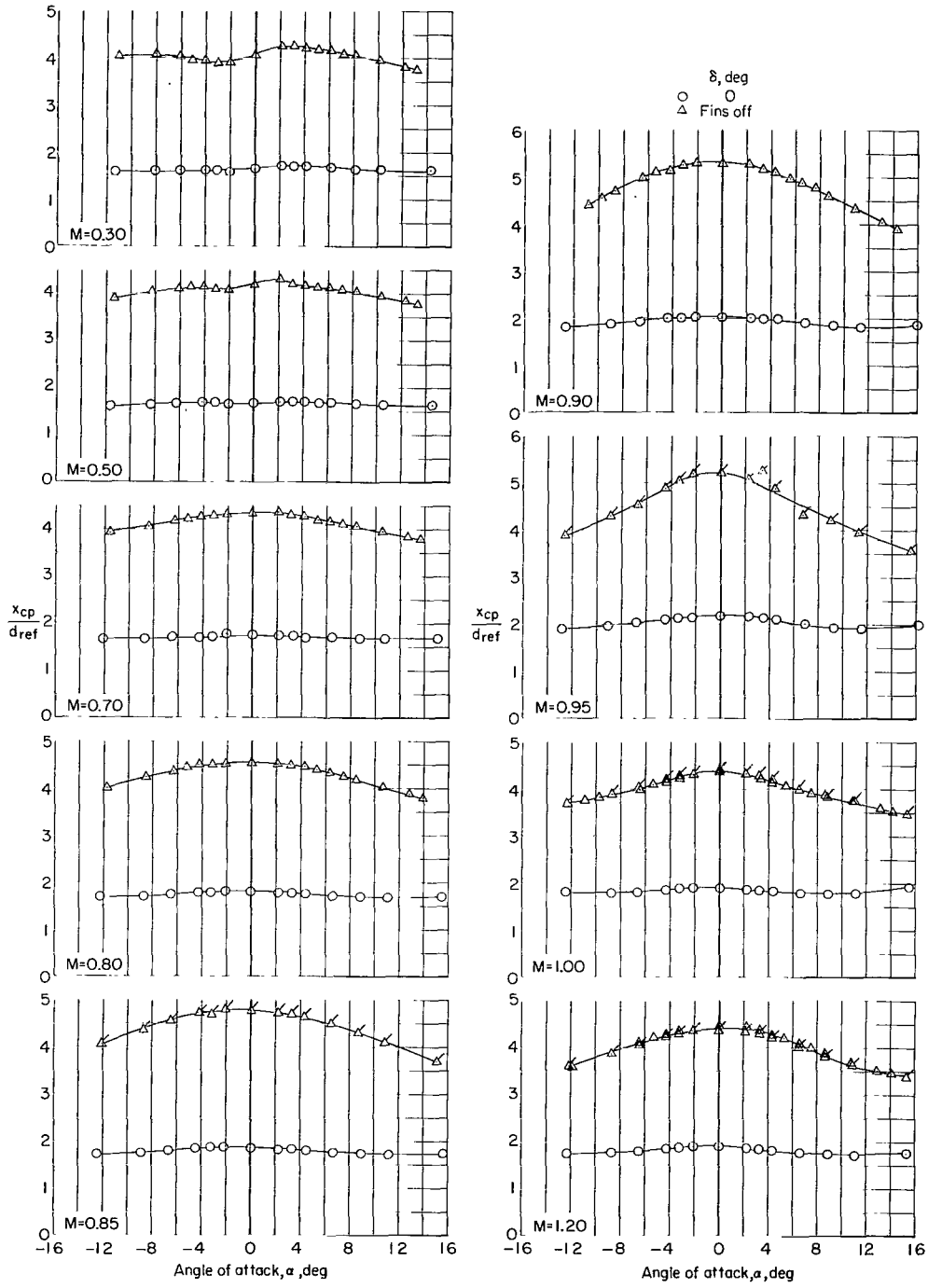

(h) x_{cp}/d_{ref} against α.

Figure 12.- Concluded.

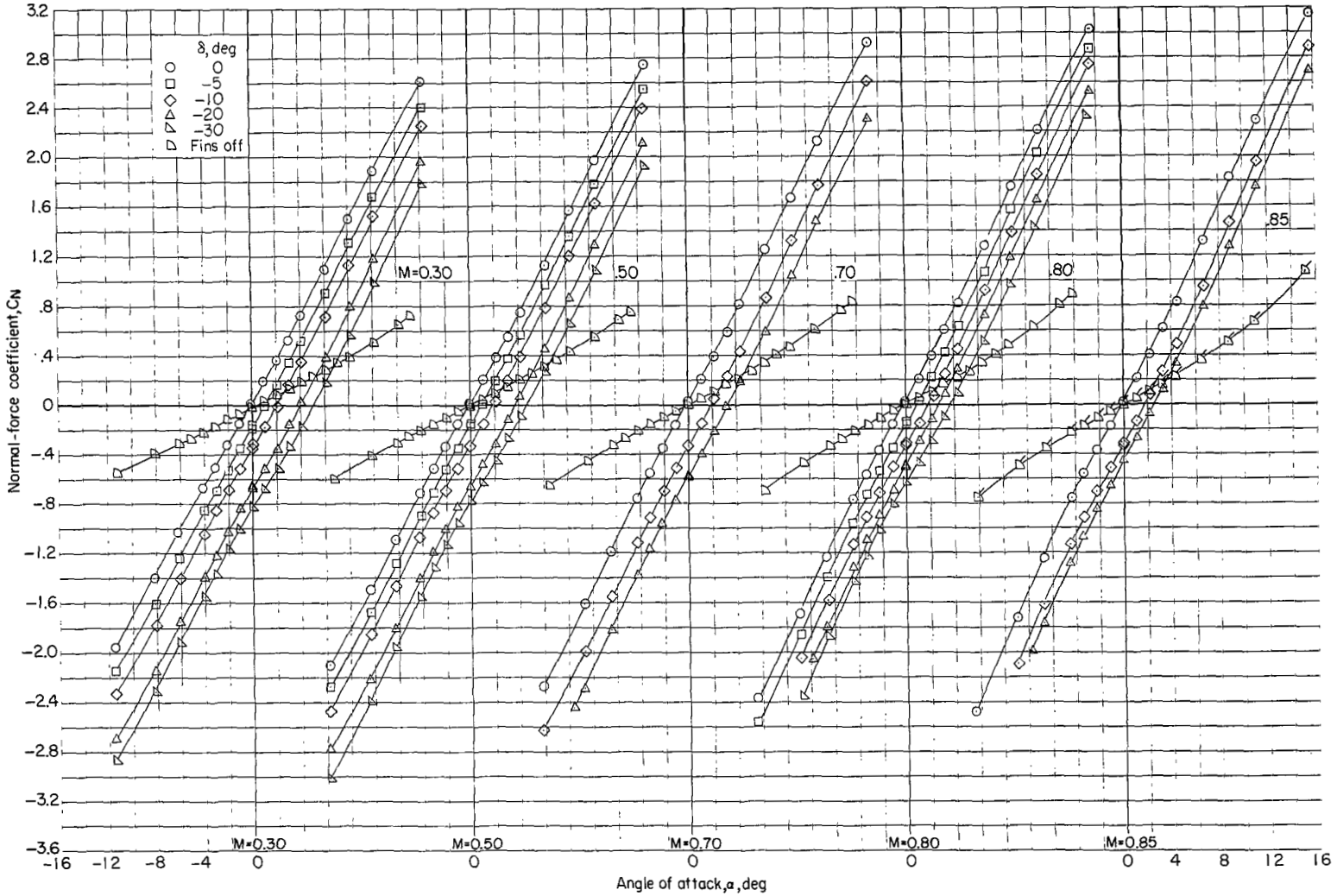

(a) C_N against α.

Figure 13.- Effect of deflection of trailing-edge controls on longitudinal aerodynamic characteristics. Shroud nose 1; large fins; shroud skirt off. (Flagged symbols indicate points from repeat run.)

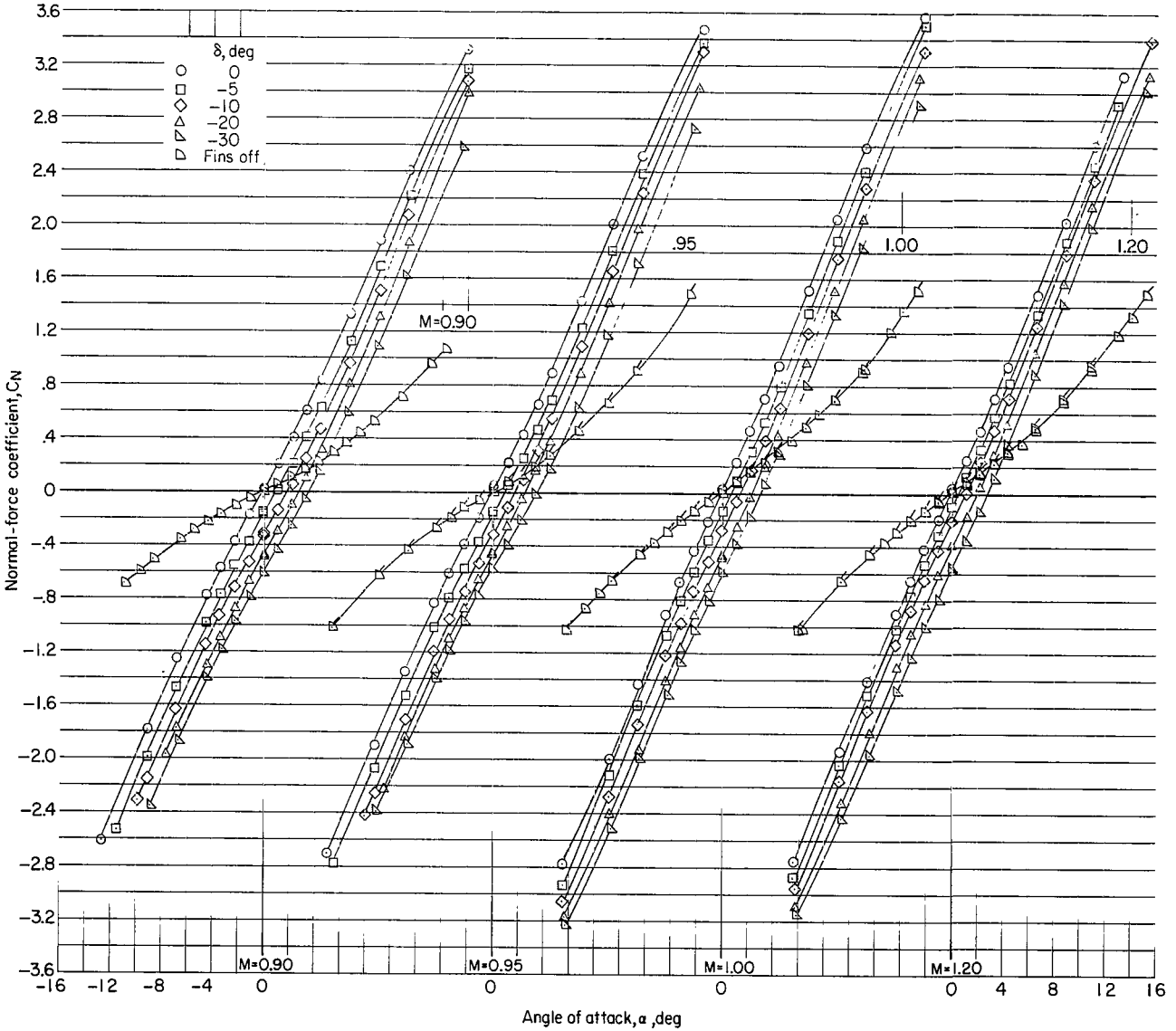

(a) C_N against α. Concluded.

Figure 13.- Continued.

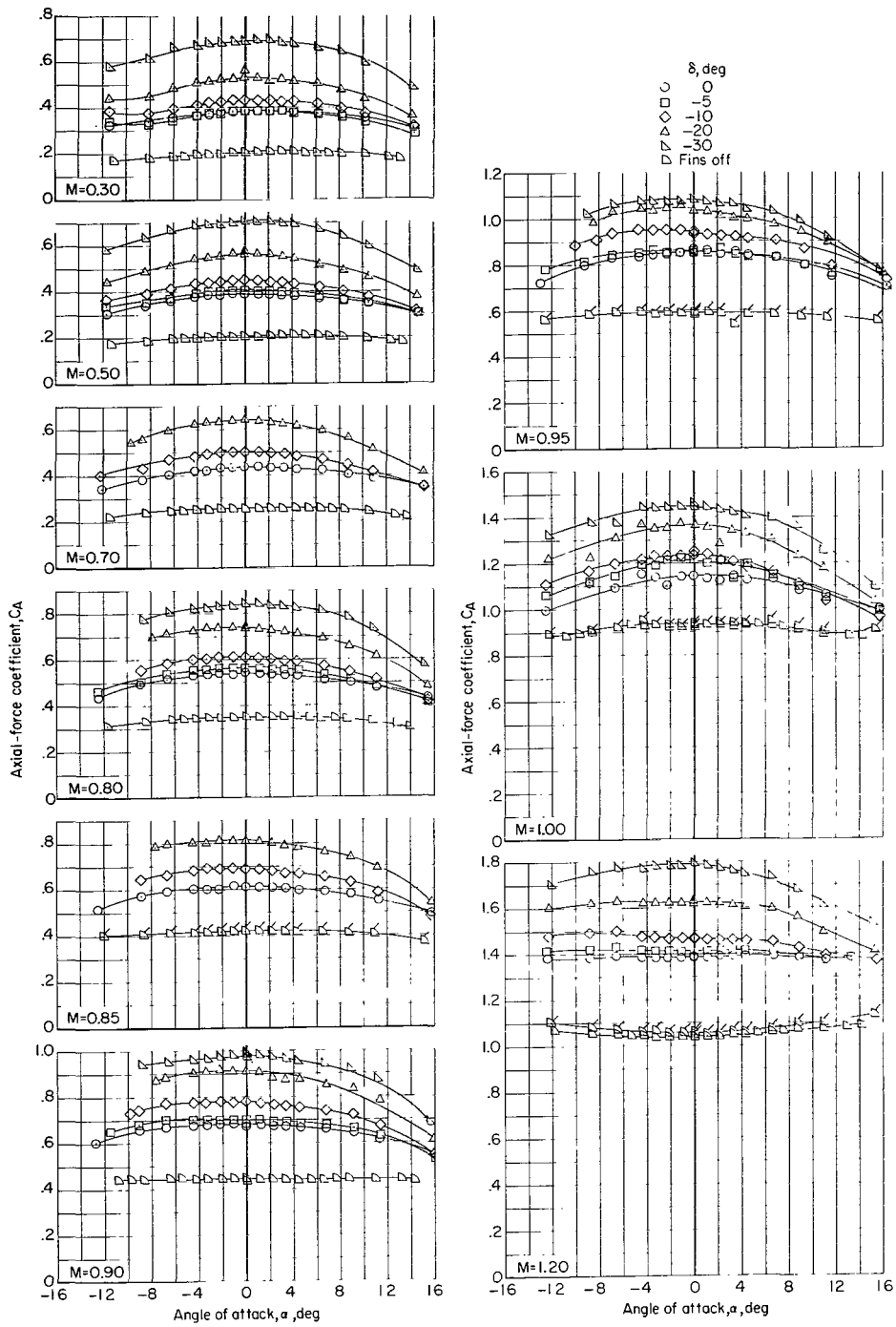

(b) C_A against α.

Figure 13.- Continued.

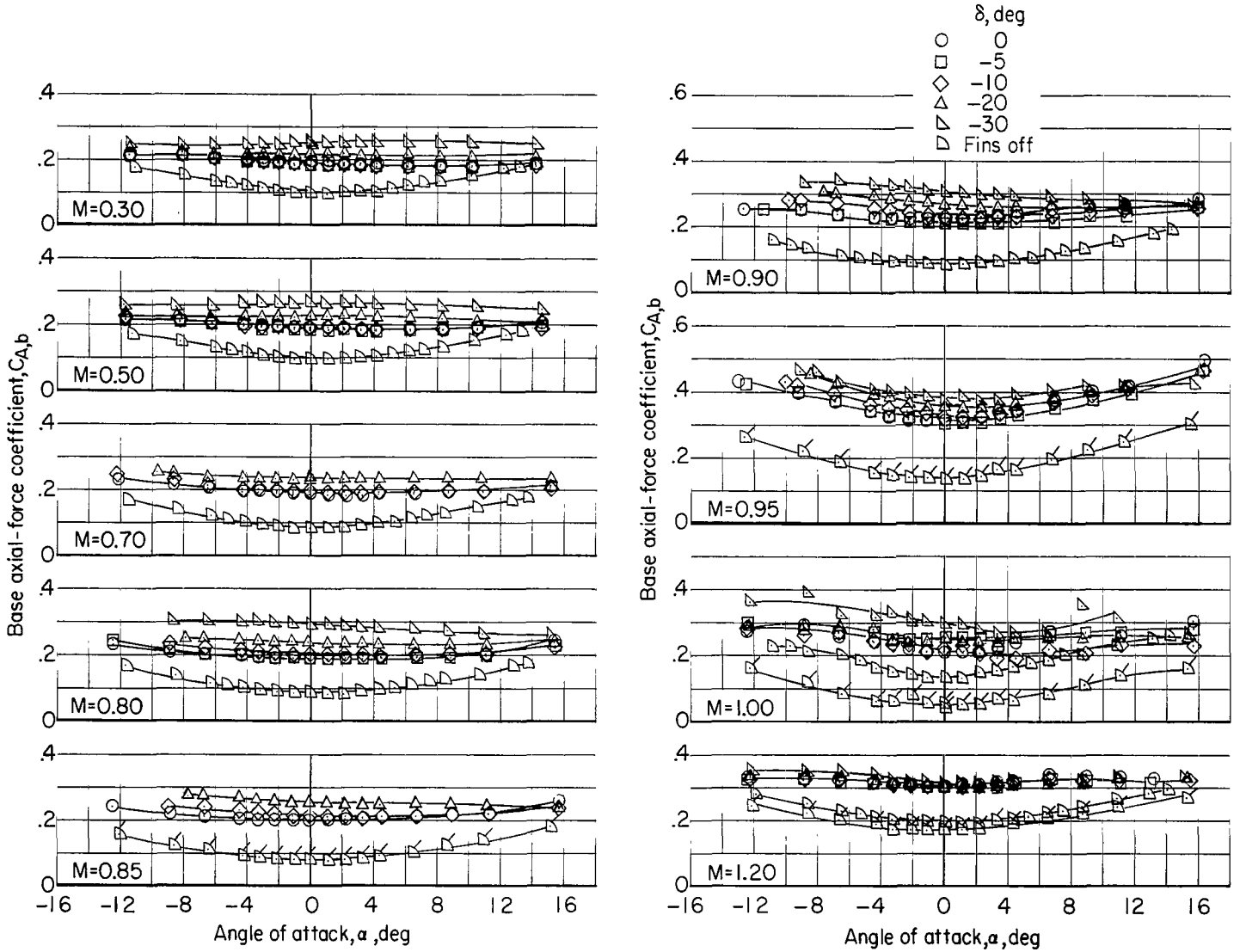

(c) $C_{A,b}$ against α.

Figure 13.- Continued.

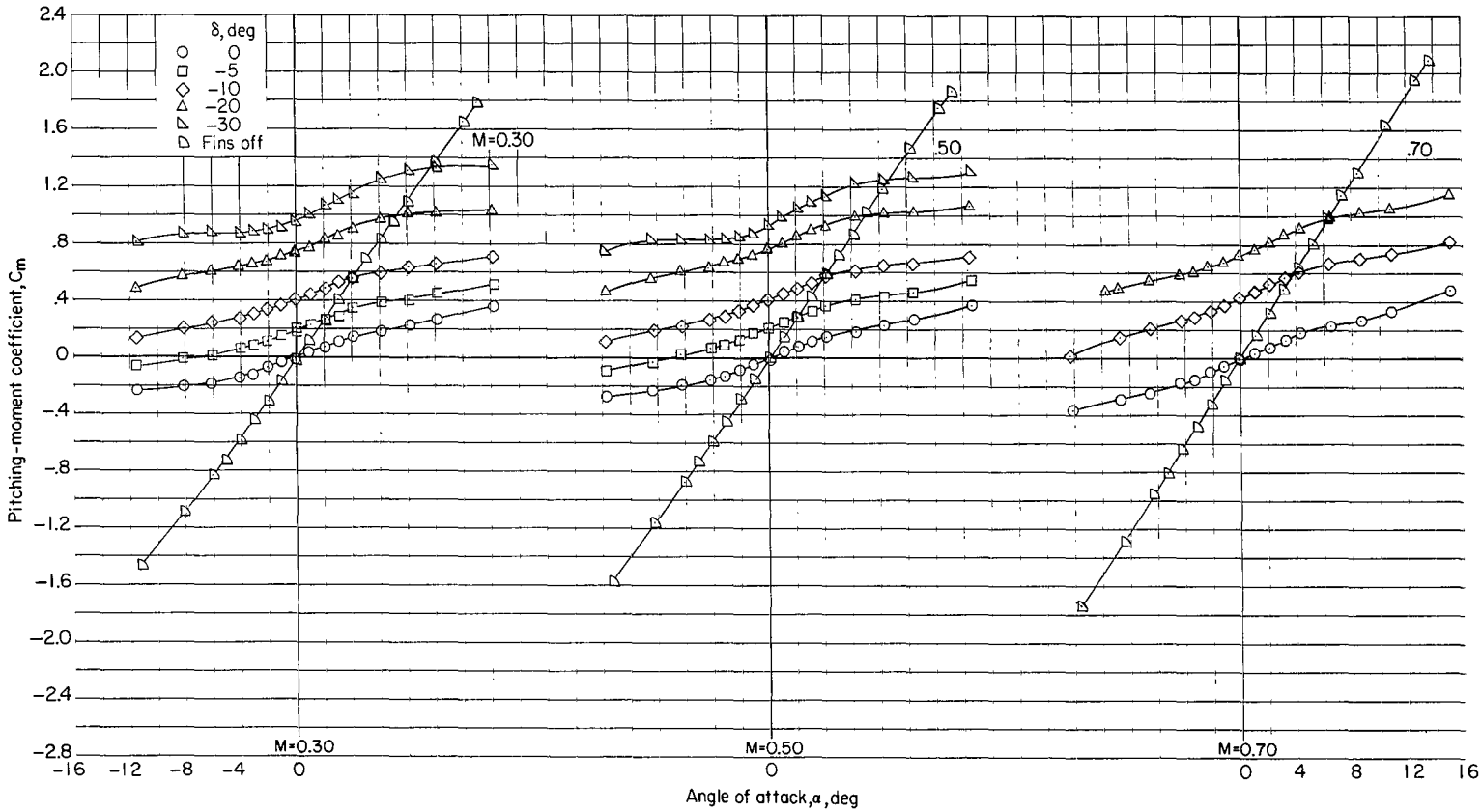

(d) C_m against α.

Figure 13.- Continued.

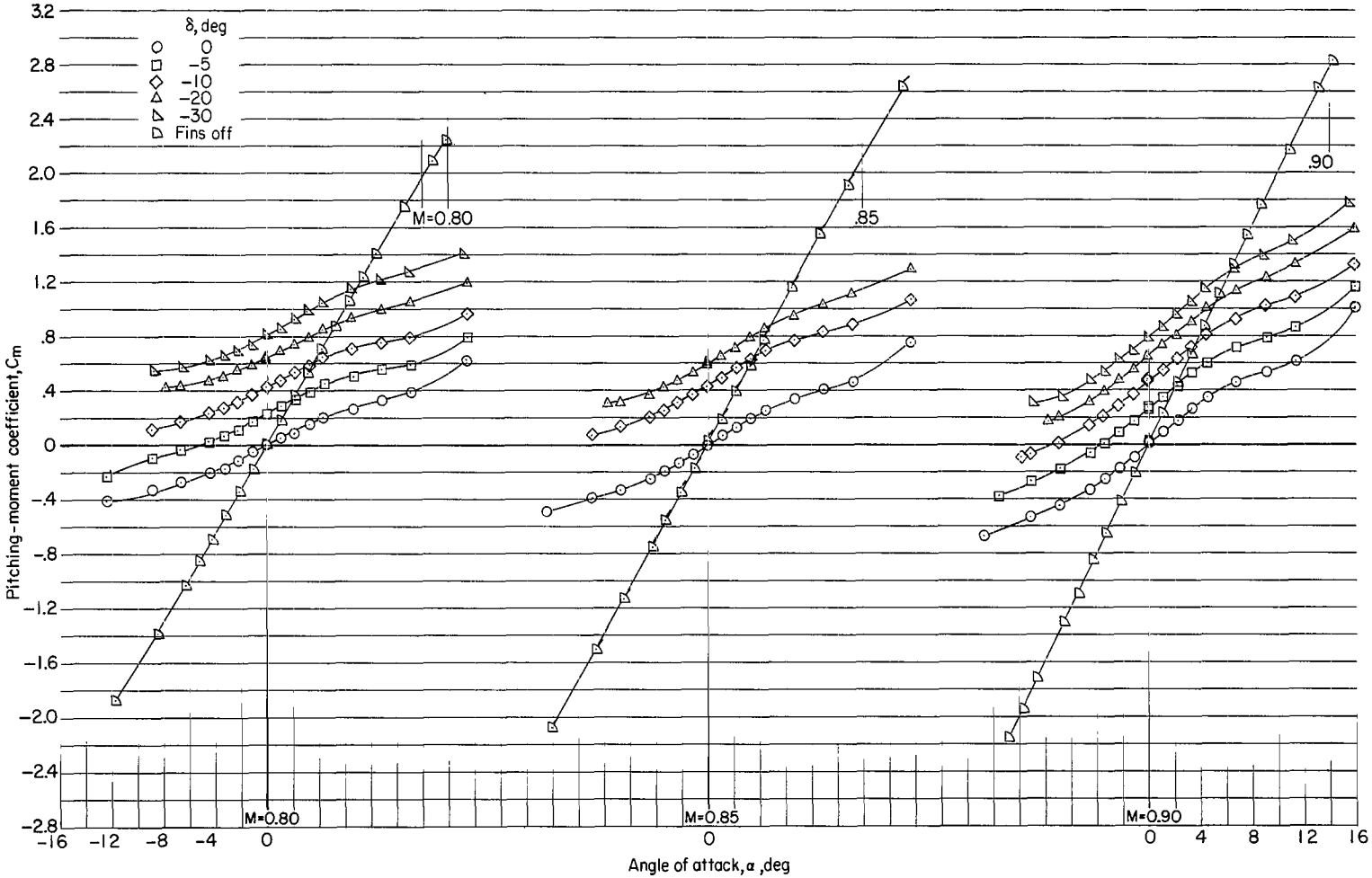

(d) C_m against α. Continued.

Figure 13.- Continued.

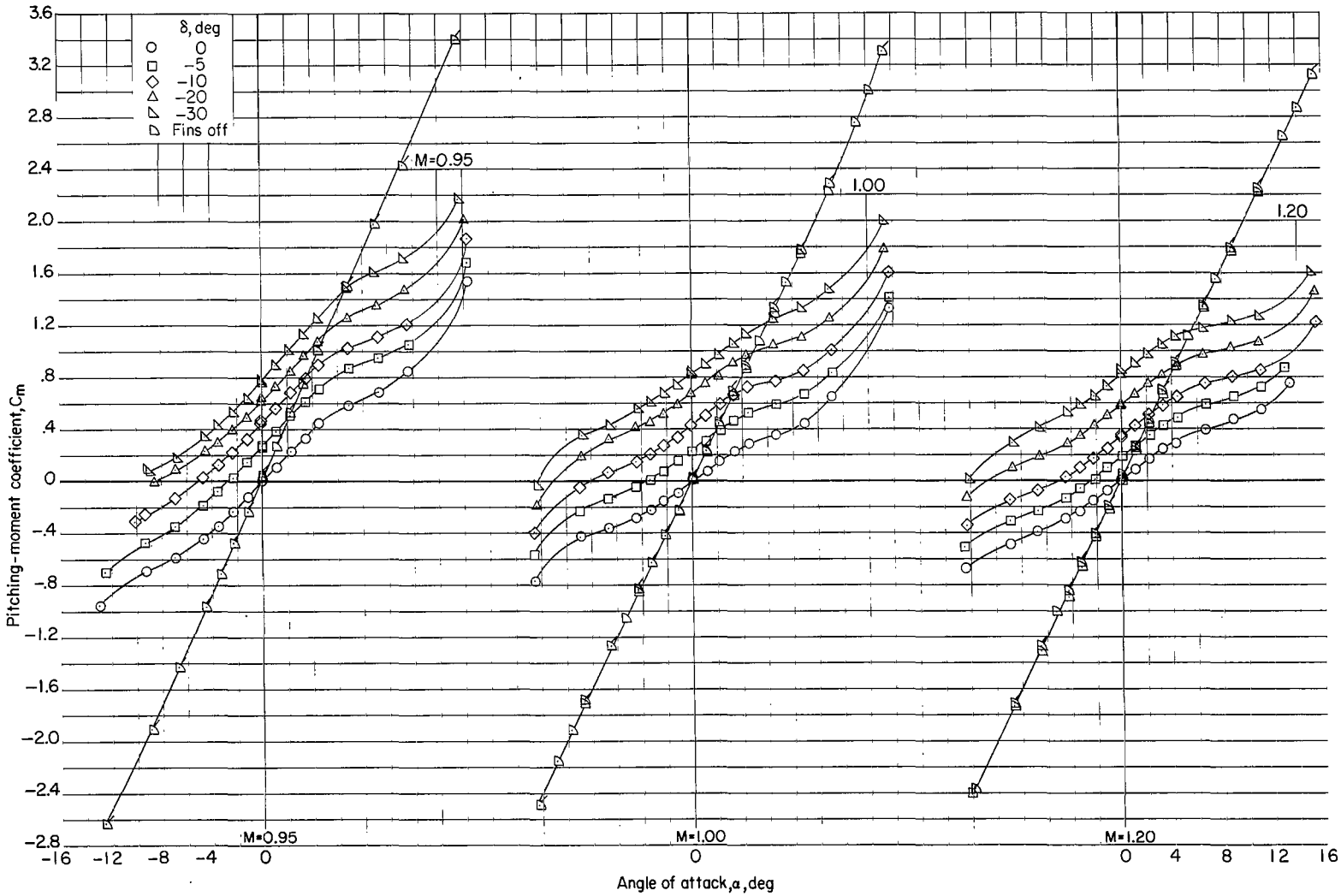

(d) C_m against α. Concluded.

Figure 13.- Continued.

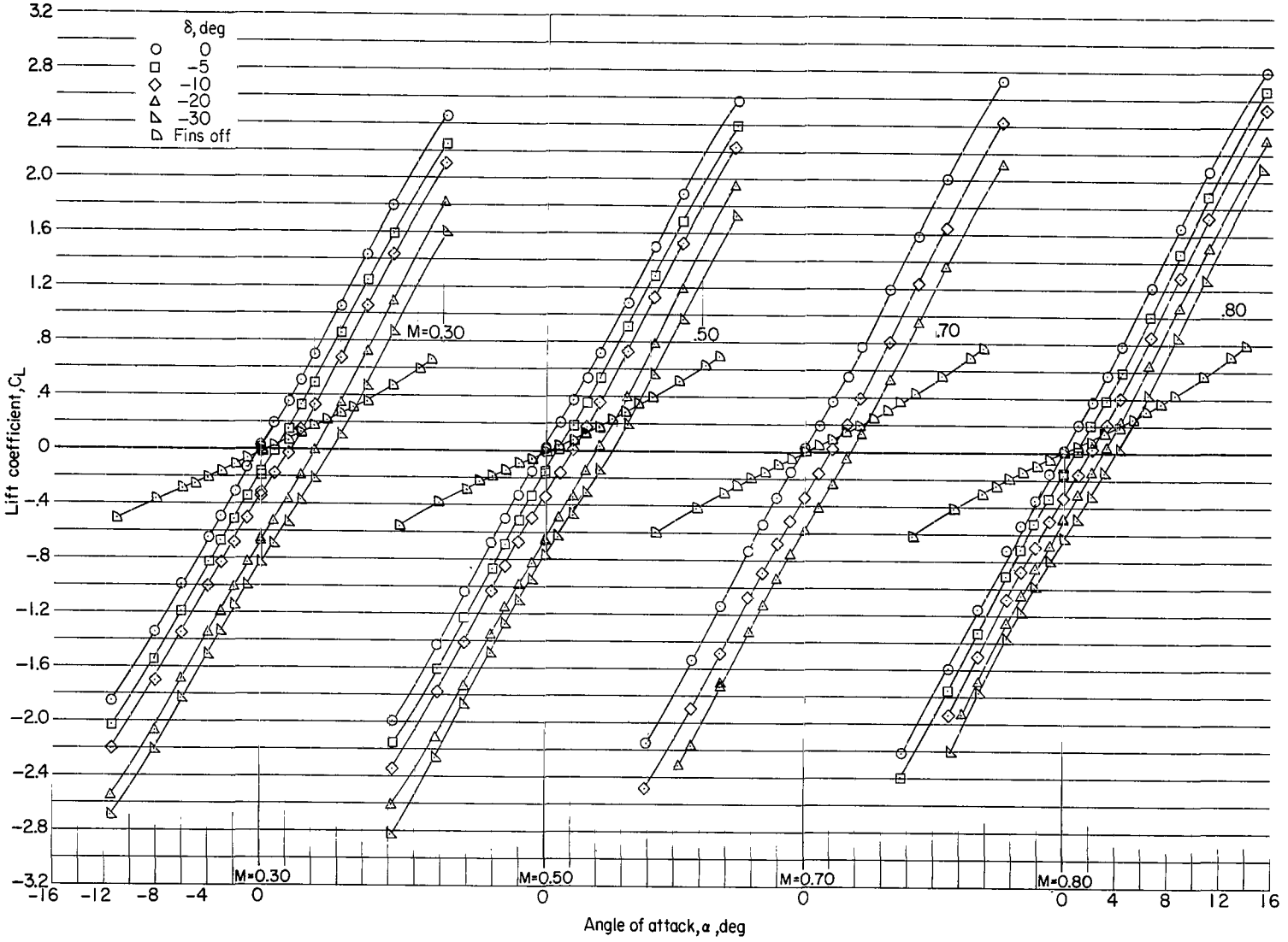

(e) C_L against α.

Figure 13.- Continued.

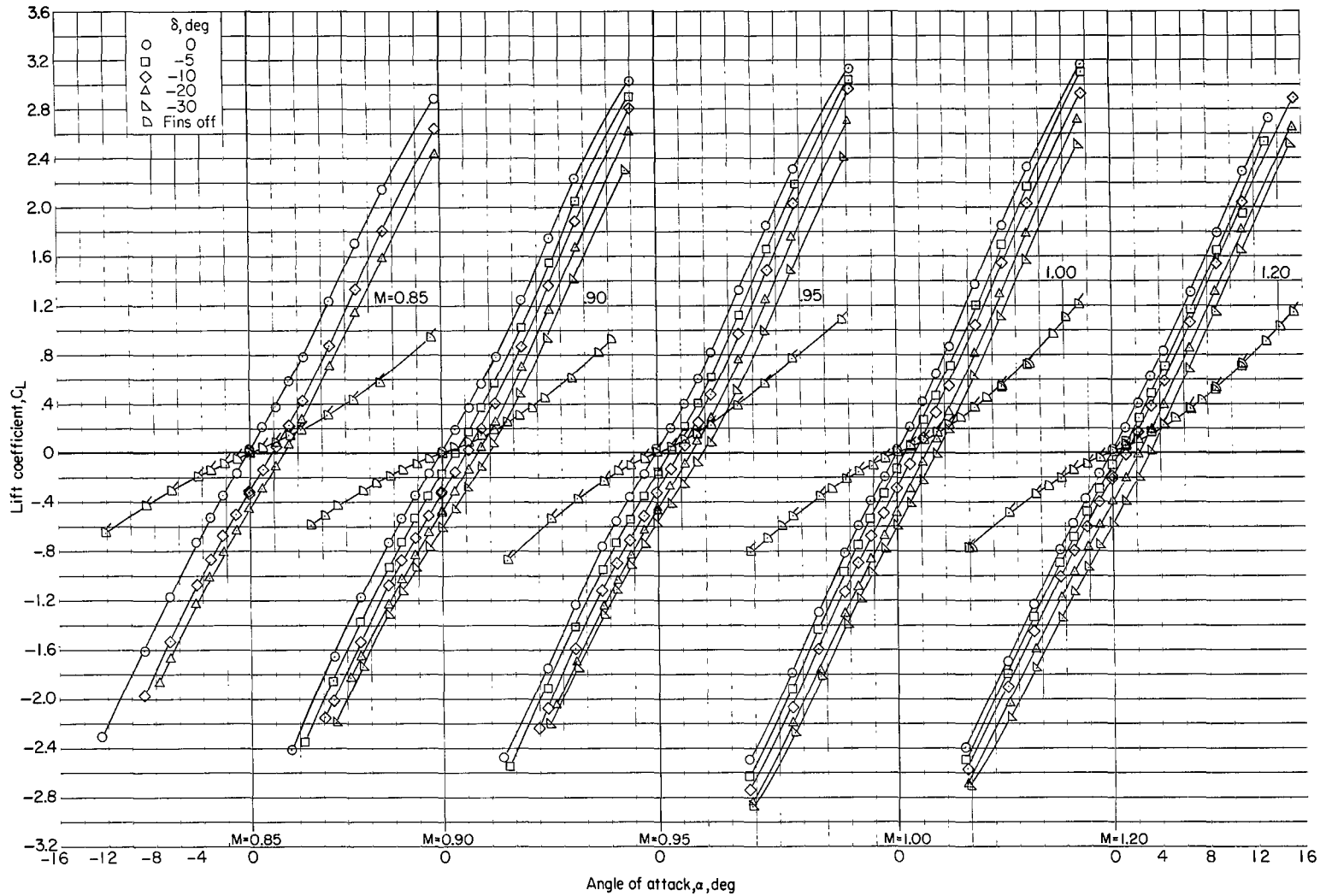

(e) C_L against α. Concluded.

Figure 13.- Continued.

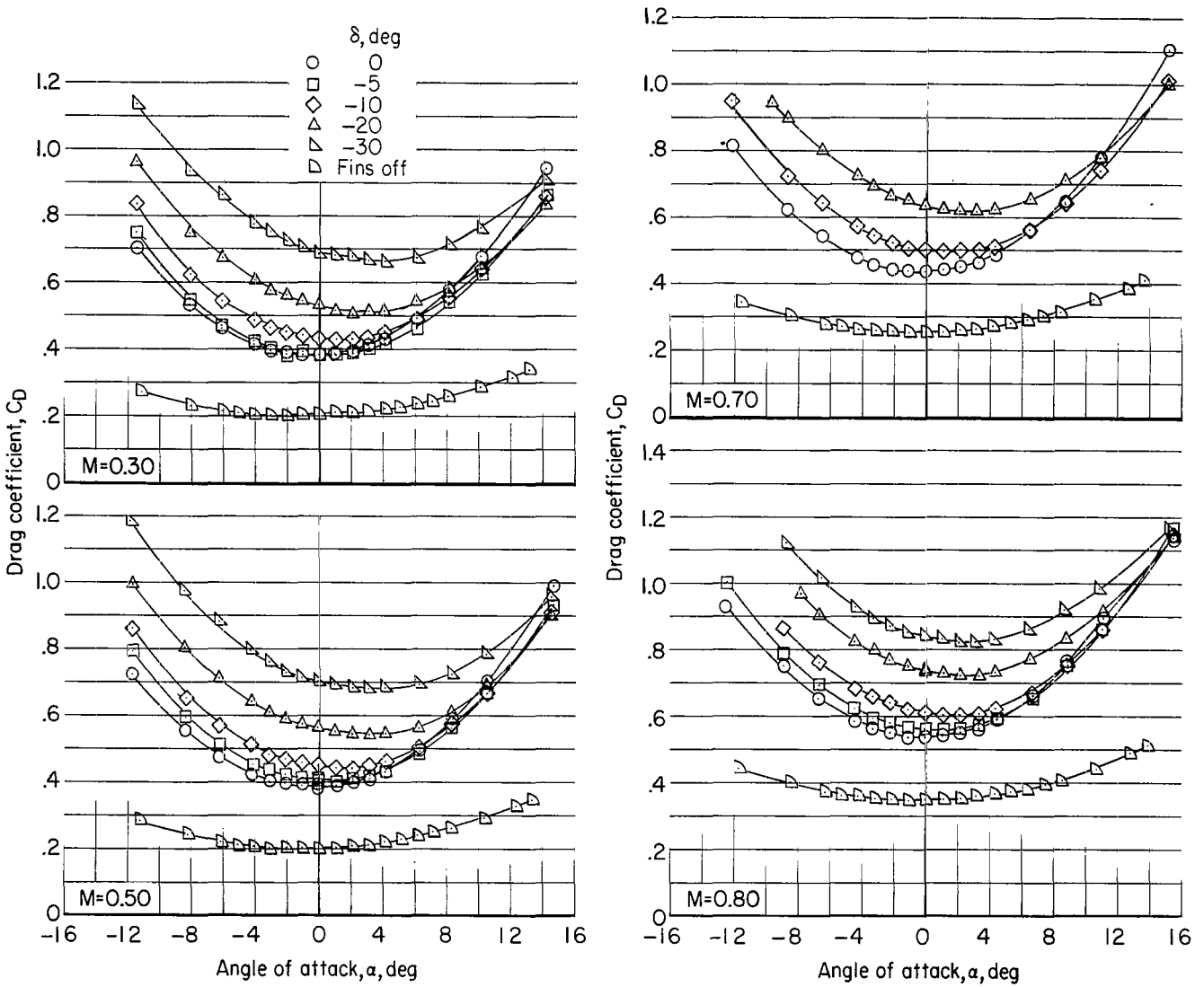

(f) C_D against α.

Figure 13.- Continued.

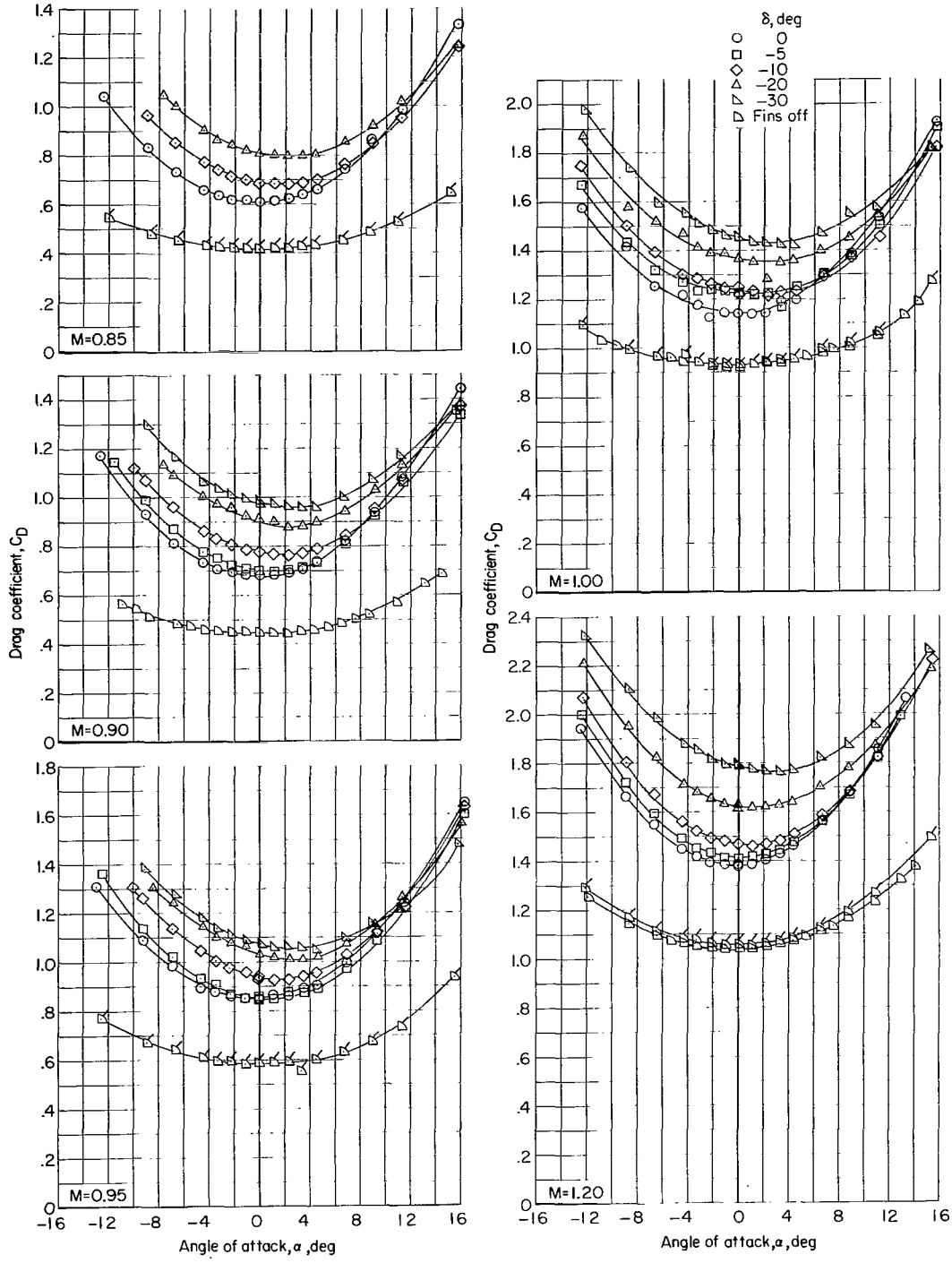

(f) C_D against α. Concluded.

Figure 13.- Continued.

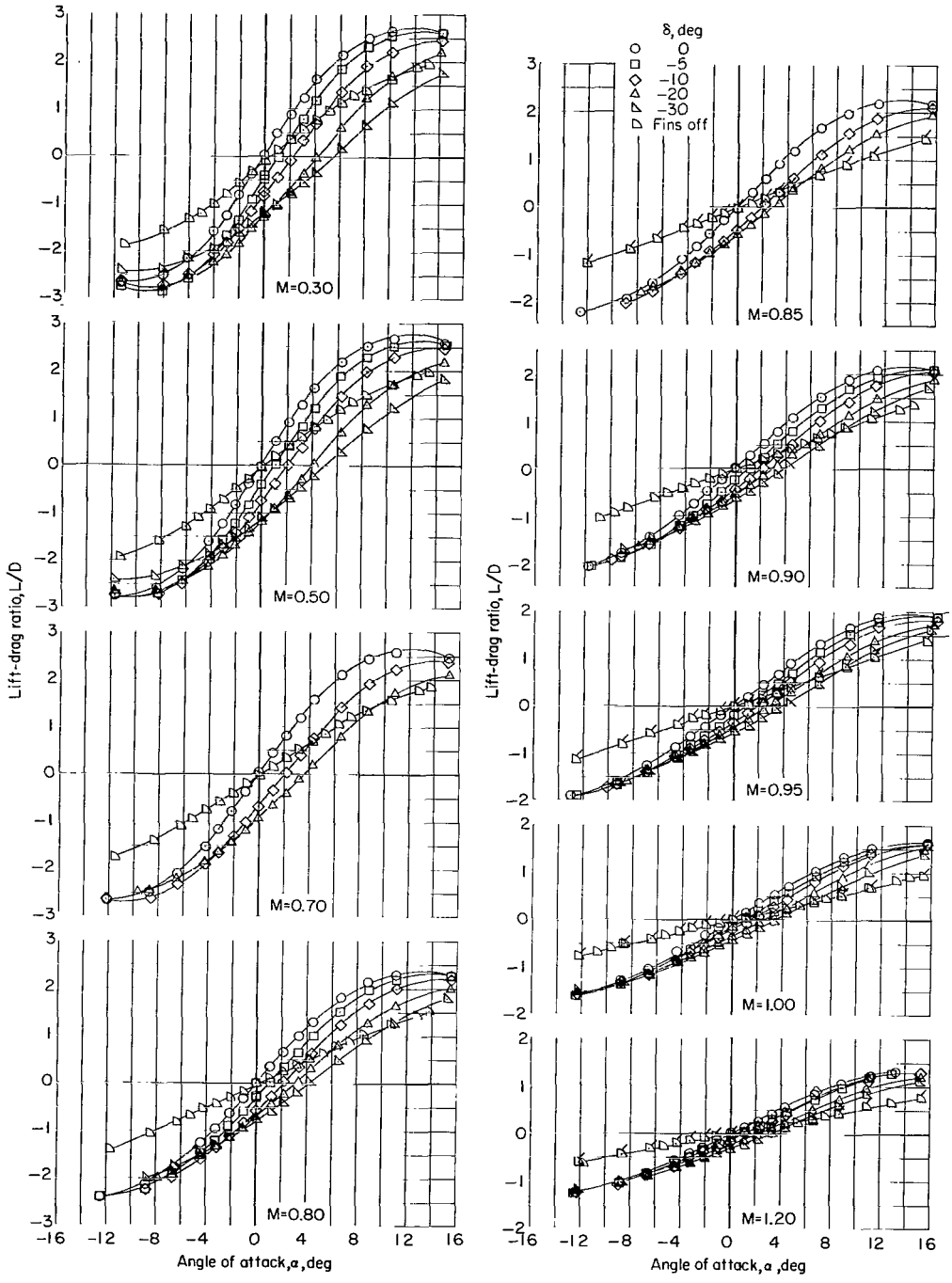

(g) L/D against α.

Figure 13.- Continued.

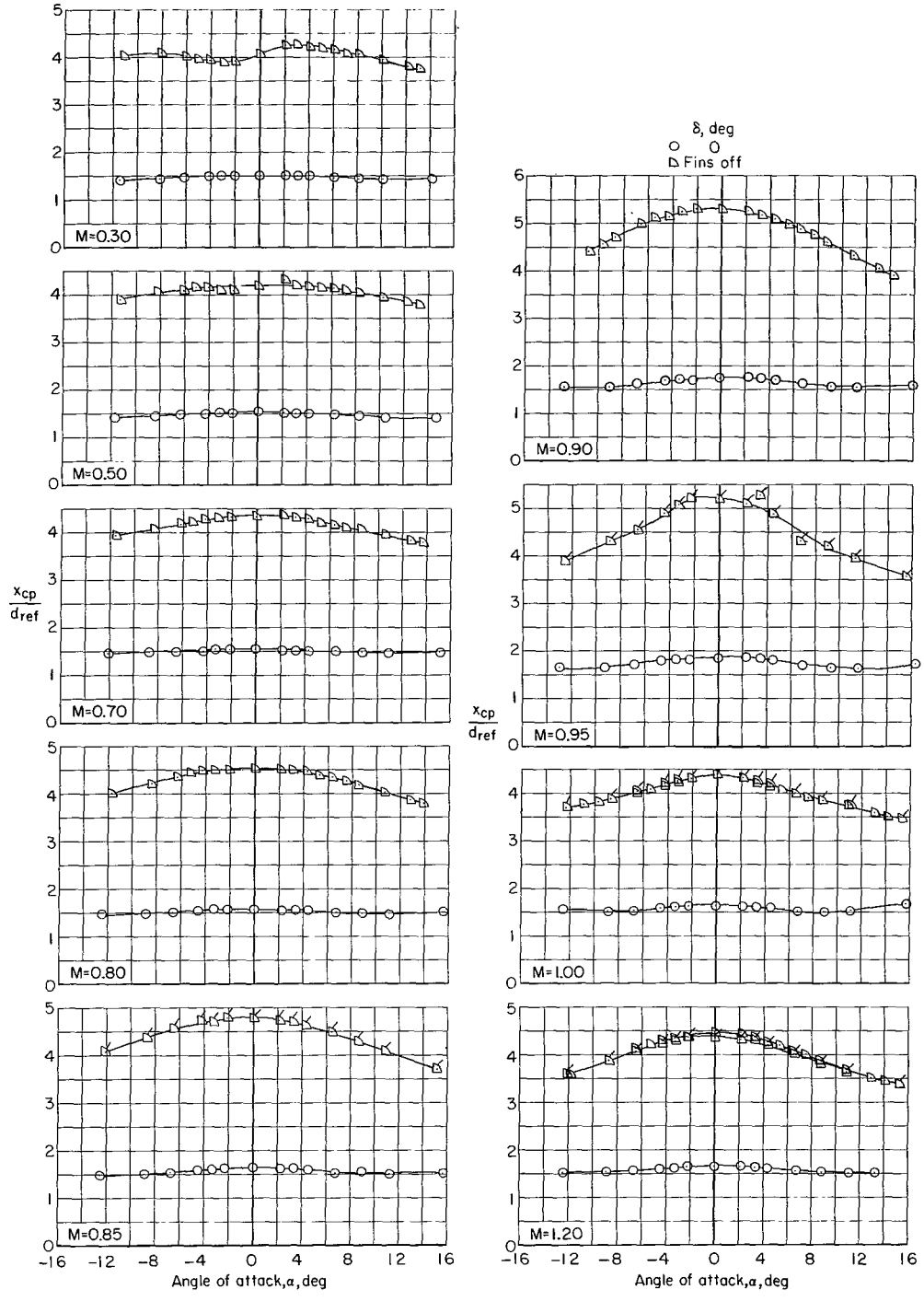

(h) x_{cp}/d_{ref} against α.

Figure 13.- Concluded.

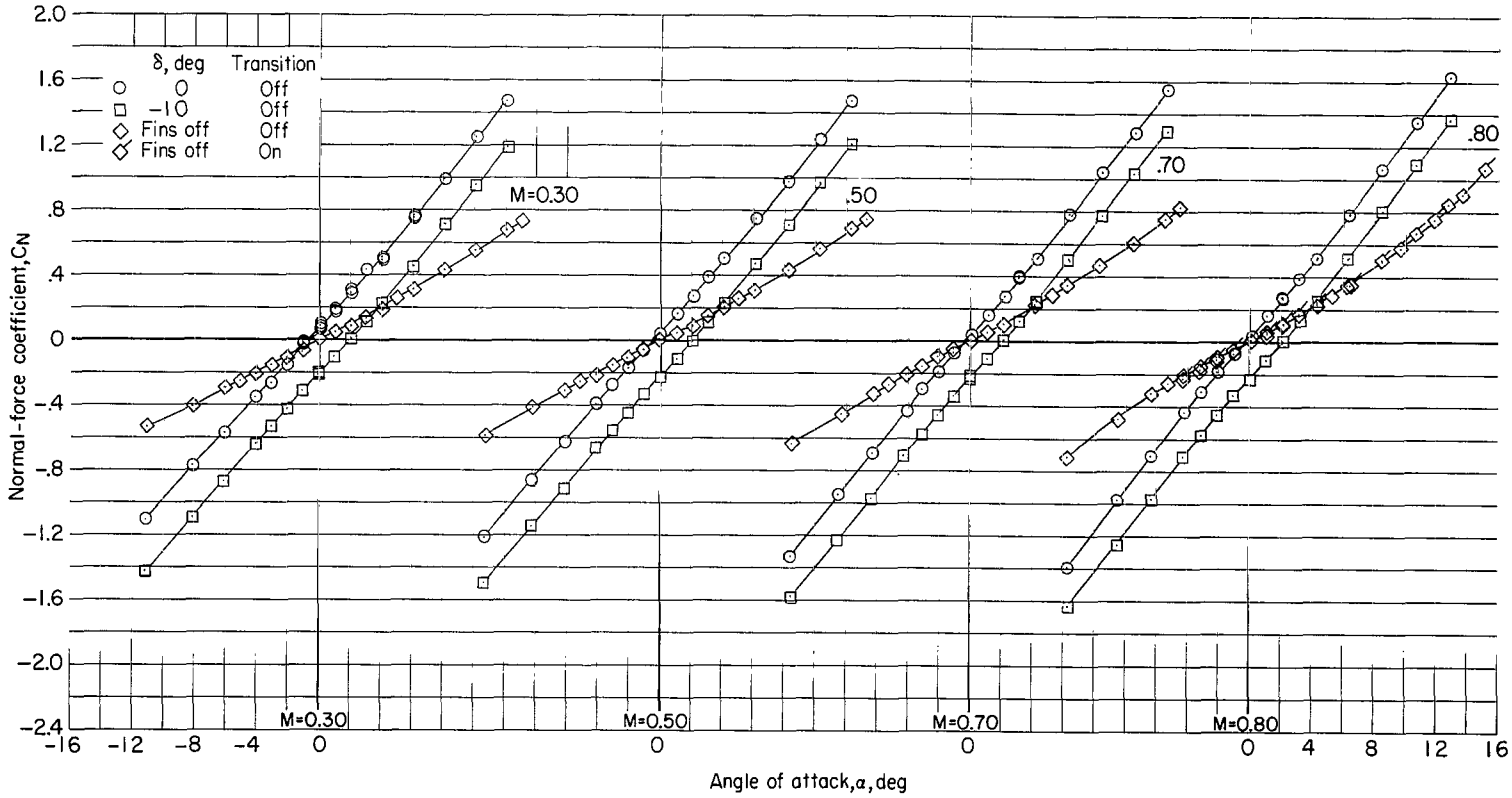

(a) C_N against α.

Figure 14.- Effect of deflection of trailing-edge controls and transition strips on longitudinal aerodynamic characteristics and on hinge moments of controls on fin 2. Shroud nose 2; small fins; shroud skirt off.

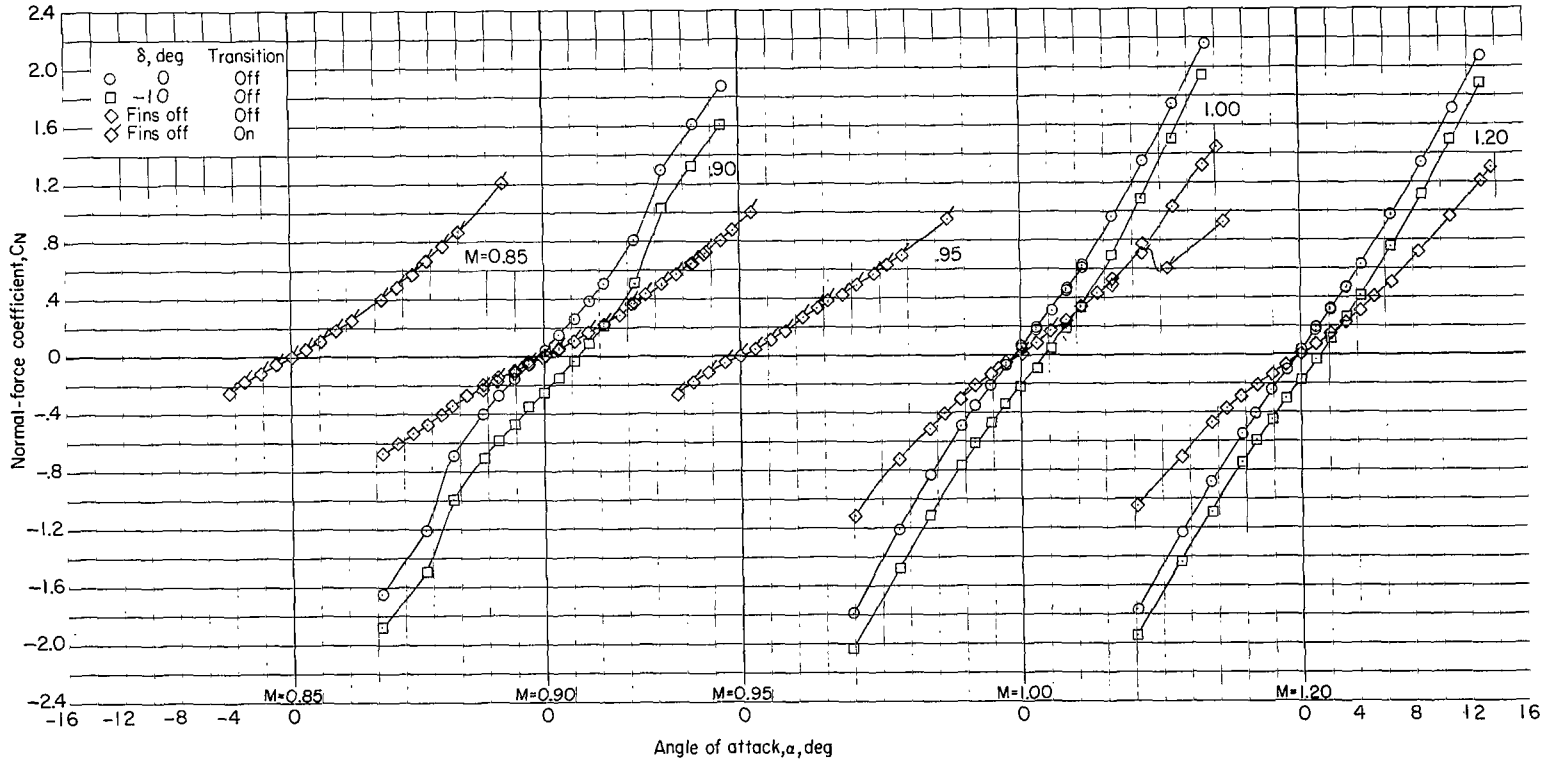

(a) C_N against α. Concluded.

Figure 14.- Continued.

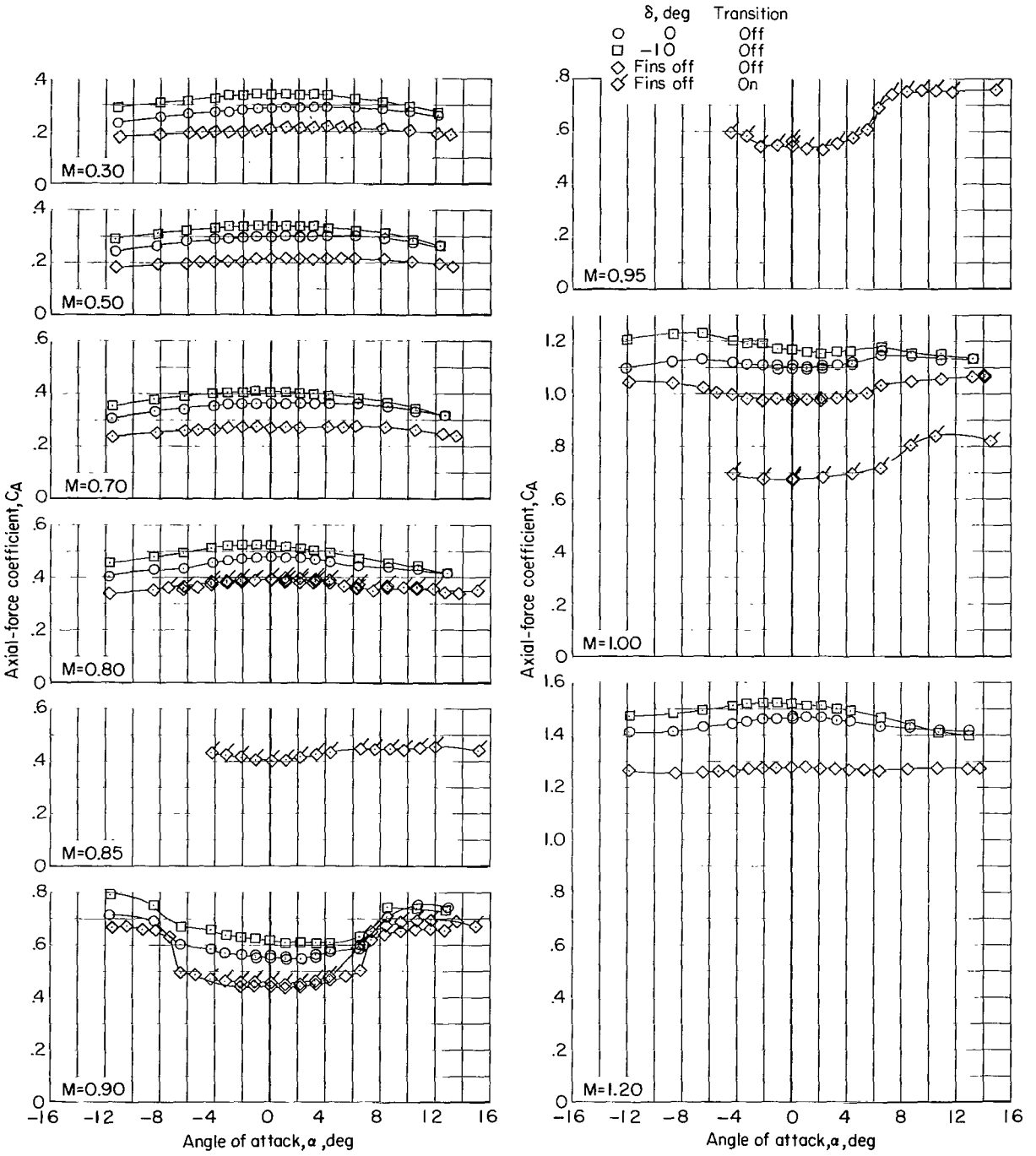

(b) C_A against α.

Figure 14.- Continued.

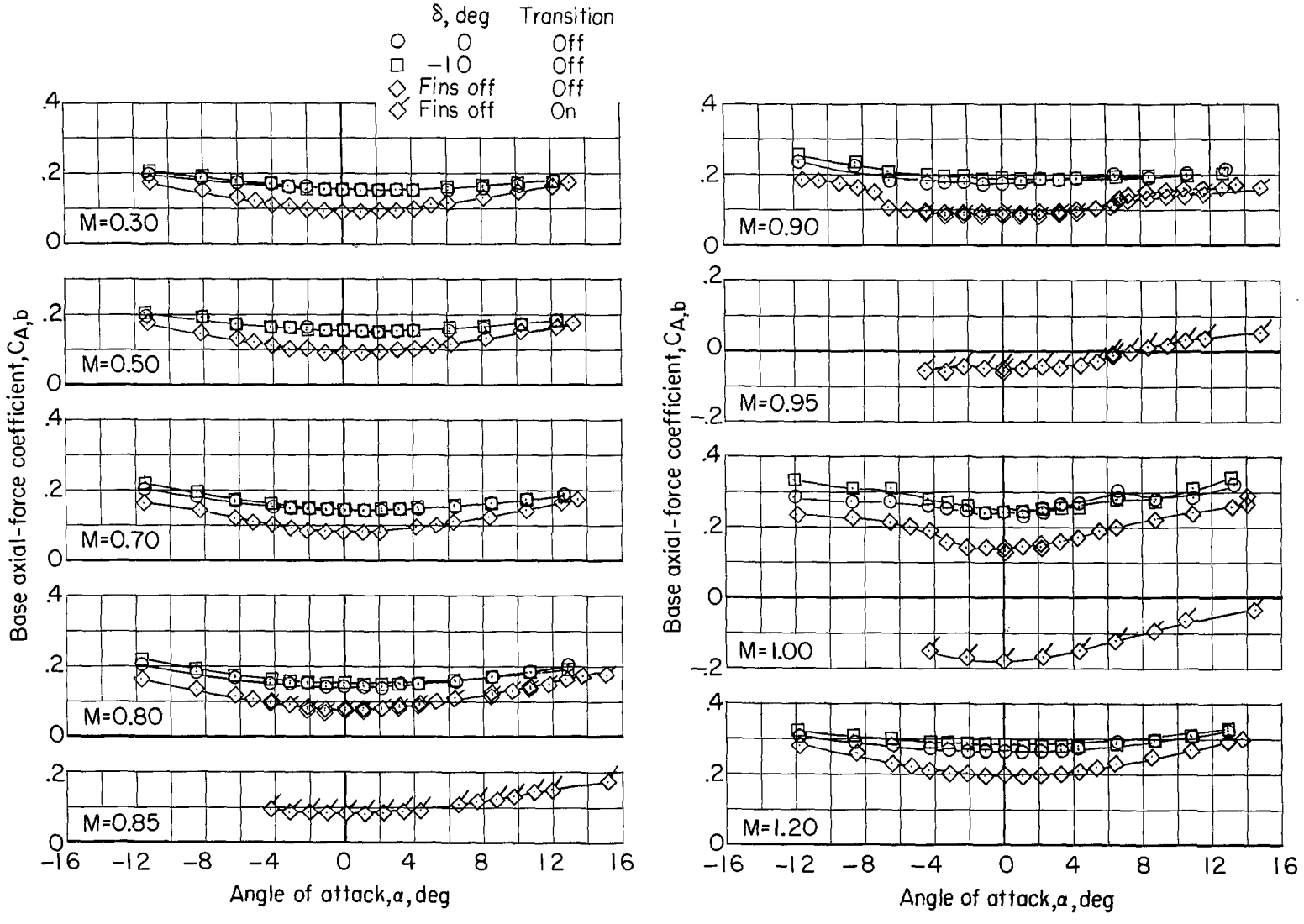

(c) $C_{A,b}$ against α.

Figure 14.- Continued.

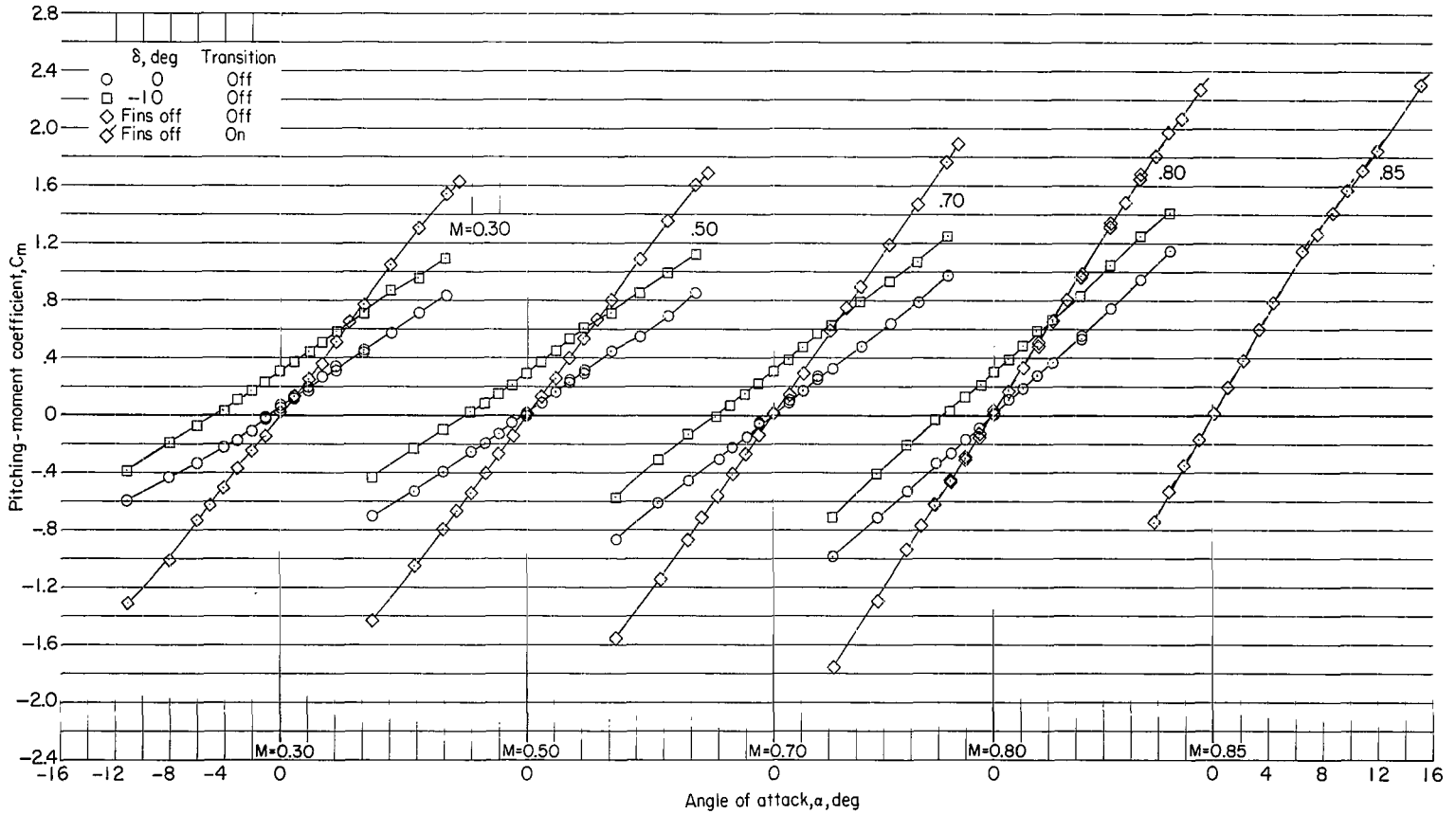

(d) C_m against α.

Figure 14.- Continued.

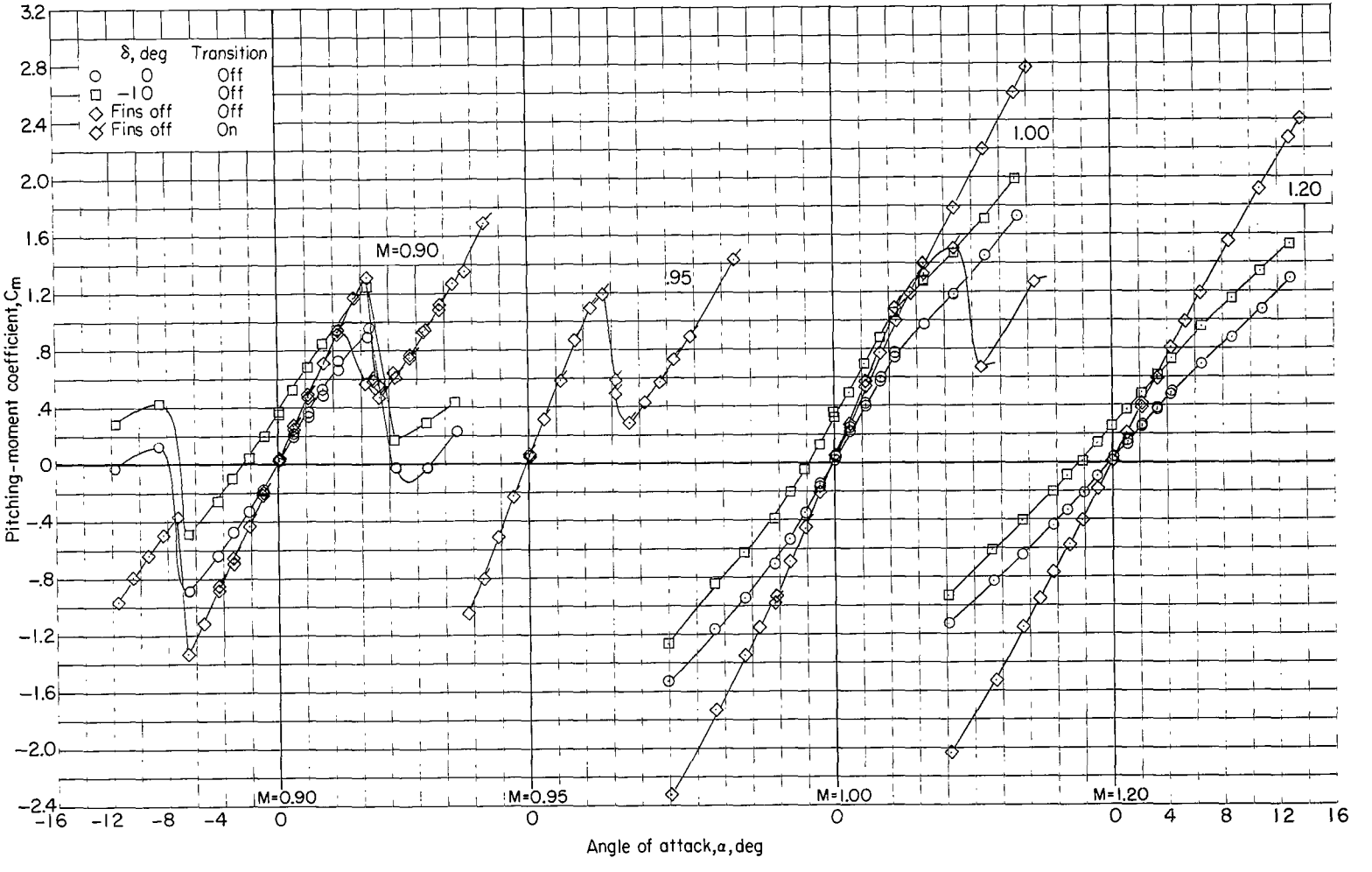

(d) C_m against α. Concluded.

Figure 14.- Continued.

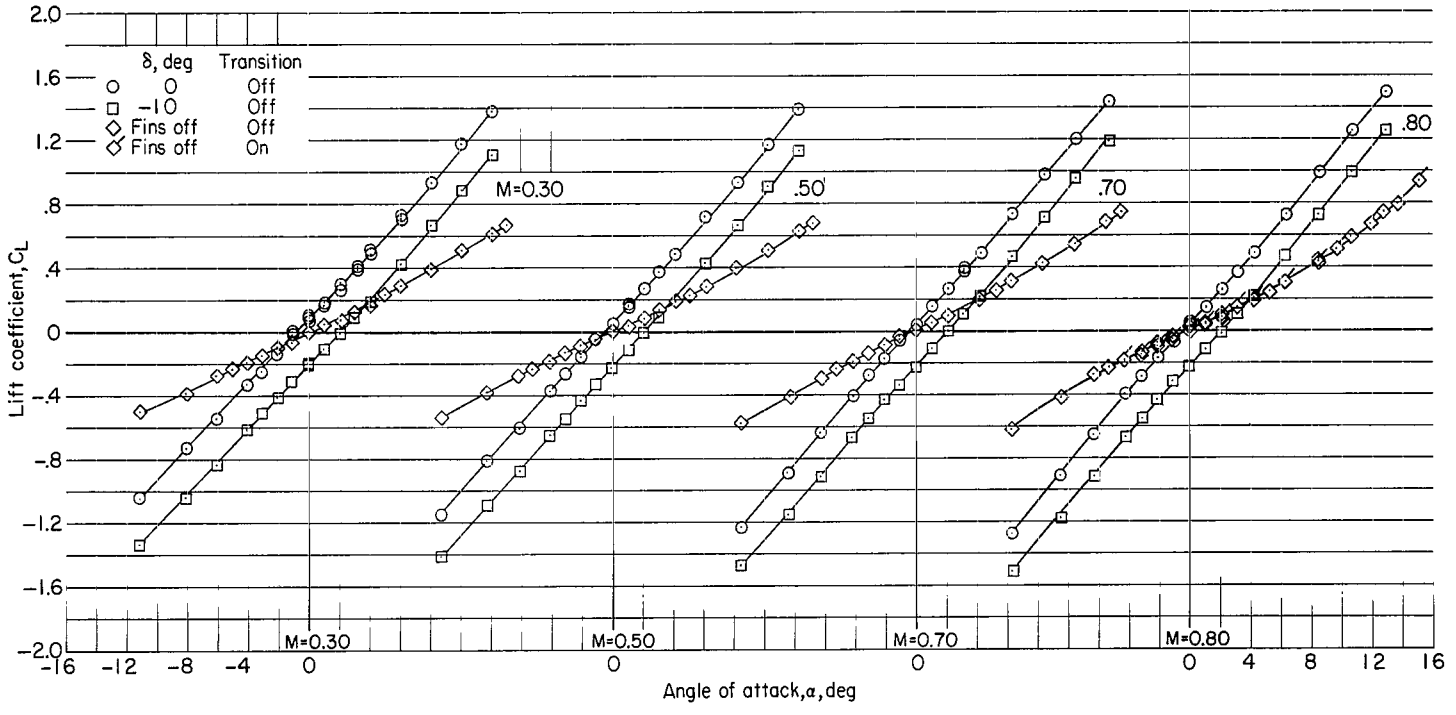

(e) C_L against α.

Figure 14.- Continued.

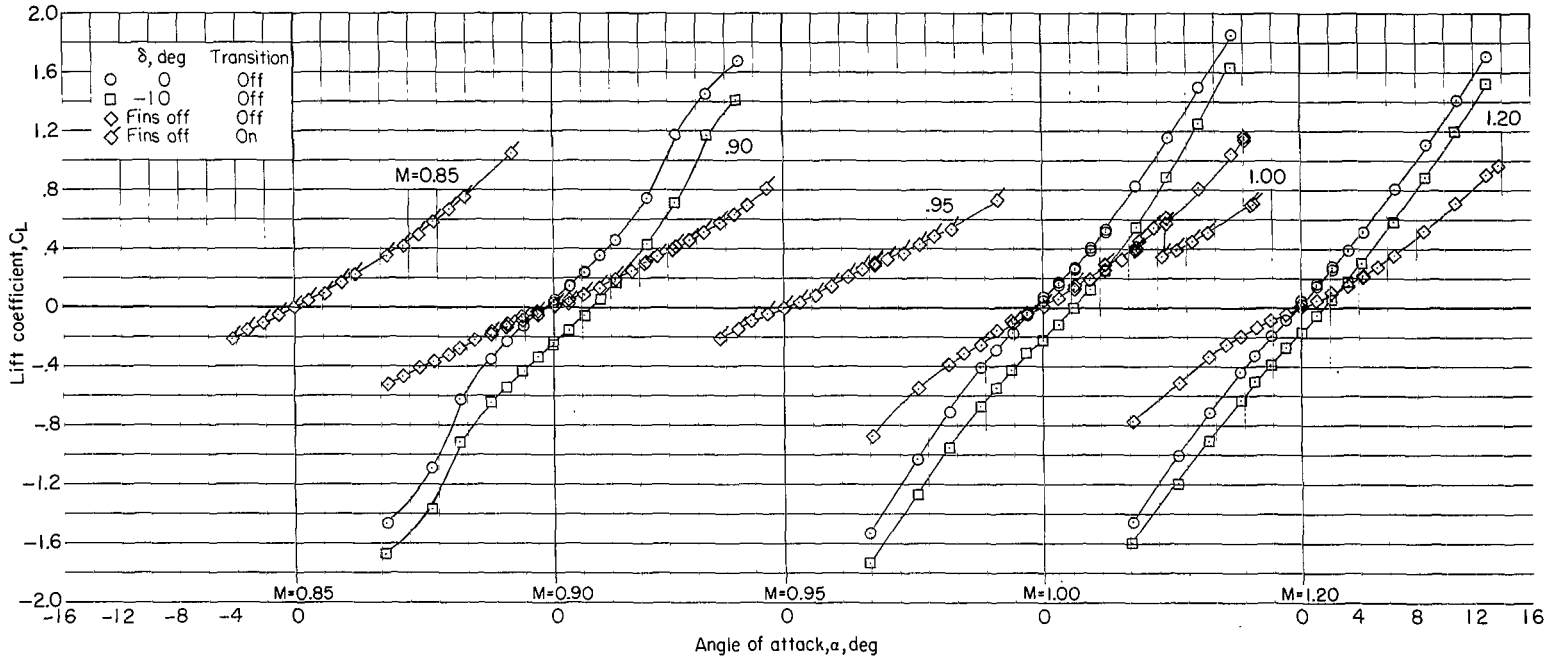

(e) C_L against α. Concluded.

Figure 14.- Continued.

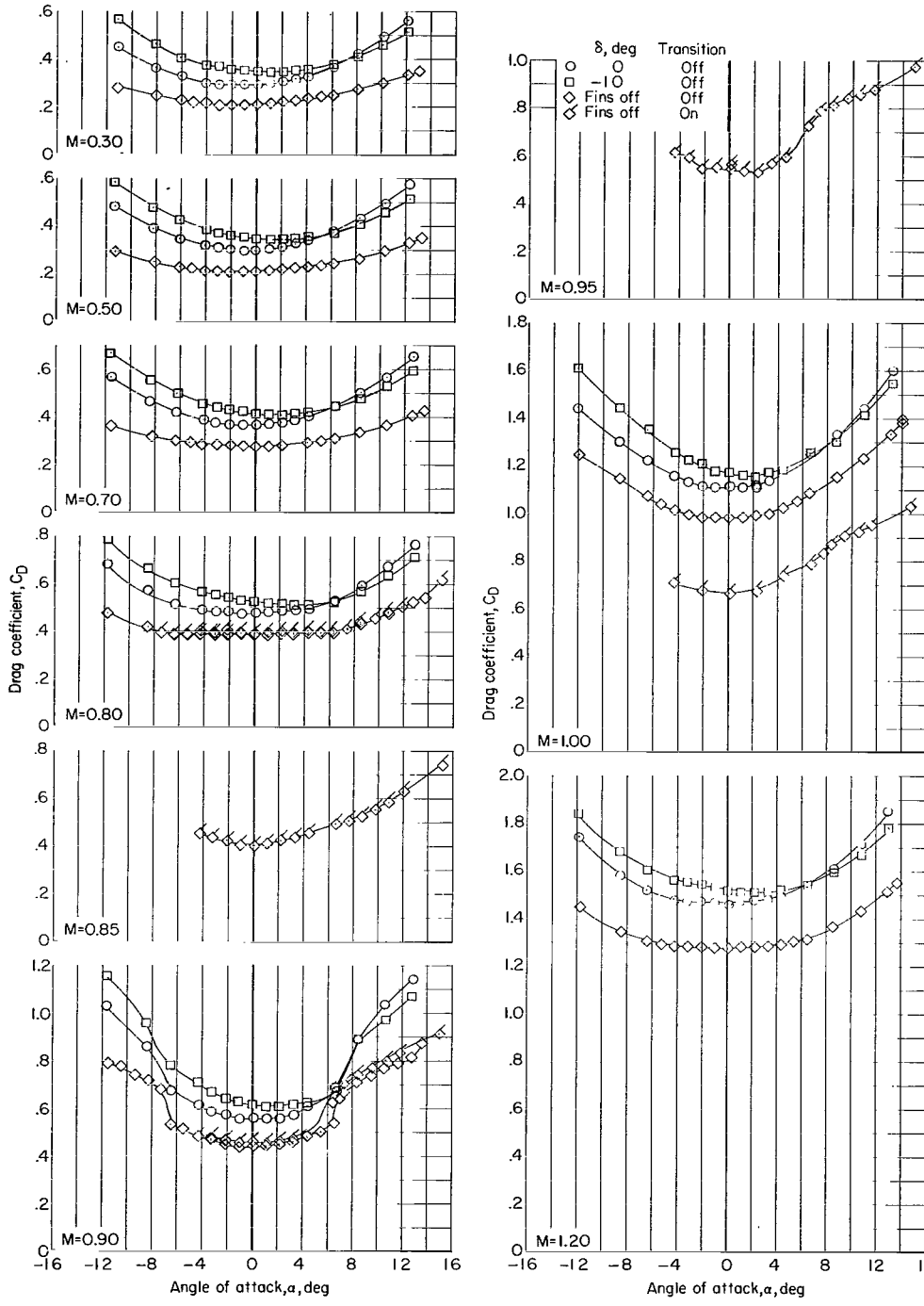

(f) C_D against α.

Figure 14.- Continued.

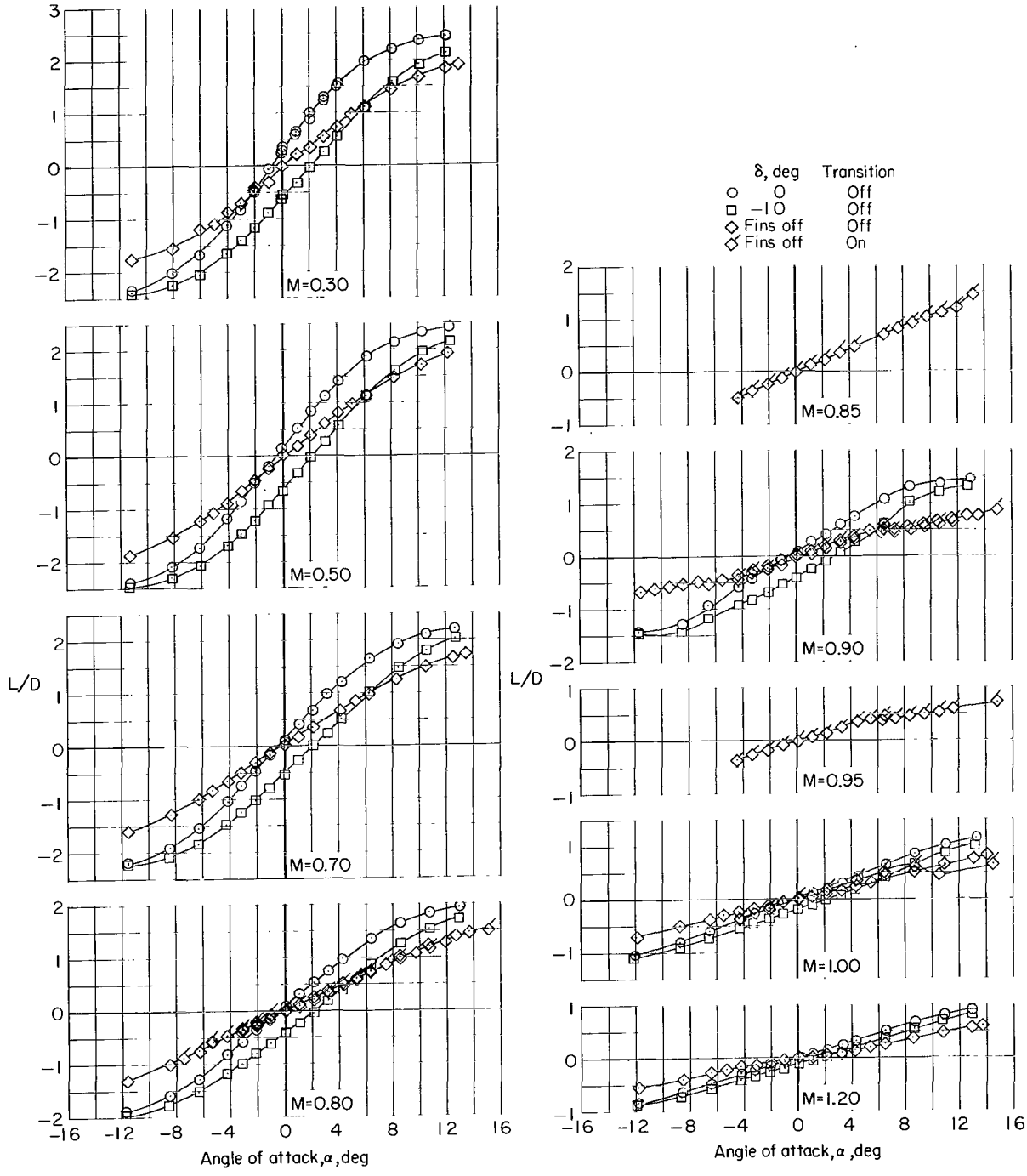

(g) L/D against α.

Figure 14.- Continued.

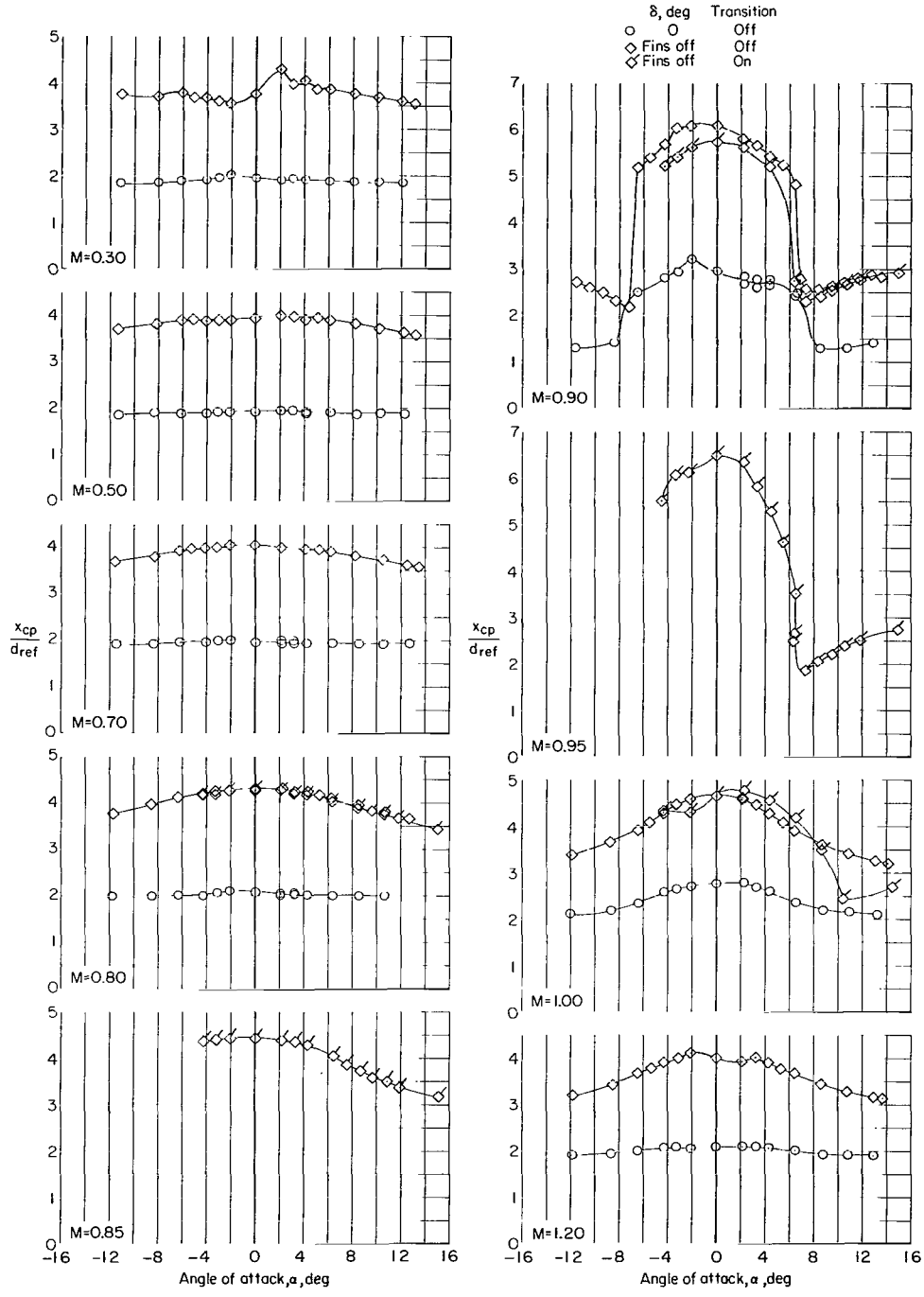

(h) x_{cp}/d_{ref} against α.

Figure 14.- Continued.

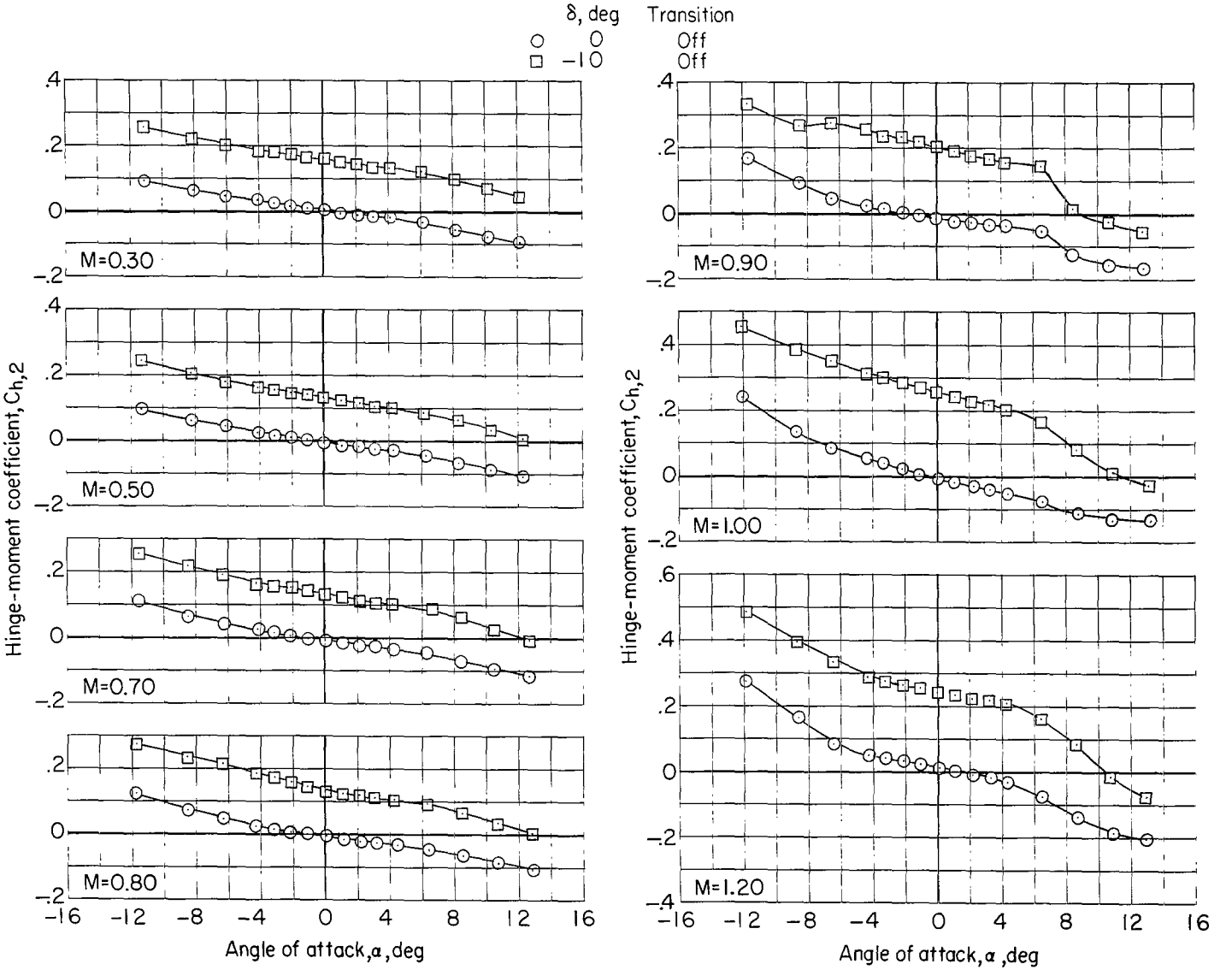

(i) $C_{h,2}$ against α.

Figure 14.- Concluded.

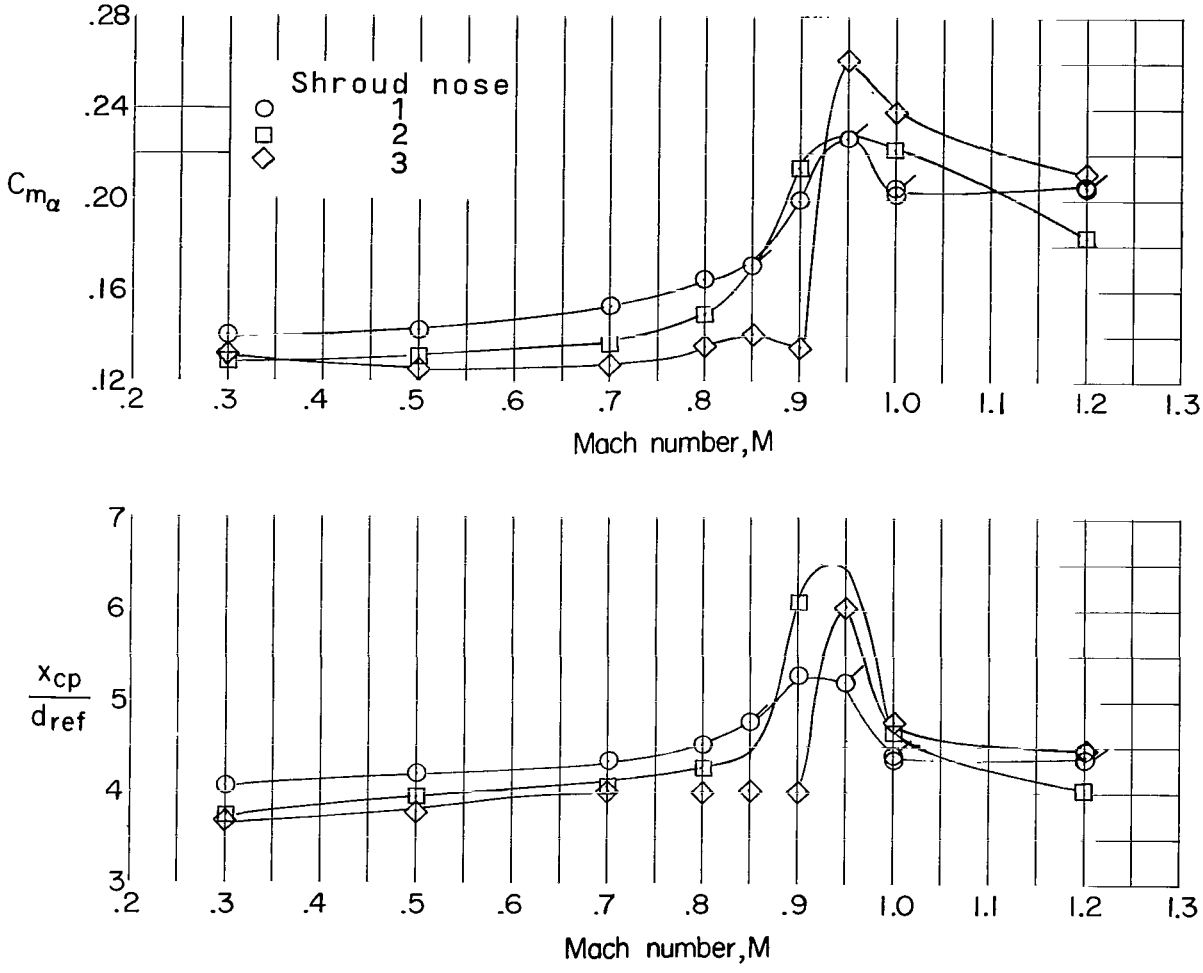

Figure 15.- Summary information on effect of shroud nose on longitudinal aerodynamic parameters. Shroud skirt off; fins off; $\alpha = 0^{o}$. (Flagged symbols indicate points from repeat run.)

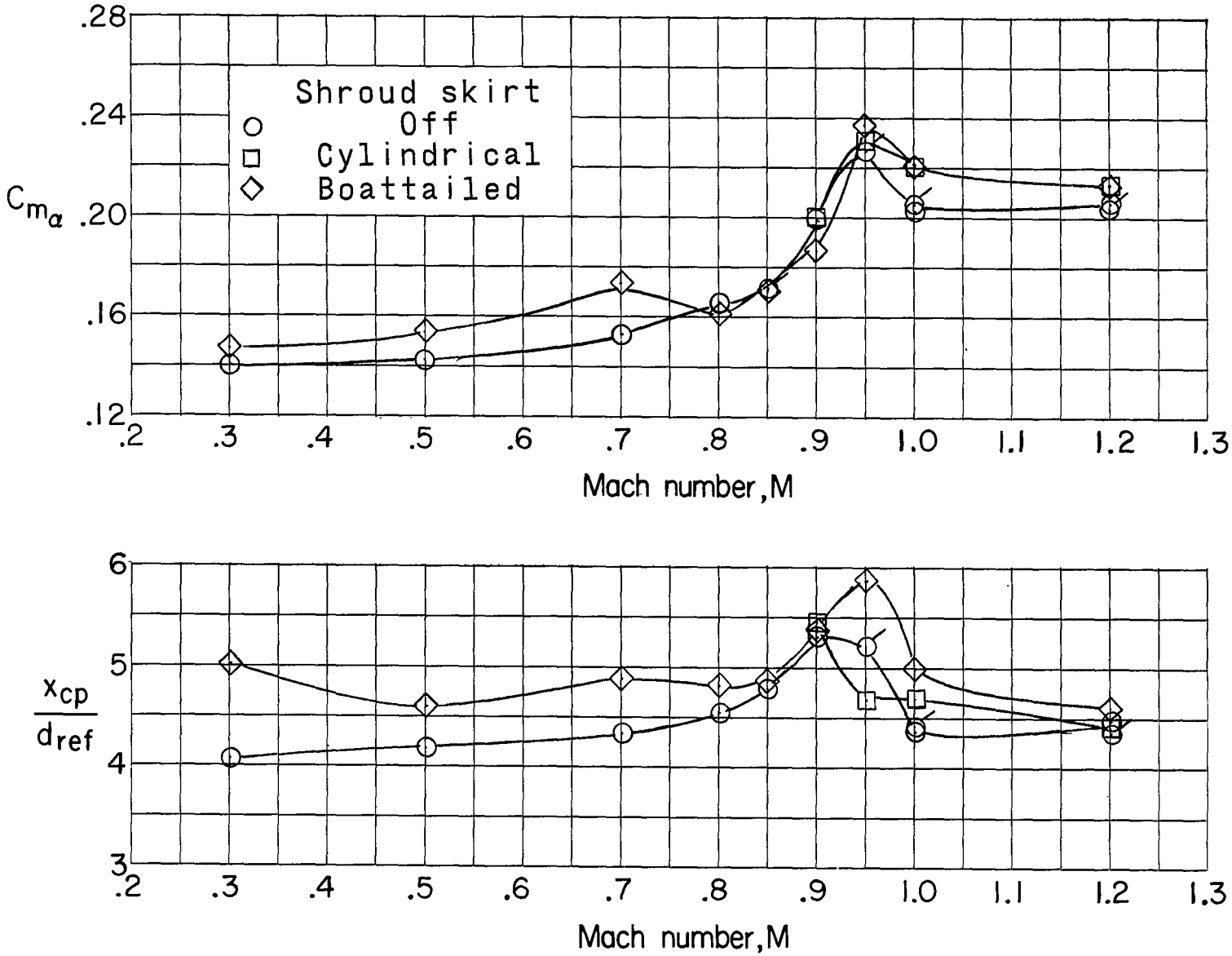

Figure 16.- Summary information on effect of cylindrical and boattailed shroud skirts on longitudinal aerodynamic parameters. Shroud nose 1; fins off; $\alpha = 0^0$. (Flagged symbols indicate points from repeat run.)

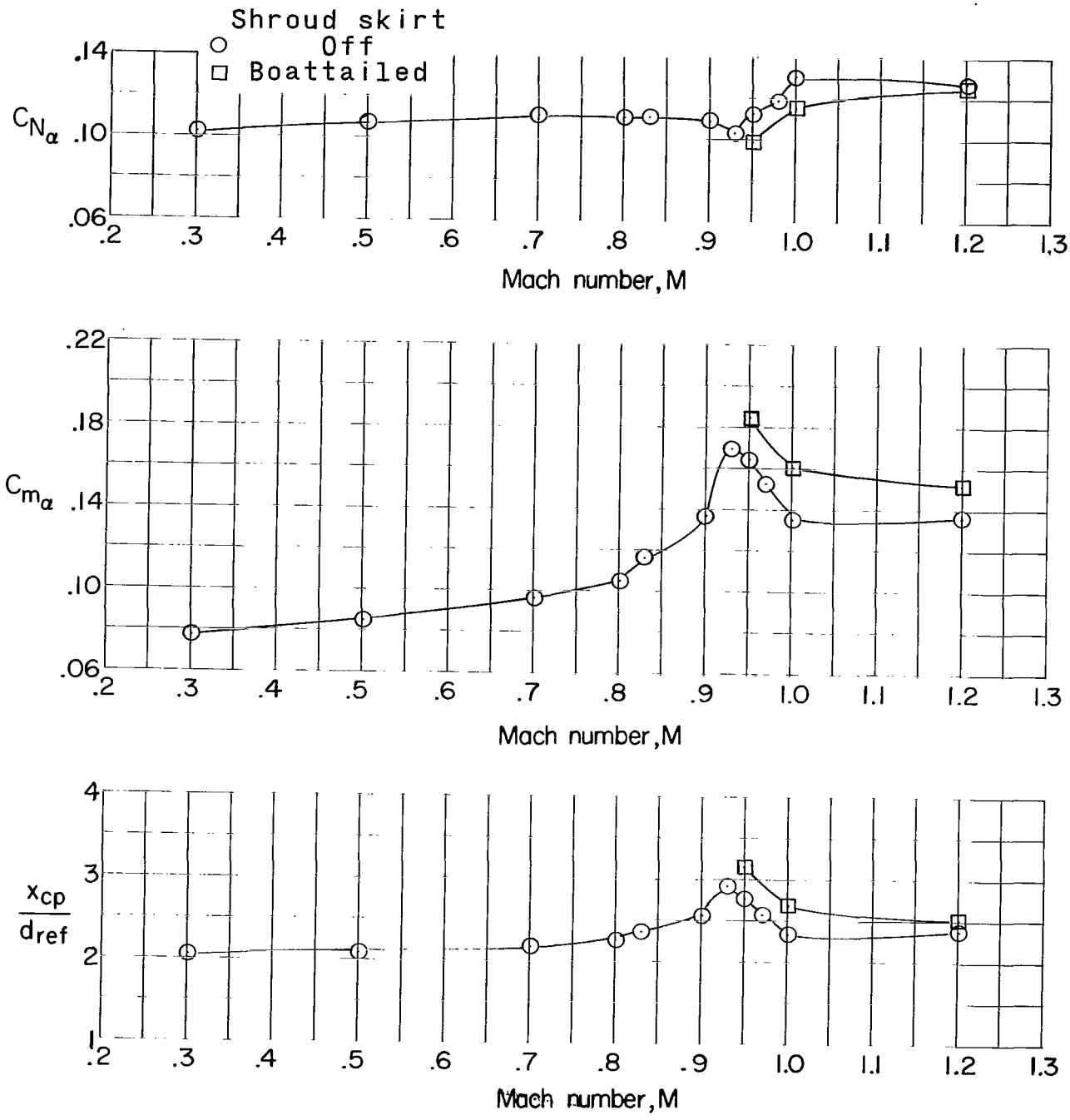

Figure 17.- Summary information on effect of boattailed shroud skirt on longitudinal aerodynamic parameters. Shroud nose 1; small fins; $\delta = 0^0$; $\alpha = 0^0$.

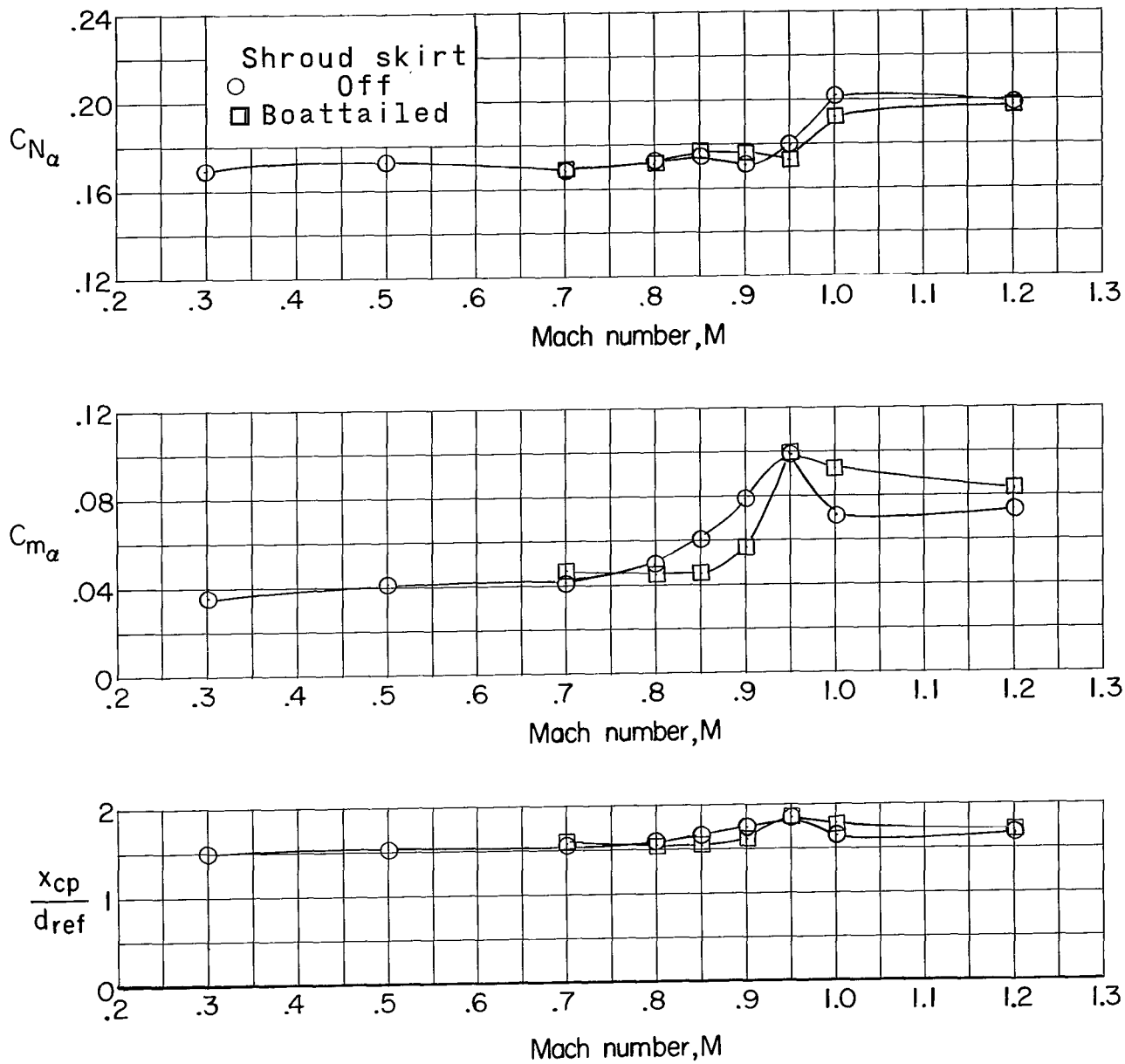

Figure 18.- Summary information on effect of boattailed shroud skirt on longitudinal aerodynamic parameters. Shroud nose 1; large fins; $\delta = 0^0$; $\alpha = 0^0$.

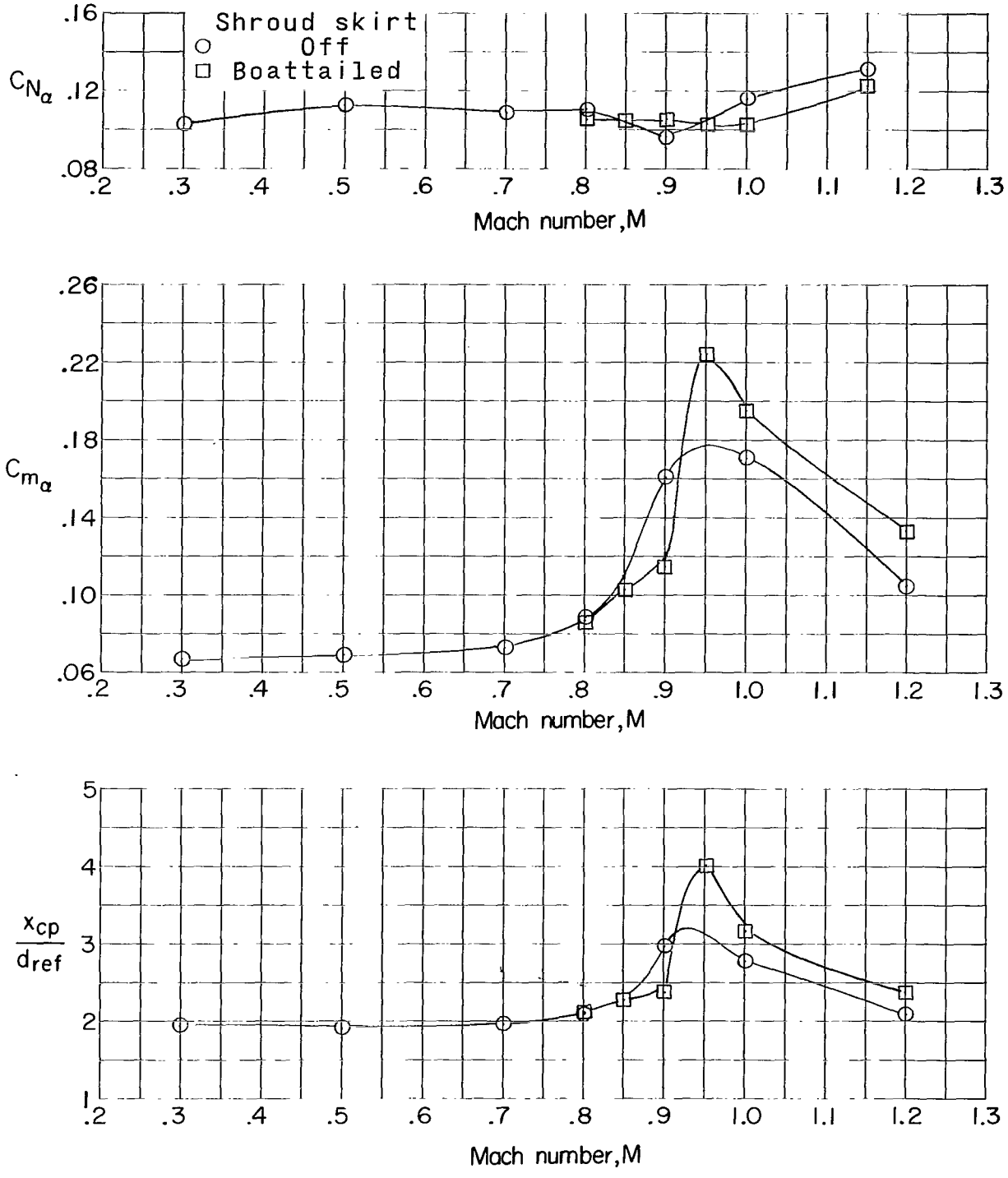

Figure 19.- Summary information on effect of boattailed shroud skirt on longitudinal aerodynamic parameters. Shroud nose 2; small fins; $\delta = 0^0$; $\alpha = 0^0$.

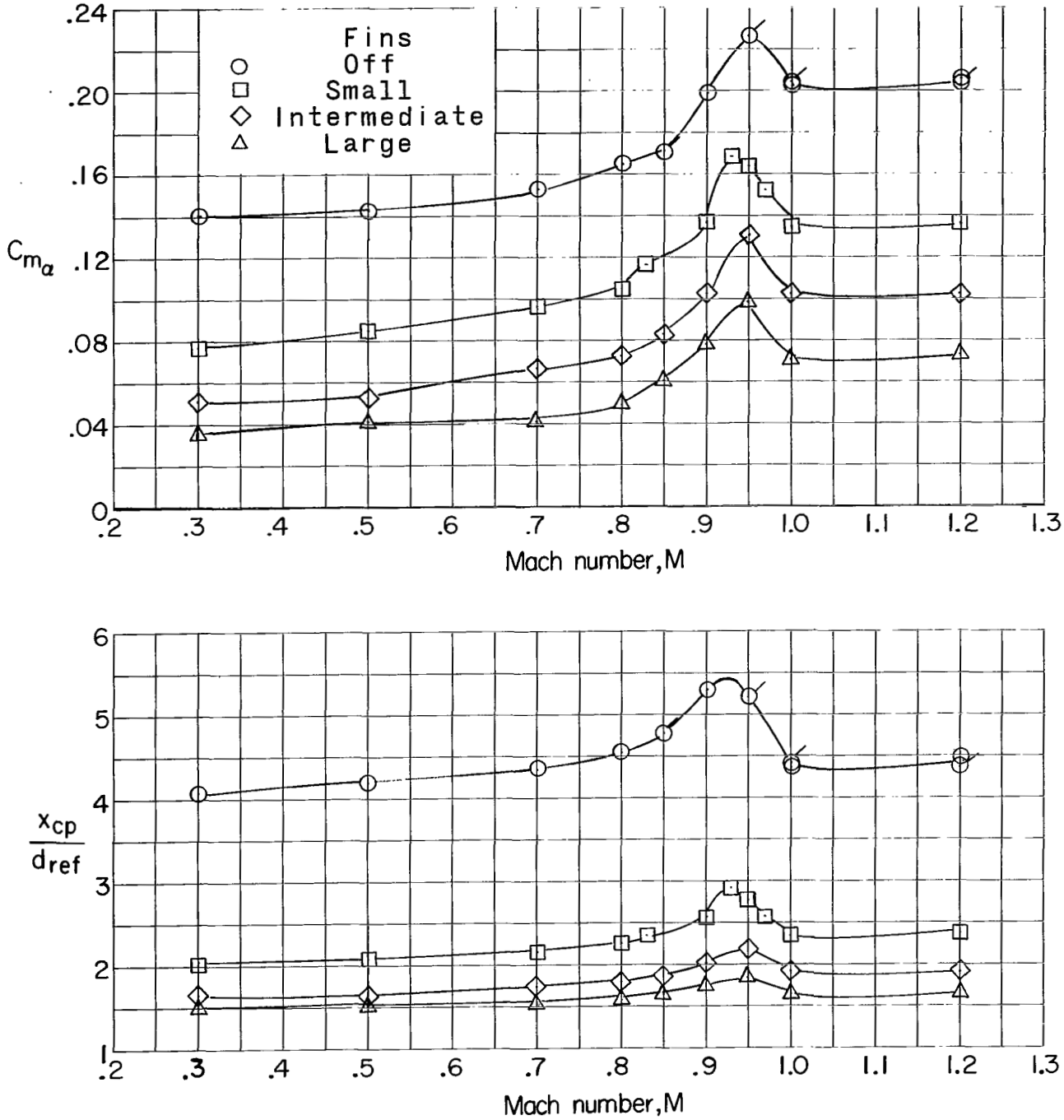

(a) C_{m_α} and x_{cp}/d_{ref} against M. $\delta = 0^0$.

Figure 20.- Summary information on effect of fin size on longitudinal aerodynamic parameters. Shroud nose 1; shroud skirt off; $\alpha = 0^0$. (Flagged symbols indicate points from repeat run.)

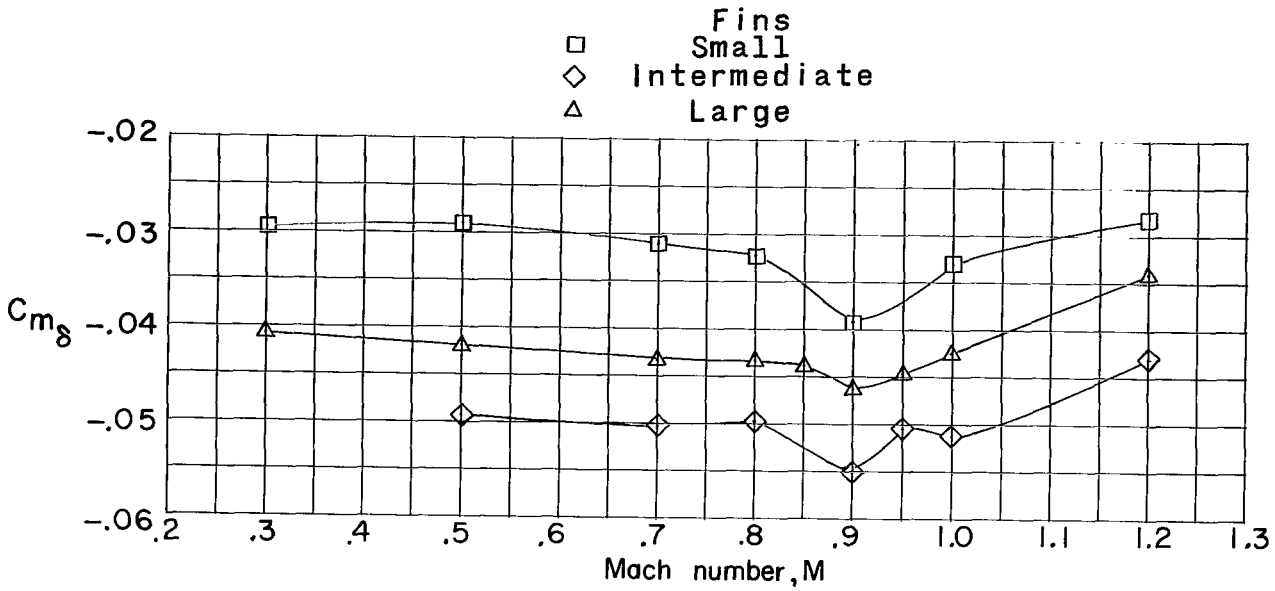

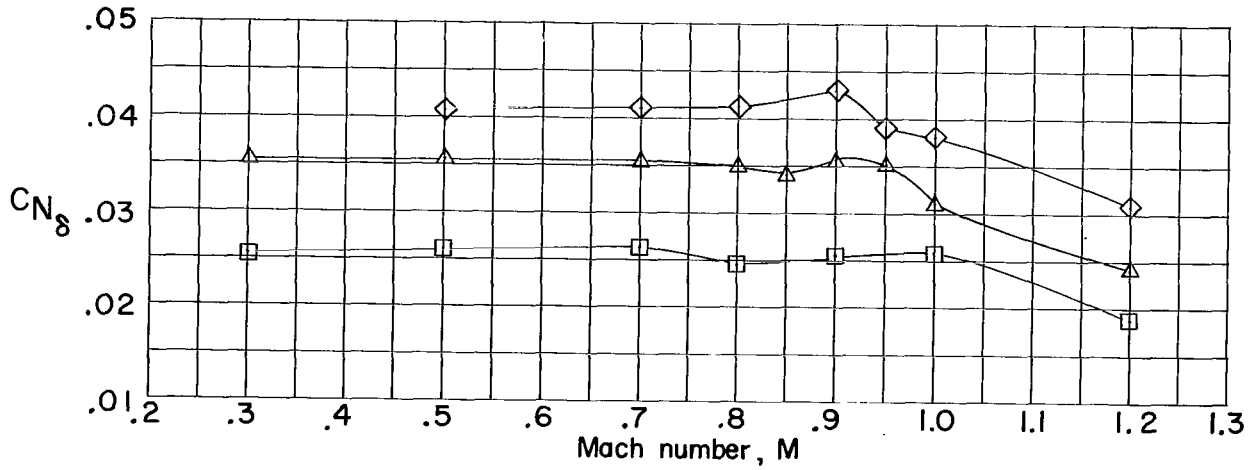

(b) C_{m_δ} and C_{N_δ} against M.

Figure 20.- Concluded.

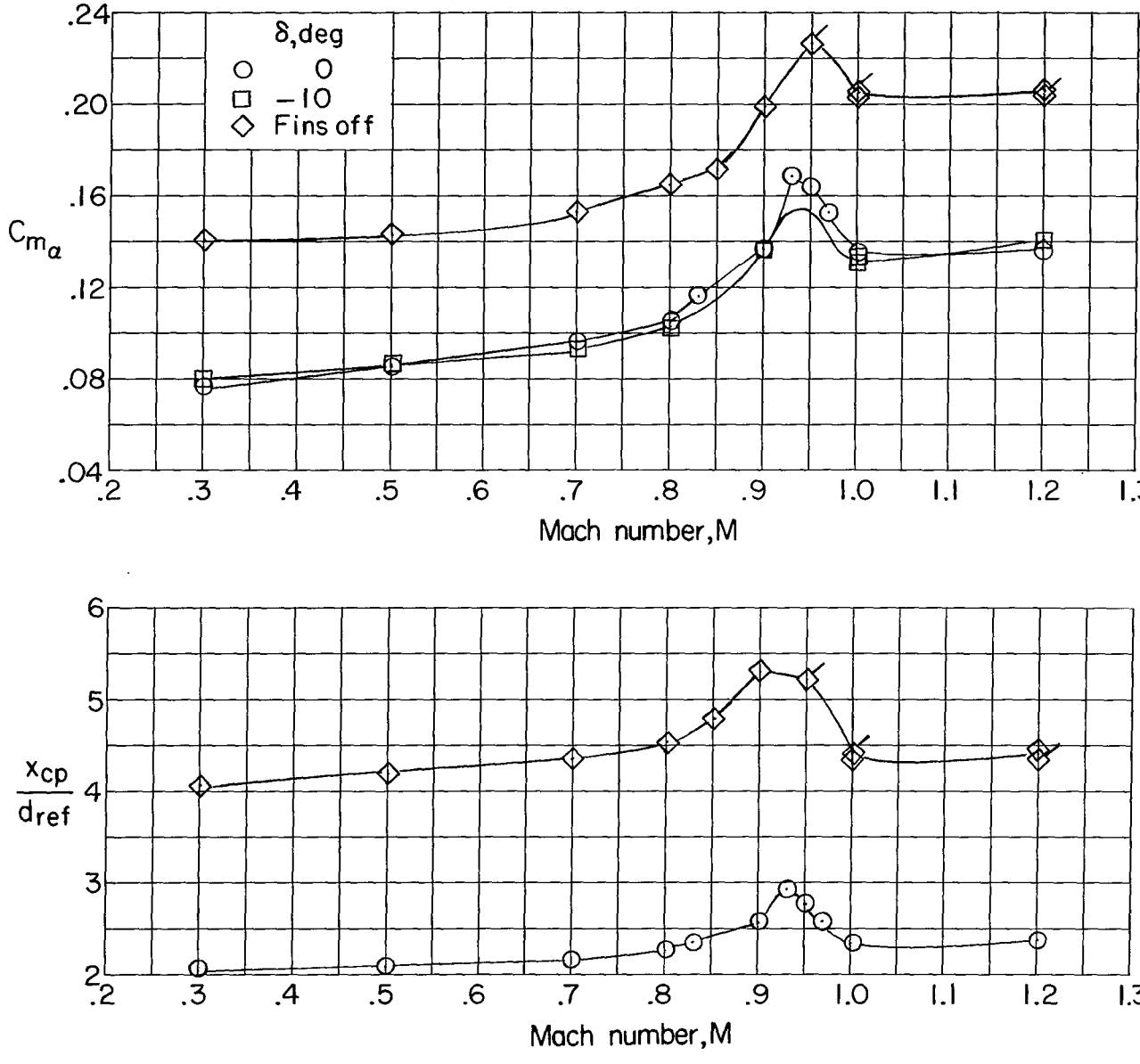

(a) C_{m_α} and x_{cp}/d_{ref} against M.

Figure 21.- Summary information on effect of deflection of trailing-edge controls on longitudinal aerodynamic parameters. Shroud nose 1; small fins; shroud skirt off; $\alpha = 0^0$. (Flagged symbols indicate points from repeat run.)

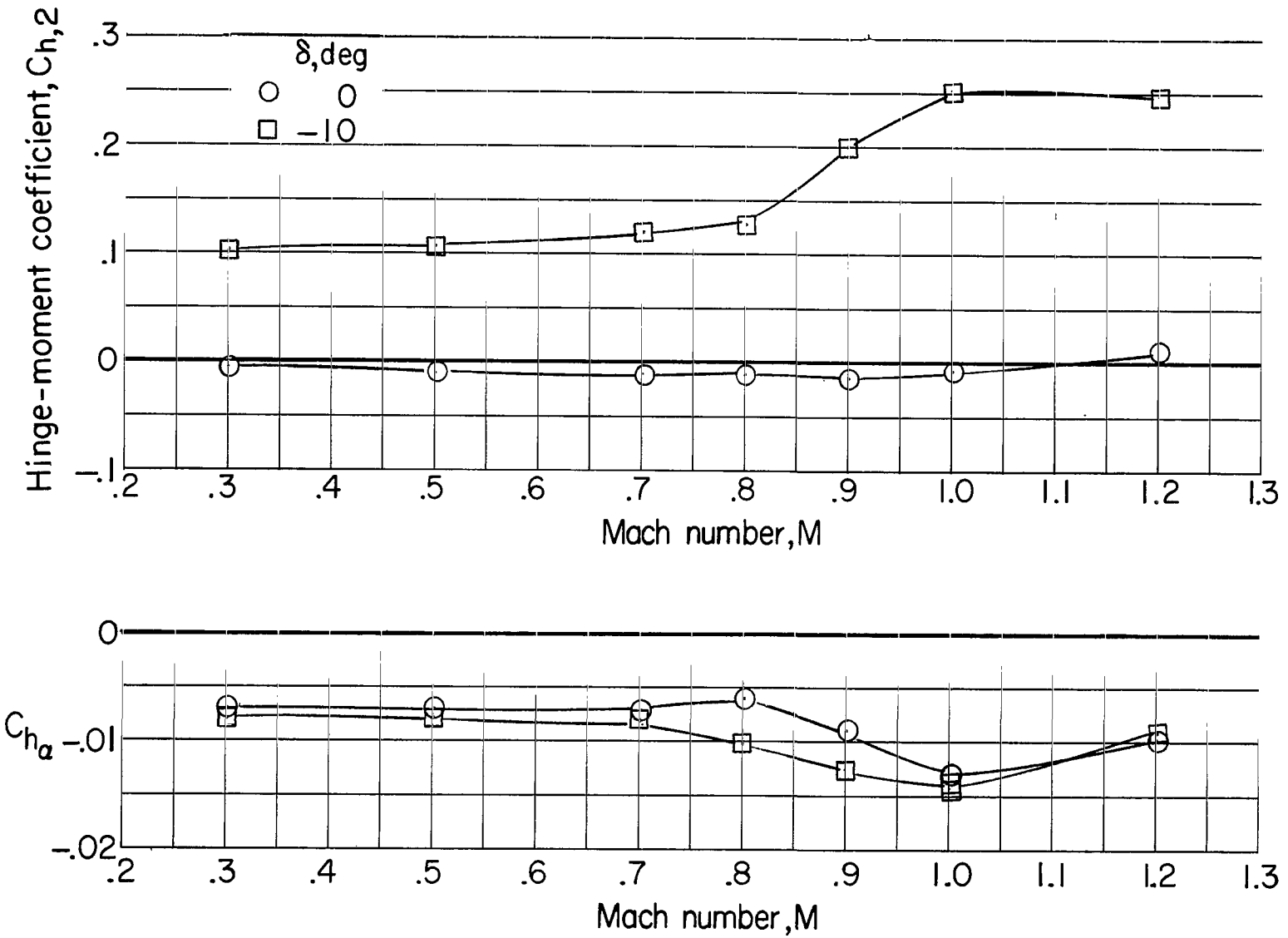

(b) $C_{h,2}$ and C_{h_α} against M.

Figure 21.- Continued.

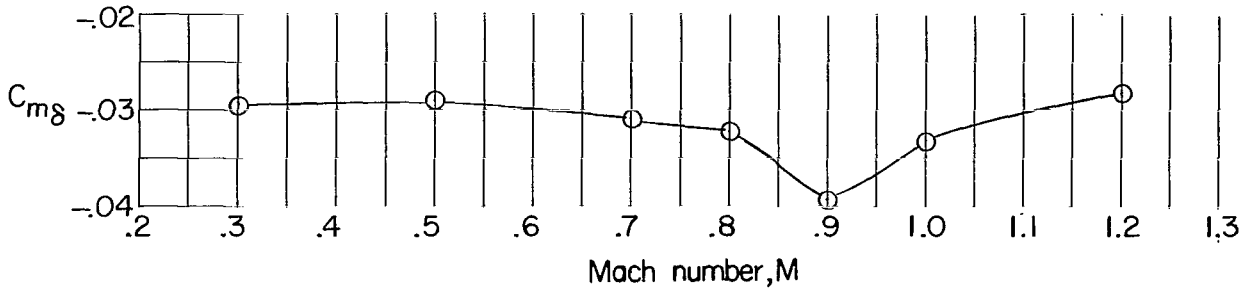

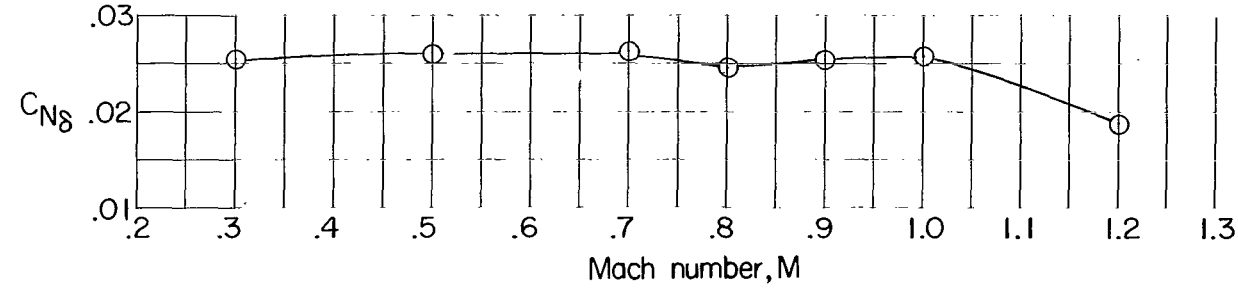

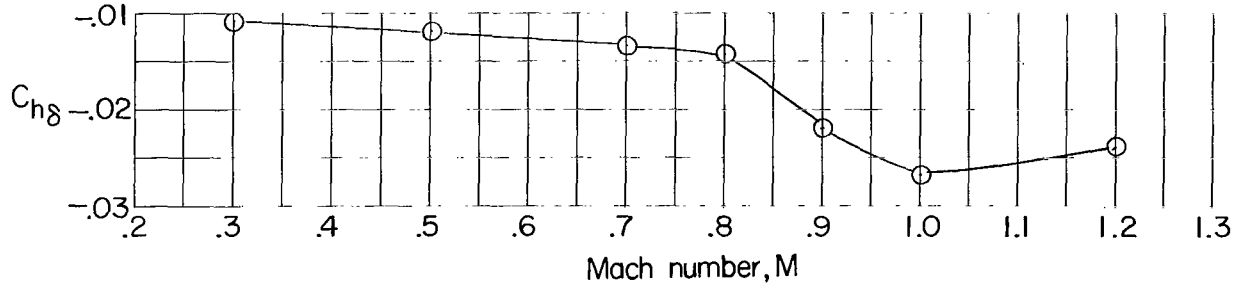

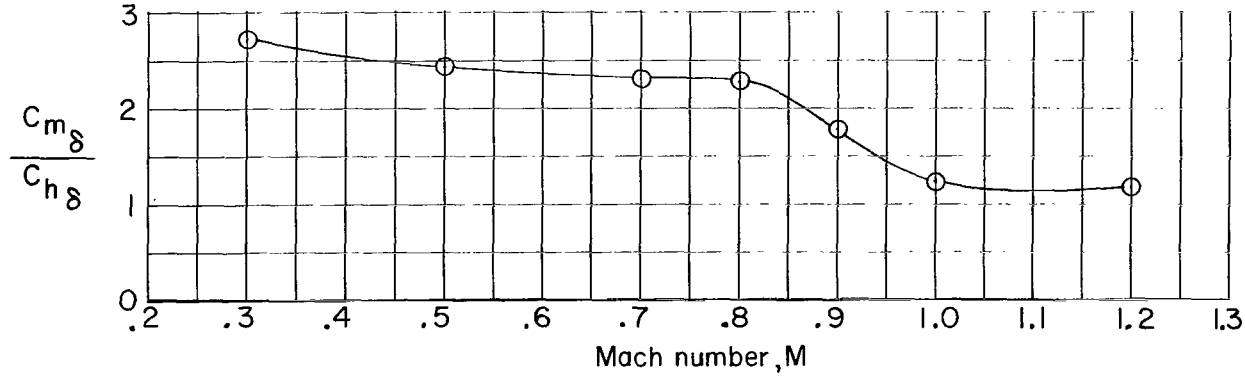

(c) C_{h_δ}, C_{N_δ}, C_{m_δ}, and $C_{m_\delta}/C_{h_\delta}$ against M.

Figure 21.- Concluded.

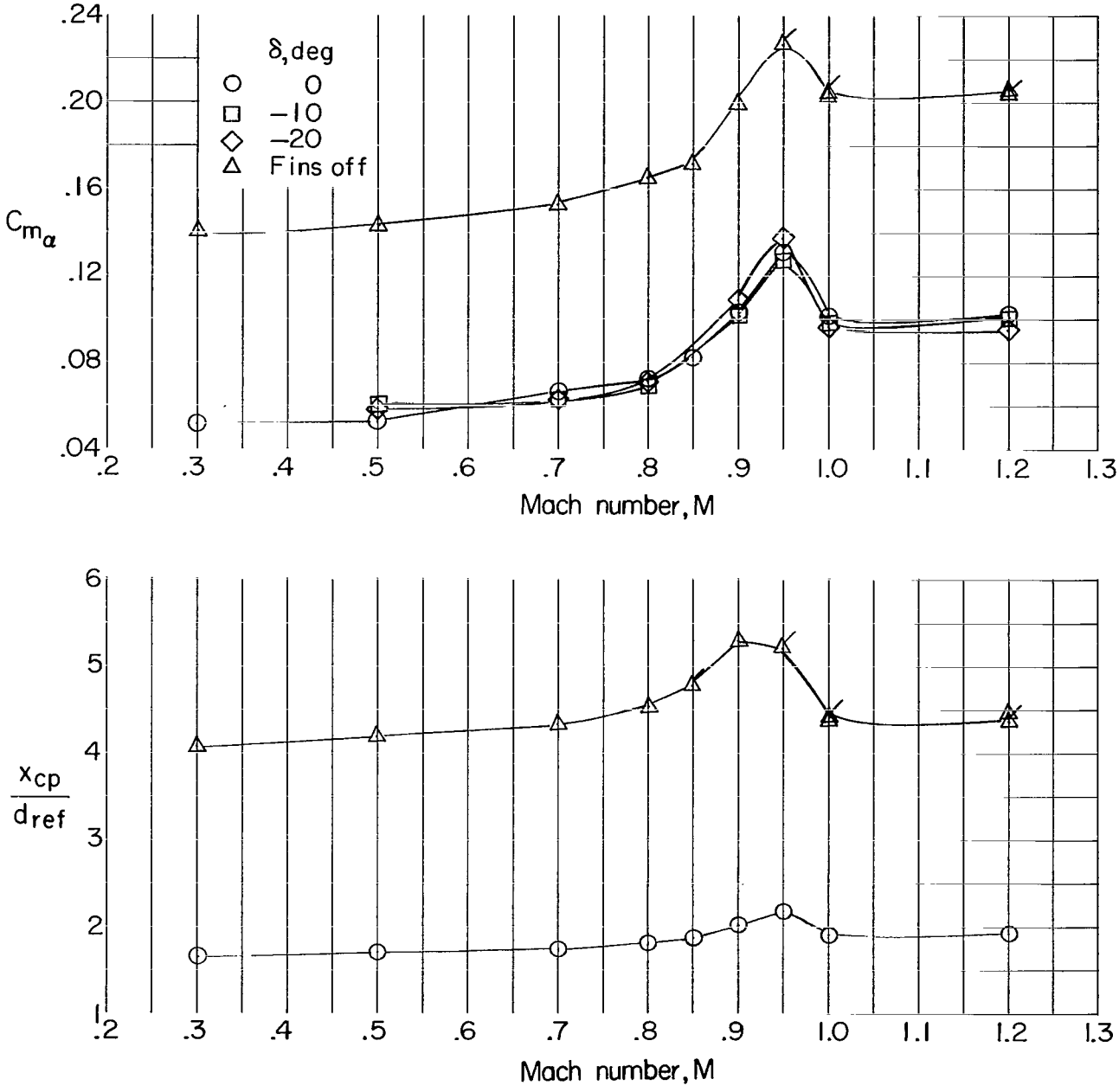

(a) C_{m_α} and x_{cp}/d_{ref} against M.

Figure 22.- Summary information on effect of deflection of trailing-edge controls on longitudinal aerodynamic parameters. Shroud nose 1; intermediate fins; shroud skirt off; $\alpha = 0^0$. (Flagged symbols indicate points from repeat run.)

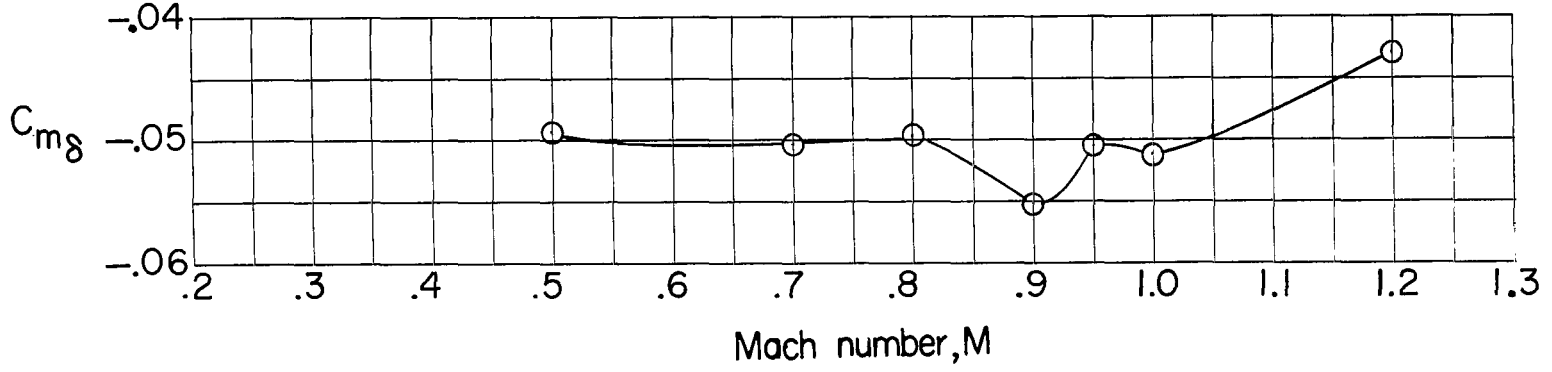

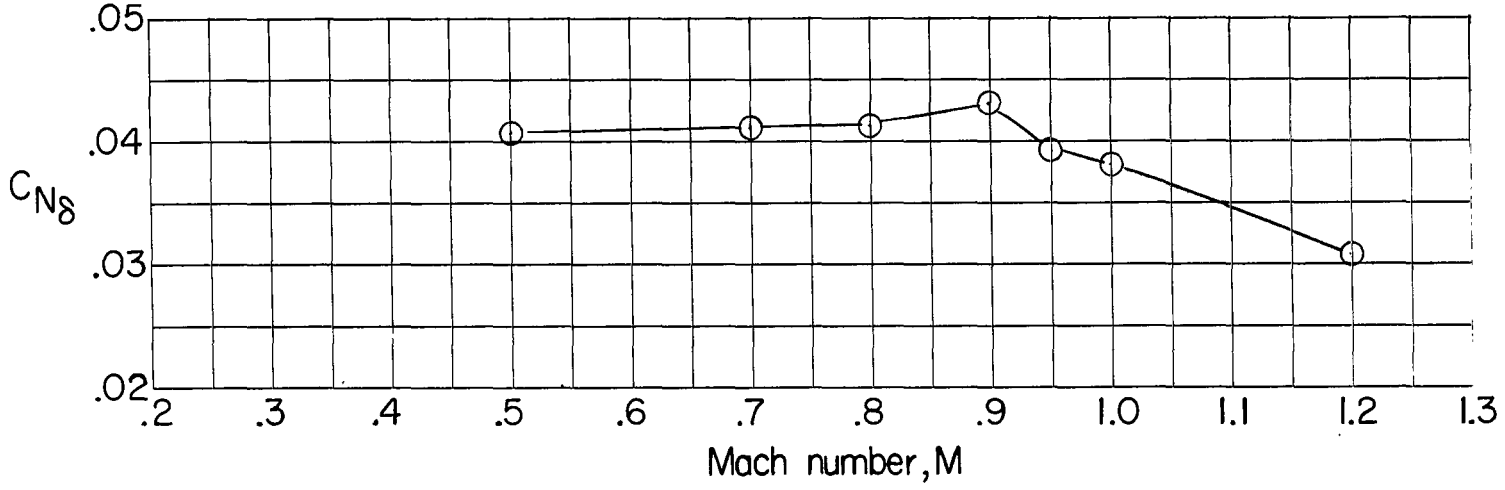

(b) C_{m_δ} and C_{N_δ} against M.

Figure 22.- *Concluded.*

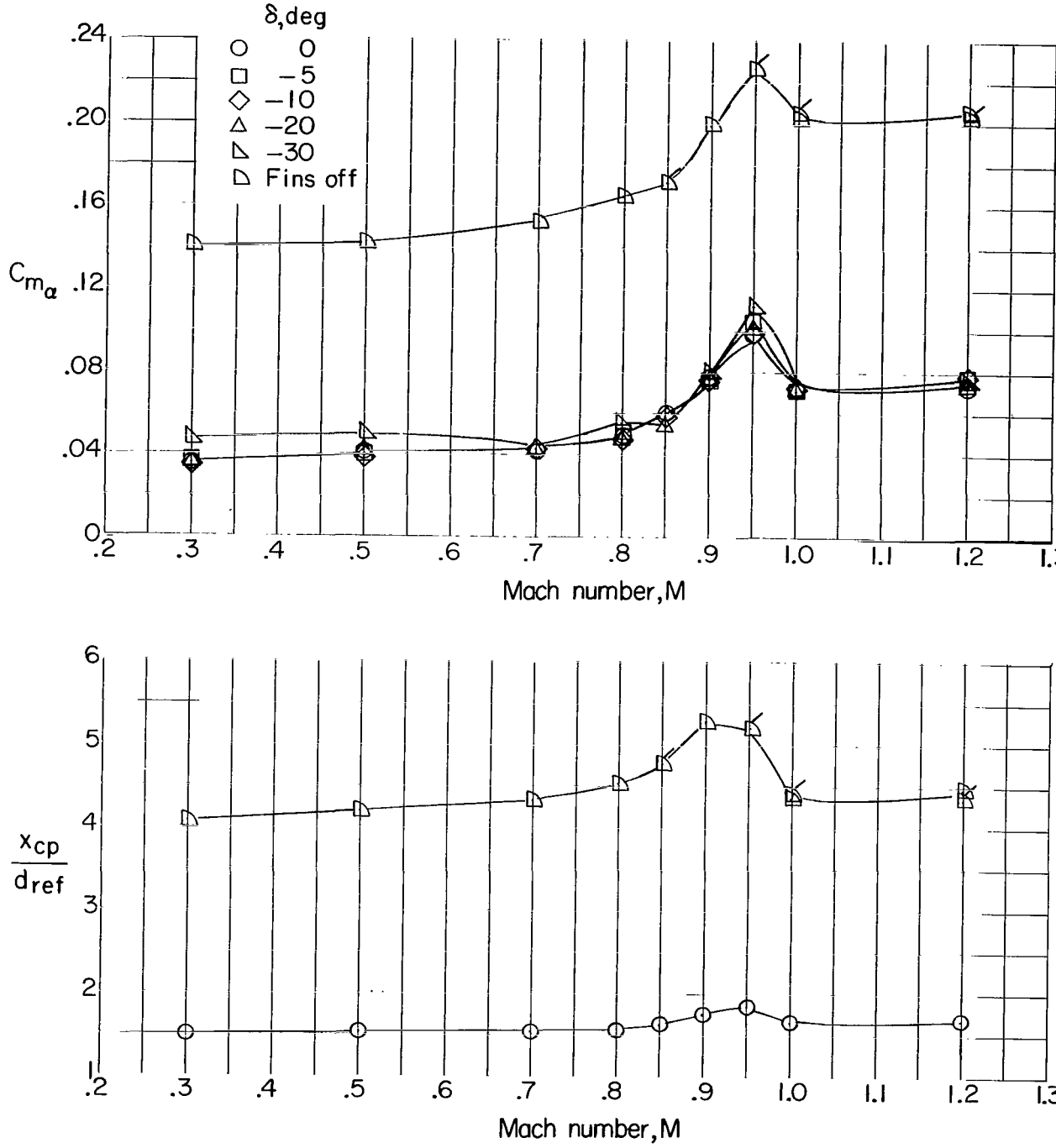

(a) C_{m_α} and x_{cp}/d_{ref} against M.

Figure 23.- Summary information on effect of deflection of trailing-edge controls on longitudinal aerodynamic parameters. Shroud nose 1; large fins; shroud skirt off; $\alpha = 0^0$. (Flagged symbols indicate points from repeat run.)

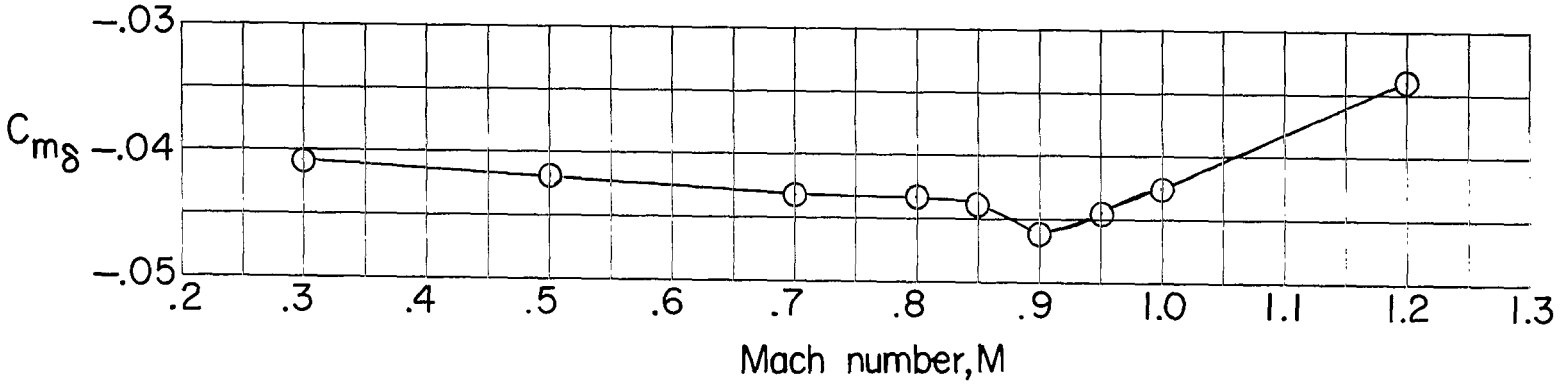

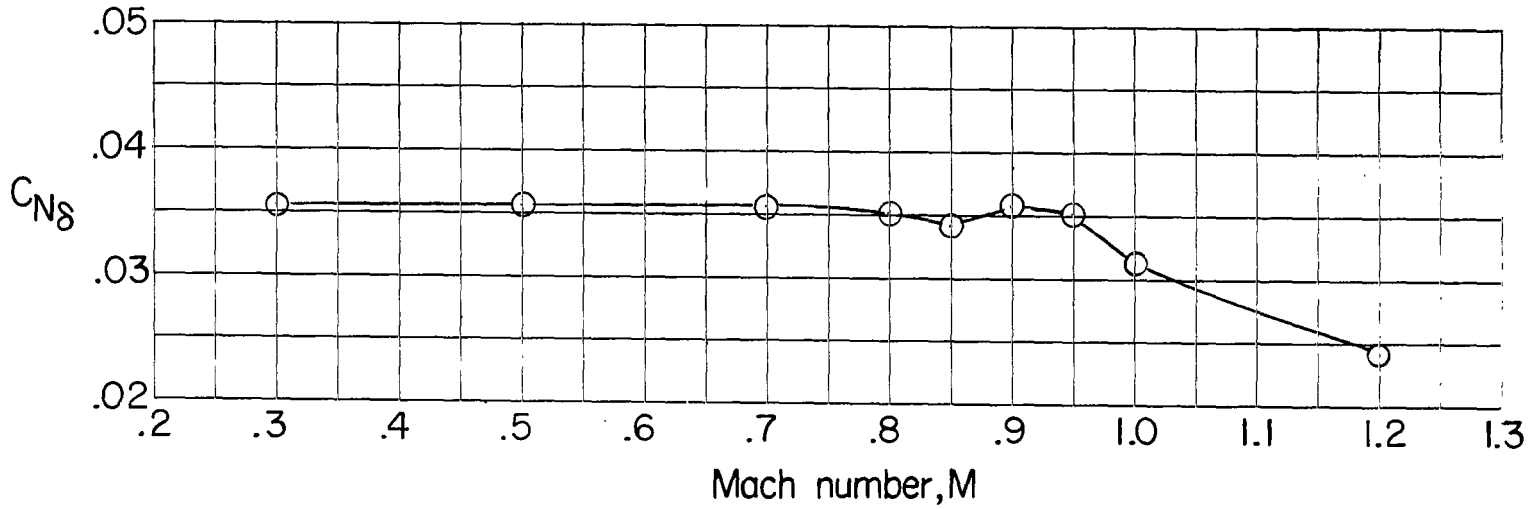

(b) C_{m_δ} and C_{N_δ} against M.

Figure 23.- Concluded.

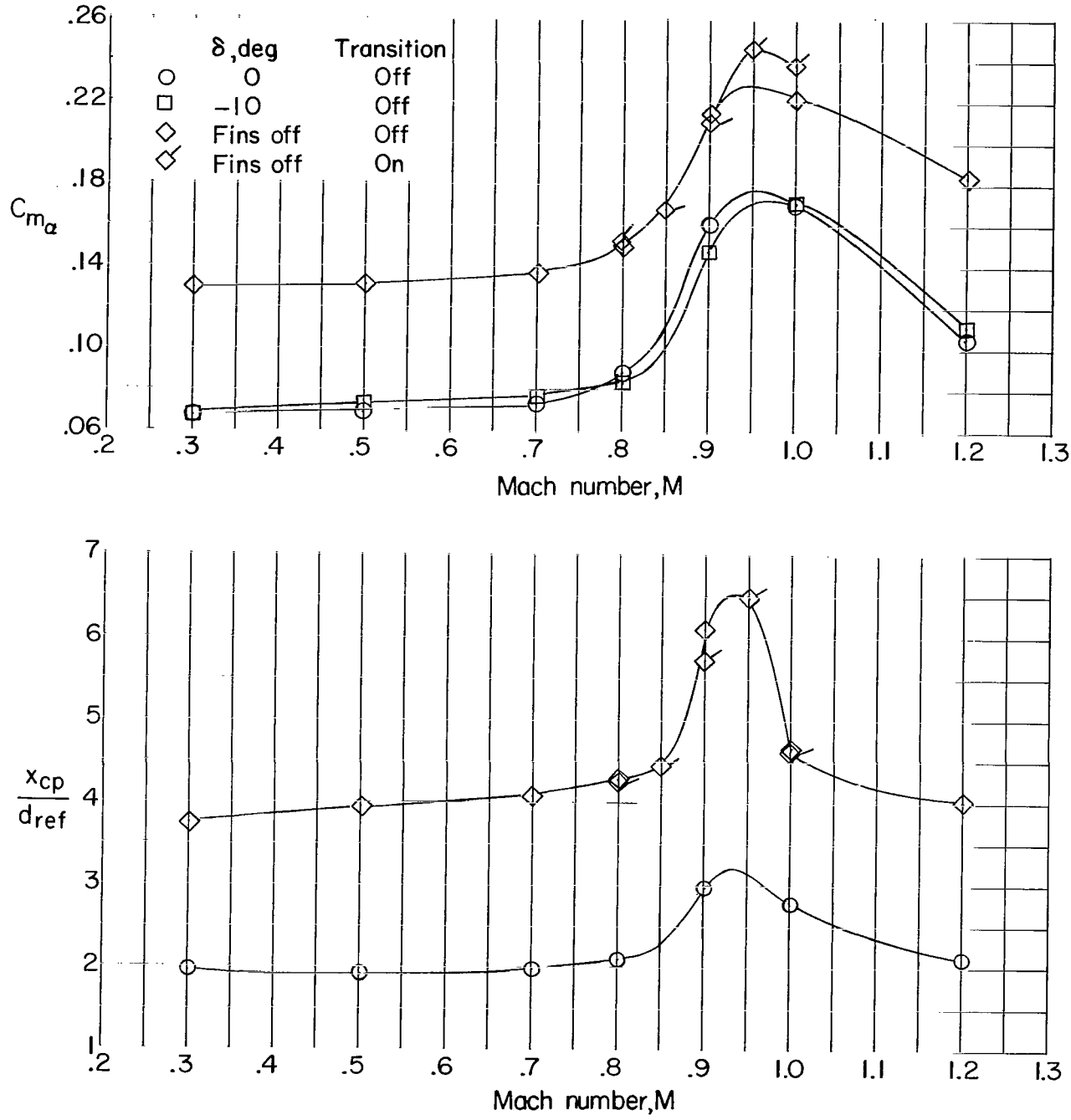

(a) C_{m_α} and x_{cp}/d_{ref} against M.

Figure 24.- Summary information on effect of deflection of trailing-edge controls on longitudinal aerodynamic parameters. Shroud nose 2; small fins; shroud skirt off; $\alpha = 0^0$.

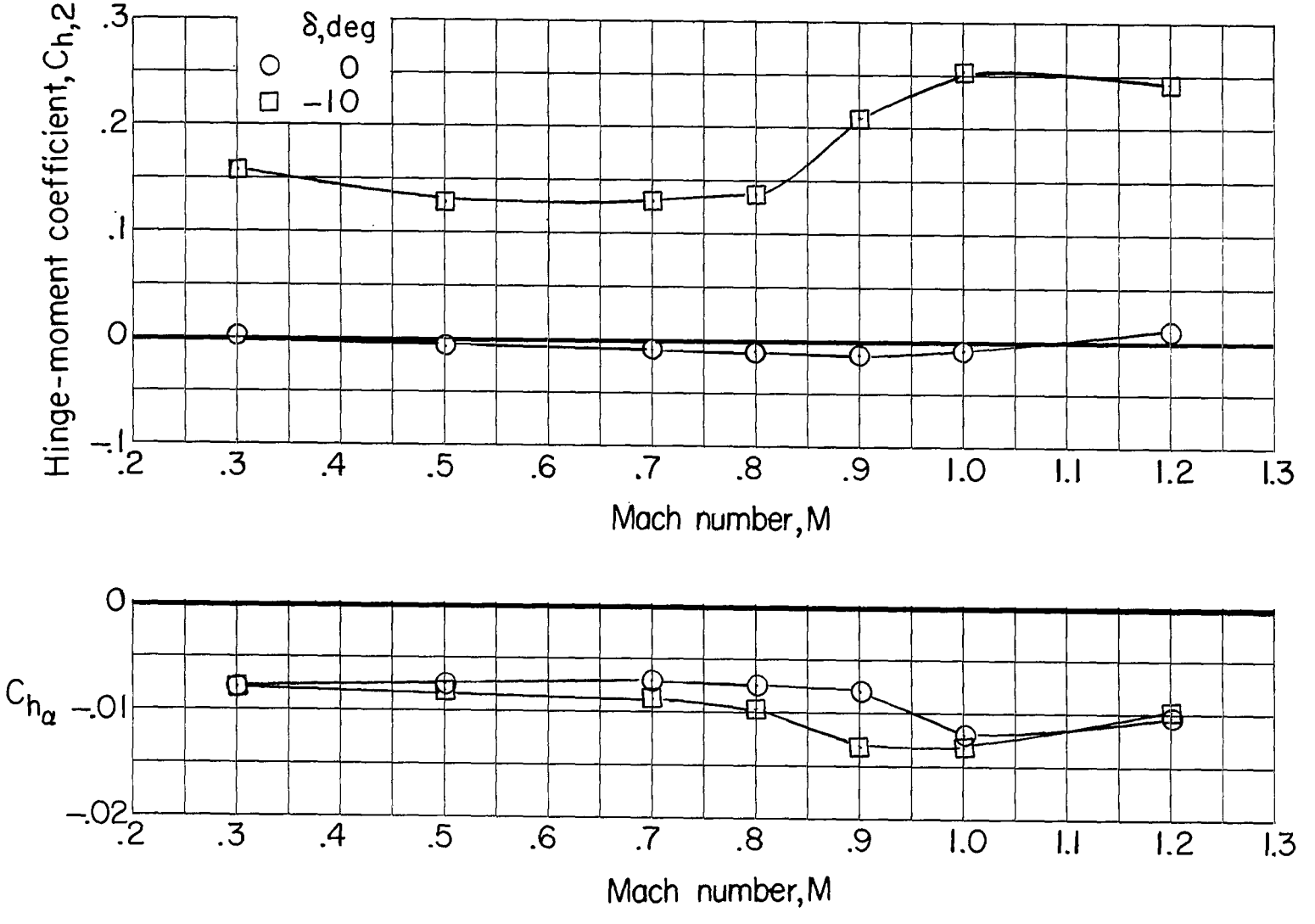

(b) $C_{h,2}$ and C_{h_α} against M.

Figure 24.- Continued.

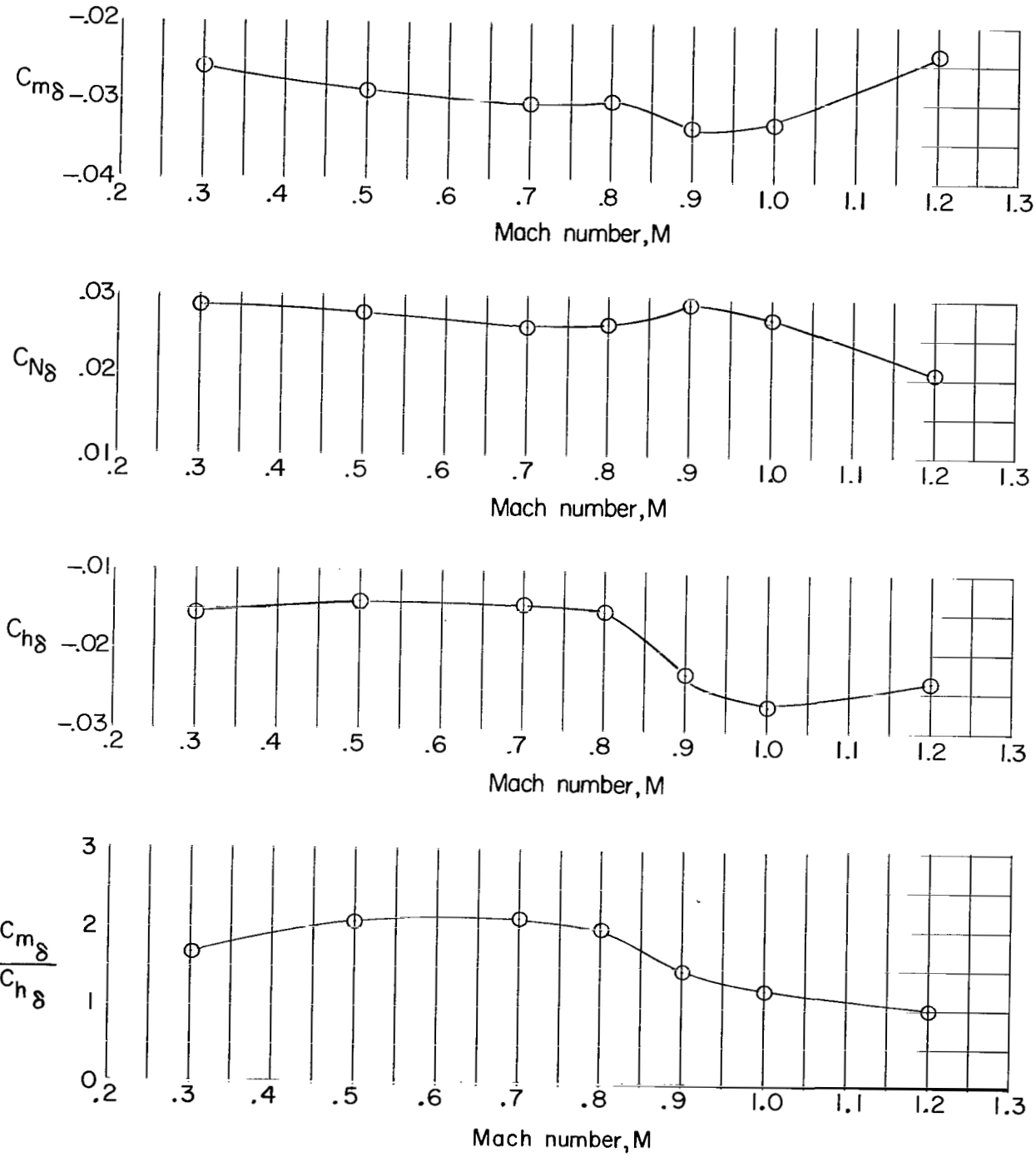

(c) C_{h_δ}, C_{N_δ}, C_{m_δ}, and $C_{m_\delta}/C_{h_\delta}$ against M.

Figure 24.- Concluded.

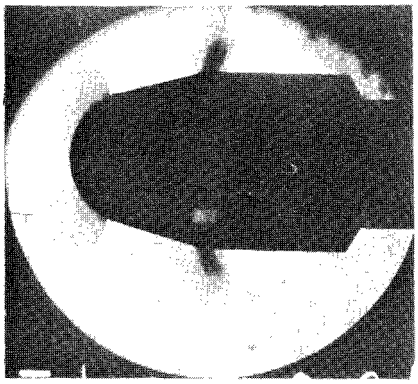

M=0.80 ; α = 0°

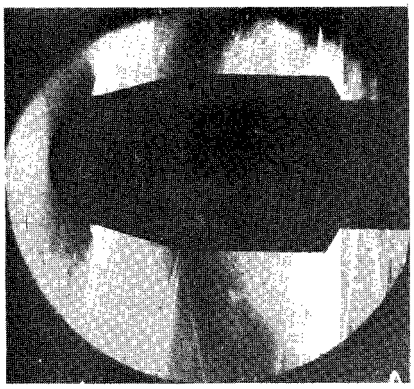

M=0.90; α = 0°

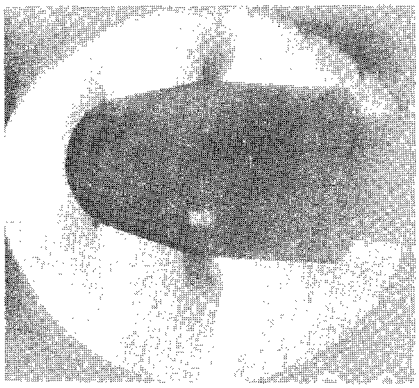

M=0.80 ; α = 2°

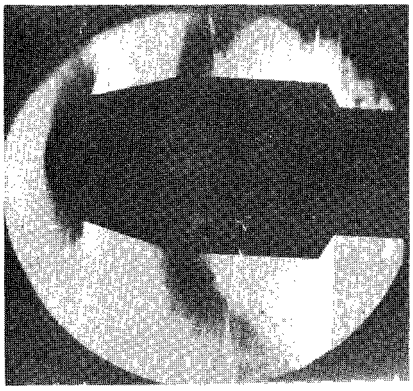

M=0.90; α = 2°

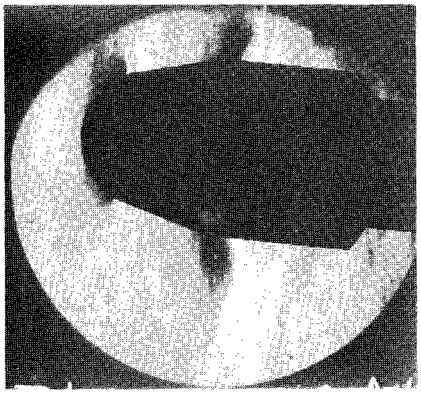

M=0.80; α = 4°

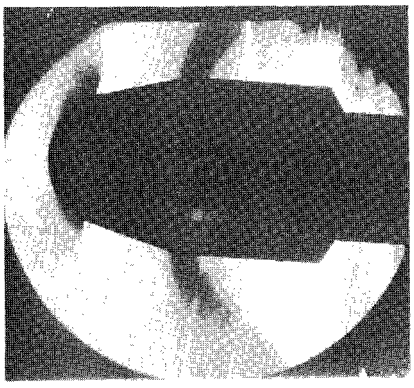

M = 0.90 ; α = 4°

(a) With shroud nose 1. L-67-964

Figure 25.- Schlieren photographs of airflow about LM aerodynamic shroud with shroud noses 1 and 2. Transition strips off.

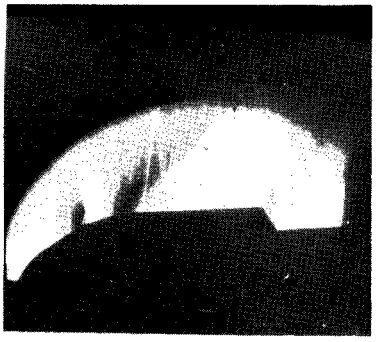

M=0.90; α = -7°

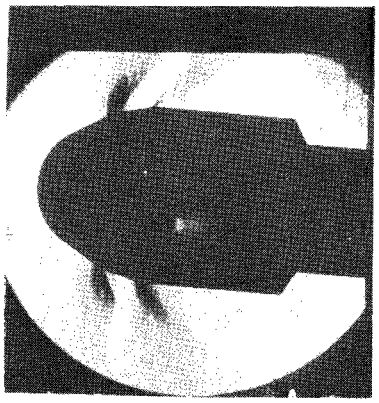

M=0.90; α = 4°

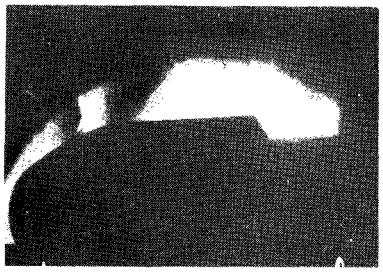

M=0.90; α = -6°

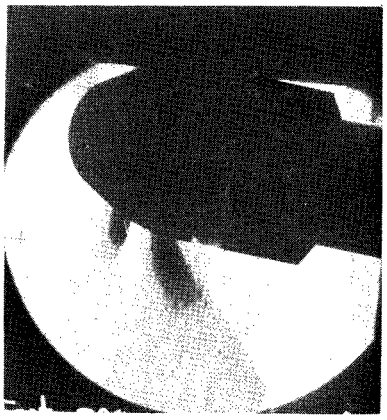

M=0.90; α = 6°

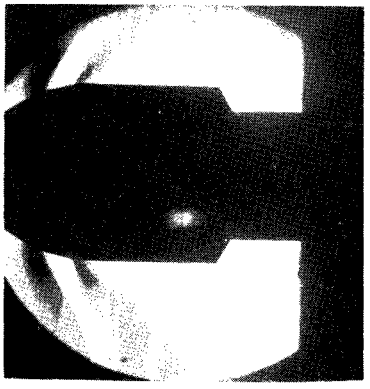

M=0.90; α = 0°

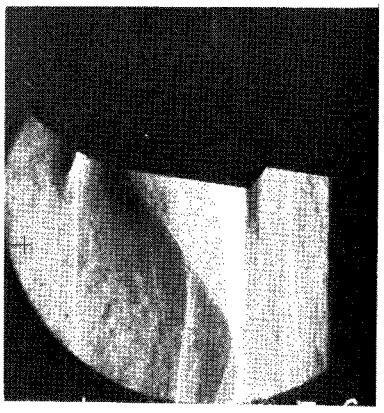

M=0.90; α = 8°

(b) With shroud nose 2. L-67-965

Figure 25.- Concluded.

"The aeronautical and space activities of the United States shall be conducted so as to contribute . . . to the expansion of human knowledge of phenomena in the atmosphere and space. The Administration shall provide for the widest practicable and appropriate dissemination of information concerning its activities and the results thereof."

—NATIONAL AERONAUTICS AND SPACE ACT OF 1958

NASA SCIENTIFIC AND TECHNICAL PUBLICATIONS

TECHNICAL REPORTS: Scientific and technical information considered important, complete, and a lasting contribution to existing knowledge.

TECHNICAL NOTES: Information less broad in scope but nevertheless of importance as a contribution to existing knowledge.

TECHNICAL MEMORANDUMS: Information receiving limited distribution because of preliminary data, security classification, or other reasons.

CONTRACTOR REPORTS: Scientific and technical information generated under a NASA contract or grant and considered an important contribution to existing knowledge.

TECHNICAL TRANSLATIONS: Information published in a foreign language considered to merit NASA distribution in English.

SPECIAL PUBLICATIONS: Information derived from or of value to NASA activities. Publications include conference proceedings, monographs, data compilations, handbooks, sourcebooks, and special bibliographies.

TECHNOLOGY UTILIZATION PUBLICATIONS: Information on technology used by NASA that may be of particular interest in commercial and other non-aerospace applications. Publications include Tech Briefs, Technology Utilization Reports and Notes, and Technology Surveys.

Details on the availability of these publications may be obtained from:

SCIENTIFIC AND TECHNICAL INFORMATION DIVISION

NATIONAL AERONAUTICS AND SPACE ADMINISTRATION

Washington, D.C. 20546